

BIOMECHANICAL ASYMMETRIES  
AND JOINT LOADING IN ELITE  
ROWERS

by

ERICA BUCKERIDGE

A Thesis submitted in fulfillment of requirements for the degree  
of Doctor of Philosophy of Imperial College

Department of Surgery and Cancer and Department of Bioengineering

Imperial College London

2013

# **Declaration of Originality**

I declare that all material in this thesis which is not my own work has been identified and that no material has previously been submitted and approved for the award of a degree by this or any other University.

# Copyright Declaration

**‘The copyright of this thesis rests with the author and is made available under a Creative Commons Attribution Non-Commercial No Derivatives licence. Researchers are free to copy, distribute or transmit the thesis on the condition that they attribute it, that they do not use it for commercial purposes and that they do not alter, transform or build upon it. For any reuse or redistribution, researchers must make clear to others the licence terms of this work’**

# Abstract

Rowing is a technical sport which requires a high skill level in order to optimise performance and reduce the risk of injury. Previous studies investigating the biomechanics of rowing technique and performance have focussed on two-dimensional lumbar-pelvic kinematics as well as more detailed three-dimensional descriptions of the lower extremity. However, limited research has examined lower limb asymmetries during rowing, with the majority of studies focussing on the action of a single leg.

This study aims to quantify lower limb asymmetries during ergometer rowing, and the effect that asymmetries might have on the dynamics of the lumbar-pelvic joint, a commonly injured area in rowers, and subsequent performance. Kinematic asymmetries of the lower limbs were quantified using an electro-magnetic motion capture system. Symmetry of foot force production was also examined through custom force measuring footplates, with the design and output of these being developed and refined as part of this project. Inter-segmental loading of the lower limb and lumbar-pelvic joints were estimated with a five-segment inverse dynamics model, which utilised foot force and kinematic data as inputs. A final aim was to examine the effect of changing foot stretcher height on rowing performance and technique from a biomechanical perspective.

The results indicate that rowing is in fact an asymmetrical activity, with significant bilateral differences identified at the footplates. From a movement perspective knee and hip joints were bilaterally asymmetrical, with hip range of motion asymmetries significantly associated with lumbar-pelvic flexion in the sagittal plane. Inter-segmental joint moments were not influenced by the presence of foot force asymmetries. However,

they were influenced by increased rowing intensity. Large lumbar-pelvic extension moments were present during the rowing stroke, and these increased with respect to stroke rate. This is unlikely to be a measure of greater performance, as corresponding increases in performance measures such as foot and handle force were not observed. In fact, it may be an indicator of technique decline at higher work rates, as larger peak lumbar-pelvic moments occurred alongside increases in lumbar-pelvic flexion and loading of the seat – both of which are considered deleterious to performance. Therefore, rowers may be at greater risk of developing lower back pain when training at high intensities. A performance intervention, which involved raising the height of the foot-stretchers, was found to have little positive effect on the horizontal forces measured at the feet. In addition, there was a negative influence on stroke length and lumbar-pelvic posture. From a coaching perspective these results provide information regarding athlete set-up and their immediate implications on rowing performance.

These studies have shown that elite rowers demonstrate biomechanical asymmetries of the lower limbs, and these could negatively influence the dynamics of the lumbar-pelvic joint and predispose them to low back pain. High intensity rowing and increases in foot stretcher height were also seen to increase lumbar-pelvic flexion through the rowing stroke. Key kinematic characteristics of the lower limbs which positively influence force production were also identified, thus providing rowing coaches with important biomechanical insight into performance optimisation and reduction of injury risk.

# List of Publications

## Publications

- Buckeridge, E., Hislop, S., Bull, A.M.J., and McGregor, A.H. (2012). Kinematic asymmetries of the lower limbs during ergometer rowing. *Med Sci Sport & Ex.*, 44, 2147-2153.
- Buckeridge, E., Bull, A.M.J., and McGregor, A.H. (2012). Foot force patterns and asymmetries in elite rowers. *Sports Biomechanics* (Accepted).

## Presentations

- 17th European Congress of Sports Science, Bruges, Belgium, July 2012: “The effect of incremental training intensities on joint dynamics in elite rowers”.
- The Biomedical Basis of Elite Performance, Queen Elizabeth II Conference Centre, London, UK, March 2012: “Kinematic asymmetries of the lower limbs during ergometer rowing”.
- Imperial College division of Surgery Research Symposium, London, December 2011: “Foot force asymmetries in elite scullers and rowers”.

# Acknowledgements

I wish to thank, first and foremost, my supervisors Alison McGregor and Anthony Bull. Thanks for giving me the opportunity to carry out this research, and for the many years of support, guidance and encouragement. It's been a privilege to work with two people who have brought such expertise and enthusiasm to this project.

Many thanks to all the coaches, athletes and support staff at GB Rowing. The team's continued success has been a real inspiration to me and has made me strive for gold in my own research! I would like to extend particular thanks to Paul Thompson and Rosie Mayglothling for their continued encouragement and support. Many thanks to Liz Arnold. I couldn't have asked for a better or more helpful physio to spend all that time with in the lab! A big thank you to Alex Wolf who has shown a great deal of interest in this project, and shared much of his ideas and enthusiasm with me along the way.

I have many people to thank at Imperial College for both their academic and social support. Andy Murphy, Jeroen Bergmann, Paul Strutton, Lynsey Duffell, Reva Vaze, Antoinette Hardijzer, Megan Sperry and Samuel Bird. Thanks to each of you for your technical support, advice, and collaborative efforts. A big thank you to Rob Aplin who has been an invaluable part of this research and I thank you for the many fascinating discussions and help during lab sessions...and especially the baked goods! Thank you to my 'bodyguards' Sham and Jose. TFCTID....enough said!

Thanks to Chris for everything!! Finally, thanks to my family for their unwavering support and dealing so well with my roller coaster of emotions. I hope the completion of this thesis has made you proud.

# Nomenclature and Abbreviations

<b><math>\alpha</math></b>	Alpha angle i.e. flexion-extension inter-segmental angle
<b><math>\beta</math></b>	Beta angle i.e. abduction-adduction, side flexion inter-segmental angle
<b><math>\gamma</math></b>	Gamma angle i.e. internal external rotation, twist inter-segmental angle
<b><math>\Delta L5/S1</math></b>	Change in L5/S1 flexion-extension during the critical drive phase
<b>AJC</b>	Ankle joint centre
<b>AP</b>	Anterior-posterior axis
<b>ASI</b>	Asymmetry Index
<b>ASIS</b>	Anterior superior iliac spine
<b>ANOVA</b>	Analysis of variance
<b>BM</b>	Body mass
<b>CM</b>	Centre of mass
<b>CMD</b>	Coefficient of multiple determination
<b>COP</b>	Centre of pressure
<b>CV</b>	Coefficient of variance
<b>d</b>	Moment arm
<b>DC</b>	Direct current
<b>EMG</b>	Electromyography
<b>FEM</b>	Body segment – the thigh
<b>FOB</b>	Flock of Birds
<b>FOOT</b>	Body segment – the foot
<b>GRF</b>	Ground reaction force
<b>HJC</b>	Hip joint centre
<b>HWV</b>	Athlete group - heavyweight females
<b>I</b>	Moment of inertia
<b>IDA</b>	Inverse dynamics analysis
<b>JCS</b>	Joint co-ordinate system
<b>KJC</b>	Knee joint centre
<b>L4/L5</b>	Junction of fourth and fifth lumbar vertebrae
<b>L5/S1</b>	The junction of the fifth lumbar and first sacral vertebrae
<b>LBP</b>	Lower back pain
<b>LEPI</b>	Anatomical point - the lateral femoral epicondyle
<b>LMAL</b>	Anatomical point - the lateral malleolus



<b>LASIS</b>	Anatomical point - the left anterior superior iliac spine
<b>LPSIS</b>	Anatomical point - the left posterior superior iliac spine
<b>LUM</b>	Body segment – the lumbar spine
<b>LWM</b>	Athlete group - lightweight men
<b>M</b>	Moment
<b>MAE</b>	Mean absolute error
<b>MET5</b>	Anatomical point - the dorsal aspect of the fifth metatarsal head
<b>MEPI</b>	Anatomical point - the medial femoral epicondyle
<b>MHF</b>	Maximum handle force
<b>ML</b>	Medio-lateral axis
<b>ML drift</b>	Medio-lateral drift on the seat
<b>MMAL</b>	Anatomical point - the medial malleolus
<b>MRI</b>	Magnetic resonance imaging
<b>P1</b>	Foot-stretcher Position 1
<b>P2</b>	Foot-stretcher Position 2
<b>P3</b>	Foot-stretcher Position 3
<b>P4</b>	Foot-stretcher Position 4
<b>PEL</b>	Pelvis segment
<b>PLA</b>	Point loading apparatus
<b>RASIS</b>	Anatomical point - the right anterior superior iliac spine
<b>RF</b>	Foot force ratio
<b>ROM</b>	Range of motion
<b>RPSIS</b>	Anatomical point - the right posterior superior iliac spine
<b>R</b>	Reaction force
<b>S1</b>	Flock of Birds sensor 1
<b>S2</b>	Flock of Birds sensor 2
<b>S3</b>	Flock of Birds sensor 3
<b>S4</b>	Flock of Birds sensor 4
<b>SCULL</b>	Athlete group - heavyweight female scullers
<b>SI</b>	Superior-inferior axis
<b>SWEEP</b>	Athlete group - heavyweight female sweep rowers
<b>T12/L1</b>	The junction of the twelfth thoracic and first lumbar vertebrae
<b>TIB</b>	Body segment – the shank
<b>VIF</b>	Variance inflation factor
<b>UT1</b>	Utilisation training 1

<b>UT2</b>	Utilisation training 2
<b>UTS</b>	Ultimate tensile strength
<b>X</b>	The laboratory medio-lateral axis
<b>Y</b>	The laboratory vertical axis
<b>Z</b>	The laboratory anterior-posterior axis

# Contents

<b>Declaration of Originality .....</b>	<b>2</b>
<b>Copyright Declaration .....</b>	<b>3</b>
<b>Abstract.....</b>	<b>4</b>
<b>List of Publications .....</b>	<b>6</b>
<b>Acknowledgements .....</b>	<b>7</b>
<b>Nomenclature and Abbreviations.....</b>	<b>8</b>
<b>Contents .....</b>	<b>11</b>
<b>List of Figures.....</b>	<b>16</b>
<b>List of Tables .....</b>	<b>22</b>
<b>Chapter 1: Introduction to Rowing.....</b>	<b>25</b>
1.1 Rowing: The basics .....	26
1.2 Lower back pain in rowing .....	30
<b>Chapter 2: Previous Research and Current Objectives.....</b>	<b>33</b>
2.1 Rowing Research at Imperial College.....	33
2.1.1 System Development .....	34
2.1.2 Experimental Research: lumbar-pelvic kinematics .....	37
2.1.3 Further system developments: instrumentation and three dimensional kinematics .....	41
2.2 Development of Study Aims.....	44
2.2.1 Specific Study Aims .....	45
2.3 Structure of Thesis .....	46
<b>Chapter 3: Lower Limb Kinematic Asymmetries in Elite, Club and Novice Rowers.....</b>	<b>49</b>
3.1 Introduction .....	49
3.1.1 Kinematic investigations of the rowing stroke .....	49
3.1.2 Asymmetries and Lower Back Pain.....	52
3.1.3 Lower limb asymmetries in rowing .....	54
3.2 Methodology .....	55
3.2.1 Participants.....	55
3.2.2 Instrumented ergometer and motion capture .....	56
3.2.3 Subject preparation and digitisation .....	58
3.2.4 Experimental protocol.....	59
3.2.5 Data acquisition .....	60

3.2.6	Data analysis .....	61
3.2.7	Statistical analysis .....	69
3.3	Results .....	70
3.3.1	Performance related parameters.....	70
3.3.2	Lower limb kinematics .....	71
3.3.3	Lumbar-pelvic kinematics .....	73
3.3.4	Summary of results .....	75
3.4	Discussion .....	75
3.5	Conclusion.....	81
<b>Chapter 4: Development of Instrumented Footplates: Design, instrumentation and calibration .....</b>		<b>82</b>
4.1	Introduction .....	83
4.1.1	Measuring contact forces in sport .....	83
4.1.2	Measuring foot forces in rowing.....	89
4.2	Footplate Design .....	92
4.2.1	Design Specifications .....	92
4.2.2	Instrumentation .....	94
4.2.3	Physical Design.....	97
4.2.4	Basic Force Measuring Principles .....	100
4.2.5	Stress Analysis .....	102
4.2.6	Application of Strain Gauges.....	107
4.2.7	Bridge circuit .....	108
4.2.8	Justification of a full bridge circuit.....	109
4.2.9	Amplification and signal conditioning .....	112
4.3	Calibration.....	113
4.3.1	Normal Force Calibration .....	114
4.3.2	Centre of Pressure Calibration .....	118
4.3.3	Shear Force Calibration .....	119
4.3.4	Footplate Error Analysis .....	123
4.3.5	Cross-talk Compensation.....	124
4.4	Development of biofeedback system .....	125
4.4.1	Foot force Biofeedback to GB Rowing .....	126
4.5	Summary .....	128
<b>Chapter 5: Application of Instrumented Footplates: Foot force production and asymmetries in elite rowers.....</b>		<b>129</b>
5.1	Introduction .....	130

5.1.1	The Leg drive.....	130
5.1.2	Foot force asymmetries in rowing .....	131
5.2	Methodology .....	133
5.2.1	Participants.....	133
5.2.2	Experimental Protocol .....	134
5.2.3	Data Acquisition .....	135
5.2.4	Data Analysis .....	135
5.2.5	Statistical Analysis.....	140
5.3	Results .....	141
5.3.1	Reliability.....	141
5.3.2	Total foot force .....	144
5.3.3	Foot force asymmetry .....	147
5.3.4	Longitudinal foot force and asymmetry.....	149
5.3.5	Summary of results .....	150
5.4	Discussion .....	151
5.5	Conclusion.....	156
<b>Chapter 6: Modelling the Relationship between Rowing Technique, Asymmetry and Performance.....</b>		<b>158</b>
6.1	Introduction .....	158
6.1.1	How does technique influence force application? .....	159
6.1.2	Do asymmetries at the feet increase injury risk? .....	161
6.1.3	Investigating the kinetic chain in rowing.....	162
6.1.4	Statistical modelling of performance .....	163
6.2	Methodology .....	165
6.2.1	Participants.....	165
6.2.2	Experimental set-up .....	166
6.2.3	Subject Preparation and Digitization .....	168
6.2.4	Experimental protocol.....	169
6.2.5	Data acquisition .....	169
6.2.6	Data analysis .....	172
6.2.7	Statistical Analysis.....	179
6.3	Results .....	182
6.3.1	Does technique influence force application? .....	182
6.3.2	Do foot force asymmetries influence performance?.....	189
6.3.3	How do forces at the feet influence the kinetic chain? .....	195

6.3.4	Summary of results .....	200
6.4	Discussion .....	201
6.5	Conclusion.....	212
<b>Chapter 7: The effect of incremental training intensities on joint dynamics in elite rowers.....</b>		<b>213</b>
7.1	Introduction .....	213
7.1.1	Prevalence and aetiology of lower back injuries in rowing.....	213
7.1.2	Inter-segmental inverse dynamic modelling.....	215
7.1.3	Limitations of inter-segmental modelling.....	217
7.1.4	Applications of inter-segmental inverse dynamic modelling .....	218
7.2	Methodology .....	222
7.2.1	Participants.....	222
7.2.2	Data Collection .....	223
7.2.3	Data Analysis.....	224
7.2.4	Statistical Analysis.....	233
7.3	Results .....	234
7.3.1	Influence of stroke rate on joint dynamics and performance.....	234
7.3.2	Gender Differences .....	238
7.3.3	Interaction effects .....	239
7.3.4	Summary of Results.....	244
7.4	Discussion .....	245
7.5	Conclusion.....	251
<b>Chapter 8: Effect of changes in foot-stretcher height on rowing technique and performance .....</b>		<b>253</b>
8.1	Introduction.....	254
8.2	Methodology .....	258
8.2.1	Participants.....	258
8.2.2	Experimental set-up .....	258
8.2.3	Experimental protocol.....	261
8.2.4	Data analysis .....	262
8.2.5	Statistical analysis.....	265
8.3	Results.....	265
8.3.1	Foot force application technique.....	266
8.3.2	Rowing performance.....	268
8.3.3	Joint kinematics .....	269
8.3.4	Joint kinetics .....	270

8.3.5	Summary of results .....	274
8.4	Discussion .....	275
8.5	Conclusion.....	283
<b>Chapter 9:</b>	<b>Summary and Future Work.....</b>	<b>284</b>
9.1	Summary of work.....	285
9.1.1	Research Contributions.....	294
9.2	Future recommendations .....	294
<b>References.....</b>		<b>298</b>
<b>Appendix A:.....</b>		<b>313</b>
<b>Appendix B:.....</b>		<b>316</b>
<b>Appendix C:.....</b>		<b>322</b>
<b>Appendix D:.....</b>		<b>328</b>
<b>Appendix E:.....</b>		<b>330</b>
<b>Appendix F: .....</b>		<b>333</b>
<b>Appendix G: .....</b>		<b>336</b>
<b>Appendix H: .....</b>		<b>339</b>
<b>Appendix I:.....</b>		<b>341</b>
<b>Appendix J: .....</b>		<b>343</b>
<b>Appendix K: .....</b>		<b>352</b>

# List of Figures

Figure 1.1: Diagrams depicting the drive and recovery phases of the rowing stroke.....	<b>29</b>
Figure 1.2: Side view of spinal column (left) and larger view of two vertebra and intervertebral disc (right) ( <a href="http://www.spineuniverse.com/anatomy/lumbar-spine">http://www.spineuniverse.com/anatomy/lumbar-spine</a> ).....	<b>31</b>
Figure 2.1: Plan view of laboratory set-up showing the placement of the FOB transmitter in relation to the ergometer.....	<b>35</b>
Figure 2.2: Diagram depicting the sagittal plane orientations of body segments measured by the Flock of Birds. ....	<b>38</b>
Figure 2.3: Layout of the thesis with blue boxed section representing chapters containing developmental and experimental studies. ....	<b>48</b>
Figure 3.1: Instrumentation of the Concept II ergometer at the flywheel (a), handle (b), and seat (c). ....	<b>57</b>
Figure 3.2: Location of FOB Sensor 2 and Sensor 3 during athlete testing. Sensor 1 was attached bilaterally symmetrically to Sensor 4. ....	<b>58</b>
Figure 3.3: The digitisation stylus with Sensor 3 attached for the purposes of anatomical landmark digitisation. ....	<b>59</b>
Figure 3.4: (a) is the anterior and side views of the pelvis and its anatomical co-ordinate system, (b) is the thigh and its anatomical co-ordinate system and (c) is the hip joint co-ordinate system.....	<b>64</b>
Figure 3.5: Sagittal plane view of linked thigh and shank segments, depicting the computation of knee joint flexion/extension angles. ....	<b>66</b>
Figure 3.6: Plan view of rower's pelvis and lower limbs depicting the process of calculating pelvic twist angle.....	<b>67</b>
Figure 3.7: Horizontal handle displacement trace depicting the stroke length derivation process.....	<b>67</b>
Figure 3.8: Centre of pressure trajectory on the seat for a single normalised stroke. Red dot is the catch, solid black trace is the drive phase, green dot is the finish, dotted black trace is the recovery phase. Units are cm. ....	<b>68</b>
Figure 3.9: Bilateral joint angles over a normalised rowing stroke (top row; elite rower, middle row; club rower, bottom row; novice rower). Blue line represents right side, red line represents left side. 0° is full joint extension; hip flexions are negative, knee flexions are positive. Vertical lines represent MHF, finish and 10% recovery positions, from left to right. ....	<b>73</b>



Figure 3.10: Average (error bars indicate standard deviation) L5/S1 flexion-extension angles at the catch, MHF, finish and 10% recovery positions during four incremental steps. Flexion is positive and extension is negative. * statistically significant difference from finish and recovery ( $P<0.05$ ). # is statistically significant difference from recovery ( $P<0.05$ ). .....	<b>74</b>
Figure 4.1: Dimensions of the two main components of the footplate; Beam A (top) and Beam B (bottom).....	<b>98</b>
Figure 4.2: (a) Beam A and B loading scenario showing the application of normal force to Beam A (blue arrows) and shear force to Beam B (red arrows), (b) assembled footplate showing the addition of the Side Plate and Loading Plate, (c) underside view of the footplate showing where the ends of Beam A form attachments to the ends of the Loading Plate, and the connections between Beam B and the Mounting Component. ....	<b>99</b>
Figure 4.3: Example of a tensile stress-strain curve. ....	<b>101</b>
Figure 4.4: Equivalent Von Mises stresses (MPa) of a 1000 N load applied perpendicular to the footplate loading surface. ....	<b>104</b>
Figure 4.5: Vertical axis displacements (mm) of the footplate construct in response to a 1000 N split load. ....	<b>106</b>
Figure 4.6: Strain gauges are bonded to beam A and beam B at the locations indicated above. Corresponding number of strain gauges are bonded on the reverse of each beam.....	<b>107</b>
Figure 4.7: Wheatstone bridge circuit.....	<b>109</b>
Figure 4.8: (a) Beam B's attachment to side plate and Beam A (b) side view of right footplate (c) Beam A and Beam B attached to side plate (d) loading plate attached to Beam A. ....	<b>112</b>
Figure 4.9: Diagram of right footplate attached to rigid horizontal surface with PLA aligned to calibration point. ....	<b>115</b>
Figure 4.10: Location of 36 normal calibration points along footplate surface. ....	<b>116</b>
Figure 4.11: Raw voltage outputs of normal force (front, red), normal force (rear, blue), shear force (green). ....	<b>117</b>
Figure 4.12: Diagram of footplate attached to rigid vertical surface with weights suspended via a calibration plate. ....	<b>120</b>
Figure 4.13: Location of three shear calibration points along footplate surface. ....	<b>121</b>
Figure 4.14: Raw voltage outputs of normal force (front) (red), normal force (rear) (blue), shear force (green). ....	<b>122</b>
Figure 4.15: Linear regression line to predict shear force values. ....	<b>123</b>

- Figure 4.16: Diagram of footplate showing normal and shear forces resolved into its vertical and horizontal components.  $F_y$  is vertical force,  $F_z$  is horizontal (anterior-posterior) force,  $x_1$  is normal force and  $x_2$  is shear force.....**126**
- Figure 4.17: Screenshot of footplate biofeedback and acquisition program. Red traces are horizontal forces, white traces are vertical forces and green bars are longitudinal COP displacement from the rear of the footplate.....**127**
- Figure 5.1: Centre of pressure traces of the right and left footplate depicting the time normalisation process.....**136**
- Figure 5.2: Illustrative example of the calculation of impulse (i.e. area under the curve) using the trapezoidal method. ....**139**
- Figure 5.3: Illustrative example of parameters calculated within a stroke: A is value of peak vertical force, B is the timing of peak vertical force, and C is the vertical impulse i.e. area under the curve above between 0% and minimum force. Parameters for the horizontal force component and resultant force were calculated in the same way.....**139**
- Figure 5.4: (a) Change in peak resultant force and (b) change in peak vertical force with respect to stroke rate. Thick dashed line is LWM, solid line is SCULL and dotted line is SWEEP. Error bars are  $\pm$  SD. ....**144**
- Figure 5.5: (a) Change in resultant impulse and (b) change in vertical impulse with respect to stroke rate. Thick dashed line is LWM, solid line is SCULL and dotted line is SWEEP. Error bars are  $\pm$  SD. ....**144**
- Figure 5.6: (a) Change in horizontal impulse and (b) change in peak horizontal force with respect to stroke rate. Thick dashed line is LWM, solid line is SCULL and dotted line is SWEEP. Error bars are  $\pm$  SD.....**145**
- Figure 5.7: Resultant, vertical and horizontal foot force traces at (a) Rate 18, (b) Rate 24, (c) Rate 28 and (d) Free Rate. Blue lines are LWM, green lines are SCULL and red lines are SWEEP. Standard deviations for this data ranged from  $\pm 0.2$  to  $\pm 4.0$  N/kg for Rate 18,  $\pm 0.2$  to  $\pm 3.6$  N/kg for Rate 24,  $\pm 0.2$  to  $\pm 3.8$  N/kg for Rate 28 and  $\pm 0.5$  to  $\pm 2.6$  N/kg for Free Rate. ....**146**
- Figure 5.8: Average (error bars SD) resultant, vertical and horizontal impulse ASI (top graph) and magnitude (bottom graph) at Free Rate during three testing sessions. \* denotes significant difference where  $P < 0.05$ .....**150**
- Figure 6.1: Instrumentation of the Concept II ergometer at the flywheel (a), handle (b), feet (c) and seat (d). ....**167**
- Figure 6.2: Screenshot of the integrated rowing biofeedback and acquisition program. Top left graphic displays 2D motion of rowers' lower back and lower limbs; bottom left graphic is COP applied to the rowing seat (depicted by green

dot); top right are the footplate biofeedback graphs; and bottom right is the handle force trace. ....	<b>170</b>
Figure 6.3: Scatterplot depicting a linear relationship between peak resultant foot force and resultant foot force at MHF. ....	<b>183</b>
Figure 6.4: Assessment of the assumptions of normality and constant variance with respect to resultant foot force at MHF. ....	<b>186</b>
Figure 6.5: Assessment of the assumptions of normality and constant variance with respect to RF at MHF. ....	<b>189</b>
Figure 6.6: Assessment of the assumptions of normality and constant variance with respect to $\Delta L5/S1$ . ....	<b>192</b>
Figure 6.7: Scatterplot depicting a linear relationship between resultant foot force at MHF and seat force at MHF. ....	<b>197</b>
Figure 6.8: Assessment of the assumptions of normality and constant variance with respect to seat force at MHF. ....	<b>198</b>
Figure 6.9: Scatterplot depicting a linear relationship between resultant foot force at MHF and MHF. ....	<b>199</b>
Figure 6.10: Assessment of the assumptions of normality and constant variance with respect to peak handle force. ....	<b>200</b>
Figure 6.11: Free body diagram of the trunk and lower limbs of a rower in a static condition. No propulsive forces are generated at the handle and foot-stretchers, and the weight of the rower is balanced by vertical reaction forces at the seat and foot-stretchers. ....	<b>208</b>
Figure 6.12: Forces acting on the rowing system at the foot-stretchers ( $F_{\text{foot}}$ ), handle ( $F_{\text{handle}}$ ), seat ( $F_{\text{seat}}$ ) and oars ( $F_{\text{oar}}$ ). Drag forces were not considered in this diagram. ....	<b>208</b>
Figure 6.13: An optimised free body diagram where reaction force at the seat is zero, and lines of action for the weight of the rower acting through the centre of mass ( $W$ ), handle reaction force ( $R_{\text{handle}}$ ) and resultant foot reaction force ( $R_{\text{foot}}$ ) all intersect at a single point to provide zero moment about the rower. Dashed blue lines are the lines of action of the force vectors (presuming no acceleration for simplicity). ....	<b>210</b>
Figure 7.1: Two-dimensional representation of a five segment closed-chain link-segment model of the foot, shank and thigh, pelvis and lumbar spine, with forces and moments acting on all segments. Grey circles represent the location of each segments' centre of mass, and the accelerations acting at the centre of mass is shown for just the shank. Red arrows represent extension moments at each joint. ....	<b>229</b>

Figure 7.2: Three dimensional moments acting about the L5/S1 and bilateral hip coordinate systems. The left thigh is assumed to mirror the right thigh, thus negating pelvis moments about the Y and Z axis, whilst doubling moments about the X axis. ....	<b>230</b>
Figure 7.3: Ankle, knee, hip and L5/S1 joint moment traces in the sagittal plane at Rate 18 (blue) and Free Rate (red) for (a) HWW and (b) LWM. Standard deviations for this data ranged from $\pm 0.03$ to $\pm 0.32$ Nm/kg for ankle moments, $\pm 0.15$ to $\pm 1.13$ Nm/kg for knee moments, $\pm 0.09$ to $\pm 1.61$ Nm/kg for hip moments and $\pm 0.36$ to $\pm 3.63$ Nm/kg for L5/S1 moments.....	<b>239</b>
Figure 7.4: Changes in (a) Peak Ankle Moment, (b) Peak Knee Moment, (c) Peak Hip Moment, and (d) Peak L5/S1 Moment with respect to stroke rate. Thick dashed line is LWM, solid line is HWW. Error bars are $\pm$ SD.....	<b>240</b>
Figure 7.5: Change in proportion of joint work done with respect to stroke rate for (a) HWW and (b) LWM. * represent an overall change in % Work done for that joint with respect to stroke rate ( $P < 0.05$ ).....	<b>242</b>
Figure 7.6: Change in joint work done relative to work done at Rate 18, for (a) HWW and (b) LWM. Red dotted line represents 100% of work done at Rate 18. * represent an overall change in % Work done for that joint relative to Rate 18 ( $P < 0.01$ ). ....	<b>243</b>
Figure 7.7: Changes in (a) MHF, (b) Peak Resultant Foot Force, (c) Peak Seat Force, and (d) Peak L5/S1 ROM with respect to stroke rate. Thick dashed line is LWM, solid line is HWW. Error bars are $\pm$ SD.....	<b>244</b>
Figure 8.1: Foot-stretchers are fixed to the adjustable footplates to demonstrate two different heights. The left foot-stretcher depicts the lowest heights (Position 1) and the right foot-stretcher depicts the highest height (Position 4). ....	<b>259</b>
Figure 8.2: Two different foot-stretcher heights adjusted in the traditional way by slotting the end of the foot-stretcher into holes arranged at incremental heights. ....	<b>260</b>
Figure 8.3: Feet constrained to the foot-stretchers at two different positions, showing the bilateral differences in placement of each strap relative to the foot. ....	<b>260</b>
Figure 8.4: Scale of perceived effect of footplate height on rowing performance, relative to the rowers' traditional foot-stretcher set-up.....	<b>262</b>
Figure 8.5: Mean + SD of (a) RF at the catch and (b) RF at MHF at P1, P2, P3 and P4. * is a significant difference from P1 ( $P < 0.01$ ).....	<b>267</b>
Figure 8.6: Mean $\pm$ SD for seat force at (a) the catch, (b) MHF, and (c) the finish positions. Significant differences between footplate positions are given by square brackets. * $P < 0.01$ . ....	<b>269</b>

Figure 8.7: Mean  $\pm$  SD of (a) L5/S1 compressive force and (b) L5/S1 shear force with respect to footplate position. White, light grey, dark grey and black bars are P1, P2, P3 and P4 respectively. Significant differences between footplate positions are given by square brackets. #  $P < 0.05$ . .....**272**

Figure 8.8: Mean  $\pm$  SD of (a) ankle compressive force and (b) ankle shear force with respect to footplate position. White, light grey, dark grey and black bars are P1, P2, P3 and P4 respectively. Significant differences between footplate positions are given by square brackets. \*  $P < 0.01$ , #  $P < 0.05$ . .....**273**

# List of Tables

Table 1.1: Zones of exercise intensity. Adapted from McArthur (1997). .....	27
Table 3.1: Population details for elite, club and novice rowers in kinematic asymmetry study. Mean $\pm$ SD. ....	56
Table 3.2: Structure and description of the ergometer Step test.....	60
Table 3.3: Raw data output file from step test.....	61
Table 3.4: Bilaterally digitised anatomical landmarks made whilst the rower was seated on the rowing machine.....	63
Table 3.5: External performance measures at Steps 1-4 for all rowing groups (Mean $\pm$ SD). Maximum handle force (MHF), medio-lateral (ML). ....	71
Table 3.6: Hip and knee ROM, and ASI and pelvic twist in the three groups of rowers (Mean $\pm$ SD). ....	72
Table 3.7: Proportion of lumbar-pelvic flexion explained by kinematic asymmetries. .	75
Table 4.1: Summary of force transducer specifications. ....	96
Table 4.2: Experimental protocol for normal footplate calibration. ....	116
Table 4.3: Experimental protocol for AP footplate calibration .....	122
Table 4.4: Mean absolute error (MAE) values for right and left footplates. For <i>Normal</i> and <i>Shear</i> MAE is percentage of applied load. For <i>COP</i> , MAE is mean error in mm. ....	123
Table 5.1: Coefficient of multiple determination (CMD) values for bilaterally summed foot force traces, across all four rates and all three groups.....	142
Table 5.2: Coefficient of variance values (average $\pm$ SD) for foot force parameters for all three groups across all four rates. ....	143
Table 5.3: Asymmetry index values (average $\pm$ SD) for foot force parameters for all three groups across all four stroke rates. All values are % ASI.....	148
Table 6.1: Anatomical placement of FOB sensors. ....	168
Table 6.2: Anatomical landmarks digitized during static recordings. ....	169

Table 6.3: Headers of the raw output file consisting of force, length and kinematic data. .....	<b>172</b>
Table 6.4: Method of determining joint centre locations.....	<b>174</b>
Table 6.5: Kinematic variables that are significantly correlated with resultant foot force at MHF. Variables subsequently extracted by Stepwise Regression are highlighted in grey. ....	<b>184</b>
Table 6.6: Descriptive statistics of the multiple regression model's dependent variable (top) and predictor variables. ....	<b>185</b>
Table 6.7: Kinematic variables that are significantly correlated with RF at MHF. Variables subsequently extracted by Stepwise Regression are highlighted in grey. ....	<b>187</b>
Table 6.8: Descriptive statistics of the multiple regression model's dependent variable (top) and predictor variables. ....	<b>188</b>
Table 6.9: Aspects of foot force asymmetry that are significantly correlated with $\Delta L5/S1$ . Variables subsequently extracted by Stepwise Regression are highlighted in grey. ....	<b>190</b>
Table 6.10: Descriptive statistics of the multiple regression model's dependent variable (top) and predictor variables. ....	<b>191</b>
Table 6.11: Aspects of foot force asymmetry that are significantly correlated with ML drift. Variables subsequently extracted by Stepwise Regression are highlighted in grey. ....	<b>193</b>
Table 6.12: Descriptive statistics of the multiple regression model's dependent variable (top) and predictor variables. ....	<b>193</b>
Table 6.13: Aspects of foot force asymmetry that are significantly correlated with pelvic twist. Variables subsequently extracted by Stepwise Regression are highlighted in grey. ....	<b>194</b>
Table 6.14: Descriptive statistics of the multiple regression model's dependent variable (top) and predictor variables. ....	<b>195</b>
Table 6.15: Pearson's product moment correlation coefficients (R-value) between maximum handle force, resultant foot force at MHF and seat force at MHF .....	<b>196</b>
Table 6.16: Descriptive statistics of the multiple regression model's dependent variable (top) and predictor variables. ....	<b>196</b>
Table 7.1: Anthropometric measures from Zatsiorsky et al. (1990).....	<b>226</b>
Table 7.2: Kinetic, kinematic and performance parameters derived from the Step files. .....	<b>233</b>

Table 7.3: Three dimensional inter-segmental moment values (average $\pm$ SD) at key positions in the stroke are shown for Rate 18 and Free Rate. All values are in Nm/kg where kg is the rowers' body mass. * is where there is an overall significant difference ( $P<0.05$ ) for the parameters with respect to stroke rate. ....	<b>236</b>
Table 7.4: Three dimensional inter-segmental force values (average $\pm$ SD) at key positions in the stroke are shown for Rate 18 and Free Rate. All values are in Nm/kg where kg is the rowers' body mass. * is where there is an overall significant difference ( $P<0.05$ ) for the parameters with respect to stroke rate. ....	<b>237</b>
Table 8.1: Kinetic, kinematic, performance and asymmetry data derived from experimental trials at each footplate position. ....	<b>264</b>
Table 8.2: Descriptive data of rowing performance at each footplate position. ....	<b>265</b>
Table 8.3: Distribution of rower responses to perceived effect of P1-P4 on rowing performance. ....	<b>266</b>
Table 8.4: Mean power output, MHF and stroke length values (average $\pm$ SD) are shown for P1 – P4. ....	<b>268</b>
Table 8.5: Sagittal plane angles (average $\pm$ SD) at key positions in the stroke are shown for P1 – P4. All values are in degrees ( $^{\circ}$ ). $0^{\circ}$ is full joint extension; ankle dorsi-flexion, knee hyper-extension, hip flexion and L5/S1 flexion are negative. ....	<b>270</b>
Table 8.6: Sagittal plane joint moment values (average $\pm$ SD) at key positions in the stroke are shown for P1 – P4. All values are in Nm/kg where kg is the rowers' body mass. ....	<b>274</b>



# **Chapter 1:**

## **Introduction to Rowing**

Rowing is a sport in which the parameters of injury, performance and training are all intimately related and in dynamic equilibrium. Within the context of prior and current work in this field, the subject of this thesis is to investigate the interrelationships between these key parameters, whilst focusing on novel technological approaches to conduct studies into a previously less-considered variable. In particular, the effect of asymmetries on rowing.

Rowing is rapidly becoming one of Great Britain's most successful Olympic sports, with GB Rowing topping the rowing medal table at both the 2008 and 2012 Olympics games. In 2004 GB Rowing won four medals (one gold) at the games. This number increased to six (two golds) and nine (four golds) in 2008 and 2012 respectively. Along with the increased success of the sport, scientific interest surrounding the sport has also grown. Sports scientists strive to develop means of enhancing rowing performance, through investigations of optimal rowing technique (Bull and McGregor, 2000, Torres-Moreno et al., 2000, Soper and Hume, 2004, Strahan et al., 2011), efficiency and transfer of power from lower to upper limbs (Baudouin and Hawkins, 2002, Hofmijster et al., 2009, van Soest and Hofmijster, 2009), minimisation of injury risk (Stallard, 1980, Teitz et al., 2002, McGregor et al., 2007), and the use of biofeedback tools in training (Page and Hawkins, 2003, Loh et al., 2004, Fothergill, 2010). There are also numerous investigations into correlates of performance with key physiological characteristics (Fukunaga et al., 1986, Ingham et al., 2002, Smith, 2000), so that these traits can be developed to facilitate even greater success in future Olympic cycles.

## 1.1 Rowing: The basics

There are two distinct types of ‘on-water’ rowing. There is sweep rowing, where a single oar is handled by each member of the crew (crew size can be 2, 4 or 8). In sweep rowing there are *bow* side rowers, who place the blade of the oar to their left, and there are *stroke* side rowers, who place the blade of the oar to their right. The second category of on-water rowing is sculling, where each athlete handles two symmetrical blades (crew size can be 1, 2 or 4). In addition, athletes are categorised as heavy/open weight rowers, or lightweight rowers (men; individual < 72 kg, crew average < 70 kg, women; individual < 59 kg, crew average < 57 kg). Consequently, based on the rowers’ gender, boat size and preferred rowing style, it is possible to categorise their boat class, for example, men’s lightweight double sculls.

Olympic rowing races cover a distance of 2000 m, with the aim being to complete the race in the shortest time possible (ranging from under six minutes for larger male crews, to over seven minutes for lightweight females). Consequently, rowers require not only explosive power, which is essential for a dynamic sprint start, but also a high level of aerobic fitness to sustain them over 2000 m. The energy pathways utilised to complete a rowing race is approximately 75% aerobic energy and 25% anaerobic energy (Ingham et al., 2002), and this is reflected in their training which covers various intensities of rowing. This is described in detail below.

**Table 1.1: Zones of exercise intensity. Adapted from McArthur (1997).**

<b>Training Zone</b>	<b>Stroke rate (per min)</b>	<b>Heart rate (% max)</b>	<b>Work</b>
Utilisation Training 2 (UT2)	18-20	65-75%	60-90 min
Utilisation Training 1 (UT1)	22-24	75-85%	45-60 min
Aerobic Threshold	24-28	80-90%	2 x 20 min
Oxygen transport	28-36	90-100%	6 x 5 min
Anaerobic Threshold	max	max	15 strokes

A large proportion of training that occurs prior to the racing season is high volume, low intensity endurance work at UT1 and UT2, in order to develop baseline aerobic fitness. In addition to this high volume endurance training, muscle power and movement speed are trained at intensities corresponding to oxygen transport and anaerobic threshold, particularly as the race season approaches. These involve short bursts of 30 sec to 5 minutes of rowing where lactate accumulates in the muscles with the aim of improving anaerobic fitness. In addition to aerobic capacity and anaerobic fitness, effective rowing also requires good flexibility, core strength and muscle co-ordination (Thompson, 2005). Muscle co-ordination is particularly important as rowing is a cyclic activity which requires a precise, fluid technique to rapidly and efficiently accelerate the boat through a distance of 2000 m. Large forces must be transmitted to the oars to effectively propel the boat through the water. Power is generated by the quadriceps during the ‘drive phase’, and it is essential that this force is effectively transmitted through the rower’s trunk which acts as a link in the kinetic chain, both generating and transferring forces from the legs and arms to the oar (Caplan et al., 2010).

The above transmission of force from the lower to upper limbs is achieved through accurate sequencing of limb motion (Figure 1.1). Firstly, the legs initiate the drive through rapid extension of the knees, followed by a posterior lean of the torso to maintain power through the core, finally drawing the hands towards the body to finish the stroke (Nolte,

2004). The mechanical loading that occurs between the start of the stroke (i.e. catch) and the point of maximum handle force (MHF) will be referred to as the *critical* drive phase. Following MHF inertial forces limit the ability to apply high forces, therefore force production becomes dependent on maintaining a strong trunk posture. Opening up the body too early (i.e. posteriorly rotating the trunk prior to full leg extension thus taking the catch with the back rather than legs) would cause mechanical advantage to be lost and the rower becomes dependent on movement of their body mass to continue increasing velocity of the boat.

The recovery phase is essentially the opposite of the drive phase where the rower is in an extended finish position, and moves forward on the seat whilst rotating their torso anteriorly into a flexed catch position. The recovery phase is important, particularly on the water, for setting the rower up into a powerful position to generate high forces at the catch. Inability to execute the rowing stroke correctly or with poor technique affects efficiency of power transmission and consequent rowing performance (Hofmijster et al., 2008). In addition, poor technique is thought to be a major cause of chronic rowing injuries, particularly affecting the lumbar spine region (Bull and McGregor, 2000).

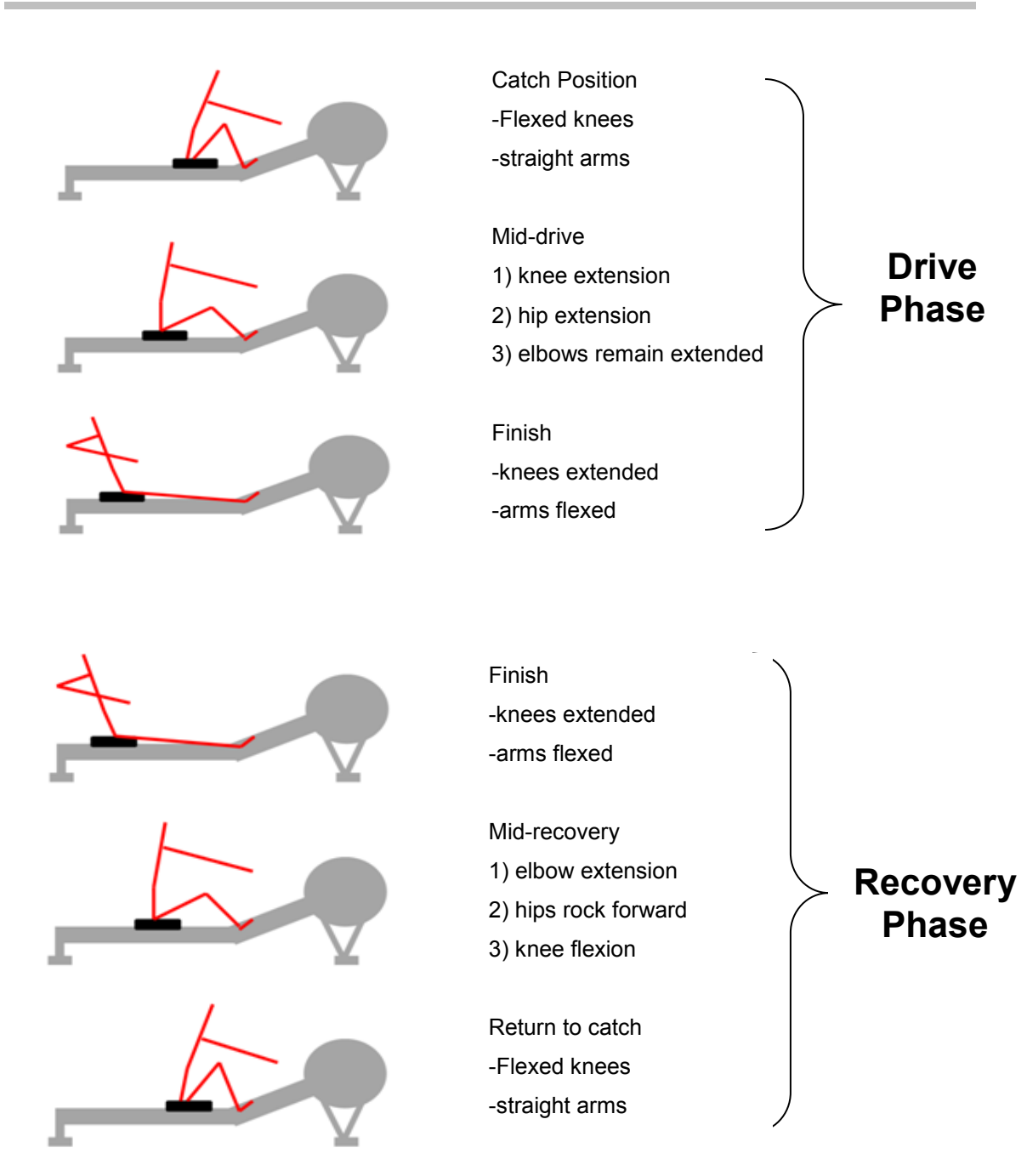


**Figure 1.1: Diagrams depicting the drive and recovery phases of the rowing stroke.**

## **1.2 Lower back pain in rowing**

Rowing is regarded as one of the most physically demanding endurance sports, imposing great challenges on the aerobic system and a large number of upper limb, lower limb and core muscle groups. Nevertheless, it is considered to be a safe, low impact sport with little risk of acute injuries (Hickey et al., 1997). However, elite rowers have been known to suffer from overuse injuries such as rib stress fractures, shoulder pain, wrist tenosynovitis, chronic knee pain, and most commonly lower back pain (LBP), which accounts for nearly a quarter of all rowing injuries (Karlson, 2000, Rumball et al., 2005).

In a sporting context the primary functions of the spine and its associated muscles and ligaments are to provide support and stability to the rest of the body's structures, transmit loads from the lower to upper extremities and to permit movement such as flexion, extension, rotation and lateral motion. The spinal column consists of seven cervical, twelve thoracic and five lumbar vertebrae, with the sacrum consisting of five and the coccyx three to five fused vertebrae (Figure 1.2). In daily living the most commonly injured locations of the spine are the L4/L5 and L5/S1 discs (Humphreys and Eck, 1999), owing to the large range of motion and compressive forces that occur there. For example, (Cholewicki et al., 1991) estimated compressive loads and moments at L4/L5 during heavy lifting to be 17,192 N and 988 Nm, respectively. It has also been noted that increased lumbar flexion is the most influential factor affecting compressive loads (Bono, 2004). As such, it is widely believed that LBP may be a result of accumulated loads from cyclic activities, in combination with repeated flexion and extension of the lumbar spine.

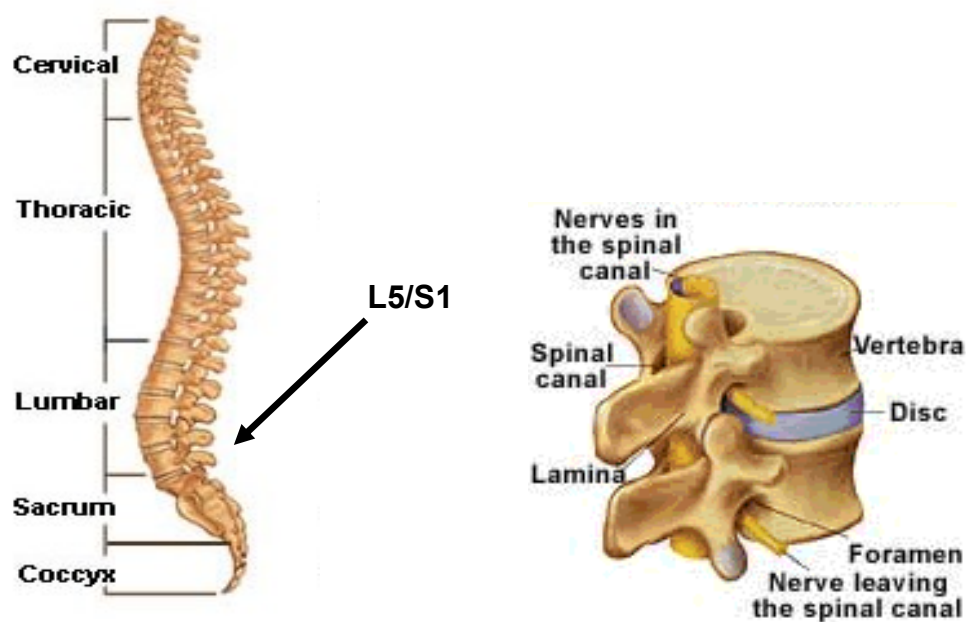


Figure 1.2: Side view of spinal column (left) and larger view of two vertebrae and intervertebral disc (right) (<http://www.spineuniverse.com/anatomy/lumbar-spine>).

The most common structural abnormalities associated with LBP in athletes are degenerative disc disease, sacroiliac joint dysfunction and spondylolysis (Bono, 2004, Rumball et al., 2005). There is a multitude of research showing that cyclic repetitive compression leads to vertebral fracture (Parkinson and Callaghan, 2007a, Parkinson and Callaghan, 2007b). Furthermore, loading whilst in a flexed posture results in a significantly lower tolerance to compression compared to a moderately flexed or neutral posture (Gallagher et al., 2005). In sporting tasks such as rowing or weightlifting, where LBP is also highly prevalent, the lumbar spine is exposed to excessive compressive loads whilst in a flexed position. During a rowing stroke the average compressive forces acting on the lumbar spine are nearly 4000 N for men and over 3000 N for women. In fact the peak loads estimated at the lumbar spine during a rowing stroke is >6000 N and >5000 N for men and women, respectively (Reid and Mcnair, 2000). In addition, rowers are in a flexed position for 70% of the stroke cycle, which

means that they are often transmitting large loads through their trunk whilst their back is in a flexed, vulnerable position (Reid and McNair, 2000). As well as flexion-extension motions, sweep rowing can also induce rotations about the vertical axis of the spine due to its asymmetrical nature. Axial torque/twist in combination with repetitive flexion-extension motion is thought to be a precursor for disc pathology (Farfan et al., 1970). Furthermore, it has been stated that combinations of flexion and twisting have an exacerbating role in the herniation mechanism of the vertebral disc (Gordon et al., 1991).

As mentioned previously, the trunk acts as a link in the kinetic chain during the rowing stroke transferring very large forces from the lower limbs to the upper limbs. Given the repetitive action of the rowing stroke, in combination with the large magnitude of the forces imposed upon the lumbar spine whilst it is flexing and also potentially rotating, there exists an amplified potential for the development of lower back injuries in rowers (Holt et al., 2003).

Due to this pertinent and debilitating problem of LBP in rowing, much of the biomechanics research in this field has focussed on quantifying the action of the lumbar-pelvic region and its subsequent effect on injury risk and performance. The research conducted in this area, focussing largely on the previous work conducted at Imperial College, will be described in the following chapter.



## **Chapter 2:**

### **Previous Research and Current Objectives**

This chapter contains a detailed history of the rowing biomechanics research undertaken at Imperial College. The review provides a summary of the development of an instrumented rowing system. It also outlines the experimental studies that have been conducted as a result of the on-going development of the system, focussing on lumbar-pelvic kinematics of the rower and their performance measures. The chapter ends by highlighting gaps in the group's research, which will clearly set the context and objectives for the developmental and experimental work undertaken in this thesis. This chapter reviews only the previous work undertaken at Imperial College in order to determine where advancements in the group's research must be made. However, future chapters will place the work of this thesis in the context of wider literature to highlight its relevance and novelty within the broad field of rowing biomechanics research.

#### **2.1 Rowing Research at Imperial College**

Imperial College and GB Rowing have been working in collaboration for the past 12 years. The main aim of this collaboration is to produce world leading research in the field of rowing biomechanics. Through kinematic measures at the lumbar-pelvic and lower limb joints/segments, in addition to performance related parameters such as stroke length, power and handle force, extensive research has been conducted into rowers' spinal kinematics with respect to performance. A further aim of this collaboration is to deliver effective and timely feedback to elite rowing squads, thus providing

biomechanical feedback on performance, movement and postural characteristics of their ergometer rowing technique.

### **2.1.1 System Development**

The experimental rowing set-up at Imperial College was instigated as a research tool for the measurement of lumbar spine and pelvis kinematics during indoor rowing. Using an electro-magnetic motion tracking system called the Flock of Birds (FOB), it was proposed that kinematics of the spine and pelvis could be recorded in real-time to enable rapid assessments of indoor rowing technique and posture. The FOB is a direct current (DC) system which simultaneously provides six degrees of freedom data (i.e. 3D position and orientation) of up to four sensors/receivers, with respect to a long range magnetic field transmitter (Figure 2.1). A DC electromagnetic tracking system was used because it reduces distortion of the field and thus errors imparted by eddy currents which can form in nearby metallic objects. Three position and three orientation values:  $x$ ,  $y$ ,  $z$  and  $z_{ang}$ ,  $y_{ang}$ ,  $x_{ang}$  respectively, are given for each receiver. The  $x,y,z$  values describe positions along each of the three axes making up a transmitter-fixed axis system. The  $z_{ang}$ ,  $y_{ang}$ ,  $x_{ang}$  values are euler angles that describe three successive rotations where the orientation of the transmitter will match the orientation of the receiver.

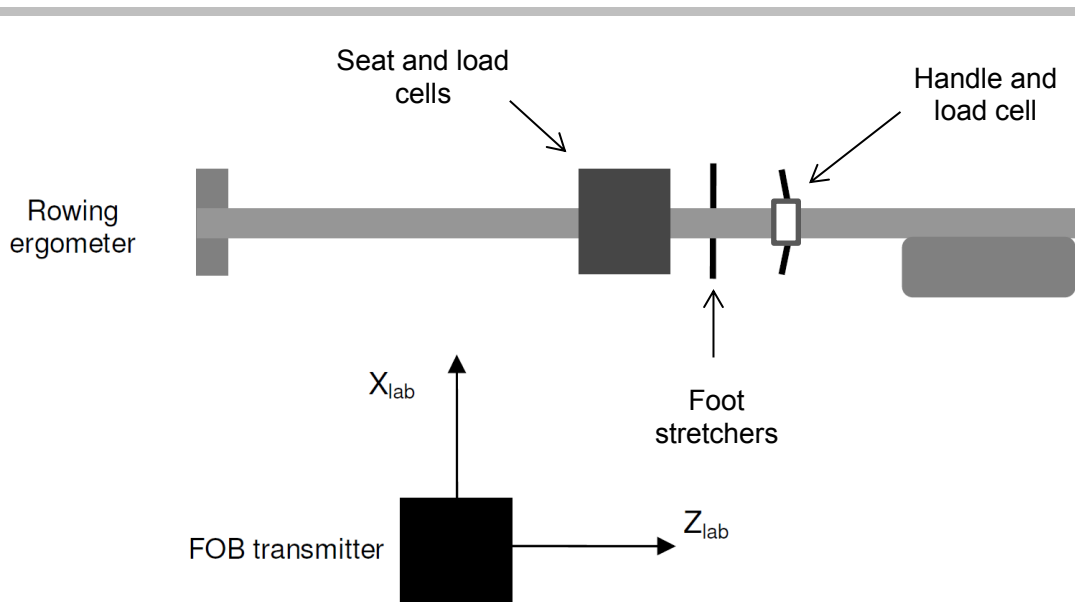


**Figure 2.1: Plan view of laboratory set-up showing the placement of the FOB transmitter in relation to the ergometer.**

At the centrepiece of the Imperial College measurement system is an indoor rowing machine (i.e. ergometer) as seen in Figure 2.1. Rowing on ergometers has become increasingly popular, allowing training to continue despite bad weather; enabling hands on training to be provided by coaches; with useful display of real-time feedback such as split projections (i.e. average time to complete 500 m) and power output made available to the athlete (Soper and Hume, 2004). Some differences between boat and ergometer dynamics have been noted (Ritchie, 2008), but kinematics during the rowing stroke have not been shown to significantly differ between the two conditions (Lamb, 1989, Elliott et al., 2002). Ergometers are often the basis of instrumentation for mechanical and biomechanical research studies (Hawkins, 2000, Page and Hawkins, 2003, Soper and Hume, 2004) because their indoor nature allows for a controlled surrounding environment which is conducive to the employment of further sensors and transducers as measurement tools during rowing data collection. In fact, much of the performance assessments that Great Britain's elite athletes undergo are done on ergometers, enabling

additional physiological, biomechanical and performance measures to be made. Therefore, it is important and relevant for biomechanical testing to be performed on ergometers (Lamb, 1989).

In its early stages (i.e. 1998-2001), a standard commercial Concept II (model D) rowing machine was utilised in conjunction with the FOB motion tracking system and a load cell at the handle to measure pulling force. Bull and McGregor (2000) initially used this set-up to examine whether FOB could effectively measure lumbar spine, pelvis and femoral orientation in the sagittal plane, and to see whether it would be sensitive enough to discriminate between various rowing styles. For example, 'shooting the slide' when the leg drive and posterior seat motion are disconnected from the force produced at the handle, or excess posterior lean at finish. The results showed significant differences in lumbar spine and pelvic orientations, as well as joint flexions between different rowing techniques. For example, the seat shoving technique showed a more upright pelvis and lumbar spine at the finish position, whilst others demonstrated greater anterior rotation. Fatigued rowing exhibited greater lumbar-pelvic flexion compared to non-fatigued abnormal techniques.

This study also recorded magnetic resonance images (MRI) of the rowers in their *catch* and *finish* positions, and found that the average error in the sagittal plane between the sensor orientation recording and the underlying vertebrae was  $\pm 1^\circ$ . This confirmed that FOB could be used to effectively and accurately measure spinal motion during ergometer rowing, with potential use as a bio-feedback tool for athletes and coaches. Furthermore, Steer et al. (2006) reported good repeatability of all kinematic parameters recorded during indoor rowing using the FOB set-up.

### **2.1.2 Experimental Research: lumbar-pelvic kinematics**

The experimentally validated FOB has been subsequently utilised for experimental studies which quantify lumbar spine and pelvis segment orientations of club level rowers, relative to the global vertical axis established by the transmitter (Figure 2.2). Holt et al. (2003) investigated spinal motion during one hour of low intensity rowing (stroke rate: 18-20 strokes per minute; heart rate 130-150 beats per minute) in 13 male club rowers, and found a marked increase in lumbar-pelvic range of motion during the stroke towards the end of the one hour piece. This was attributed to a compensatory increase in back extensor muscle activity to maintain force production in the face of trunk fatigue, and may have implications towards lower back injuries. However, when this protocol was performed by six elite female rowers, no significant changes in lumbar spine or pelvis kinematics were noted (Mackenzie et al., 2008), despite a non-significant 3° reduction in femoral extension at the finish of the stroke and a small reduction (approximately 10 N) in force output towards the end of the hour. The above studies suggest that elite rowers are better able to maintain their technique during an hour long training session compared to club rowers, although these studies were not powered for between cohort comparisons.

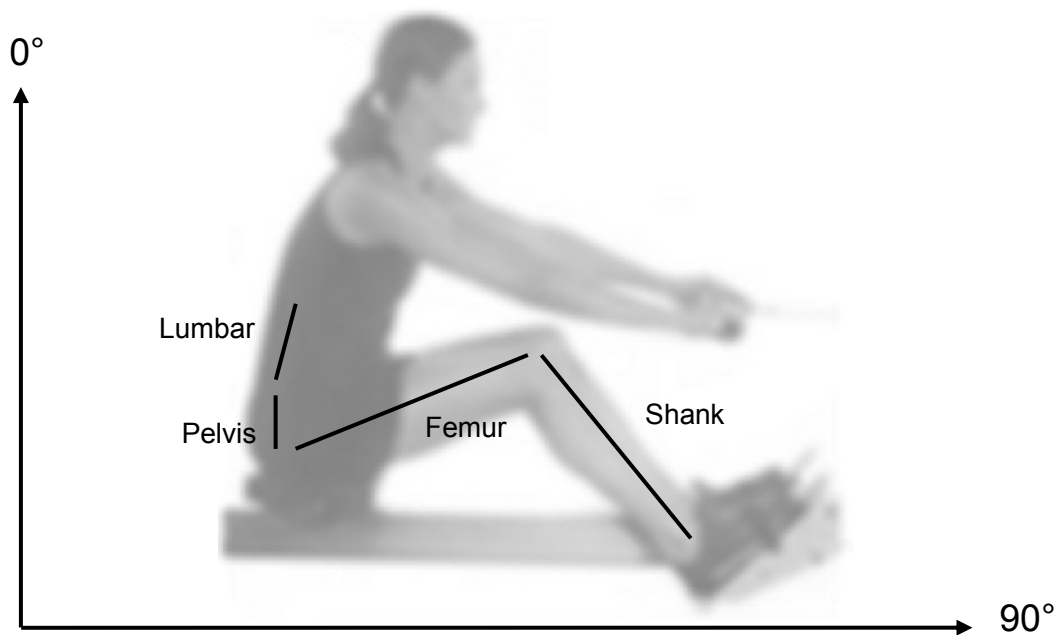


**Figure 2.2: Diagram depicting the sagittal plane orientations of body segments measured by the Flock of Birds.**

---

In addition to prolonged rowing, incremental training intensities have also been examined with respect to spinal kinematics (McGregor et al., 2004, McGregor et al., 2005). This is pertinent because rowers train at different intensities in order to target distinct adaptations for example, aerobic fitness and strong core and leg power. Consequently it is important to know how the kinematics of the spine differ with increasing levels of intensity, because the spine is an important link in the transfer of force generated during the leg drive and expressed at the handle. In a study by McGregor et al. (2004), ten club level rowers performed at three progressively higher intensities on an indoor rowing machine whilst instrumented with FOB sensors. Their results showed a progressive reduction in knee extension at the finish and a reduction in anterior pelvic and lumbar rotations at the catch of the stroke, which are common technical errors in rowing. Interestingly, there was also a trend towards peak handle force reduction at progressive intensities. When the same parameters were investigated in elite rowers, peak handle force was seen to increase with respect to intensity.

Furthermore, in elite rowers the changes in pelvic kinematics at higher intensities were non-significant (McGregor et al., 2005). Whilst greater lumbar rotation at the catch and reduced femoral extension was observed at the finish of the stroke, these parameters were not as notable as those seen in the club rowers in the study of McGregor et al. (2004). Therefore, the above comparison of club level and elite rowers demonstrated notable differences in their biomechanical response to increasing intensities of ergometer rowing.

An advantage of the research conducted at Imperial is that multiple groups of athletes are tested (e.g. lightweights, heavyweights, males and females) at different time points over successive seasons. McGregor et al. (2007) examined the same seven athletes on the ergometer at the same point in the season two years apart. The aim was to investigate longitudinal changes in rowing biomechanics as a result of two years of training. Improvements in ergometer performance included significant increases in handle force and stroke length. In terms of kinematics, the athletes demonstrated improved anterior pelvic and lumbar rotation at the catch and a greater consistency in the degree of pelvic extension achieved at the finish, at all successive intensities. Consequently, the data indicates that two years of training can significantly improve ergometer performance and technique, and the instrumented rowing machine and FOB are useful tools for monitoring athlete progress longitudinally.

The aforementioned study by McGregor et al. (2007) was conducted on a group of female rowers only, but there is evidence to suggest that males and females row differently, in terms of force production and in particular, their lumbar-pelvic motion (McGregor et al., 2008). This latter study compared a group of heavyweight female rowers and heavyweight male rowers whilst performing the same rowing protocol i.e.

incremental step test. Women were found to be less powerful, producing less handle force and mean power per stroke. However, they were better at optimising their technique through achieving a significantly greater anterior rotation of the pelvis at the catch position (by more than  $7^\circ$  compared to males) and minimising flexion at the lumbar-pelvic joint, resulting in a superior lumbar-pelvic ratio. There were no gender differences in lumbar rotation at the catch, which indicated that males had a poorer posture as characterised by greater lumbar-pelvic flexion, given their lack of anterior pelvic rotation. This study confirmed that males and females row differently in terms of power output and optimisation of technique. Therefore, despite normalising to body weight and height, differences in technique and performance parameters may persist and should be considered when investigating a mixed group of male and female rowers.

Research from Imperial College shows that the FOB motion capture system can be used to accurately record human motion during indoor rowing. Based on lumbar-pelvic kinematics, it has the capacity to discriminate between different styles of rowing (Bull and McGregor, 2000), fatigue in less experienced rowers (Holt et al., 2003), various intensities (McGregor et al., 2004), longitudinal changes (McGregor et al., 2007) and gender differences (McGregor et al., 2008). However, these studies focus largely on the lumbar-pelvic region and report just two-dimensional data in the sagittal plane. Subsequent work has seen further development of the system in terms of instrumentation of the ergometer and kinematic measurement techniques, in order to achieve a greater biomechanical understanding of the rowing stroke.



### **2.1.3 Further system developments: instrumentation and three dimensional kinematics**

Through kinematic measures at the lumbar-pelvic and lower limb joints, and performance related parameters such as stroke length, power and handle force, Imperial College has conducted extensive research into rowers' spinal kinematics with respect to performance, fatigue, trunk strength and rowing intensity. More recently, through development of novel instrumentation at the ergometer seat and expansion of motion analysis capabilities (Loh et al., 2004), measurements have been extended to 3D kinematics of the lumbar spine and lower limbs, as well as resultant force and centre of pressure parameters at the seat (Murphy et al., 2010). This has allowed for a more complete assessment of elite rowers' technique and performance, where specific aspects of rowing technique could be used to predict rowing performance and potential injury risk (Murphy, 2009).

As described in the previous section, the FOB has been used extensively to assess motion of the lumbar spine, pelvis and femoral segments in the sagittal plane. However, FOB has the capacity to measure six degrees of freedom, thus quantify 3D motion. Bull et al. (2004) assessed the accuracy of out of plane rotations of externally fixed sensors against MRI measurements of the spine and noted an average error in ab/adduction rotations of  $5.0^\circ$  and an average error of  $4.4^\circ$  for rotations about the vertical axis. This out of plane accuracy, combined with accuracy of sagittal plane rotations of  $\pm 1^\circ$  and translational errors of  $< 2$  mm, suggests that externally fixed FOB sensors can be used to quantify deviations from ideal rowing technique in 3D. Further to this, it was necessary to carry out a sensitivity analysis of the FOB kinematic model used to derive joint angles. How the output variables of a model responds to changes in their input

parameters are an important part of the development and evaluation phase, and tells the user how much confidence should be placed in the results (Robertson, 2004). For example, Chaffin and Erig (1991) found that predictions of static strength were extremely sensitive to errors in postural kinematic inputs, but less sensitive to errors in anthropometric inputs, when values for stature, body weight and postural angles were systemically changed. In addition, an inverse dynamics model of vertical jumping was shown to be particularly sensitive to simulated changes in joint centre positions. For example, when joint centre positions were moved an equivalent of 10% of their proximal segment length, the model output (i.e. total work) demonstrated errors of up to 28% (Nagano et al., 2000). In the case of this study, the inputs to the kinematic model are 3D translations and 3D rotations of the FOB sensors. The measurement errors of these sensors are noted above, and a sensitivity analysis of the kinematic model showed lumbar-pelvic sagittal plane angles to have greatest robustness, and sagittal plane ankle angles to have greatest sensitivity to changes in input parameters (Appendix A). This is important to note, so that subsequent results are interpreted with caution.

Subsequently, a detailed 3D kinematic analysis of the foot, shank, thigh and lower back, in combination with kinetic outputs from the rowing machine, was undertaken and related to performance measures, external kinetics and injury mechanisms (Murphy, 2009). Statistical modelling was performed on the data to determine which measured variables are useful in predicting performance, and the discrete aspects of technique that could positively influence these predictors. It was postulated that there were five main predictors of good rowing performance:

1. Finish occurring later in the stroke
2. Rapid rate of handle force production

3. Long stroke length
4. Large power output
5. Suspension of body weight away from seat (quality of seat suspension)

Furthermore, the above could be positively influenced when the rower exhibits the following characteristics in the technique:

1. Minimal flexion of the lumbar-pelvic joint (L5/S1) at the catch position
2. Minimal flexion of L5/S1 at max handle force (i.e. lumbar-pelvic posture from catch maintained)
3. Minimal flexion of L5/S1 at the finish.
4. Large knee flexion at the catch position (i.e. good knee compression)
5. Inferior ankle joint centre at the finish position (i.e. heels down at finish)
6. Superior ankle joint centre at the catch position (i.e. heels up at catch)

The data suggests that high level performance can be predicted by monitoring discrete aspects of elite rowing technique. Interestingly, these detailed 3D analyses showed only kinematics in the sagittal plane were important in influencing high level performance. Developments to the rowing machine and motion capture techniques provide useful tools for collecting data that describe rower kinematics and external forces. This would further enable the effects of factors such as exercise intensity, fatigue, and longitudinal training to be observed in order to predict athletic performance and injury risk.

## 2.2 Development of Study Aims

The previous sections in this chapter outlined the developments that had been made to the instrumented rowing machine and motion analysis techniques. However, the data acquisition system for testing elite rowers' is restricted to measuring the kinematics of the lumbar spine and pelvis segments, and the right side of the lower extremity only, thus assuming perfect symmetry of the lower limbs. Theoretically rowing is a symmetrical activity, but it has recently been suggested that bilateral differences exist between the lower limbs (Baca et al., 2006a, Hislop, 2008, Janshen et al., 2009). Therefore it is necessary to investigate kinematic asymmetries of the lower limbs through an adaptation of the current unilateral motion capture set-up. Furthermore, there is need for development of instrumented foot-stretchers. Imperial's ergometer system measures contact forces at the handle to give peak force outputs, and at the seat, to give centre of pressure and quality of suspension values. However, no instrumentation has been developed for the foot-stretchers. There has been a limited number of studies which describe the development of instrumented foot-stretchers with regards to the magnitude and bilateral differences in forces that are produced (Macfarlane et al., 1997, Pudlo et al., 2005, Colloud et al., 2006, Baca et al., 2006a). These will be discussed in greater detail in subsequent chapters. However, no study has yet scrutinised the foot force of multiple groups of elite rowers over numerous testing sessions, particularly where the focus has been on investigating force production asymmetries.

The development of bilaterally instrumented footplates would provide a measure of peak pressures applied to the foot-stretchers, vertical and horizontal foot force components and leg drive asymmetry. Furthermore, this paves the way for the

development of an inverse dynamics model, where foot force data can be combined with kinematic data from the FOB (and anthropometric values) to enable joint forces and moments to be quantified. Again, there have been limited investigations of joint loading during rowing, with none evaluating the pelvis and lumbar spine as separate segments (Hase et al., 2004, Cerne et al., 2011). As such, there is a major gap in rowing biomechanics research where the magnitude of loads which span the lower limb and particularly lumbar-pelvic joints are not accurately known. These measures would provide useful quantitative information pertaining to performance potential and injury risk during rowing, especially as the lumbar spine is thought to endure repeated high loads whilst undergoing notable ranges of motion (Reid and McNair, 2000). As a consequence of the hardware developments and progress in modelling that are to be made, this project will provide insights into the pattern of bilateral rowing technique through measurements of lower limb force production, and detail the mechanisms by which asymmetrical rowing affects spinal kinematics and joint loading.

### **2.2.1 Specific Study Aims**

To structure the research studies contained within this thesis, five main research aims were developed:

1. Investigate kinematic asymmetries of the lower limbs through an adaptation of the current unilateral motion capture set-up.
2. Develop instrumented footplates which enable foot force asymmetries and magnitudes to be quantified.
3. Examine the influence of newly acquired foot forces and asymmetries on previously established predictors of performance and technique.

4. Develop and implement an inter-segmental model of the lower limb and lumbar-pelvic joints to quantify joint forces and moments.
5. Examine the effect of raising foot-stretcher height on discrete aspects of performance and technique.

### **2.3 Structure of Thesis**

The format of this thesis will be such that all studies are presented as a standalone chapter (Chapters 3-8; Figure 2.3) with its own introduction, literature review, methods, results, discussion and reference list. **Chapter 1** was a general introduction to rowing to familiarise the reader with concepts and terminology that will be frequently used throughout this thesis. **Chapter 2** provided a detailed literature on the work previously accomplished at Imperial College, and identified research themes which this thesis aims to cover. Following this chapter, there will be a further seven chapters, for which the layout and contents are described below:

**Chapter 3:** The traditional unilateral motion capture set-up is adapted so that bilateral kinematics of the lower-limbs and lumbar-pelvic segments can be recorded. It aims to look at the influence of hip and knee joint asymmetries on the quality of lumbar-pelvic kinematics in groups of rowers with varying degrees of experience.

**Chapter 4:** Contains a detailed description of the development of bilateral force measuring footplates, including; design, instrumentation and calibration.

**Chapter 5:** Footplates developed in Chapter 4 are tested in a laboratory environment. Reliability of foot force traces, magnitudes of peak force and bilateral foot force asymmetries are investigated in three groups of elite rowers.

**Chapter 6:** Footplate data acquisition is synchronised with kinematics and other external force data. Elite rowing performance during an incremental step test is statistically modelled to examine the influence of foot force magnitude and asymmetries on previously identified markers of good performance and technique.

**Chapter 7:** A five segment inverse dynamic model is developed, so that inter-segmental forces and moments of the ankle, knee, hip and lumbar-pelvic joints can be estimated during ergometer rowing. Elite rowers' data recorded during incremental step tests are presented, and the implication of high intensity rowing on joint kinetics is discussed.

**Chapter 8:** The effect of changing foot-stretcher height on rowing technique and performance is investigated in a group of high-level male rowers. Changes in vector orientation of foot force, joint dynamics and various performance parameters are examined with respect to raised height of the foot-stretchers, relative to the seat.

**Chapter 9:** An overall discussion and summary of work done and suggestion for future research.

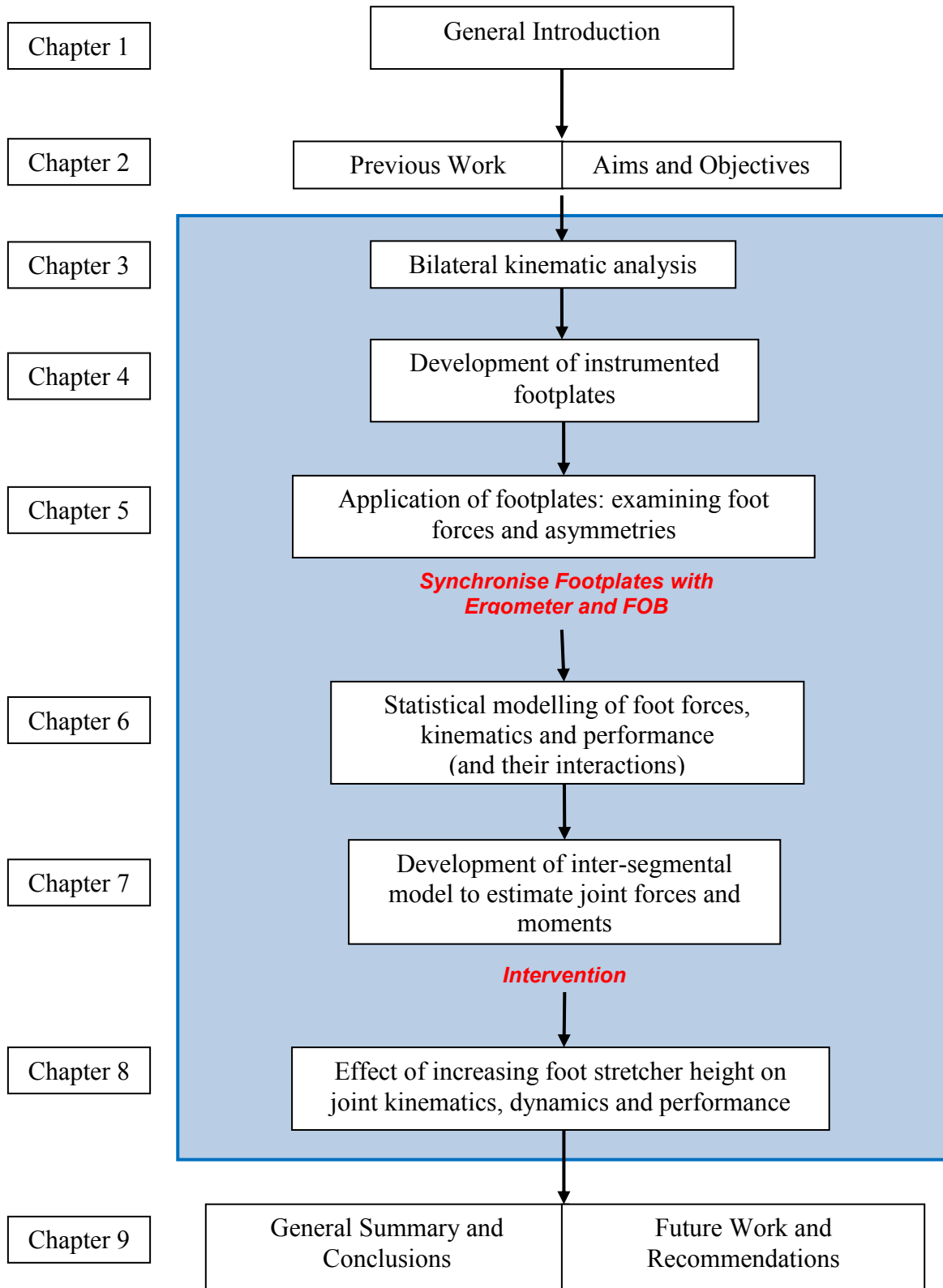


Figure 2.3: Layout of the thesis with blue boxed section representing chapters containing developmental and experimental studies.



## **Chapter 3:**

# **Lower Limb Kinematic Asymmetries in Elite, Club and Novice Rowers**

In Chapter 2 it was shown that a system now exists whereby measures of handle force, seat force and stroke length (Chee, 2006, Murphy et al., 2010), as well as 3D kinematics of rowers' lumbar-pelvic and lower limb joints (Murphy, 2009), could be made. This enabled robust, real-time measures and detailed biomechanical feedback of rowing technique and performance to be given to athletes and coaches. The goal of this chapter is to adapt the traditional motion capture set-up and develop a bilateral kinematic model, in order to quantify bilateral lower limb joint kinematics. This will be used to identify potential lower limb asymmetries during the rowing stroke and their possible impact on lumbar-pelvic kinematics.

### **3.1 Introduction**

#### **3.1.1 Kinematic investigations of the rowing stroke**

Kinematics describes the motion of points, bodies or systems, without consideration of the forces and moments that cause the motion. These can include; 3D joint angles, joint positions, segment velocities and segment orientations, all of which are fundamental for the analysis of human movement. An important consideration in sports biomechanics is ascertaining the way in which an athlete moves, in order to determine the quality of their technique. This is especially pertinent in a 'closed chain' activity such as rowing,

where the movement pattern can be predicted, and thus, optimal technique can be honed during training. Therefore, studying the kinematics of a rower is essential in terms of identifying aspects of technique that are lacking or being performed incorrectly, and to enable refinements of the skill which will improve athlete performance, whilst minimising risk of injury.

Numerous studies have focussed on kinematics of the lower limbs and trunk during rowing. Elliott et al. (2002) employed simple 2D video analysis to digitise the shoulder (acromion process), hip (greater trochanter), knee (lateral epicondyle) and ankle (lateral malleolus) in order to quantify trunk, thigh and shank orientations, as well as knee angle in the sagittal plane. They found similarities in kinematics at different stroke rates, and between ergometer and on-water rowing. Using optical motion tracking, Caplan & Gardner (2010) examined knee and hip angles, as well as trunk and shank orientation at several points during the rowing stroke. They investigated the effect of increasing foot-stretcher height on 2D rower kinematics, and found that as foot-stretcher height was increased; greater hip flexion at the catch, greater knee extension during mid-drive and mid-recovery, and greater posterior trunk orientation at the catch, finish and mid-recovery, was evident. This information not only gives insight into rowers' movement patterns, but demonstrates how they respond to changes in their ergometer set-up, thus informing coaches how to setup a rower for optimal performance output. A similar motion capture technique was employed by Pollock et al. (2009) who also used optical tracking to capture kinematic data of the spine, pelvis and lower limbs, in order to calculate 2D joint angles and trunk and lumbar segment orientations, to investigate co-ordination of segment rotations during a 2000 m ergometer test. Page and Hawkins (2003) and Panjkota et al. (2009) have both also both developed methods to analyse 2D

kinematics of rowers' trunk and lower limbs, largely for the purpose of individual performance feedback.

As mentioned in Chapter 2, 2D and 3D analysis of lumbar-pelvic and right lower limb kinematics had been performed by Bull & McGregor (2000) and Murphy (2009), respectively. Two-dimensional analysis yielded information regarding the ability to discriminate between good and poor technique (Bull and McGregor, 2000), fatigue during prolonged rowing (Holt et al., 2003), high intensity rowing (McGregor et al., 2004), influence of longitudinal training (McGregor et al., 2007) and gender differences (McGregor et al., 2008), by quantifying lumbar-pelvic kinematics of rowers. Murphy (2009) further developed the system by Bull & McGregor (2000) to enable rower kinematics to be obtained in 3D. Three-dimensional analysis elucidated that the kinematic variables which were associated with good performance include; superior displacement of the heels at the catch (heels up), inferior displacement of the heels at the finish (heels down), and increased compression of the knee at the catch (vertical shins). Furthermore, kyphosis of the lumbar-pelvic region at any point in the rowing stroke was found to be detrimental to rowing performance, whilst increasing the risk of attaining lower back injuries. This latter point is endorsed by Strahan et al. (2011) who found that electromagnetic motion analysis of the spine and pelvis during ergometer rowing exhibited large lumbar-pelvic flexions at the catch beyond 85% of its maximum range of motion (ROM), where the pelvis was posteriorly rotated, and the lumbar spine was flexed. Loading the spine while it is near end range flexion increases the risk of lower back injuries because this increases the loading of the passive spinal structures (Caldwell et al., 2003). Excessive degrees of lumbar flexion can result in sprained ligamentous structures, and in combination with large compressive forces, which are prevalent in rowing, can induce damage to intervertebral discs (Adams and Dolan,

1995). Consequently, kinematic analysis of rowing technique can be extremely useful in providing feedback to coaches and athletes, regarding technique and risk of injury development.

### **3.1.2 Asymmetries and Lower Back Pain**

There is a wealth of research that examines rowing kinematics with respect to performance and injury, with particular focus on the trunk and pelvis (Bull and McGregor, 2000, Mackenzie et al., 2008, Strahan et al., 2011). With regards to lower limb asymmetries, a study by Janshen et al. (2009) found some bilateral differences in leg muscle activation and foot pressure. Overall, there is a distinct lack of research into bilateral leg kinematics and their asymmetries, and their interaction with spinal kinematics. Although rowing is mainly a sagittal plane activity it may be incorrect to assume that the left and right sides of the body perform symmetrically, particularly due to medio-lateral drift (ML drift) that has been identified on the seat during the rowing stroke (Murphy, 2009). A key contributor of centre of pressure (COP) motion at the seat is the drive through the legs. Asymmetrical loading through the footplates may result in compensatory rotations of the lower limb and pelvis, thus resulting in ML drift on the seat during the drive phase. Therefore, an important parameter to investigate would be asymmetry of the lower limbs, and its potential impact on ML seat motion and subsequent kinematics during the rowing stroke. If an interaction between asymmetries and lumbar-pelvic kinematics are identified it may perhaps be possible to make simple measures of lower limb ROM asymmetries and infer the possibility of attaining lower back injuries.

Although it has not been directly investigated in the rowing population, asymmetries of the lower limbs and pelvis have been linked with lower back pain and altered trunk motions (Al-Eisa et al., 2006b). It is supposed that when pelvic asymmetries are present, this alters body mechanics and puts various body segments under strain, thus contributing to musculoskeletal pain (Al-Eisa et al., 2004b). For example, asymmetries in lifting movements cause compensatory pelvic rotations about the transverse plane and trunk co-contractions, which may explain an increased risk of low back disorders (Kingma et al., 1998). Furthermore, asymmetrical lifting has been found to significantly increase spinal loading in those with low back pain, compared to those without (Marras et al., 2004), thus further emphasising a possible link between asymmetrical kinematics and low back pain.

It is clear that in functional tasks, where asymmetries exist at the lower limbs or pelvis, there are associations with altered trunk mechanics and thus low back pain (Lund et al., 2002, Al-Eisa et al., 2006b, Marras et al., 2004). Despite rowing being performed in a seated position with body weight supported, (Al-Eisa et al., 2006a) gave evidence to suggest that pelvic asymmetry can also affect the dynamics of trunk motion whilst sitting, thus putting the lumbar spine under greater stress. They showed that the link between pelvic asymmetry and asymmetric trunk motion was maintained in a seated position, as pelvic asymmetry was significant in predicting lateral flexion and axial rotation asymmetries whilst seated. Therefore, lower limb asymmetries could be a potential cause of increased lumbar loading and sub-optimal kinematics at the lumbar-pelvic joint in a seated, high loading activity such as rowing. Asymmetries in lower limb joint angles and angular extension velocities may result in twisting of the pelvis with respect to the seat, which may in turn produce ML drift on the seat in addition to its sagittal plane motion during the drive and recovery phases.

### **3.1.3 Lower limb asymmetries in rowing**

Sculling and sweep rowing require different trunk and upper limb kinematics due to the asymmetrical nature of sweep rowing, which requires the rower to rotate their trunk, causing the upper limbs to follow an asymmetrical arced trajectory. Additionally, there are some differences in lower limb kinematics where scullers' legs move in parallel whereas a sweep rower's outside leg (leg opposite oar) is positioned more laterally than the inside leg (Herberger, 1987). As described in Section 3.1.1, many studies have investigated kinematics of the rowing stroke (Torres-Moreno et al., 2000, Holt et al., 2003, Page and Hawkins, 2003, Pollock et al., 2009). However, concurrent measures of bilateral leg kinematics are rare, with measurements often being made on one side of the body (Bull and McGregor, 2000), or combining joint angles for the left and right side of the body to give a mean angle for each joint (Caplan and Gardner, 2010). Using 2D video cameras pointing towards the right and left sides of the rower with reflective markers fixed to bony landmarks, sagittal plane angles between hips, knees and ankles were found to exhibit similar ROM in a small group of seven national rowers (Janshen et al., 2009). However, it may be incorrect to assume that the left and right sides of the body perform symmetrically, particularly in novice and club level rowers with lesser technical experience than elite rowers. The rowing stroke is similar to a lifting task where it is advocated to lift with symmetrical co-ordinated movements in order to minimise torsional loading and thus lower back disorders (Kingma et al., 1998). Consequently, executing the rowing stroke with asymmetrical lower limb motion may result in compensatory pelvic motions and co-contractions of muscles such as the transverses abdominis and erector spinae, in order to keep the trunk stabilised, thus influencing the action of the spine. Past work has shown that rowing technique

deteriorates at progressively higher work rates by demonstrating an increase in lumbar-pelvic flexion (McGregor et al., 2004), which in itself has been shown to be an important risk factor for rowing injuries (Murphy, 2009).

The aims of this study were to examine lower limb kinematic asymmetries and their consequent impact on lumbar-pelvic kinematics, during varying intensities of ergometer rowing, and between rowers of varying standards. It was hypothesised that ergometer rowing would be symmetrical with respect to motion of the legs, and that deviations from this symmetry would result from rowing experience (i.e. novice, club, elite), work rate, or stroke position (i.e. catch, maximum handle force, finish, recovery).

## **3.2 Methodology**

### **3.2.1 Participants**

The study received ethical approval from the Imperial College Research Ethics Committee, and informed consent was obtained from all subjects (Appendix B). Twenty two male rowers were recruited into this study from local rowing clubs in London. Of these, 6 were novice rowers, 8 were club level rowers, and 8 were elite rowers. Group classification criteria are outlined in Table 3.1. The sample size was deemed large enough for a moderate effect size of 0.5 and statistical power of 95% with an alpha significance level of 0.05. Subjects with a leg difference of more than 1 cm were excluded from this study because anatomical asymmetries may influence the results of this study. Additionally, rowers with a current episode of low back pain or any other serious illness or injury were excluded from participation in this study.

**Table 3.1: Population details for elite, club and novice rowers in kinematic asymmetry study. Mean  $\pm$  SD.**

<b>Group</b>	<b>N=</b>	<b>Age (years)</b>	<b>Mass (kg)</b>	<b>Height (cm)</b>	<b>Experience</b>	<b>2 km personal best (min:sec)</b>
Elite	8	24.6 $\pm$ 4.5	87.9 $\pm$ 10.5	189.9 $\pm$ 8.5	> 3 years *	6:05 $\pm$ 0.11
Club	8	21.3 $\pm$ 1.5	80.8 $\pm$ 8.6	184.4 $\pm$ 6.8	> 1 year	6:28 $\pm$ 0.08
Novice	6	20.8 $\pm$ 3.1	84.4 $\pm$ 6.4	186.0 $\pm$ 7.6	$\leq$ 0.5 year	6:38 $\pm$ 0.14

\*Rowed in a World Rowing Championship

### **3.2.2 Instrumented ergometer and motion capture**

All rowers performed their trials on a modified Concept II model D ergometer (Figure 3.1). The ergometer was instrumented at the handle with a uniaxial load cell (ELHS model, Entran, Lexington, Kentucky, USA) to measure pulling force on the handle (2.5 kN range, 0.5% combined non-linearity and hysteresis). The flywheel was instrumented with a linear encoder with 5000 increments per revolution (ERN120, Heidenhain Ltd., Traunreut, Germany) to enable measurements of stroke length. The seat was instrumented with four uniaxial load cells (ELPM model, Entran, Lexington, Kentucky, USA) to measure COP and vertical forces on the seat (1.25 kN range,  $\pm$ 0.15% hysteresis, 0.15% non-linearity) (Murphy et al., 2010). Signals from the instrumented rowing machine were hardware synchronised and connected to a PC through a multi-channel signal conditioning unit (SC-2345, National Instruments, Austin, Texas, USA).



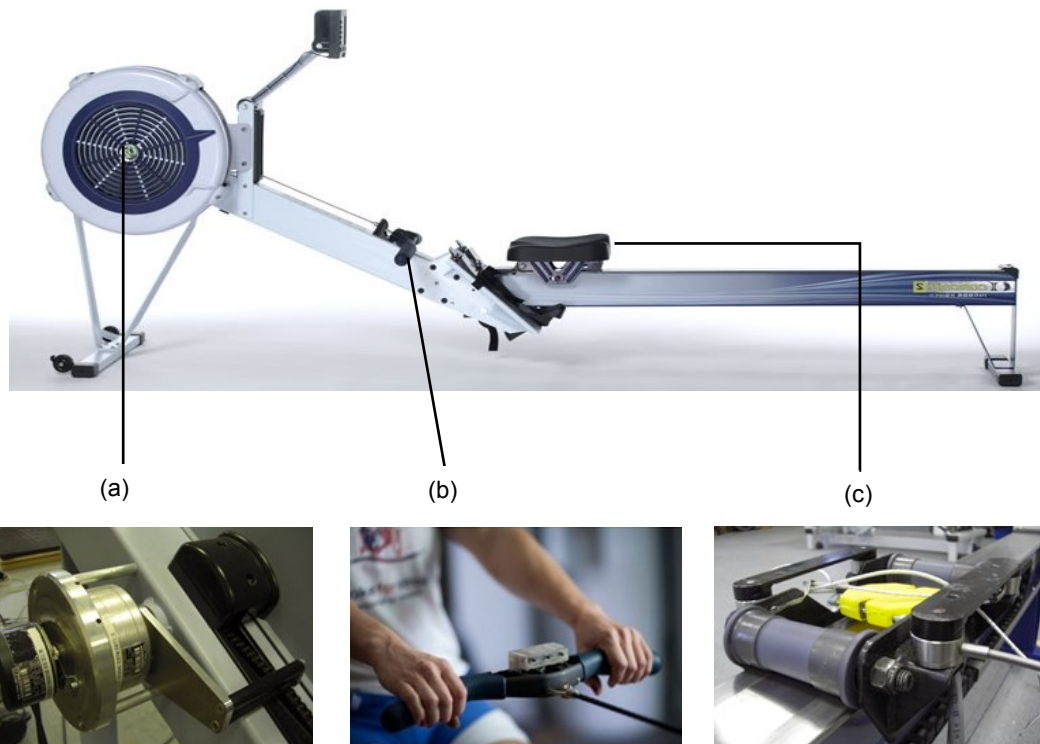


**Figure 3.1: Instrumentation of the Concept II ergometer at the flywheel (a), handle (b), and seat (c).**

---

Rower kinematics were recorded using the FOB motion capture system (Ascension Technology, Burlington, USA). The system consists of an extended range electromagnetic transmitter, situated at a location that would optimise measurement accuracy (Murphy et al., 2011), and four receivers (S1 – S4) whose three dimensional (3D) translations ( $x$ ,  $y$ ,  $z$ ) and rotations ( $\alpha$ ,  $\beta$ ,  $\gamma$ ) could be quantified within the electromagnetic field. Previous work has validated this system's suitability for measuring spinal and lower limb motion (Bull et al., 1998, Bull and McGregor, 2000, Bull et al., 2004, Murphy, 2009).

### 3.2.3 Subject preparation and digitisation

The lumbar FOB sensor (S3) was placed at the thoraco-lumbar junction (T12/L1), the pelvic sensor (S2) was attached to the lumbar-pelvic junction (L5/S1) and the remaining two sensors were attached to the anterior tibial spine at a point midway between the knee and ankle on the right (S4) and left (S1) legs (Figure 3.2). Adhesive pads (PALstickies™, PAL Technologies Ltd, Scotland) were used to secure the sensors to skin.

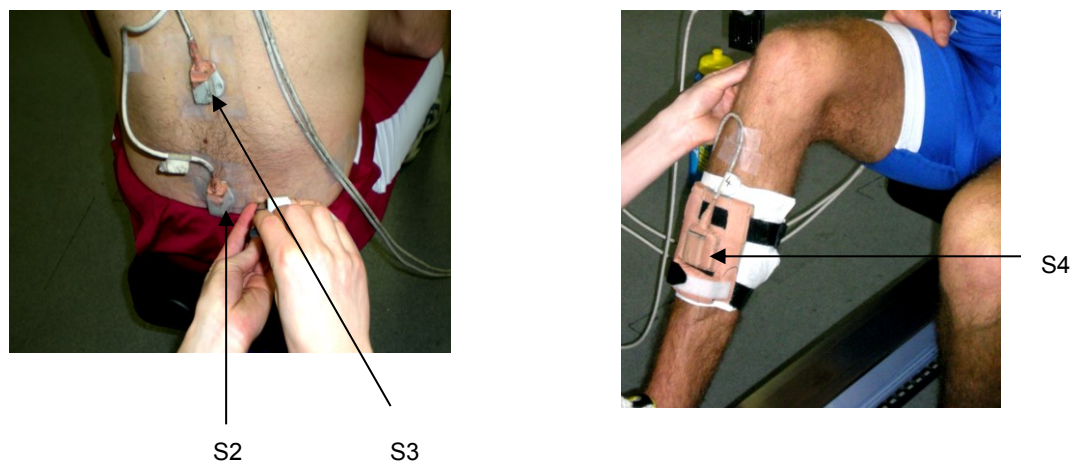


**Figure 3.2: Location of FOB Sensor 2 and Sensor 3 during athlete testing. Sensor 1 was attached bilaterally symmetrically to Sensor 4.**

Prior to recording, multiple bony landmarks were digitised by attaching S3 to a digitisation stylus. Whilst the rower was seated on the ergometer, the tip of the digitisation stylus was placed on the landmark of interest and rotated about that point in order to create a cloud of 3D position data. A sphere fitting procedure was then used to work out the 3D vector offset of that point relative to the sensors already attached to the body segments, so that the trajectories of the landmarks could be tracked at all points during the rowing stroke.

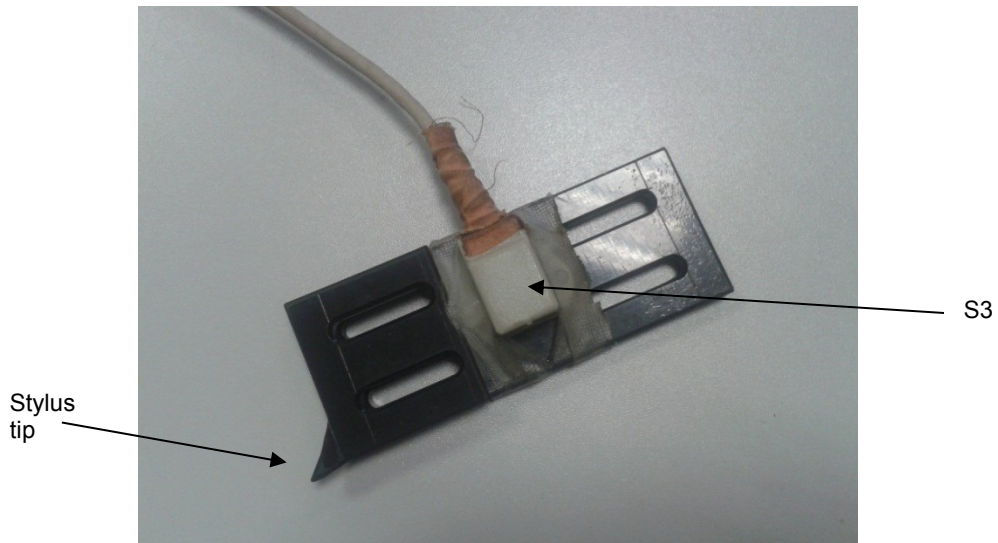


**Figure 3.3:** The digitisation stylus with Sensor 3 attached for the purposes of anatomical landmark digitisation.

---

The hip joint centre was determined through a functional test. This involved strapping the S3 digitising stylus to the subject's thigh, and in a standing position, the subject rotated their thigh to capture their full range of motion about the hip, enabling a sphere fitting procedure to find the centre of rotation. The 3D vector offsets of anatomical landmarks are entered into a kinematic model to enable dynamic tracking of joint centres and calculations of joint angles during the rowing trials, as described in Section 3.2.6.

### **3.2.4 Experimental protocol**

Each subject performed a 10 minute warm up on the ergometer prior to testing. They then performed the following step test with at least a 5 minute rest period between steps:

**Table 3.2: Structure and description of the ergometer Step test**

<b>Step</b>	<b>Rate</b>	<b>Description</b>	<b>Duration</b>
1	18 strokes per minute	Pace consistent with the athletes' standard utilisation training 2 pace (where athletes aim to keep their heart rate between 130-150 beats per minute).	4 minutes
2	20 strokes per minute	Pace consistent with the athlete's personal best score for 30 minutes at rate 20.	4 minutes
3	Race Pace	500 m at a pace consistent with the athlete's personal best 2000 m pace.	500 m
4	Maximum Effort	Maximal rate and power output.	30 strokes

### **3.2.5 Data acquisition**

Custom software was written in Labview (Version 7.1, National Instruments, Austin, Texas, USA) to initialise and synchronise the signals from the instrumented rowing machine and FOB, to acquire measurement data from all sensors at a rate of 75 Hz, and write the data to an ASCII file. The raw output file consisted of the following arrays of data in Table 3.3.

**Table 3.3: Raw data output file from step test**

<b>Column Number</b>	<b>Measured Parameter</b>	<b>Column Number</b>	<b>Measured Parameter</b>
1	Handle Force	23	S2 $\beta$ angle
2	Chain Length	24	S2 $\gamma$ angle
3	Chain Angle	25	S2 Binary marker
4	Stroke Marker	26	S3 x position
5	Front left seat force	27	S3 y position
6	Front right seat force	28	S3 z position
7	Rear left seat force	29	S3 $\alpha$ angle
8	Rear right seat force	30	S3 $\beta$ angle
9	ML seat coordinate	31	S3 $\gamma$ angle
10	AP seat coordinate	32	S3 Binary marker
11	Seat Force	33	S4 x position
12	S1 x position	34	S4 y position
13	S1 y position	35	S4 z position
14	S1 z position	36	S4 $\alpha$ angle
15	S1 $\alpha$ angle	37	S4 $\beta$ angle
16	S1 $\beta$ angle	38	S4 $\gamma$ angle
17	S1 $\gamma$ angle	39	S4 Binary marker
18	S1 Binary marker	40	Time stamp
19	S2 x position	41	Initial AP handle position
20	S2 y position	42	Initial SI handle position
21	S2 z position	43	AP handle coordinate
22	S2 $\alpha$ angle	44	SI handle coordinate

AP = anterior-posterior, ML = medio-lateral, SI = superior-inferior

### **3.2.6 Data analysis**

A custom kinematic model was written in MatLab (Mathworks Inc., Natick, MA) which served the function of:

- (i) Sphere fitting the digitised anatomical landmarks in Table 3.4 to provide 3D anatomical landmark positions in the global co-ordinate system.
- (ii) Transforming the global anatomical landmark positions into local sensor offsets during the static digitisation trials.

$$P^{Local} = inv(T_{Local}^{Global}) \times P^{Global} \quad \text{Equation 3.1}$$

- (iii) Applying the local sensor offsets derived during the static trials, to the global sensor position/orientation recorded during the dynamic trials, in order to derive global positions of 3D anatomical landmarks during rowing trials.

$$P^{Global} = T_{Local}^{Global} \times P^{Local} \quad \text{Equation 3.2}$$

For (ii) and (iii),  $T_{Local}^{Global}$  represents the coordinate transform to go from the local coordinate frame to the global coordinate frame and  $P^{Global}$  and  $P^{Local}$  represents anatomical landmark positions in the global and local coordinate frames respectively.

- (iv) Translation of the global origin (centre of electromagnetic transmitter) to a local origin (mid-point of left and right fifth metatarsal) so that anatomical landmarks are bilaterally positioned about a central point.
- (v) Calculation of inter-segmental joint angles.

**Table 3.4: Bilaterally digitised anatomical landmarks made whilst the rower was seated on the rowing machine.**

<b>Anatomical Landmark</b>	<b>Right / Left</b>	<b>Stores as vector offset from:</b>
Dorsal aspect of the fifth metatarsal head (MET5)	Right	Global offset
	Left	Global offset
Distal apex of the lateral malleolus (LMAL)	Right	S4
	Left	S1
Distal apex of the medial malleolus (MMAL)	Right	S4
	Left	S1
Lateral femoral epicondyle (LEPI)	Right	S4
	Left	S1
Medial femoral epicondyle (MEPI)	Right	S4
	Left	S1
Posterior superior iliac spine (PSIS)	Right	S2
	Left	S2
Anterior superior iliac spine (ASIS)	Right	S2
	Left	S2
Hip joint centre (HJC)	Right	S2
	Left	S2

### 3.2.6.1 Calculation of lumbar-pelvic joint angles

Lumbar-pelvic joint (L5/S1) angles were determined by subtracting the value of the pelvic sensor from the lumbar sensor.

$$L5/S1[\alpha\beta\gamma] = S1[\alpha\beta\gamma] - S2[\alpha\beta\gamma] \quad \text{Equation 3.3}$$

### 3.2.6.2 Calculation of hip joint angles

Bilateral hip joint angles were calculated using the joint co-ordinate system (JCS) (Grood and Suntay, 1983) where the hip joint co-ordinate frame was derived from the pelvis and thigh co-ordinate frames. The definition of pelvis and thigh co-ordinate frames can be visualised in Figure 3.4.

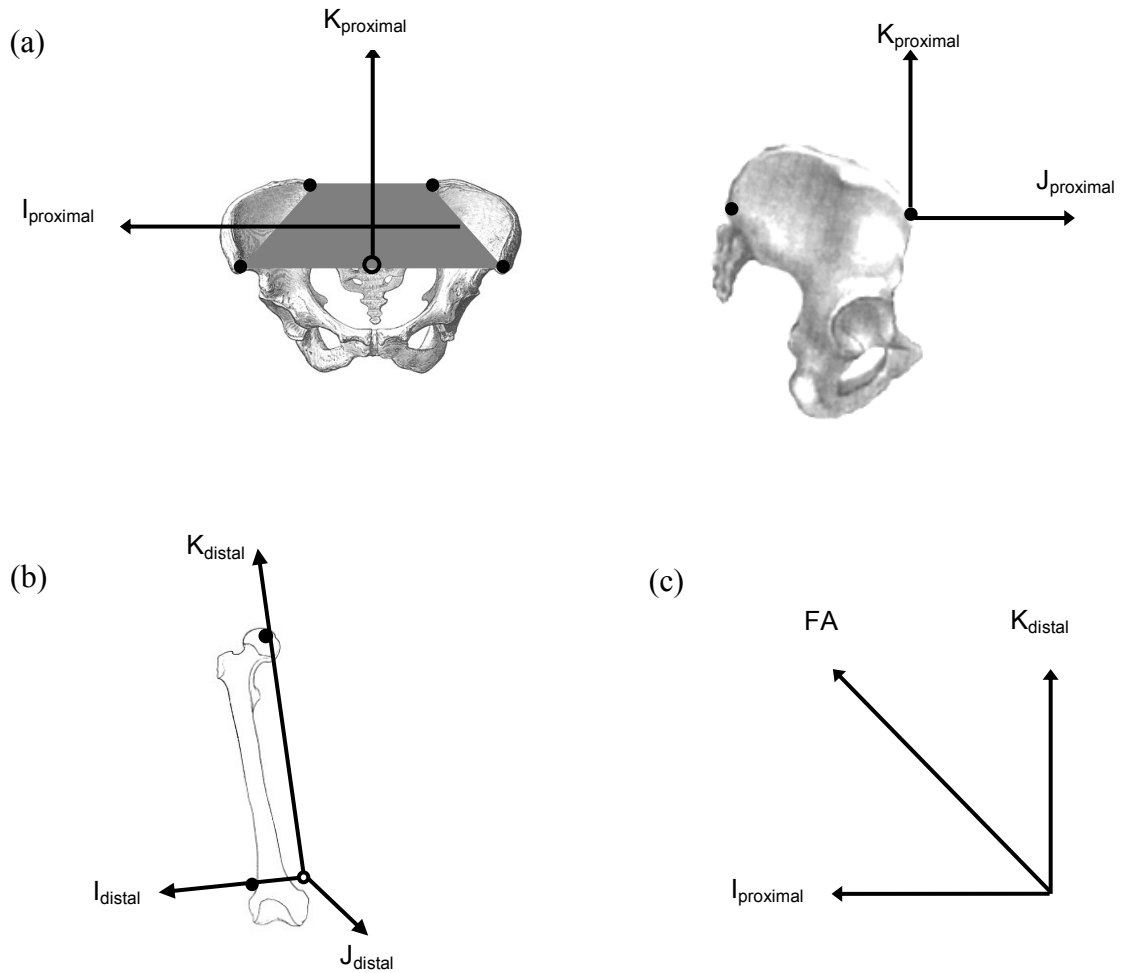


**Figure 3.4: (a) is the anterior and side views of the pelvis and its anatomical co-ordinate system, (b) is the thigh and its anatomical co-ordinate system and (c) is the hip joint co-ordinate system.**

$I_{proximal}$  was defined by the line joining the mid-point of the right PSIS and ASIS to the line joining the mid-point of the left PSIS and ASIS, and was positive to the right.  $J_{proximal}$  was perpendicular to  $I_{proximal}$  and intersected the midpoint of the right and left ASIS, and was positive anteriorly.  $K_{proximal}$  was mutually perpendicular to the  $I_{proximal}$  and  $J_{proximal}$  axes following the right hand rule.

For both the right and left thigh, the segment axes were defined as follows.  $I_{distal}$  intersected the medial and lateral epicondyles and was positive towards the lateral epicondyle,  $J_{distal}$  was perpendicular to  $I_{distal}$ , intersected HJC and was positive in the



proximal direction, and  $K_{\text{distal}}$  was mutually perpendicular to  $I_{\text{distal}}$  and  $J_{\text{distal}}$  and was positive anteriorly.

The hip joint co-ordinate system was defined as  $I_{\text{proximal}}$ ,  $K_{\text{distal}}$  and a floating axis (FA) which is the cross product of  $I_{\text{proximal}}$  and  $K_{\text{distal}}$ . Consequently, this system is not necessarily orthogonal.

$$FA = \frac{K_{\text{distal}} \times I_{\text{proximal}}}{|K_{\text{distal}} \times I_{\text{proximal}}|} \quad \text{Equation 3.4}$$

Flexion/extension of the joint occurred about  $I_{\text{proximal}}$  and was the angle between the pelvis segment's coronal axis ( $K_{\text{proximal}}$ ) and FA.

$$\alpha = 90 - \cos^{-1}(K_{\text{proximal}} \cdot FA) \quad \text{Equation 3.5}$$

Rotations along the sagittal plane occur in the same direction bilaterally, so Equation 3.2 was used for the calculation of both left and right hip angles.

### 3.2.6.3 Calculation of knee joint angles

It was intended that the JCS technique would be used to obtain kinematics for the ankle and knee as well as hip joints. However, during data collection there were problems with digitisation of the medial and lateral malleoli landmarks (see Appendix C). As a result, it was not possible to use the JCS to calculate ankle and knee kinematics. Ankle kinematics were not calculated in this study, whilst an alternative method was used for knee joint angles.

Knee flexion/extension angles were calculated as the angles between a vector joining the hip joint centre and the proximal origin of the shank (defined as the midpoint of

MEPI and LEPI), and the longitudinal line of the respective shank sensors (Figure 3.5).

The limitations associated with this method will be addressed in Section 3.4.

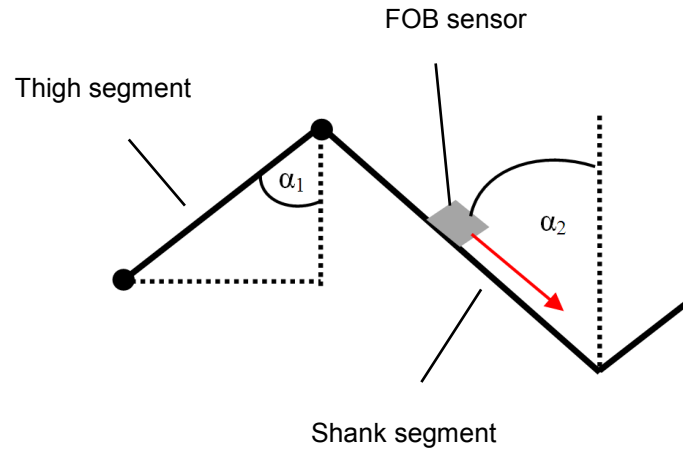


**Figure 3.5: Sagittal plane view of linked thigh and shank segments, depicting the computation of knee joint flexion/extension angles.**

#### 3.2.6.4 Calculation of pelvic twist angle

Pelvic twist was calculated based on the positions of the left and right ASIS landmarks (Figure 3.6). It was defined as the angle that the unit vector between the ASIS landmarks made with the unit vector between the MET5 landmarks. This was solved by the inverse cosine of the dot product.

$$Pelvic\ Twist = \cos^{-1} \left( \frac{a \cdot b}{|a||b|} \right) \quad \text{Equation 3.6}$$

Where  $a$  is the unit vector between the bilateral ASIS landmarks, and  $b$  is the unit vector between the bilateral MET5 landmarks. A positive angle was defined as clockwise pelvic twist, and a negative angle was defined as anti-clockwise pelvic twist.

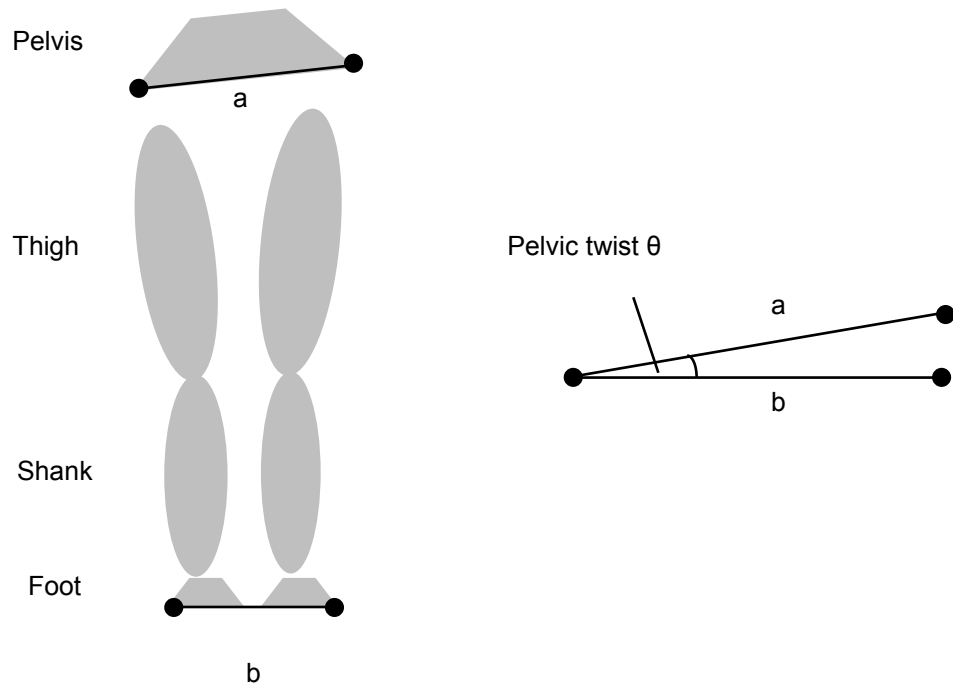


Figure 3.6: Plan view of rower's pelvis and lower limbs depicting the process of calculating pelvic twist angle.

### 3.2.6.5 Derivation of performance parameters

Performance parameters were calculated as follows. Stroke length was the difference between the maximum and minimum handle displacement values (Figure 3.7).

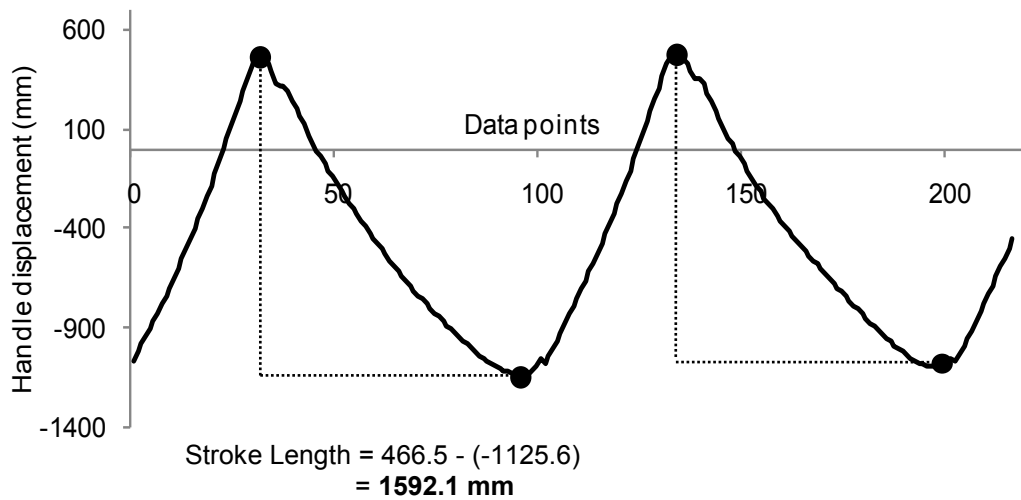
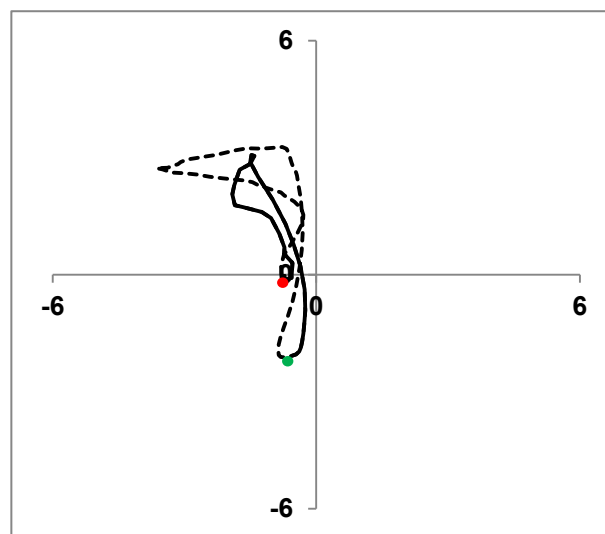


Figure 3.7: Horizontal handle displacement trace depicting the stroke length derivation process.

Mean external power per stroke was defined as the work done during the drive phase i.e. integral of the handle displacement-handle force curve divided by stroke time. Seat centre of pressure was quantified based on the values of the seat's load cells. Deviations in COP from the seat's midline resulted in ML drift, with cumulative drift values calculated per stroke (Figure 3.8).



**Figure 3.8:** Centre of pressure trajectory on the seat for a single normalised stroke. Red dot is the catch, solid black trace is the drive phase, green dot is the finish, dotted black trace is the recovery phase. Units are cm.

#### 3.2.6.6 *Time normalisation*

All data were normalised to 101 data points, based on the handle force, with 0% representing the catch of the stroke and 100% representing the completion of the stroke prior to the subsequent catch point. In this study, the catch was considered to be a point which corresponded to the start of propulsion, and was defined as the onset of tensile force at the handle where the force first exceeds 75 N. This has been found to be a highly robust and repeatable measure of the catch (Holt et al., 2003, McGregor et al., 2005). The finish was defined as the point at which tensile force production was less than 50 N. Of all the normalised strokes recorded within a trial, ten strokes in the

middle of each trial were extracted for statistical analysis. This is so that any acceleration or deceleration phases at the start and end of each piece are discarded, and ten highly repeatable and consistent strokes could be analysed (Appendix D).

All measured parameters were sampled at four points in each stroke; catch, MHF, finish, and at 10% into the recovery phase. Good organisation of the recovery phase sequence (arms straightening, anterior rotation of the trunk and pelvis, knees flexing to bring the weight of the rower onto the feet), prepares the rower for the change of direction at the catch and progression of the drive phase (Thompson, 2005). Thus, measuring 10% of the recovery can help assess the recovery sequence.

#### 3.2.6.7 *Quantifying asymmetry*

The absolute of the symmetry index (ASI) proposed by Robinson et al. (1987) was used to assess the degree of asymmetry in hip ROM and knee ROM and was calculated using Equation 3.7:

$$\text{ASI (\%)} = \frac{2|X_{right} - X_{left}|}{(X_{right} + X_{left})} \cdot 100 \quad \text{Equation 3.7}$$

$X_{right}$  is the value of the right limb and  $X_{left}$  is the value of the left limb. An ASI value of zero indicates perfect symmetry, and increasingly positive values indicate increasing magnitudes of bilateral asymmetry.

#### 3.2.7 **Statistical analysis**

All statistical analyses were performed using SPSS (version 19, IBM Corporation, New York, USA). Group means and standard deviations from ten strokes of each trial were

computed, and normality of the data set was tested using the Shapiro-Wilk test. A two-way mixed model analysis of variance (ANOVA) was run to determine whether bilateral differences in hip and knee joint angles were statistically significant, and to look for differences in parameters such as maximum handle force, mean external power, stroke length, ML drift, and knee and hip ROM, with respect to rowing experience, stroke positions and work rates. A two-way mixed model ANOVA was also employed to examine differences in ASI of the hip and knee joints with respect to rowing experience and work rate. Where an overall significance was seen, Bonferroni post-hoc tests were conducted to locate differences. A multiple linear regression model was employed to evaluate whether asymmetries in hip ROM and knee ROM could predict lumbar-pelvic flexion at the catch and MHF. Significance level for all tests was set at  $P < 0.05$ .

### **3.3 Results**

#### **3.3.1 Performance related parameters**

The means and standard deviations for all performance related parameters are presented in Table 3.5. Maximum handle force and mean external power were the two performance parameters found to be significantly greater in elite rowers compared to both club and novice rowers ( $P < 0.01$ ). There were also significant increases in these parameters at each of the four progressive work rates ( $P < 0.01$ ). However, only mean external power demonstrated a significant interaction effect for work rate and experience ( $P < 0.05$ ). Additionally, there was a progressive increase in ML drift at each of the four progressive work rates ( $P < 0.01$ ), with novice rowers exhibiting significantly

greater ML drift on the seat compared to elite and club rowers ( $P<0.05$ ). However, stroke length did not differ between groups ( $P=0.64$ ).

**Table 3.5: External performance measures at Steps 1-4 for all rowing groups (Mean  $\pm$  SD). Maximum handle force (MHF), medio-lateral (ML).**

Step	Group	MHF (N)	Power (W)	ML Seat drift (mm)	Stroke Length (mm)
1	Elite	921.9 $\pm$ 86.7	253.8 $\pm$ 24.1	115.6 $\pm$ 76.0 <sup>&amp;</sup>	1506.3 $\pm$ 70.0
1	Club	871.8 $\pm$ 68.4 <sup>§</sup>	238.8 $\pm$ 27.5 <sup>§</sup>	118.7 $\pm$ 74.1 <sup>&amp;</sup>	1552.5 $\pm$ 104.3
1	Novice	823.1 $\pm$ 100.3 <sup>§</sup>	211.1 $\pm$ 20.7 <sup>§</sup>	211.1 $\pm$ 20.7	1486.3 $\pm$ 81.3
2	Elite	1031.5 $\pm$ 93.0*	311.5 $\pm$ 30.1*	125.8 $\pm$ 51.7 <sup>&amp;</sup>	1537.5 $\pm$ 60.3
2	Club	921.5 $\pm$ 66.5* <sup>§</sup>	278.0 $\pm$ 25.8* <sup>§</sup>	131.5 $\pm$ 70.5 <sup>&amp;</sup>	1576.3 $\pm$ 100.9
2	Novice	885.2 $\pm$ 106.8* <sup>§</sup>	246.9 $\pm$ 19.8 <sup>§</sup>	246.9 $\pm$ 19.8	1491.7 $\pm$ 78.7
3	Elite	1016.1 $\pm$ 64.8*	437.2 $\pm$ 36.8* <sup>£</sup>	378.8 $\pm$ 33.6 <sup>§</sup>	1512.5 $\pm$ 70.0
3	Club	888.6 $\pm$ 79.8* <sup>§</sup>	383.4 $\pm$ 36.0* <sup>£§</sup>	135.3 $\pm$ 48.7 <sup>&amp;</sup>	1530.0 $\pm$ 117.4
3	Novice	872.6 $\pm$ 84.3* <sup>§</sup>	378.8 $\pm$ 33.6 <sup>§</sup>	169.6 $\pm$ 55.4 <sup>&amp;</sup>	1485.0 $\pm$ 77.7
4	Elite	1066.3 $\pm$ 79.4*	581 $\pm$ 73.1* <sup>£</sup>	135.3 $\pm$ 48.7 <sup>&amp;</sup>	1545.0 $\pm$ 70.0
4	Club	920.4 $\pm$ 73.1* <sup>§</sup>	474.0 $\pm$ 52.9* <sup>£§</sup>	169.6 $\pm$ 55.4 <sup>&amp;</sup>	1516.3 $\pm$ 113.0
4	Novice	954.8 $\pm$ 79.8* <sup>§</sup>	477.6 $\pm$ 61.6 <sup>§</sup>	378.8 $\pm$ 33.6	1525.0 $\pm$ 57.1

\* statistically significant difference from step 1 ( $P<0.05$ ), <sup>£</sup> statistically significant difference from step 2 ( $P<0.05$ ), <sup>§</sup> statistically significant difference from Elite ( $P<0.05$ ), <sup>&</sup> statistically significant difference from Novice ( $P<0.05$ )

### 3.3.2 Lower limb kinematics

With regards to ROM of the lower extremities, hip ROM was higher in elite compared to club and novice rowers, although this difference was not statistically significant (Table 3.6). Elite rowers also appeared to exhibit greater knee extension at the finish position, with 7 out of 8 elite rowers hyper-extending one or both of their knees, whereas this was only evident in 2 of 6 novice rowers. Knee ROM demonstrated no statistical differences between novice, club and elite rowers ( $P=0.21$ ). In terms of the effect of work rate on kinematics; knee and hip angles demonstrated a reduction in ROM as work rate increased ( $P<0.01$ ).

**Table 3.6: Hip and knee ROM, and ASI and pelvic twist in the three groups of rowers (Mean  $\pm$  SD).**

	<b>Elite</b>	<b>Club</b>	<b>Novice</b>
Right knee ROM ( $^{\circ}$ )	134.5 $\pm$ 14.1	135.1 $\pm$ 14.1	140.4 $\pm$ 9.0
Left knee ROM ( $^{\circ}$ )	135.3 $\pm$ 14.9	138.3 $\pm$ 14.9	139.6 $\pm$ 13.8
Knee ROM ASI (%)	3.0 $\pm$ 2.1	5.4 $\pm$ 5.3	5.0 $\pm$ 5.7
Right hip ROM ( $^{\circ}$ )	97.2 $\pm$ 10.6	94.9 $\pm$ 10.7	90.6 $\pm$ 8.4
Left Hip ROM ( $^{\circ}$ )	92.7 $\pm$ 9.0	93.2 $\pm$ 8.2	87.2 $\pm$ 8.1
Hip ROM ASI (%)	6.4 $\pm$ 3.4 *	6.3 $\pm$ 5.9 *	9.0 $\pm$ 10.3 *
Absolute Pelvic Twist ( $^{\circ}$ )	14.5 $\pm$ 6.2	10.9 $\pm$ 5.8	12.3 $\pm$ 6.4

\* significant difference to knee ROM ASI ( $P<0.05$ )

Bilateral differences in sagittal plane kinematics were observed at the hip ( $P<0.01$ ) and knee joints ( $P<0.01$ ), however, there were no subsequent interactions between asymmetry and; rowing experience (hip  $P=0.76$ , knee  $P=0.37$ ) or work rates (hip  $P=0.09$ , knee  $P=0.27$ ). Hip asymmetries were evident at all four points in the rowing stroke ( $P<0.01$ ) whereas knee angles only exhibited asymmetries at MHF and 10% recovery ( $P<0.01$ ). ASI values for hip ROM and knee ROM were not sensitive to work rate or rowing experience, however, hip ROM was more asymmetrical than knee ROM ( $P<0.05$ ). This is demonstrated in the bilateral hip and knee angle trajectories in Figure 3.9. The figure below shows three rowers to have hip asymmetries towards the same side. However, six of 22 rowers demonstrated opposite asymmetries where the left hip exhibited greater flexion through the stroke.



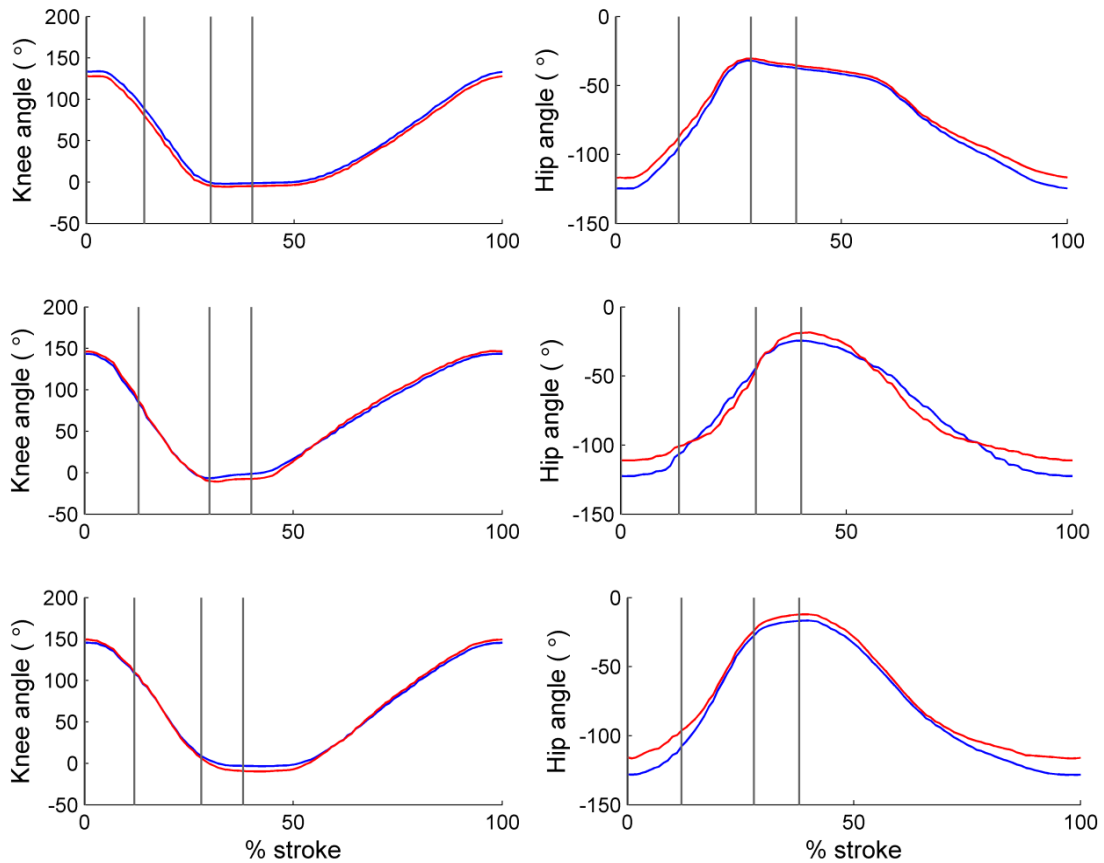


**Figure 3.9: Bilateral joint angles over a normalised rowing stroke (top row; elite rower, middle row; club rower, bottom row; novice rower). Blue line represents right side, red line represents left side. 0° is full joint extension; hip flexions are negative, knee flexions are positive. Vertical lines represent MHF, finish and 10% recovery positions, from left to right.**

### 3.3.3 Lumbar-pelvic kinematics

Lumbar-pelvic kinematics in the sagittal plane was sensitive to stroke position, with L5/S1 angle differing at all stroke positions ( $P<0.01$ ) except between catch and MHF (Figure 3.10). There was a significant interaction effect between work rate and stroke position ( $P<0.01$ ) where an increase in work rate saw corresponding increases in L5/S1 flexion at the catch, and a reduction in L5/S1 flexion at the finish (Figure 3.10). Lumbar-pelvic joint kinematics in the frontal plane significantly differed between MHF and 10% recovery ( $P<0.01$ ). However, rowing experience, stroke position and work rate had no effect on L5/S1 kinematics in the transverse plane ( $P>0.05$ ).

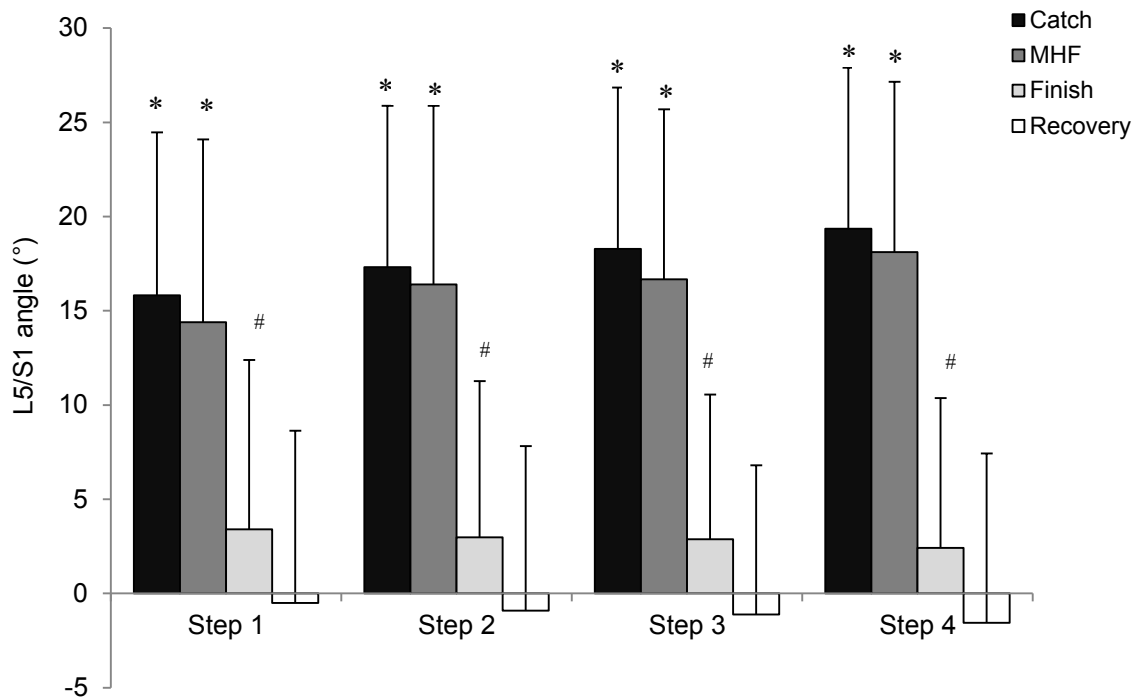


**Figure 3.10: Average (error bars indicate standard deviation) L5/S1 flexion-extension angles at the catch, MHF, finish and 10% recovery positions during four incremental steps. Flexion is positive and extension is negative. \* statistically significant difference from finish and recovery ( $P < 0.05$ ). # is statistically significant difference from recovery ( $P < 0.05$ ).**

In addition, there were no changes in pelvic twist as a result of rowing experience, work rate or stroke position, nor did the direction of pelvic twist correlate with the direction of knee and/or hip asymmetry. Hip and knee ROM asymmetries were significantly correlated with L5/S1 angle at the catch and MHF (Table 3.7). Regression analysis indicated that both hip and knee ROM asymmetry were significant in predicting L5/S1 flexion ( $P < 0.05$ ). However, hip ROM asymmetry showed a better relationship with L5/S1 flexion compared to knee ROM asymmetry, explaining a greater proportion of the variance in the dependent variable.

**Table 3.7: Proportion of lumbar-pelvic flexion explained by kinematic asymmetries.**

		<b>R</b>	<b>R<sup>2</sup></b>
CATCH	Hip ROM ASI	0.59*	0.35*
	Knee ROM ASI	0.28*	0.08*
MHF	Hip ROM ASI	0.60 *	0.36*
	Knee ROM ASI	0.33*	0.11*

\* = P<0.05

### **3.3.4 Summary of results**

- Mean stroke power and MHF were greatest in elites and smallest in novice rowers. In all rowers these parameters increased with respect to stroke rate.
- No group differences in joint kinematics, with hip and knee ROM decreasing with respect to stroke rate.
- Lumbar-pelvic flexion also showed no group differences and increased with progressive stroke rate, with largest joint flexions at the catch and MHF positions.
- Greater degree of asymmetry was observed at the hips compared to the knees.
- Hip range of motion asymmetry was significantly correlated to L5/S1 flexion at the catch and MHF, explaining 36% of its variance.

## **3.4 Discussion**

This study investigated kinematic asymmetries of the lower limbs during ergometer rowing. Using an adaptation of the system described by Bull and McGregor (2000) it was found that ergometer rowing is not symmetrical with respect to lower limb kinematics, and this carries implications for both rowing performance and injuries.

In terms of rowing performance, there was an upward trend of handle force, stroke length and mean external power for all groups of rowers as work rate increased. In accordance, both Murphy (2009) and McGregor et al. (2004) found elite rowers to increase handle force and power output with respect to rate. Although McGregor et al. (2004) found no changes in stroke length as work rate increased, whilst Murphy (2009) observed just small increases in stroke length. Conversely, work rate had the opposite effect on hip and knee ROM, with a consistent reduction in ROM. This was because rowers became progressively less effective at flexing their hips and knees at the catch, and were not extending their knees as fully at the finish of the stroke. Again this has been demonstrated in elite and club level athletes who have shown a reduction in knee flexion at the catch (Murphy, 2009) and reduced knee extension at the finish (McGregor et al., 2004). In general, elite rowers had the largest hip ROM throughout the stroke and extended their knees the most at the finish. These observations correspond with suggestions from Murphy (2009) that effective knee extension at the finish makes it easier to anteriorly rotate the pelvis during the recovery phase. Therefore, the greater performance parameters achieved by elite rowers (i.e. MHF, mean external power) may be due to more effective knee and hip kinematics, thus putting the pelvis in a stronger position at the catch. However, none of the kinematic parameters measured in this study were found to be significantly different between rowers of different standards. It has previously been noted that ML drift on the seat is a predictor of performance on the rowing machine (Murphy, 2009), and at all rates it was found that elite and club rowers have significantly less ML drift on their seat than novice rowers. However, the mechanisms that resulted in these groups' lower ML drift scores cannot be accounted for by the results of their lower limb kinematic measures or associations with pelvic twist, as these did not significantly differ between groups. Therefore, additional non-

kinematic factors such as asymmetries in knee extensor strength and hamstring flexibility may also contribute to the superior performance measured in elite and club rowers; these were not assessed in this study.

Bilateral differences between lower limb joint angles were observed in elite, club and novice rowers at all work rates (Table 3.6). Rowers were tested at incremental work rates based on the findings of McGregor et al. (2004), who found that with increased ratings, technique of rowers progressively deteriorated, which can be characterised by a reduction in pelvic anterior rotation at the catch (Murphy, 2009). However, the current study indicates that such a decline in technique is not coupled with an increase in lower limb asymmetry, as consistent levels of asymmetry were observed throughout the step test. Asymmetrical hip joint angles were evident at all four points in the stroke, whereas knee joint asymmetry occurred at just MHF and 10% recovery. Additionally, ASI values of hip ROM were significantly greater than knee ROM, further emphasising that the hips are at greater risk of asymmetrical motion compared to the knees (Figure 3.9).

Prior research has been carried out looking into the effects of the asymmetrical rowing motion. It was hypothesised that muscle asymmetries and imbalances may be a cause of the high incidence of LBP seen in rowers. However, no significant difference in knee extensor strength, measured using an isokinetic dynamometer, or muscle activity, measured using electromyography (EMG), was identified between the dominant and non-dominant legs in sweep rowers (Parkin et al., 2001). Rowers have been recognised as having poor hamstring strength relative to their quadriceps, and this hamstring weakness is believed to contribute to lower-back injuries by impacting the lumbar-pelvic rhythm, and thus increasing stresses placed on the spine (Koutedakis et al., 1997). Consequently, the degree to which the hips are able to flex at the catch, in addition to

the symmetry of this movement, could have a direct impact on the flexion and rotational quality of the lumbar-pelvic joint throughout the rowing stroke. Therefore, if lower limb asymmetries contribute to sub-optimal lumbar-pelvic kinematics at the start of the drive phase, this could influence the likelihood of attaining a back injury. Stallard (1980) stated that lumbar flexion and rotations at the start of the drive phase results in stretched spinal ligaments and tight apposition of the spinal joint facets, and any imbalances at this time will strain the lumbar spine causing ligament and joint capsule injury. This study demonstrated that L5/S1 is flexed between 15° and 21° at the start of the drive phase, and significant changes to these kinematics occurred as the stroke progressed. This indicates that rowers were not able to hold a strong, stable trunk position from catch to finish which is known to be deleterious to performance (Murphy, 2009).

Parkin et al. (2001) did not observe bilateral asymmetries in isometric and isokinetic strength parameters of the knee flexor or extensor groups. However, it was expected that asymmetrical lower limb kinematics would impact on the action of the pelvis and lumbar spine. This is because lower limb asymmetries would induce pelvic asymmetries at the base of the spine, which may transfer to a distortion of the spine itself, thus leading to theories that rowing asymmetry is related to spinal injury (Reid and McNair, 2000). The results here demonstrate that knee ROM asymmetry had poor predictive relationships with L5/S1 flexion at the catch and MHF, explaining just 8% and 11% of variance in L5/S1 flexion, respectively. A moderately predictive correlation was found between hip ROM asymmetry and L5/S1 flexion at both the catch position and MHF, accounting for 35% and 36% of variance in L5/S1 flexion, respectively. It is not surprising that hip asymmetries explain a greater proportion of variance in L5/S1 kinematics, due to the origin and insertion of the iliopsoas muscle group; a hip flexor

which crosses both hips and lumbar spine. Consequently, tight or overactive hip flexors will directly result in anterior pelvic tilt (Schache et al., 2000). Biarticular muscles such as the biceps femoris, semitendinosus and rectus femoris all work on both the knee and hip joints. Therefore, the knees can only affect lumbar-pelvic motion via the hips, and cannot directly impact the action of the pelvis, resulting in very low predictive power in the regression model.

Hip asymmetries were found to influence L5/S1 flexion in this study, despite a lack of correlation with pelvic twist. Distal segments of the lower and upper extremities are fixed in rowing, thus asymmetries at the lower limbs must be compensated for, through flexion and rotation of L5/S1, in order to maintain symmetrical handle motion in the sagittal plane. The direction of pelvic twist did not correlate with lower limb asymmetry, suggesting rotation about the transverse plane was not sensitive enough to mediate the effect of hip asymmetry on L5/S1 kinematics, and that other means of compensation took place. Whilst it cannot be established as a cause and effect relationship, there was clearly an association between hip ROM asymmetries and L5/S1 kinematics in the sagittal plane, as demonstrated by the regression analysis. Consequently, the moderate correlation of the hips' effect on L5/S1 kinematics at the catch and MHF indicates a need to carry out bilateral measurements of sagittal plane hip ROM in rowers of all standards. Goniometers are commonly employed for the measurement of segment and joint angles, such as asymmetry of hip ROM (Ellison et al., 1990), knee flexion (Rheault et al., 1988) and pelvic tilt (Walker et al., 1987). Therefore, simple measures of hip ROM asymmetry could be an effective way of preempting lower back problems in rowers, and facilitates coaches and physical trainers in implementing interventions to improve hip symmetry, and potentially kinematics of the lower back.

It must be noted that there was a limitation in the number of FOB sensors, therefore the medial and lateral femoral epicondyles were tracked with respect to the tibial sensors, rather than sensors attached to the thigh. This method can result in mal-tracking of the epicondyles, partially due to AP translation of the tibia during flexion-extension motions (Bull et al., 2008), resulting in fluctuations of the thigh segment's length up to 20 mm in this study. However, this would cause knee angles at the catch and MHF to be affected by less than 2°. Furthermore, the length changes were bilaterally similar, with a root mean square error of 3.5±1.3 mm (calculated for 10 strokes for all 22 rowers). Therefore, digitizing the femoral epicondyles relative to the tibial sensor had little impact on asymmetry values obtained at the knees and hips. The largest varus/valgus motion of the shank sensor for any subject was 19.7° with a group average of 9.6±5.3°. A 20° varus/valgus motion of the shank can affect knee flexion angles by up to 6°. However, there were no significant differences in frontal plane motion between the left and right the shank sensors ( $P<0.05$ ). As such, sagittal plane asymmetries observed in this study were due to kinematic differences rather than measurement limitations.

With regards to the kinematics of the lower limb joints, only a two dimensional analysis was conducted for this study. However, the intention of this study was to measure simple kinematics, which could be carried out in medical screenings, providing information as to a rower's asymmetry. Furthermore, investigations into 3D kinematics during rowing have indicated that the majority of segmental motion occurs in the sagittal plane (Halliday et al., 2004), with these kinematics being the most pertinent in predicting performance and injury risk (Murphy, 2009).



### **3.5 Conclusion**

This study has shown the rowing stroke on an ergometer to be asymmetrical, with significant bilateral differences between the knees and hips at specific positions in the stroke, with asymmetries also observed in joint ROM. A symmetrical stroke, in terms of force production at the lower limbs, would result in more equal loading of the spine, thus reducing the likelihood of injury (Stallard, 1980). Consequently, more work should be done to discern the link between asymmetry of the rowing stroke and back injury. Instrumented foot-stretchers that measure vertical and horizontal foot forces would be invaluable in quantifying the bilateral forces transferred during the rowing stroke, and also provide other means of assessing technique and performance through the relationship between symmetry of applied forces, joint moments and power output. Nevertheless, the results of this study indicate a link between asymmetrical hip ROM and L5/S1 kinematics. If asymmetrical kinematics can be identified in rowers through simple measurements of hip ROM, then techniques that predispose an athlete to injury can be identified and altered accordingly via biofeedback to the athlete and coach, thus going some way to prevent future injury.

## **Chapter 4:**

### **Development of Instrumented Footplates: Design, instrumentation and calibration**

The previous chapter identified a link between kinematic asymmetries at the hip and lumbar-pelvic rotations in the sagittal plane, thus giving insight into possible mechanisms that contribute to lower back pain in rowers. Theoretically it is possible to have perfect kinematic symmetry of the lower limbs even when the rower is only exerting pressure onto one foot-stretcher, causing a moment about the lumbar spine which would have to be countered by stabilising lower back muscles. Therefore, it is evident that in order to carry out a comprehensive analysis of lower limb asymmetries and its impact on spinal dynamics, it is necessary to quantify kinetic symmetry of forces applied to the foot-stretchers, during the drive of the rowing stroke. The first step to achieving this would be to develop instrumented footplates which measure bilateral foot forces exerted by the rower onto each foot-stretcher.

This chapter will firstly give an overview of work in the literature which have utilised instrumented devices such as force plates and load cells to record force outputs exerted by an athlete. Secondly, this chapter will outline the work that has been carried out towards developing the instrumentation and software for real-time data acquisition and biofeedback of foot force on a Concept II ergometer. The application of this technology for analysis of elite athlete foot force and asymmetries will be presented in Chapter 5.

## **4.1 Introduction**

### **4.1.1 Measuring contact forces in sport**

#### *4.1.1.1 Traditional force plate studies*

Force transducers are instruments used to measure force and are often used as tools for functional assessments in clinical and sporting environments. Transducers are often incorporated in force plates (or force platforms), and these measure ground reaction forces (GRF) generated by a body that comes into contact with the plate. Therefore, force plates can be used to measure balance during quiet standing or forces generated during motion across the plate. A force plate usually quantifies three dimensional forces during the entire contact phase, thus it is possible to quantify peak GRF, impulse, timing of peak forces, rate of force development, amongst other parameters, for performance and injury considerations across sporting disciplines (Munro et al., 1987, Kollias et al., 2004, Walsh et al., 2006).

Often, assessments of leg power and muscular strength are made by examining force production during a vertical jump take-off. Vertical GRF and its rate of development is similar in subjects performing an Olympic snatch and vertical jump (Garhammer and Gregor, 1992). Therefore, vertical jump performance can give surrogate measures of muscular strength and mechanical power, which are important requirements for success in weightlifting (Garhammer and Gregor, 1979). Propulsive forces have also been measured during a swimming start, using a submersible force plate as part of a system to examine and improve swimmers' take off technique (Arellano et al., 2000). The study found weak correlations between measured force parameters and swim

performance, and called for individual analyses in order to provide appropriate feedback. In addition to examining technique and performance, force plates have been used to assess injury risks by quantifying forces during high impact activities such as jump landings. Ground reaction forces during ballet jump landings were found to generate significantly less GRF than vertical jump landings. This was because greater ankle stability and stiffness 'on pointe' meant a lower jump height where less GRF could be produced (Chockley, 2008). Gymnasts, however, generated greater GRF during 60 and 90 cm drop landings compared to recreational athletes. Therefore, a gymnast's frequent exposure to large GRF may influence their high rate of lower extremity injuries (Seegmiller and McCaw, 2003). These studies provide information regarding technique and stress-related injuries, as high impact forces can increase shin splints and stress fractures (Ozguven and Berme, 1988). Consequently, the measurement of GRF can have wide applications in sports biomechanics in terms of assessing performance, injury mechanisms, and subject-specific analyses.

#### *4.1.1.2 Custom Transducers*

Force platforms are commercially available and easy to use as they often come with custom software. However they are heavy, expensive and are generally limited to the measurement of ground reaction forces. In order to measure contact forces on specialised sporting equipment, it is often necessary to develop bespoke instrumentation using force transducers such as load cells or foil strain gauges. Instrumentation of bicycle pedals have been most prevalent, with load cells employed to measure reaction forces of all three orthogonal axes (Wootten and Hull, 1992, Wheeler et al., 1992). Strain gauges have also been employed to quantify normal and tangential pedal forces (Reiser et al., 2003). These enabled pedal loads to be accurately quantified, thus aiding

the conception and design of pedal components that attenuate torsional moments at the shoe-pedal interface, consequently influencing the patho-mechanics associated with knee pain during cycling (Wheeler et al., 1992).

Other sports which have benefitted from biomechanical instrumentation include athletics, where starting blocks have been instrumented with load cells and strain gauges to quantify peak forces, impulse and reaction times during a sprint start (Gander et al., 1994, Pain and Hibbs, 2007). Using this technology Pain and Hibbs (2007) found minimum sprint start reaction times can be under 85 ms, which is less than the current false start criterion of 100 ms, as proposed by the International Association of Athletics Federations. This type of technology is also extremely useful as a quantitative coaching aid, allowing informed adjustments in force application, and supplementing coaches' qualitative feedback and instructions (Harland et al., 1995). Similarly, force transducers have been incorporated into downhill skis to precisely quantify durations and magnitudes of resultant forces during individual phases of ski turns (Vaverka et al., 2012), again providing useful objective coaching feedback. For example, ski force vectors provide information on the average turn duration which in turn gives indirect information about speed. Biomechanical feedback through these custom instrumented tools enables quantitative performance data to be delivered to athletes. Therefore it can be pivotal in informing athletes and coaches of adjustments that need to be made in order to optimise their technique and achieve performance gains.

#### *4.1.1.3 Kinetic asymmetries in gait and sport*

Reaction forces measured by force plates and transducers are useful for the assessment of performance potential and injury risks by quantifying peak forces and loading

patterns. However, by utilising or developing bilaterally symmetrical transducers or force plates, it is possible to quantify kinetic asymmetry. With regards to biomechanics research, the lower extremities are often assumed to behave symmetrically during activities such as running (Hunter et al., 2005), jumping (Cleather and Bull, 2010) and rowing (Halliday et al., 2004). This is largely due to logistics such as equipment limitations and cost, and as such studies often rely on unilateral data collection (Bull and McGregor, 2000), or in some cases, bilaterally average the right and left sides (Caplan and Gardner, 2010).

Symmetry of force production is an important consideration in sports and activities of daily living because asymmetries are thought to be a factor which influences LBP (Al-Eisa et al., 2006a). It also indicates the functional health of an individual during rehabilitation of a unilateral lower limb injury, by providing a measure of its force producing ability compared to the unimpaired limb (Flanagan et al., 2003). Studies investigating healthy, asymptomatic subjects have shown that they exhibit symmetrical GRF and muscle activations during activities of daily living (Burnett et al., 2011). However, some clinical studies have identified asymmetries in GRF and lower limb joint moments even in healthy control subjects during tasks such as walking (Seeley et al., 2010), and sit-to-stand (Highsmith et al., 2011). As such kinetic asymmetries between the lower limbs are widely identified in gait and rehabilitation studies which investigate pathological gait. For example, those pertaining to amputees (Nolan et al., 2003, Mattes et al., 2000), chronic stroke patients (Kim and Eng, 2003), and hip and knee arthroplasty patients (McCroory et al., 2001, Oken et al., 2010, Stacoff et al., 2007). All these studies have found large bilateral asymmetries in vertical GRF parameters, with their asymmetry values significantly greater than their healthy matched controls.

The majority of the above studies investigated asymmetries exclusively using force plates, and have thus bilaterally examined parameters such as peak GRF, impulse, timing of peak force, stride time and rate of force development. Information from bilateral GRF has also been used to investigate differences in loading asymmetries between runners with and without previous tibial stress fractures (Zifchock et al., 2006). Consequently, they are useful for informing runners of the likelihood and locations of injuries, based on the magnitude and direction of their asymmetries.

Instrumented treadmills have also been developed which have two force plates embedded in the belt to enable the degree of lower limb asymmetry, in terms of bilateral kinetics, to be quantified (Dingwell et al., 1996). However, with regards to sporting application, there has been surprisingly little research on kinetic asymmetries and none in sprinting, despite the wealth of literature investigating biomechanics of sprinting performance (Hunter et al., 2005, Hunter et al., 2004, Bezodis et al., 2008). Asymmetrical activities such as badminton, which employ lateral side stepping and cross stepping movements, have used force plates to examine ground reaction force asymmetries (Kuntze et al., 2009). They were able to determine the demands placed on the leading and trailing limb, thus predicting the contribution of these movements to the occurrence of lower limb overuse injuries. Bicycle pedals have also been bilaterally instrumented by Carpes et al. (2006) for the purpose of quantifying pedalling asymmetries during a 40 km time trial. The data showed that the dominant leg was always responsible for greater peak torques at the crank arm. Interestingly, they found that during the first and last 10 km of the time trial, pedal torques were higher and significantly more symmetrical compared to the middle section of the trial. This suggests that symmetry is related to torque production and limb dominance.

Recently, more in-depth analysis of bilateral asymmetries have become evident in the literature, with asymmetry measures of kinematics and inter-segmental joint moments, in addition to GRF parameters. Flanagan and Salem (2007) investigated bilateral asymmetries of the lower limbs in healthy adults during bar-bell squatting by quantifying joint angles, inter-segmental moments and GRF. They found significant bilateral differences in kinetic parameters. However, none of the 18 subjects followed the pattern of asymmetry exhibited by the group mean, suggesting that single subject analysis of lower limb asymmetry is also important in an investigation of bilateral asymmetry. Furthermore, it should not be assumed that net joint torques are equal on the right and left sides during the squat exercise, with joint biomechanics on both sides of the body being made during bilateral tasks.

#### *4.1.1.4 Bio-feedback for coaching*

In sports biomechanics research, force plates and transducers have been useful in determining performance potential, the capacity to generate forces at different contact points, and potential exposure to injuries through assessments of peak loads and asymmetries. Providing the above information on the quality of an athlete's performance and ways in which they can improve is a fundamental coaching paradigm. Technology that assists sports coaching by providing real time bio-feedback of an athlete's technical ability can provide timely, constant, and objective support to supplement the coach's qualitative feedback. Instrumentation-driven biofeedback provides a unique tool for quantifying and visually displaying performance information. For example, data on force and power output during indoor rowing can be delivered to an athlete in real time, thus providing immediate feedback on performance and consistency levels (Hawkins, 2000). In a rowing boat instrumented with force



transducers at the feet and handle, immediate kinetic feedback enabled the coach to provide suggestions regarding changes in pattern and timing of force development, and both athlete and coach could observe whether changes were effective (Smith and Loschner, 2002). Biofeedback has also been shown to be highly successful in improving performance of top level shooters by refining motor skills and providing information that trains better decision making (Mullineaux et al., 2012). The dynamical systems theory of motor learning would suggest that immediate kinetic information feedback positively supports the improvement of motor skills, making this form of immediate feedback a highly recommended instrument for training (Smith and Loschner, 2002). Therefore, the development of custom transducers for the purpose of measuring athletes' force and power output during training sessions, and its consequent feedback mechanisms, can be an invaluable coaching tool which can be used to accurately refine changes in technique for long term performance benefits. Therefore, the development of instrumented foot-stretchers for the Concept II rowing ergometer should coincide with the development of custom bio-feedback software. This will inform the athlete and coach of existing foot force asymmetries, thus providing a platform from which to make necessary corrections and technical improvements.

#### **4.1.2 Measuring foot forces in rowing**

Studies quantifying the forces generated at the feet in rowing are limited and use a variety of instrumentation approaches to achieve this. Limited studies have quantified foot forces during rowing. MacFarlane et al. (1997) developed custom footplates instrumented with strain gauges to measure normal reaction forces under the left and right foot. They recorded forces in the region of 900 N for experienced male rowers but only measured unilateral compressive forces, thus missing information on asymmetry

and shear forces applied to the foot-stretcher. Soper and Hume (2004) did not provide details on their foot-stretcher instrumentation, however it is known that they were capable of measuring only compressive forces. Foot-stretchers are orientated at an incline of  $41^\circ$  so a substantial component of force applied by the feet will be in the shear force direction. Therefore, by quantifying just compressive forces, it is not possible to obtain an accurate picture of the resultant forces at the feet.

It has been stated that rowing performance can be improved specifically by increasing propulsive impulse developed by the lower limbs (Baudouin and Hawkins, 2004, Caplan et al., 2010). This suggests that it is necessary to measure foot force with a minimum of two degrees of freedom so that vertical and AP foot forces are quantified. This would enable the mechanical effectiveness of the leg drive to be analysed with respect to resultant forces applied to the footplates. A number of studies have developed instrumented rowing foot-stretchers, with varying magnitudes of peak forces reported in the vertical and AP axes. Bi-axial forces at the feet have been measured by Baca et al. (2006a) using load cells to measure the compressive component and strain gauges to measure shear component of force. These were resolved into their vertical and AP components, with peak AP forces of approximately 500 N reported in elite male rowers on a Concept II rowing machine. Colloud et al. (2006) fixed biaxial strain gauge transducers to the foot-stretchers of a fixed head (Concept II) and floating head (RowPerfect) ergometers. They tested 25 male elite rowers who generated large vertical and AP forces of 791 N and 908 N respectively on the Concept II, and 690 N and 951 N respectively on the RowPerfect when rowing at race pace (i.e. 35 strokes per minute). Resultant forces on the Concept II were significantly greater than RowPerfect, purely resulting from the larger vertical forces applied to the foot-stretcher.

Halliday et al. (2004) attached a six degree of freedom load cell under the right foot-stretcher and measured vertical, AP and ML foot forces. Peak AP and vertical force averaged 556 N and 456 N and ML force was always less than 100 N when heavy-weight male rowers were rowing at a rate of 32 strokes per minute. The peak forces recorded in this study are substantially lower than those recorded by Colloud et al. (2006), despite both groups of rowers being high level heavyweight male rowers. Pudlo et al. (2005) placed two six degree of freedom force plates under two adapted foot-stretchers and recorded similar results as Halliday et al. (2004), with forces close to 500 N and 400 N for vertical and AP axes respectively, and the ML axis exhibiting less than 100 N. Whilst the accuracy and robustness of commercially available multiaxial load cells and force plates are very good, they tend to be large, heavy and expensive. A large, heavy transducer placed under the foot-stretcher may cause an athlete to alter their rowing style in response to changes in the appearance and feel of the ergometer. Furthermore, six degrees of freedom load cells are expensive, in the region of £5,000 - £15,000, with this cost being doubled in order to record bilateral foot forces for the purpose of investigating asymmetry. Therefore, cost is a major consideration in the development of bilaterally symmetrical footplates. Baca et al. (2006b) developed light, portable footplates using load cells and strain gauges which could be fitted onto a boat or ergometer to measure vertical and AP foot forces under each foot. The footplates were highly accurate, giving a linear relationship between measured and applied force. Having developed these instruments, they identified that bilateral foot force asymmetries are exacerbated when rowing on-water, compared to on an ergometer (Baca et al., 2006a). However, their study tested only four rowers, thus there is a lack of statistical power in this study to make clear conclusions based on this data - although when applying this technology to individual elite athletes, statistical power is not a

consideration. Examination of foot force data from the above studies suggests that the newly designed footplates must be able to measure all forces in the sagittal plane i.e. vertical and AP axes. Consequently, from here on AP forces will be referred to as horizontal forces. Both axes must be able to operate over a wide range of deflections in order to accommodate peak forces in the region of 800 N. Furthermore, the design of the footplates should not result in changes to the appearance or feel of the ergometer, therefore the instrumentation should be inconspicuous and affordable so that two identical footplates can be developed. Based on these requirements, the footplate design criteria were developed and outlined below.

## **4.2 Footplate Design**

### **4.2.1 Design Specifications**

In order to develop footplates which are most appropriate for the purpose of measuring foot force outputs during rowing, the following design specifications were outlined:

1. Measure bi-axial forces in the sagittal plane.
2. Measure force from right and left footplates independently during the full rowing stroke.
3. Footplates are able to sustain peak loads expected during the rowing stroke. These are approximately 800 N for heavyweight male rowers in the vertical and horizontal axes (Colloud et al., 2006).
4. Maintain original Concept II foot-stretcher position and orientation set-up.
5. Maintain the look and feel of the ergometer.
6. Obtain calibration coefficients of the force transducers which accurately quantify force and centre of pressure within an acceptable degree of error.

7. Make it possible to re-test the calibration of transducers easily and regularly.
8. Minimise the occurrence of cross talk between orthogonal axes.

A primary concern regarding the footplates is that the calibrated force output is computed to an acceptable degree of accuracy, usually with a level of error equivalent to 2% or less (Bobbert and Schamhardt, 1990). To ensure accurate measures of foot force, the footplate design should be such that the material is not susceptible to creep under expected magnitudes of loading, and that deflections in the material are repeatable under the same loading conditions.

Based on the review it was decided that forces will be measured in the sagittal plane only i.e. vertical and horizontal axes. In order to achieve this, both normal and shear forces must be measured (through appropriate design, instrumentation and calibration) and then resolved into vertical and horizontal forces. For investigations into kinetic asymmetry to be possible, two symmetrical footplates must be developed and it is imperative that they have a similar level of accuracy. Furthermore, the design of the footplate should reflect that of a traditional Concept II foot-stretcher, and any added instrumentation should not result in notable changes in the feel, position or orientation of the foot-stretchers. As two identical foot-stretchers must be developed, it is important to keep in mind the cost of both designing the construct and buying the transducers, to ensure that they can be made as cost effectively as possible.

The footplates must be able to function accurately and with good repeatability under high loading conditions. They must have the capacity to repeatedly withstand normal forces of >1000 N without risk of fatigue failure or reaching its upper measurement limit. The device must be thoroughly calibrated in all measurement axes so that the voltage output from the transducer is a true representation of the applied forces. With

large forces repeatedly applied to the footplates, it is important that the calibration can be retested regularly and with relative ease. This will ensure that potential drift of transducers that occurs over time is accounted for with regular re-calibrations.

Finally, cross-talk between the normal force and shear force axes must be minimised to ensure that the transducers measure force purely along its defined axis. Theoretically, the two axes (i.e. vertical and horizontal) should be perfectly orthogonal and would not produce an output on the other measurement channel. However, it is inevitable that in many cases there will be a degree of cross-talk, where a sensor reports an output value for its axis when some of the force was developed along a different axis. It is necessary to minimise cross-talk through appropriate design of the footplate construct, and to correct for any cross-talk errors, through mathematical manipulation of the load cell's output. The development of bespoke bilateral footplates which comply with the above specifications are subsequently described in this chapter.

#### **4.2.2 Instrumentation**

The transducer used for measuring force is key in determining the physical design, thus will be established prior to developing the foot plate. Considerations for choosing the most appropriate transducer include price, availability, reliability, ease of use and size.

Sensors that are frequently used in force measurement include capacitors, conductors, piezo-electric sensors and strain gauge sensors. Capacitors work on the principle that when a force is applied to it, the distance between its electrically conducting plates changes, causing a change in the current and thus voltage output. Conductors are like capacitors but consist of conductive elastomers between the plates. Thus when force is applied the elastomer deforms and reduces the electrical resistance between the two

plates. Piezoelectric sensors are non-conducting crystals (such as quartz) which generate an electrical charge when subjected to mechanical strain. The basic principle of strain gauges is to undergo a change in length when the material it is fixed to is deformed. This strain will result in an increase in electrical resistance if it occurs in the tensile direction, and a decrease in the compressive direction. Thus transducers typically function by measuring the deflection/deformation of the material as a function of the applied load.

#### *4.2.2.1 Load cells*

Commonly used force transducers are load cells which function by measuring the displacement of a structural element to determine force. The output of a load cell is therefore a calibrated association of this change in displacement or deflection.

Load cells come in many shapes and sizes and can be used to measure tension, compression and shear forces along multiple axes. Single-axis load cells measure along a single straight line, bi-axial load cells provides load measurements along two orthogonal axes and tri-axial load cells provide measurements along three orthogonal axes. They are used frequently in mechanical testing, mechanical monitoring or within devices like force plates. The most common technologies used for the sensing element within load cells are piezoelectric and strain gauge sensors. The piezoelectric technology uses a material that generates an electric charge when deformed, whereas strain gauges are typically foil type structures that change electrical resistance when stretched or compressed. Kistler force platforms (Kistler AG, Winterthur, Switzerland) consist of four piezoelectric load cells in each corner of the plate, whilst the AMTI force plate (Advanced Mechanical Technology Inc.) uses load cells that house strain gauges.

#### 4.2.2.2 *Strain gauges*

Strain gauges are the fundamental sensing element for many types of sensors including pressure sensors, position sensors and several types of load cells. They are often smaller than a postage stamp and are bonded to the surface of the material from which the measurements are taken.

The basic principle of a strain gauge is that when the material they are bonded to changes dimensions due to an external load, the pattern of resistive foil mounted on the strain gauge is stretched or compressed, causing it to change dimension and thus alter its electrical resistance. If the change in dimension is kept within an elastic region, it is possible to establish a linear relationship between changes in resistance and the force applied which causes that change. Therefore the resistance of a strain gauge is a direct reference to the applied force.

A summary describing the suitability of load cells and strain gauges for the purpose of measuring foot force are described in Table 4.1.

**Table 4.1: Summary of force transducer specifications.**

	<b>Size</b>	<b>Cost</b>	<b>Degrees of Freedom</b>	<b>Weight</b>
<b>Uniaxial Load Cell</b>	5 mm diameter 10 mm thickness	Approx £1000	Single	0.1 – 5 kg
<b>Multi-axis force torque sensor</b>	50 mm diameter 50 mm thickness	Approx £10,000	Six	5 - 15 kg
<b>Strain Gauge</b>	15 x 5 x 0.5 mm	Approx. £1	Single	< 1 g

For this particular project strain gauges are believed to be the most appropriate sensor. This is due to their small size, extremely light weight features, low cost and relative ease of implementation.



### 4.2.3 Physical Design

The preliminary footplate designs and component manufacture were completed by Chee (2006) and formed the foundation of the subsequent stress analysis, instrumentation and calibration, described later in this chapter. Based on Chee's design, the footplate structure was assembled from the following five components:

- (i) *Beam A*: a stainless steel (grade 316) fixed beam which deflects in such a way to measure normal reaction forces (Figure 4.1).
- (ii) *Beam B*: an aluminium (6082-T6) cantilever beam which deflects in such a way to measure shear forces (Figure 4.1).
- (iii) *Loading Plate*: a rectangular plate (surface area; 305 mm x 115 mm) which forms the external loading surface of the footplate where the rower's foot makes contact. The ends of Beam A attach to each end of the Loading Plate.
- (iv) *Side Plate*: a triangular plate which forms the attachment between the footplate construct and the ergometer. Beam B acts as a cantilever by connecting to this plate.
- (v) *Mounting Component*: a triangular mounting component which forms the connection between Beam A and Beam B, and ensures the two beams do not move relative to each other and are orientated orthogonally in its initial condition. It is essential that beams A and B are perfectly orthogonal to one another so that foot contact forces both normal and parallel to the footplate could be quantified.

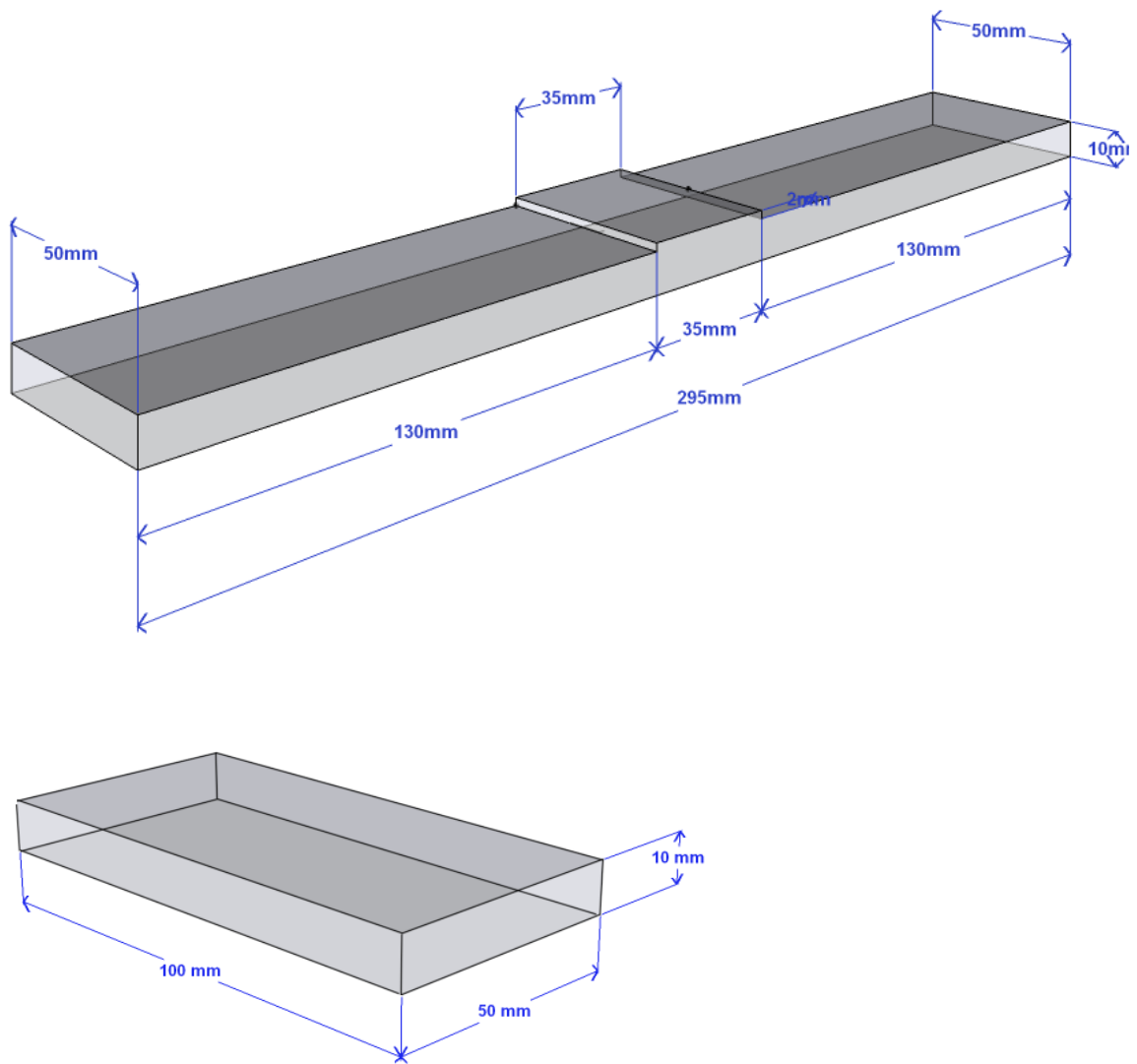


**Figure 4.1: Dimensions of the two main components of the footplate; Beam A (top) and Beam B (bottom)**

Based on the proposed design of (Chee, 2006), the loading scenario of the footplate was conceptualised in the current study. Figure 4.2a shows that when force is applied to the surface of the footplate, Beam A can deflect in two ways; anterior or posterior to the mounting component. Forces from the rower are directly applied to the Loading Plate (Figure 4.2b), with the ends of this plate making contact with the ends of Beam A. Therefore, forces from a rower are applied to Beam A through two mounting points at the extremes either end of the beam (Figure 4.2c). Beam A measures purely normal

forces at the front and rear regions of the footplate. When force is measured at two or more points it allows the point of force application to be calculated (described in Section 4.3.2).

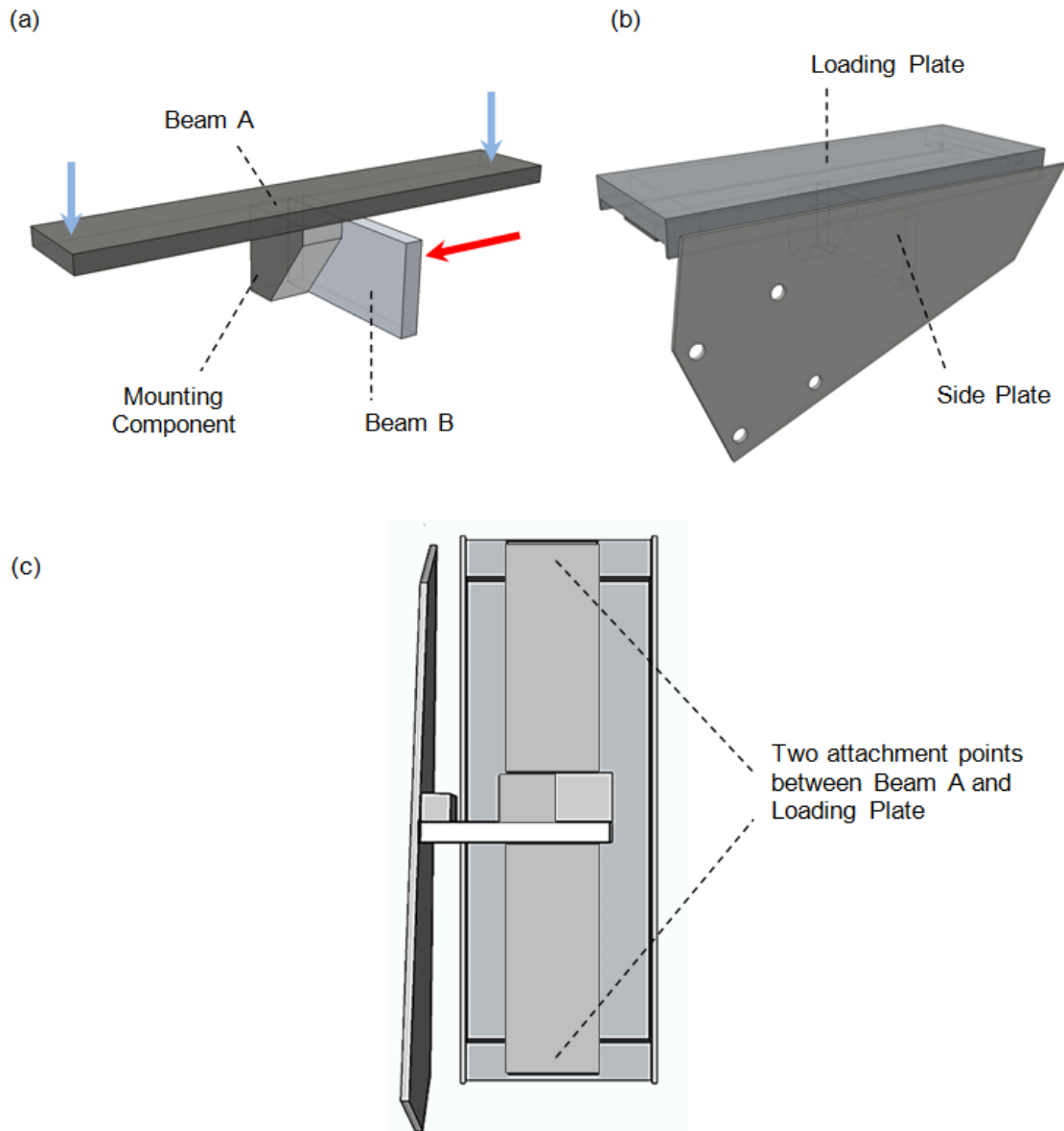


**Figure 4.2: (a) Beam A and B loading scenario showing the application of normal force to Beam A (blue arrows) and shear force to Beam B (red arrows), (b) assembled footplate showing the addition of the Side Plate and Loading Plate, (c) underside view of the footplate showing where the ends of Beam A form attachments to the ends of the Loading Plate, and the connections between Beam B and the Mounting Component.**

With regards to Beam B, one end is attached to the Side Plate (and thus the rest of the ergometer), whilst the other end forms a connection with the Mounting Component (and thus the rest of the footplate). Beam B, consequently, acts as a cantilever beam where deflections occur parallel to the Loading Plate to measure shear forces applied to the footplate. The design of the footplate construct would suggest that normal forces applied to Beam A (i.e. blue arrows) would cause a torsion of Beam B. However, the deflection of a beam under load depends also on the geometry of the beam's cross section, and consequently its stiffness. Therefore, the beam was constructed with a thickness of 10 mm in order to provide a high polar moment of inertia which improves the beam's ability to resist torsion. Consequently, this will minimise the cross-talk between Beam A and Beam B.

It was decided that strain gauges would be employed to instrument Beam B to enable measures of shear forces, and also at the front and rear of Beam A, relative to the mounting component. Two force transducers on Beam A will allow calculation of centre of pressure along the longitudinal axis of the footplate.

#### **4.2.4 Basic Force Measuring Principles**

When a tensile or compressive force is applied to a sample, stress ( $\sigma$ ) is defined as the ratio of the normal force ( $F$ ) to the cross-sectional area ( $A$ ):

$$\sigma = \frac{F}{A} \qquad \text{Equation 4.1}$$

Strain ( $\epsilon$ ) is positive in tension and negative in compression and is defined as the ratio of the change in length ( $\Delta L$ ) to the initial length ( $L_0$ ):

$$\varepsilon = \frac{\Delta L}{L_0} \quad \text{Equation 4.2}$$

Strain gauges all have the same working principle governed by Hooke's Law. Hooke's Law states that the extension of a spring is directly proportional to the applied load. Therefore, regions on the footplate where the greatest stress occurs will be where the greatest strain of the material occurs. The proportional relationship between stress and strain is modulated by the stiffness of the material according to Equation 4.3.

$$\sigma = E \cdot \varepsilon \quad \text{Equation 4.3}$$

Where E is Young's Modulus.

For most materials the relationship between stress and strain has been experimentally derived. An example of a stress-strain curve is shown in Figure 4.3. The *elastic region* is the linear region of the curve prior to the *proportional limit* which satisfies Hooke's law.

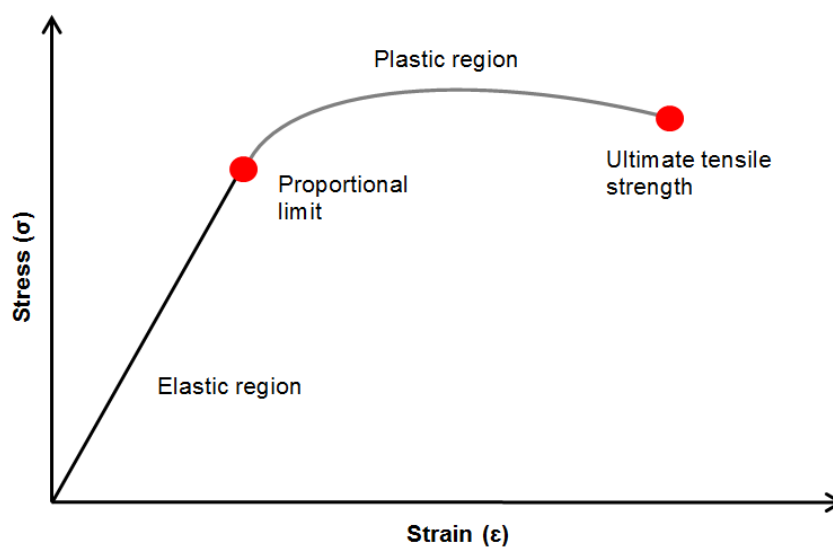


Figure 4.3: Example of a tensile stress-strain curve.

---

Based on the above principles, it is important that the material chosen for Beam A and Beam B comply with the following specifications:

1. Beams must not deflect outside of the elastic region whilst subjected to the highest possible load expected from the rower.
2. Beams must be sensitive enough to detect the range of expected forces.
3. Strain gauges are bonded to the beams for outputting data in proportion to the deflection of the beam.
4. Strain gauges can return an output over a wide enough range of deflections to accommodate those experienced during use.
5. The geometry of the beams must not significantly change during periods of high loading.

#### **4.2.5 Stress Analysis**

As mentioned, (Chee, 2006) had initiated the design process and manufactured the five components that make up the footplate construct. However, it was not known whether the structure would satisfy the specifications stated above, so an investigation of material properties and stress analysis was undertaken to ensure suitability of the chosen materials prior to instrumentation. Components fail because they break under the load imposed upon them, or the load applied is greater than anticipated. Therefore, an essential requirement of the material is that it behaves within the elastic region under the highest expected load, plus a certain safety margin.

#### 4.2.5.1 *Finite element analysis*

The finite element package MSC Marc<sup>®</sup> was used to model the footplate to ensure that the design was mechanically viable. Analysis was undertaken to ensure thickness and stiffness of the materials were within a suitable range that allowed enough deflection for the strain gauge to provide suitable measures, but would not exceed those in the elastic region of the material. Furthermore, it was important to ensure that the design minimises cross talk through high polar moment of inertia which reduces torsion of Beam B in response to the loading of Beam A.

According to the manufacturer (Vishay Micro Measurements, UK) the limitations of metallic foil strain gauges would mean that a minimum strain of  $1 \mu\epsilon$  would be measurable and a strain of no more than  $500 \mu\epsilon$  was desired. A finite element model was reverse engineered based on the manufactured footplate using 20 node brick elements, which allow deformation in all directions. The Von Mises stress was used when displaying results as it shows the resultant stress.

Loading was set at 1000 N, perpendicular to the inclined face of the loading surface. The load was split equally between four nodes where the forefoot would make contact with the footplate, and a single node where the heel would contact the plate. The resultant Von Mises stress and peak displacements can be seen in Figure 4.4 and Figure 4.5, respectively.

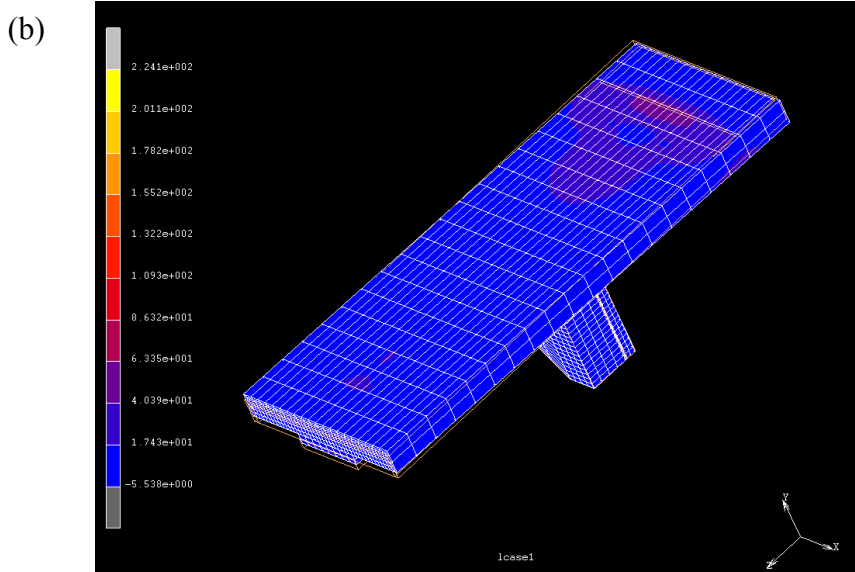
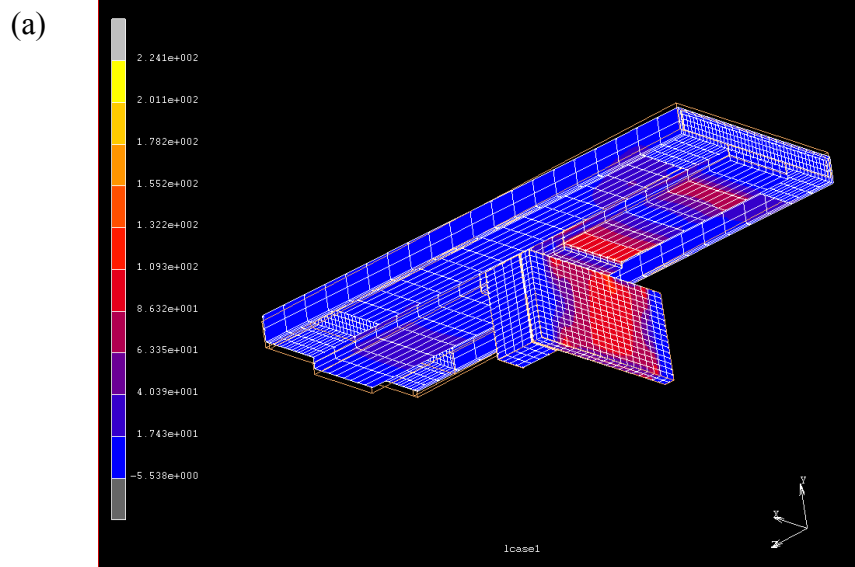


**Figure 4.4: Equivalent Von Mises stresses (MPa) of a 1000 N load applied perpendicular to the footplate loading surface.**

#### 4.2.5.2 Safety factor

Ultimate tensile strength (UTS) is the maximum tension that a material can withstand prior to breaking. Working stress is the highest stress that the material is safely allowed to undergo. Maximum force experienced by Beam A is unlikely to exceed 800 N and



will certainly never exceed 1000 N. For safety it is important that the maximum stress is always less than half the value of the UTS i.e. factor of safety should always be >2. Given the cyclical nature of rowing, where thousands of load-unload cycles will be endured by the footplates, it was also important to account for the fatigue safety factor, where fatigue strength was assumed to be two-thirds of the materials' UTS.

Regarding Beam A and Beam B, Figure 4.4a show that the largest stresses occur adjacent to their constraints, with peak values of 109 MPa. Ultimate tensile strength for stainless steel and aluminium are 579 MPa and 310 MPa, respectively. Thus, based on Equation 4.4 the lowest safety factor within the footplate construct at maximum load would be 2.84, which is greater than the recommended value of 2.

$$\text{Safety Factor} = \frac{\text{Ultimate tensile strength}}{\text{Working stress}} \quad \text{Equation 4.4}$$

Furthermore, based on the relationship between fatigue strength and UTS, where fatigue strength was assumed to be two-thirds of UTS, the fatigue safety factor was calculated using Equation 4.5. The lowest value for fatigue safety factor within the footplate construct at maximum load would be 1.89 which is higher than the recommended value of 1.

$$\text{Fatigue Safety Factor} = \frac{\text{Fatigue Strength}}{\text{Working stress}} \quad \text{Equation 4.5}$$

Figure 4.4b shows the resultant stresses at the loading surface where the loads were applied. The largest stress was seen at the centre where the force was applied, and the blue areas, signalling the areas encountering lowest stress, were seen furthest from the load. Peak stresses on the loading surface were no more than 40 MPa.

#### 4.2.5.3 Peak displacements

The finite element model of the footplate was constrained at the free end of Beam B, as this is where the attachment to the side plate and thus the rest of the ergometer would be made. Consequently, it was necessary to ensure that the footplate did not displace relative to the ergometer when large foot forces were applied by rowers. Using the same loading scenario as described in Section 4.2.5.1, peak vertical displacements were quantified to make sure that inferior displacement of the footplate loading surface did not occur to a notable degree.

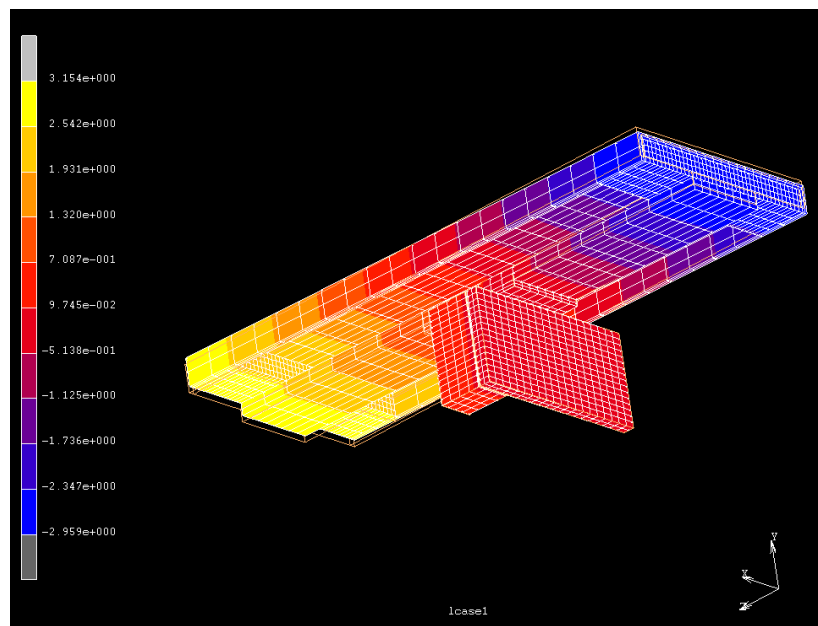


**Figure 4.5: Vertical axis displacements (mm) of the footplate construct in response to a 1000 N split load.**

A load of 1000 N is likely to cause a peak displacement of -3.0 mm at the front of the footplate and 2.5 mm at the rear of the footplate. As the footplate is constrained at the centre where Beam B is located, the middle region of the footplate will displace less than 0.1 mm. The rower should not be sensitive to these changes as these displacements are likely to be smaller than those on a standard ergometer foot-stretcher, and

particularly as the expected peak loads applied by the rower will be considerably less than 1000 N.

#### 4.2.6 Application of Strain Gauges

The output of the finite element model and an analytical analysis showed that the greatest stress, and thus strain, would occur adjacent to the central mounting component (Figure 4.4). Consequently, the strain gauges would be placed on the instrumented Beam A and Beam B as shown below, as this is where strains are expected to be greatest.

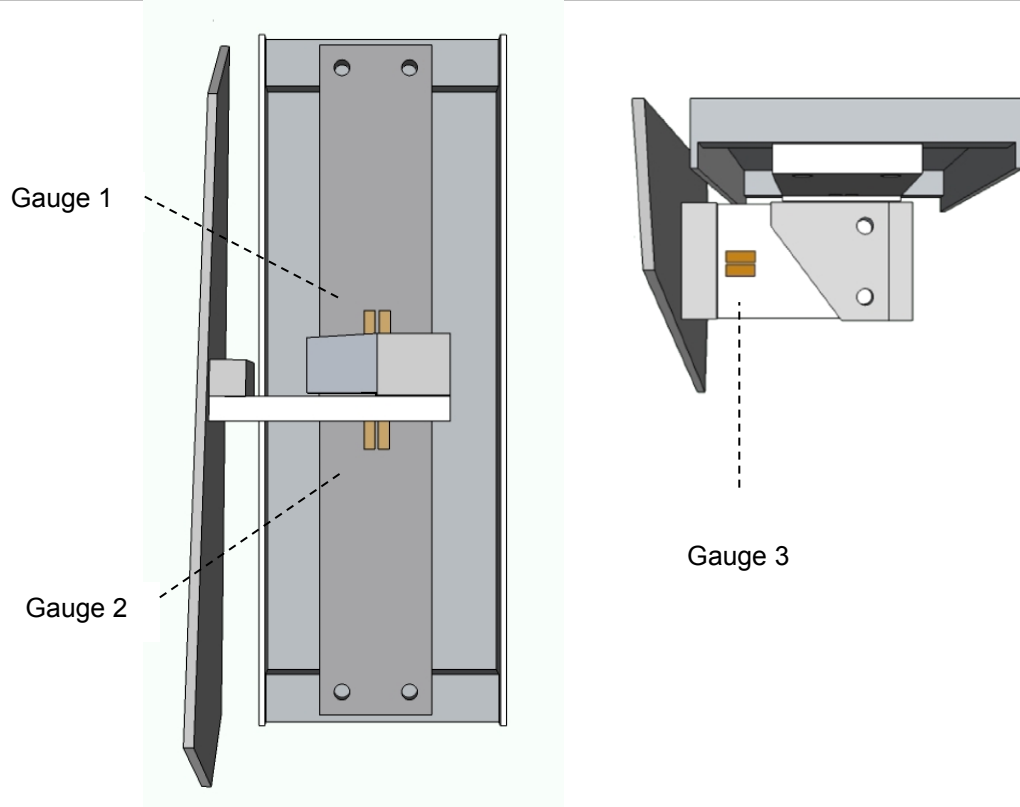


**Figure 4.6: Strain gauges are bonded to beam A and beam B at the locations indicated above. Corresponding number of strain gauges are bonded on the reverse of each beam.**

The output of the finite element model showed that under the 1000 N loading condition, the elements corresponding to the location of the strain gauges were 86  $\mu\epsilon$  for gauge 1 and 68  $\mu\epsilon$  for gauge 2 and 166  $\mu\epsilon$  for gauge 3. These are within the acceptable ranges suggested by the manufacturer and are below the general 0.2 % strain value which is used to define the proof stress.

#### **4.2.7 Bridge circuit**

When a rower pushes against the foot-stretcher, the front of the footplate will be under compression and the reverse will be in tension. The strain on each side of the foot plate should be equal but opposite in magnitude, and this fact was exploited when design of the system's instrumentation was undertaken for this study.

A Wheatstone bridge uses four resistors: one (quarter bridge), two (half bridge) or four (full bridge) of these can be strain gauges to detect the change in resistance of any one of the four arms of the bridge. To achieve maximum sensitivity and a linear output, it was decided that a full Wheatstone bridge circuit consisting of four strain gauges would be employed. The justification of this is explained in the following section. Strain gauges have nominal resistance values and they produce changes in resistance proportional to the strain they are exposed to. Thus, bridge circuits allow the change in voltage that accompanies a change in resistance to be measured. Figure 4.7 shows a bridge circuit.

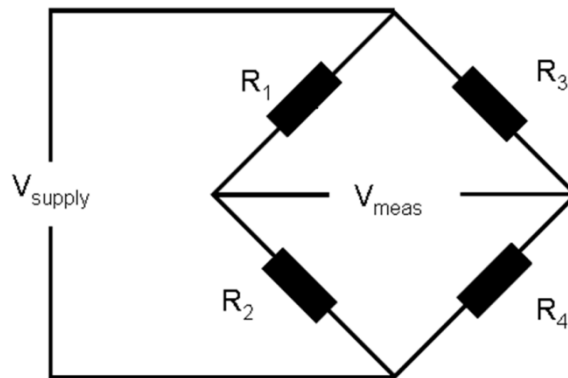


**Figure 4.7: Wheatstone bridge circuit.**

The four strain gauges are arranged such that  $R_1$  and  $R_3$  are on one side of the cantilever beam to measure tension and  $R_2$  and  $R_4$  are on the opposite side to measure the equivalent compression. Each footplate consisted of three Wheatstone bridge circuits so in total there were six channels of data outputted from the footplates.

#### **4.2.8 Justification of a full bridge circuit**

The Wheatstone bridge is a parallel circuit, and as such the bridge voltage output changes when the ratio of  $R_1 / R_2$  or  $R_3 / R_4$  changes.

The circuit acts as a potential divider so:

$$V_{meas} = \left( \frac{R_1}{R_1+R_2} - \frac{R_3}{R_3+R_4} \right) \cdot V_{supply} \quad \text{Equation 4.6}$$

But if  $R_1 = R_2 = R_3 = R_4$

$$V_{meas} = \left( \frac{R_1 - R_2}{R_1+R_2} \right) \cdot V_{supply} \quad \text{Equation 4.7}$$

If  $R_1$ ,  $R_2$ ,  $R_3$  and  $R_4$  are strain gauges with the same nominal resistance, and a local strain causes the resistance of  $R_1$  to change by a small amount ( $\Delta R_1$ ), this will affect the output of the bridge voltage.

$$V_{meas} = V_{supply} \cdot \left( \frac{R_1 + \Delta R_1}{R_1 + \Delta R_1 + R_2} \right) - \left( \frac{R_3}{R_3 + R_4} \right) \quad \text{Equation 4.8}$$

Since  $R_1 \gg \Delta R_1$

$$V_{meas} = V_{supply} \cdot \left( \frac{R_1 + \Delta R_1}{R_1 + R_2} \right) - \left( \frac{R_3}{R_3 + R_4} \right) \quad \text{Equation 4.9}$$

$$V_{meas} = V_{supply} \cdot \left( \frac{R_1 + \Delta R_1 - R_3}{R_1 + R_2} \right) \quad \text{Equation 4.10}$$

$$V_{meas} = V_{supply} \cdot \left( \frac{\Delta R_1}{R_1 + R_2} \right) \quad \text{Equation 4.11}$$

However, if  $R_1$  and  $R_3$  are mounted in the same location, but on opposite sides of a plate which is being bent, then the strain gauges will experience the strain of the same magnitude, but opposite in polarity. One strain gauge will be in compression and the other in tension. The strain gauges will undergo a change in resistance proportional to the strain they are subject to.

$$V_{meas} = V_{supply} \cdot \left( \frac{R_1 + \Delta R_1}{R_1 + \Delta R_1 + R_2} \right) - \left( \frac{R_3 - \Delta R_3}{R_3 - \Delta R_3 + R_4} \right) \quad \text{Equation 4.12}$$

$$V_{meas} = V_{supply} \cdot \left( \frac{R_1 + \Delta R_1}{R_1 + R_2} \right) - \left( \frac{R_3 - \Delta R_3}{R_3 + R_4} \right) \quad \text{Equation 4.13}$$

$$V_{meas} = V_{supply} \cdot \left( \frac{R_1 - R_3 + \Delta R_1 + \Delta R_3}{R_1 + R_2} \right) \quad \text{Equation 4.14}$$

$$V_{meas} = V_{supply} \cdot \left( \frac{2 \cdot \Delta R_1}{R_1 + R_2} \right) \quad \text{Equation 4.15}$$

Equations 4.11 and 4.15 show that by having one strain gauge in tension and another in compression, the bridge voltage is doubled compared to when only one active strain gauge is used. When four active strain gauges are used in a full Wheatstone bridge circuit, the output doubles compared to the half bridge output in Equation 4.15, and noise becomes a less significant factor in the measurement.

Amplifiers are often used to increase the size of a signal, but in doing so they proportionately increase noise. However, by employing a full Wheatstone bridge, sensitivity of the signal is doubled (compared to the half-bridge where two active strain gauges are used) without the effect of multiplying the noise. Furthermore, for a full bridge there is always a linear relationship between applied force and voltage output, whilst quarter-bridge (single active strain gauge) and half-bridge circuits provide an output that is only approximately proportional to applied strain gauge force. For these reasons a full bridge circuit was used.

Temperature changes produce thermal expansion otherwise known as ‘temperature induced strain’. If this issue is not accounted for, then small changes in temperature can result in strain and be wrongly interpreted as force induced strain by the strain gauges. All strain gauges were attached to the same piece of metal, meaning they would undergo the same temperature changes and therefore experience the same thermal expansion and contractions. Therefore, resistance would stay the same relative to each other and the bridge voltage would be unaffected by temperature fluctuations.

The assembled footplate with Beam A and Beam B instrumented with two and one full Wheatstone bridge circuits, respectively, are shown in Figure 4.8.

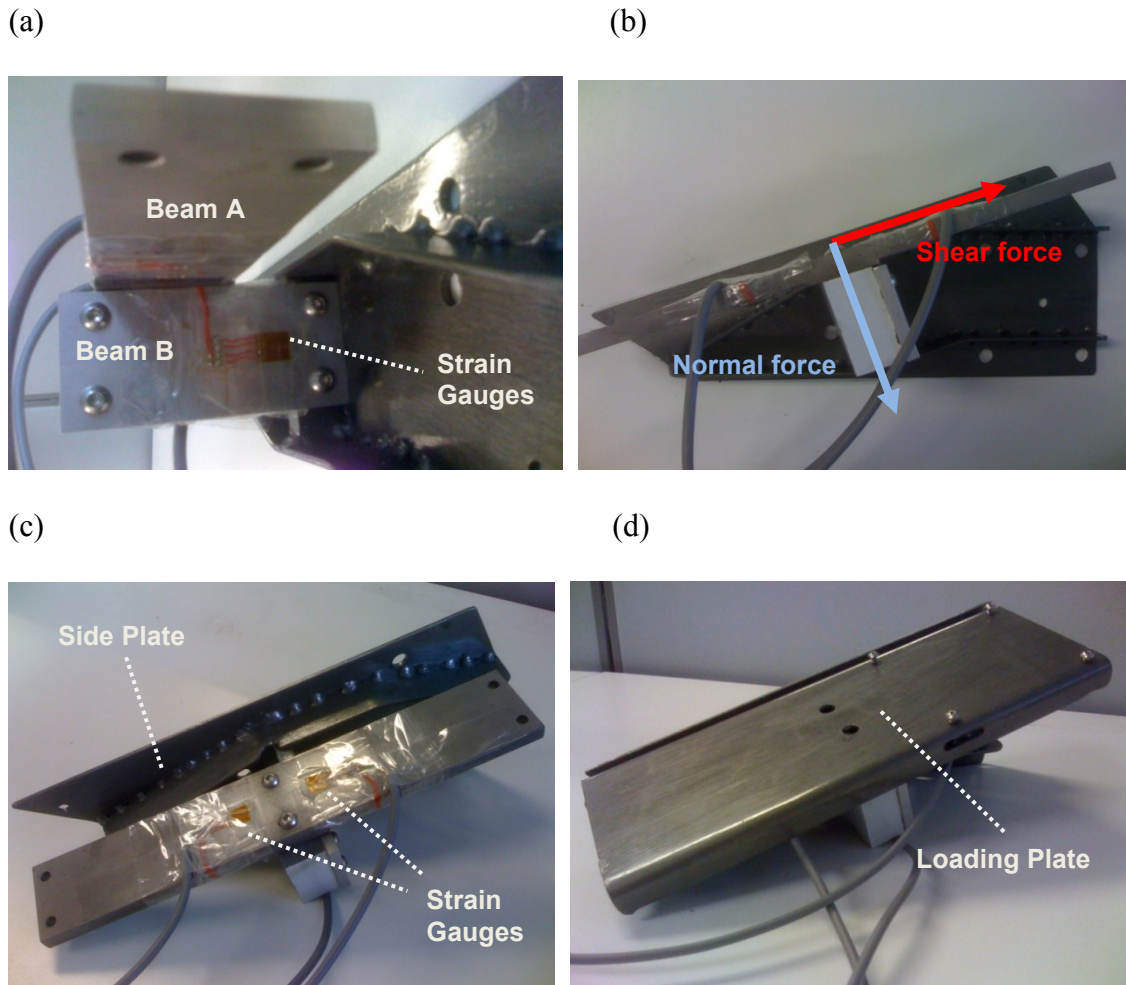


**Figure 4.8:** (a) Beam B's attachment to side plate and Beam A (b) side view of right footplate (c) Beam A and Beam B attached to side plate (d) loading plate attached to Beam A.

#### 4.2.9 Amplification and signal conditioning

The Micro Analog 2 FE-MM8 USB data acquisition system (Fylde Electronic Laboratories Ltd, UK) was used to amplify the bridge voltage and convert data from analog to digital form. The amplifier consisted of four printed circuit boards which supported two channels each, and of these, six channels were used by the footplates. The amplifier's principle gain and offset gain could be adjusted separately. The output was passed through one thousand times amplification, converting mV signals from the



strain gauges into a more substantial V signal. The analogue-to-digital converter was used to log the data to a laboratory computer.

### **4.3 Calibration**

Calibrating force measuring devices ensures that the data outputted by the system accurately represents the forces applied (Hall et al., 1996). For the purpose of this project it was necessary to carry out three separate calibrations:

- calibration of normal force (perpendicular to loading surface)
- calibration of shear force (parallel to loading surface)
- calibration of COP

It was also necessary to correct for any cross talk that occurs between orthogonal axes, as mentioned in the Design Specifications (Section 4.2.1).

The signal conditioning unit for the footplates consists of eight channels. Of these eight channels only six were required for footplate data acquisition. All the signals from the footplates were connected to the PC via a USB plug-and-play interface.

Right Footplate:

- Channel 1 = normal force (front)
- Channel 2 = normal force (rear)
- Channel 6 = shear force

Left Footplate:

- Channel 3 = shear force
- Channel 7 = normal force (rear)

- Channel 8 = normal force (front)

The calibration process allows for accurate comparisons to be made between known magnitudes of force and raw outputs from the test specimen. This allows for voltage outputs from each channel to be converted into known Newton values, by subjecting the raw outputs to calibration coefficients which are derived following a rigorous calibration process.

#### **4.3.1 Normal Force Calibration**

Calibration of normal forces applied to the footplate was performed by securing the footplate against a rigid frame using G-clamps, so that the loading surface was horizontal as verified by a digital spirit meter. A vertical point loading apparatus (PLA), as described in Hall et al. (1996) and Murphy et al. (2010) was utilized, along with several weights of known masses. The PLA consists of a support frame, through which a linear bearing assembly is slotted. At the top of the linear bearing assembly is a loading platform from where loads are applied, and at the bottom is a half sunken ball bearing through which applied loads are transmitted to the plate's surface via a single point (Figure 4.9). The caged ball bearings minimised horizontal shear forces by ensuring the loads were applied vertically.

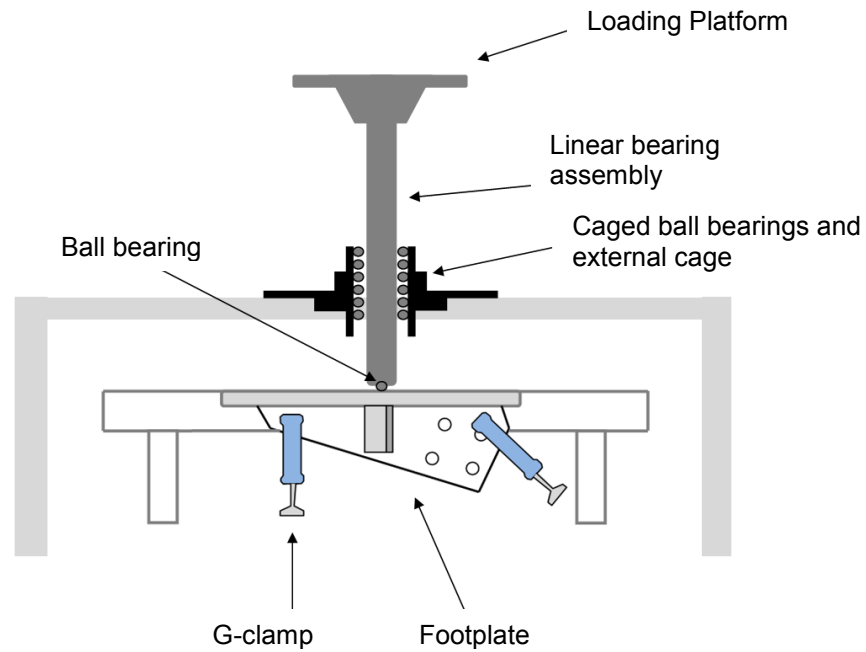


**Figure 4.9: Diagram of right footplate attached to rigid horizontal surface with PLA aligned to calibration point.**

---

Normal force calibration consisted of nine loading conditions. Starting at zero load, masses of up to 80 kg were applied to the loading platform 10 kg at a time. Signal outputs from all channels were continuously recorded for 10 seconds each time a load was added, thus a single calibration trial took a period of 1 minute 30 seconds to complete (Table 4.2). This procedure was performed at 36 locations for both footplates by aligning the ball bearing against each of the red circles on the grid in Figure 4.10.

**Table 4.2: Experimental protocol for normal footplate calibration.**

Left Footplate	Time (seconds)	Right Footplate	Time (seconds)
No Load (0 N)	10	No Load (0 N)	10
10.2 kg (100.1 N)	10	10.2 kg (100.1 N)	10
20.4 kg (200.1 N)	10	20.4 kg (200.1 N)	10
30.8 kg (300.1 N)	10	30.8 kg (300.1 N)	10
40.8 kg (400.2 N)	10	40.8 kg (400.2 N)	10
50.8 kg (498.3 N)	10	50.8 kg (498.3 N)	10
60.8 kg (596.4 N)	10	60.8 kg (596.4 N)	10
70.8 kg (694.5 N)	10	70.8 kg (694.5 N)	10
80.8 kg (792.6 N)	10	80.8 kg (792.6 N)	10

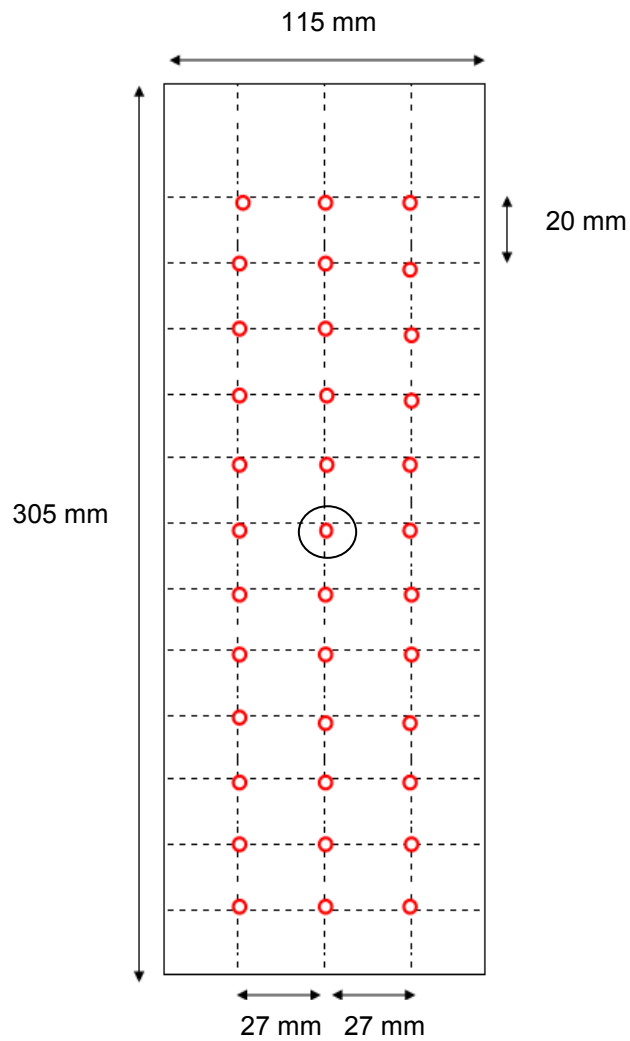


**Figure 4.10: Location of 36 normal calibration points along footplate surface.**

#### 4.3.1.1 Normal calibration results

Shown below is a raw output from a calibration trial of the right footplate at the location circled in Figure 4.10.

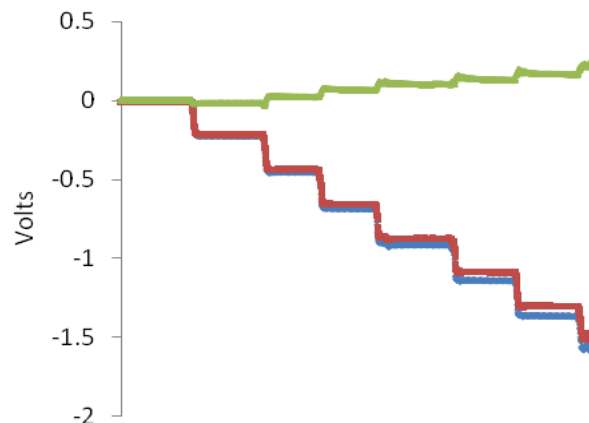


**Figure 4.11: Raw voltage outputs of normal force (front, red), normal force (rear, blue), shear force (green).**

---

A Matlab script was written which averaged the middle two seconds of data of every 10 second cycle. This was done for all three channels of data, thus giving nine averaged voltage values per channel. Once the averaged values had been derived for all 36 calibration points, the calibration coefficients for the normal force measuring transducers could be computed.

#### 4.3.1.2 Computation of normal force magnitude

With 36 calibration points and 9 data points per trial, a single array of data from each transducer consisted of 324 values.

1. Signals from Transducer A (normal force from front of footplate) and Transducer B (normal force from rear of footplate) were combined into a 324 by 2 matrix: **transducer matrix**.
2. Known force values equivalent to the raw transducer signals were put into a 324 by 1 matrix:  $\mathbf{F}_{\text{known}}$
3. Transducer matrix multiplied by a 1 by 2 matrix of calibration coefficients (C) will be equal to the applied loads:  $\mathbf{Transducer\ matrix} \cdot \mathbf{C}_1 = \mathbf{F}_{\text{known}}$
4. Therefore, by using a least squares function in Matlab, values for C can be calculated:  $\mathbf{C}_1 = \mathbf{Transducer\ matrix} \setminus \mathbf{F}_{\text{known}}$
5. Therefore, it can be inferred that:  $\mathbf{F}_{\text{calculated}} = \mathbf{F}_{\text{known}} = \mathbf{Transducer\ matrix} \cdot \mathbf{C}$

The ability of  $\mathbf{C}_1$  to predict the value applied loads on the footplate was quantified by an error analysis (Section 4.3.4) which compares  $\mathbf{F}_{\text{calculated}}$  and  $\mathbf{F}_{\text{known}}$ . Appendix E shows the linear calibration curves comparing  $\mathbf{F}_{\text{calculated}}$  and  $\mathbf{F}_{\text{known}}$ .

#### 4.3.2 Centre of Pressure Calibration

The point of force application i.e. COP can only be determined along the footplate's longitudinal axis, as the footplate does not have the capacity to measure medio-lateral forces along it x-axis. The COP location is quantified based on the calibrated output of Beam A's two transducers. Data collected during the normal force calibration trials were used to compute the COP calibration coefficients.

1.  $F_y$  front and  $F_y$  rear were combined into a 324 by 2 matrix: **transducer matrix**.
2. Known force values equivalent to the raw transducer signals were put into a 324 by 1 matrix:  $\mathbf{F}_{\text{known}}$

3. Known position values equivalent to the raw transducer signals were put into a 324 by 1 matrix:  $\mathbf{z}_{\text{known}}$
4.  $\mathbf{M}_{\text{known}} = \mathbf{F}_{\text{known}} \cdot \mathbf{z}_{\text{known}}$
5.  $\mathbf{C}_2 = \text{transducer matrix} \setminus \mathbf{M}_{\text{known}}$
6.  $\mathbf{M}_{\text{calculated}} = \mathbf{M}_{\text{known}} = \text{transducer matrix} \cdot \mathbf{C}_2$
7.  $\frac{\mathbf{M}_{\text{calculated}}}{\mathbf{F}_{\text{calculated}}} = \mathbf{z}_{\text{calculated}}$

$\mathbf{M}_{\text{known}}$  is a matrix of moments which resulted from known forces applied at known coordinates along the longitudinal surface of the footplate. The efficacy of  $\mathbf{C}_2$  at computing true z position was found by comparing  $\mathbf{z}_{\text{calculated}}$  with  $\mathbf{z}_{\text{known}}$ .

#### 4.3.3 Shear Force Calibration

Calibration of shear force was performed by securing the footplate against a rigid table leg using G-clamps, so that the Loading Place was vertically aligned (Figure 4.12). Inclination was checked to be at 90° using a digital spirit meter.

A calibration plate was designed which could be clamped to the loading surface using miniature G-clamps. The plate was made out of 6 mm thick aluminium and its width and length had the same dimensions as the footplate loading surface (Appendix F). The calibration plate had three countersunk holes drilled into its surface. Weights were applied to the footplate using this plate by inserting a countersunk screw through each hole, so that it sat flush with the calibration plate, and hanging weights from the shaft of this screw.

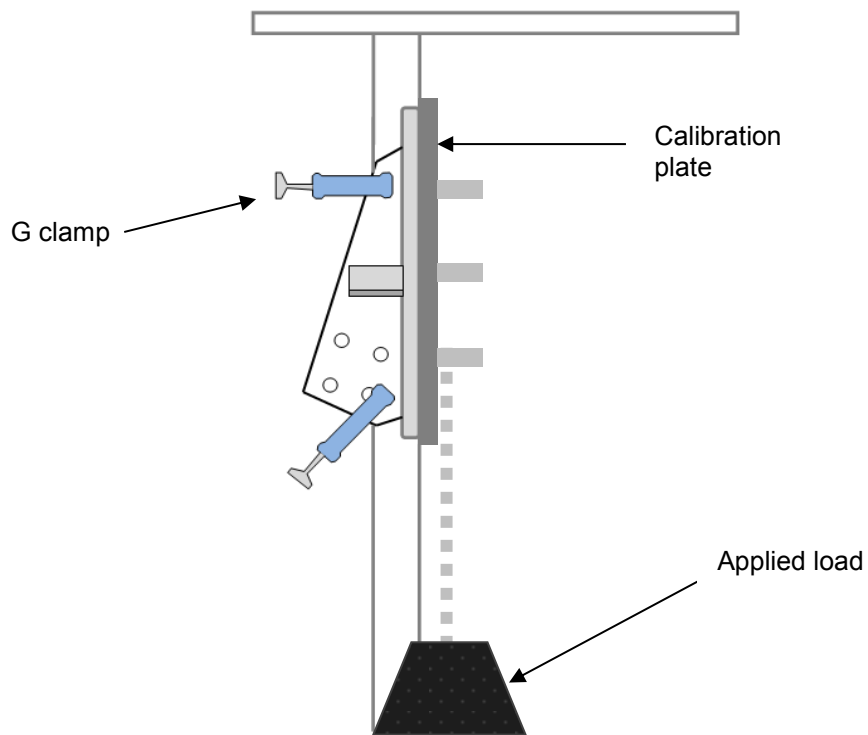


**Figure 4.12: Diagram of footplate attached to rigid vertical surface with weights suspended via a calibration plate.**

---

Shear calibration consisted of 7 loading conditions per trial; zero load, 2.6 kg load (consisting of the plate, chain and G-clamp masses) and subsequent additions of 10 kg loads until 52.6 kg. Signal outputs from all channels were continuously recorded for 10 s each time a load was added, thus a single calibration trial took a period of 1 min 10 sec (Table 4.3). The above procedure was performed at 3 locations for both footplates by hanging weights from a screw at the three calibration points as described below.



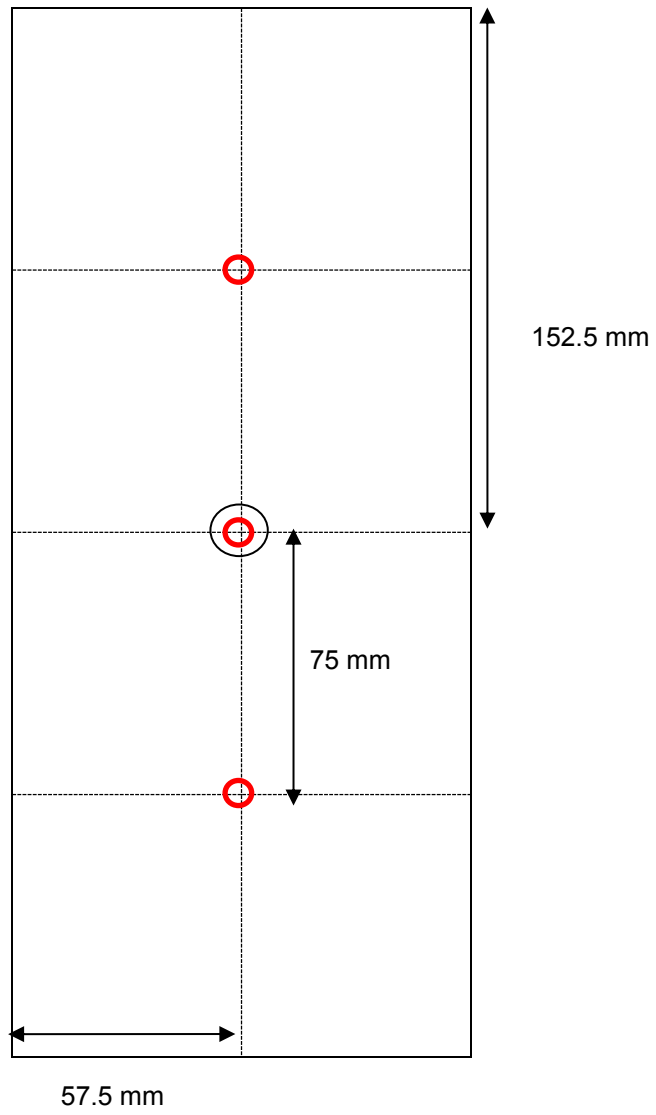


**Figure 4.13: Location of three shear calibration points along footplate surface.**

---

**Table 4.3: Experimental protocol for AP footplate calibration**

<b>Left Footplate</b>	<b>Time (seconds)</b>	<b>Right Footplate</b>	<b>Time (seconds)</b>
No Load (0 N)	10	No Load (0 N)	10
2.6 kg (25.5 N)	10	2.6 kg (25.5 N)	10
12.6 kg (123.6 N)	10	12.6 kg (123.6 N)	10
22.6 kg (221.7 N)	10	22.6 kg (221.7 N)	10
32.6 kg (319.8 N)	10	32.6 kg (319.8 N)	10
42.6 kg (498.3 N)	10	42.6 kg (498.3 N)	10
52.6 kg (596.4 N)	10	52.6 kg (596.4 N)	10

#### 4.3.3.1 Shear force calibration results

Shown below is a raw output from a calibration trial of the right footplate at the location circled in Figure 4.13.

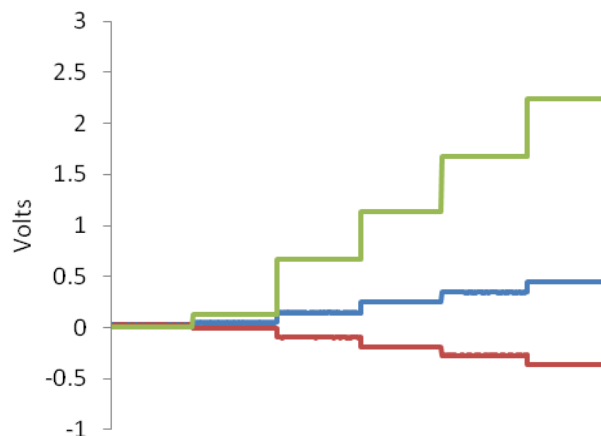


**Figure 4.14: Raw voltage outputs of normal force (front) (red), normal force (rear) (blue), shear force (green).**

In the same way as the normal force calibration, the middle two seconds of data was averaged for each 10 s cycle. Once the averaged data points had been derived at the three calibration points, calibration coefficients for the transducer measuring shear force could be computed.

#### 4.3.3.2 Computation of shear force magnitude

Only one transducer was utilised to record shear forces, so the array of known forces ( $F_{\text{known}}$ ) were plotted against the raw transducer values. A linear regression line was fitted to the data and the regression equation was used to convert the raw signals into Newtons ( $F_{\text{calculated}}$ ). Appendix E shows the linear calibration curves comparing  $F_{\text{calculated}}$  and  $F_{\text{known}}$ .

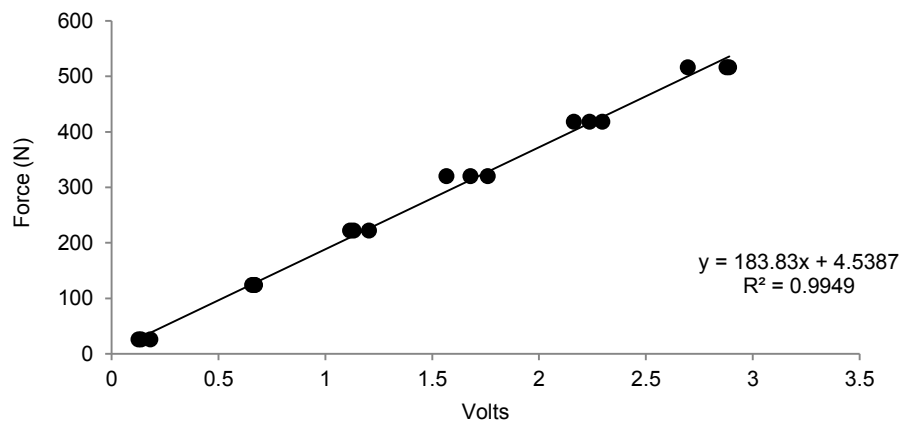


Figure 4.15: Linear regression line to predict shear force values.

#### 4.3.4 Footplate Error Analysis

Comparisons between applied load and calibrated force were made through calculations of mean absolute error (MAE) as a function of applied load. Force transducer manufacturers detail the accuracy of their systems as being within 2% for force measurement, and up to 30 mm in determining COP (Bobbert and Schamhardt, 1990). MAE of calibration errors are in Table 4.4.

Table 4.4: Mean absolute error (MAE) values for right and left footplates. For *Normal* and *Shear* MAE is percentage of applied load. For *COP*, MAE is mean error in mm.

	Normal	Shear	COP
<b>Left</b>	1.8%	4.1%	3.9 mm
<b>Right</b>	1.0%	4.9%	0.9mm

#### **4.3.5 Cross-talk Compensation**

The relevance of force transducers are to measure force along a single or multiple defined axes. The footplates designed for this project consist of sensors which are made to measure forces perpendicular and parallel to the surface of the footplate. However, as mentioned in Design Specifications (Section 4.2.1), when measuring multiple axes, some degree of cross-talk is inevitable. However, cross talk error is thought to be repeatable, so by recording the output of the channel measuring shear force during calibration of normal axis, and vice-versa, the occurrence of systematic cross-talk could be identified and eliminated. During normal calibration there was a clear response in the shear axis which systematically increased at higher loads. At any given load applied in the normal axis the shear error was 2% of the magnitude when the same load was applied in the shear direction. As this was a systematic error, cross talk could be simply corrected by removing the error term from the shear axis.

It is clear from looking at Figure 4.14 and graphs from Appendix G that during shear calibration cross-talk is evident from the two normal force transducers. However, it can also be seen that the responses from those transducers are equal and opposite. This was expected because the load cells were arranged either side of the Mounting Component on Beam A, such that torsion would produce equivalent change on both sides and thus cancel out the cross-talk response. Consequently, when calibrating Beam B, the error terms from the two load cells on Beam A cancel each other out and eliminate the need to correct for those errors.

#### 4.4 Development of biofeedback system

Biofeedback is a process by which instruments record biomechanical or physiological functions in order to provide information on the process being carried out. This is with the intention of modifying the activity in response to the instantaneous feedback, so that individuals can acquire voluntary control of that function.

For the purpose of this study, a program was developed using LabVIEW 2009 (National Instruments, USA) which displays vertical ( $F_y$ ) and horizontal ( $F_z$ ) force traces and COP of the left and right footplates in real-time. This LabVIEW program consists of a data acquisition loop which records data from all eight channels of the amplifier simultaneously at 75 Hz (Appendix H). The data then enters a number of sub-routines which serve to:

- (i) Multiply digitised signals from *Volts* to *Newtons* using the calibration coefficients derived in the previous section.
- (ii) Calculate COP of each footplate.
- (iii) Resolve normal and shear forces measured directly from the footplate into its vertical and horizontal components, using Equations 4.16 and 4.17, based on the inclination of the footplate when affixed to the ergometer (Figure 4.16).

$$F_y = x_1 \cdot \cos\theta - x_2 \cdot \sin\theta \quad \text{Equation 4.16}$$

$$F_z = x_1 \cdot \sin\theta + x_2 \cdot \cos\theta \quad \text{Equation 4.17}$$

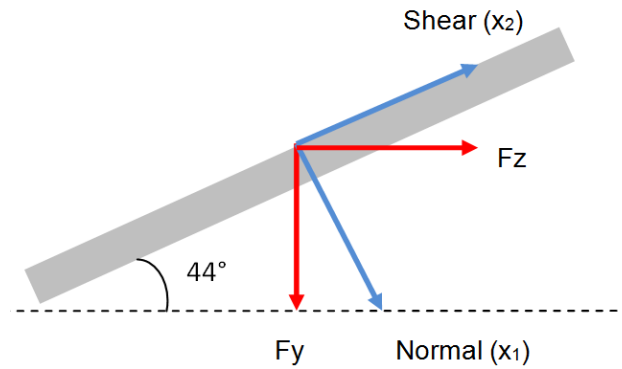


**Figure 4.16: Diagram of footplate showing normal and shear forces resolved into its vertical and horizontal components.  $F_y$  is vertical force,  $F_z$  is horizontal (anterior-posterior) force,  $x_1$  is normal force and  $x_2$  is shear force.**

---

#### 4.4.1 Foot force Biofeedback to GB Rowing

The importance of developing a biofeedback system for immediate feedback of kinetic data to the coach and athlete was highlighted in Section 4.1.1.4. It has previously been shown that objective visual feedback during training sessions can be beneficial in the sport of rowing (Page & Hawkins, 2003). Consequently, a real-time biofeedback display was created for the data outputted from the footplates, so that coaches and athletes can benefit from the biomechanical feedback seen on screen whilst rowing on the ergometer. The display shown in Figure 4.17 was developed after consultations with GB Rowing's coaching and medical staff. It was decided that key features of the real time biofeedback should include:

- Large force traces that can be seen clearly by an athlete rowing 2 metres away.
- Real-time update of force and centre of pressure traces.
- Vertical and horizontal force traces that can be clearly distinguished from each other.
- A clear bilateral comparison of left and right force traces and COP trajectories.

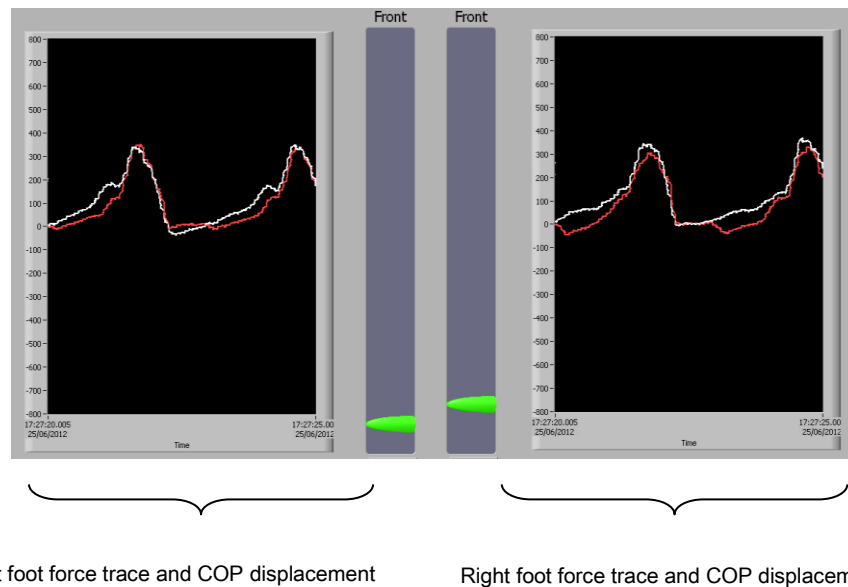


**Figure 4.17: Screenshot of footplate biofeedback and acquisition program. Red traces are horizontal forces, white traces are vertical forces and green bars are longitudinal COP displacement from the rear of the footplate.**

As shown in Figure 4.17 the biofeedback graphically displays the magnitude and shape of the vertical and horizontal force traces, and displays the movement of the foot COP along the longitudinal axis of the footplate. This information is provided for both the right and left foot, thus feedback can also be delivered based on the bilateral symmetry of the data. The data which is displayed in real time can also be logged to a spreadsheet and saved for subsequent data analysis, for the calculation of parameters such as resultant foot force, peak foot forces, impulse and foot force asymmetries. This system was implemented and used, where both the real time biofeedback and post processed quantitative feedback are delivered to GB Rowing athletes and coaches for quarterly testing sessions in the Biodynamics lab. Feedback on foot force profiles and asymmetry based on this instrumentation are important performance criteria that are examined by the medical and coaching staff in their individual athlete assessments (Thompson, 2010).

## 4.5 Summary

This chapter described the design, instrumentation and calibration of bilaterally symmetrical force measuring footplates for the Concept II rowing machine. The footplates were made from stainless steel and aluminium, and consisted of strain gauge instrumented beams which were orthogonally orientated to measure normal forces applied to the front and rear of the footplate, in addition to shear forces. Normal force and shear force had average errors of 1.8%, 4.9% respectively, whilst COP on the footplate could be derived with a mean error of 3.9 mm. Normal and shear forces were subsequently resolved into their global vertical and horizontal components, and these were input into a newly developed biofeedback system which could assess foot force production in rowers.

Following these developments, the instrumented footplates will be utilised in an applied rowing setting, for the acquisition of elite rowers' foot force. The assessment of lower limb asymmetries is a key theme in this thesis, thus bilaterally capturing elite rowers' foot force data will allow for an in-depth analysis of asymmetries during foot force production.



## **Chapter 5:**

### **Application of Instrumented Footplates: Foot force production and asymmetries in elite rowers**

The design, instrumentation and calibration of bilateral force measuring footplates were described in Chapter 4. The objective of the previous chapter was to ensure that a system was developed whereby foot force could be quantified with minimal errors, as a result of appropriate instrumentation, calibration and signal conditioning. In this chapter, the attention shifts towards the application of the system. It was established that the bespoke footplates could quantify force and COP with mean absolute errors of 1.8%, 4.9% and 3.9 mm for normal force, shear force and COP respectively, and fulfilled the design criteria outlined in Section 4.2.1. However, prior to integrating the footplate system with the instrumented ergometer system (i.e. instrumented handle, seat, flywheel and FOB described in Chapter 2), it was necessary to first test the efficacy of the footplates as a standalone feature. This would allow for a more in-depth understanding of elite rowers' force output, and further, enable detailed analysis of their foot force asymmetries, which is a key aim of this thesis. Consequently, the goal of this chapter was to collect a vast quantity of foot force data from a large group of elite rowers, and to examine their foot force patterns and the resulting bilateral asymmetries.

## **5.1 Introduction**

### **5.1.1 The Leg drive**

Rowing is considered an extremely physically demanding sport, where, in addition to the utmost fitness and strength, technical ability and skill are essential in achieving a high boat velocity (Nolte, 2004). Accurate sequencing of lower limb, trunk and pelvic motions are thus extremely important considerations in kinematic studies of elite rowers, and this has been highlighted in Section 3.1.1. Correct sequencing of the rowing stroke is important because it enables the rower to optimise the transfer of power initiated during the leg drive to the ergometer handle and oars (Hofmijster et al., 2008). The force at the handle is critical to the propulsive force developed at the blade, and in turn, force developed at the hand depends on the force generated at the foot-stretcher (Baudouin and Hawkins, 2002). Rowing performance is, therefore, fundamentally dependent on the rower's ability to develop large foot-stretcher forces and to efficiently transmit these forces to the upper limbs.

The leg drive occurs at the start of the rowing stroke (i.e. the catch) where the oars are placed in the water and the rowers' lower limbs are at their most compressed. At this point the rowers rapidly extend their knees to enable the quadriceps to generate large muscle forces, whilst the body remains anteriorly rotated and their arms remain straight. This portion of the drive phase is known as the leg drive (McArthur, 1997). Although the rowers continue to drive with the legs as they open up their backs, the initial leg drive is crucial in the subsequent sequencing of the trunk and arms because it provides the initial power that is transferred through a strong, stable core, which is ultimately transmitted to the handle/oars (Nolte, 2004).

Reaction forces at the feet are often used to assess an individual's leg power and athletic performance (Munro et al., 1987, Buckthorpe et al., 2012). Clearly, the leg drive is a key component of the rowing stroke. Therefore, the ability to quantify foot forces and their asymmetries will provide insights into constituents of an effective rowing stroke, thus enabling prediction of good rowing performance.

### **5.1.2 Foot force asymmetries in rowing**

As mentioned in Section 4.1.2 biomechanical measures of foot forces in rowing are rare, and it is even less common to see a kinetic analysis of the leg drive with reference to symmetry of the force outputs. Murphy (2009) has previously shown that elite rowers exhibit asymmetrical COP motion on the ergometer seat. A key contributor to COP motion at the seat is the drive through the legs, where it is postulated that an asymmetric drive will lead to asymmetric COP motion. Therefore, it is necessary to first examine in detail the loading through the footplates.

Baca et al. (2006a) tested four elite male rowers on; a single scull, a static Concept II ergometer and a Concept II ergometer on slides (enabling the entire ergometer system to slide back and forth). These all had portable instrumented footplates fitted onto the foot-stretchers so that vertical and horizontal forces could be measured bilaterally. They reported just the horizontal force component and found asymmetries to be present in all rowing conditions, although they were greater on the ergometer slides and boat conditions compared to the static ergometer. In an investigation of two scullers, (Colloud et al., 2001) found large bilateral asymmetries on the foot-stretchers of a Concept II ergometer. Although, interestingly, and contradicting the work by Baca (2006a), these asymmetries disappeared when the ergometer was placed on slides.

Scullers are considered to have symmetrical force outputs due to their symmetrical rowing action on the water, compared to sweep rowers. Sweep rowers have asymmetrical movement patterns when rowing on-water, with their outside arm following a larger arced trajectory compared to the inner arm, and the trunk rotating to follow the arced trajectory of the arms (McArthur, 1997). With regards to the impact of upper body and trunk asymmetry on bilateral foot force production, seven national sweep rowers were reported to exhibit asymmetrical reaction forces on the foot-stretchers, despite rowing in kinematically symmetrical conditions on a static Concept II ergometer (Janshen et al., 2009).

It is shown in these small numbers of studies that even highly experienced rowers can demonstrate notable foot force asymmetries. Initiating the drive phase of the rowing stroke with asymmetrical lower limb force production may cause compensatory pelvic rotations and moments about the lumbar spine to enable the handle trajectory to be kept in a straight line. As such, resulting moments about the lumbar spine would have to be countered by stabilising lower back muscles such as the transverses abdominis and erector spinae. Imbalanced loading of these muscles may, in turn, influence the risk of attaining lower back injuries (Oddsson and De Luca, 2003). Therefore, asymmetries may have a knock-on effect along the kinematic chain of the rowers' segments and may be compensated by lower back imbalances in order to maintain dynamic stability of the closed chain system (Colloud et al., 2001). Consequently, from the viewpoints of both performance enhancement and injury prevention, the measurements of bilateral foot forces are important, so that the degree of asymmetrical loading can be quantified.

Studies that examined kinetic asymmetries provide insight into the application of instrumented footplates, with all finding evidence of asymmetries under the feet in elite

rowers. However, due to their small sample sizes the studies were underpowered and adequate statistical analyses could not be performed on the data. There is to date no body of work which has utilised instrumented footplates to comprehensively analyse foot forces of a substantial number of elite rowers over multiple testing sessions. This chapter focuses on the comprehensive analysis of foot force data, and understanding the foot force pattern and asymmetries that elite rowers exhibit. Therefore, the aims of this study were to (a) utilise the newly developed instrumented footplates to assess the reliability of the acquired foot force curves, (b) examine the relationship between foot force and asymmetries at incremental stroke rates, and (c) assess the effect of longitudinal feedback on foot force parameters.

## **5.2 Methodology**

### **5.2.1 Participants**

The study received ethical approval from the Imperial College Research Ethics Committee, and informed consent was obtained from all subjects (Appendix B). Seventeen elite rowers participated in this study in July 2011, all of whom were selected in the GB rowing squad for the 2011 Rowing World Championships. Five were heavyweight female scullers (SCULL; mass  $78.2 \pm 2.1$  kg, age  $29.6 \pm 3.2$ ), six were heavyweight female rowers (SWEEP; mass  $73.4 \pm 4.0$  kg, age  $24.8 \pm 1.3$ ) and six were lightweight men (LWM; mass  $74.1 \pm 0.9$  kg age  $25.8 \pm 3.3$ ). Of the LWM group, two were scullers and 4 were sweep rowers, however they were considered as a single group. The sample size of seventeen was slightly greater than the required number of fifteen which was necessary to achieve a moderate effect size of 0.5 and statistical power of 95% with an alpha significance level of 0.05. All participants were right leg dominant

as defined by their preferred kicking leg. Subjects with a leg difference of more than 1 cm were excluded from this study because anatomical asymmetries may influence the results of this study. Additionally, rowers with a current episode of LBP or any other serious illness or injury were excluded from participation in this study.

Data for the main analysis of this study was obtained during a single testing session in 2011. However, for the longitudinal analysis, data recorded in February, July and October 2011 were examined. Of the original 17 subjects, 11 participated in all three sessions. However, a number of these athletes were unable to perform all four steps during each visit. Therefore, data from six rowers (3 x SCULL, 1 x SWEEP and 2 x LWM) who fully completed all three testing sessions in 2011 were analysed. These rowers satisfied all the inclusion criteria.

### **5.2.2 Experimental Protocol**

After a 10-minute warm up each athlete performed an incremental step test on a Concept II ergometer which had its traditional foot-stretchers replaced with the instrumented footplates developed in Chapter 4. The Step Test involved rowing for three minutes at each of the following stroke rates:

- 18 strokes per minute at an effort equivalent to 55% of their 2 km personal best split.
- 24 strokes per minute (no split given).
- 28 strokes per minute (no split given).
- Free rate i.e. an arbitrary stroke rate that corresponds to rowing a 500 m split at an intensity of their 2000 m personal best (McGregor et al., 2008).

Sufficient rest was permitted between each step. All rowers had previously performed this step test on multiple previous occasions, thus were familiar with the protocol.

### **5.2.3 Data Acquisition**

A programme was written in LabView (National Instruments, USA) to collect, process, and give a real time display of vertical and horizontal foot force and COP motion (Figure 4.17). All raw data was recorded at 75 Hz and saved to an ASCII file. Raw data consisted of the following arrays of data:

1. Right footplate vertical force (N)
2. Left footplate vertical force (N)
3. Right footplate horizontal force (N)
4. Left footplate horizontal force (N)
5. Right footplate centre of pressure (cm)
6. Left footplate centre of pressure (cm)

### **5.2.4 Data Analysis**

All data analysis was performed using a custom written Matlab script.

#### *5.2.4.1 Time normalisation*

To enable comparisons of rowing strokes between and within subjects, individual strokes were time normalised from 0-100%. To implement a robust time normalisation it was necessary to find a consistent and reliable means of identifying the starting point (i.e. 0%) of the rowing stroke. The start of the stroke cannot be considered the *catch*

due to the absence of handle force and handle position data, so in this case the movement of COP along the foot-stretcher surface was used to distinguish between consecutive rowing strokes. The start of each stroke was identified as the time corresponding to the bilateral average of the most anterior displacement of COP along the longitudinal axis of each foot-stretcher (Figure 5.1). Once these points were identified for all consecutive strokes, the data points in between were interpolated to 101 data points, enabling each stroke to be expressed in percentage stroke cycle (0-100%).

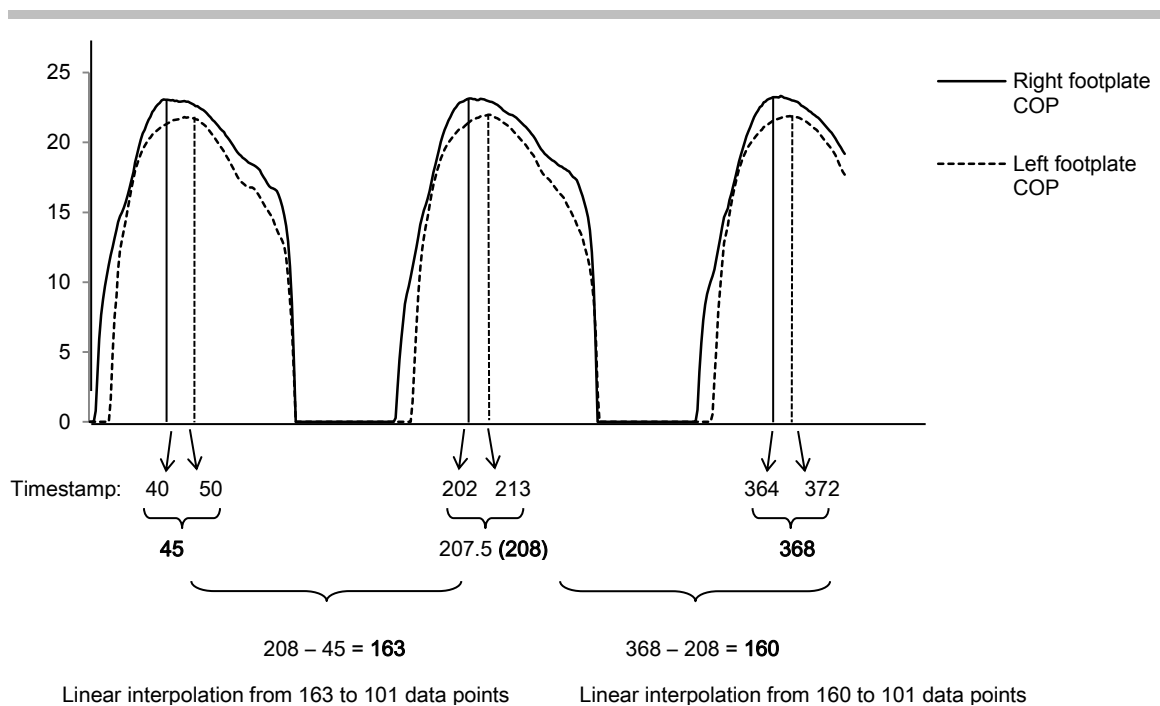


**Figure 5.1: Centre of pressure traces of the right and left footplate depicting the time normalisation process.**

Using footplate COP data is not a traditional means of identifying the start of the stroke. However, the footplates were utilised as standalone instruments in this study, so without additional kinematic or external force data, it was considered the most appropriate way of identifying the start of a stroke. All strokes within each three-minute Step were time normalised. Of all the normalised strokes recorded within a Step, ten strokes in the



middle of each trial were extracted for statistical analysis. This was so that any acceleration or deceleration phases at the start and end of each piece are discarded, and ten highly repeatable and consistent strokes could be analysed (Appendix D).

#### 5.2.4.2 *Derived foot force parameters*

From ten extracted time normalised strokes, the following foot force parameters were calculated:

1. Stroke time (s)
2. Peak resultant force (N/kg)
3. Peak vertical force (N/kg)
4. Peak horizontal force (N/kg)
5. Timing of peak vertical force (%)
6. Timing of peak horizontal force (%)
7. Resultant impulse (N.s/kg)
8. Vertical impulse (N.s/kg)
9. Horizontal impulse (N.s/kg)

The raw bilateral foot force data was summed prior to time normalisation of each stroke, so that in addition to right and left foot force, summed foot force parameters could be calculated. Consequently, all of the parameters above were calculated individually for the right footplate, left footplate and the bilateral sum of the right and left footplates. Bilateral forces were summed when considering foot force as a performance parameter, but were examined independently when investigating parameters relating to asymmetry. All forces were normalised to the rowers' body mass (BM) in kilograms.

#### 5.2.4.3 Resultant force

Vertical and horizontal components of foot force were directly measured from each footplate. Resultant force was derived from the vertical and horizontal force vectors using Equation 5.1.

$$\text{Resultant force (N)} = \sqrt{(\text{vertical force}^2 + \text{horizontal force}^2)} \quad \text{Equation 5.1}$$

Resultant foot force was calculated as it gives a value of the overall magnitude of force applied to each foot-stretcher. Consequently, it is important to obtain measures of asymmetry for this parameter.

#### 5.2.4.4 Impulse

Impulse was calculated as the area under the force-time curve between the start of the stroke (0%) and the minimum force value within the stroke (Figure 5.2). Area under the curve was calculated using the trapezoidal rule. That is, the area of a trapezium was calculated for every time interval from the start of the stroke until the point of minimum foot force occurrence, and these values were summed to obtain a single impulse value per stroke.

$$\text{Impulse (N.s/kg)} = \Delta x / 2 \cdot (y_0 + 2y_1 + 2y_2 + \dots + 2y_{n-1} + y_n) \quad \text{Equation 5.2}$$

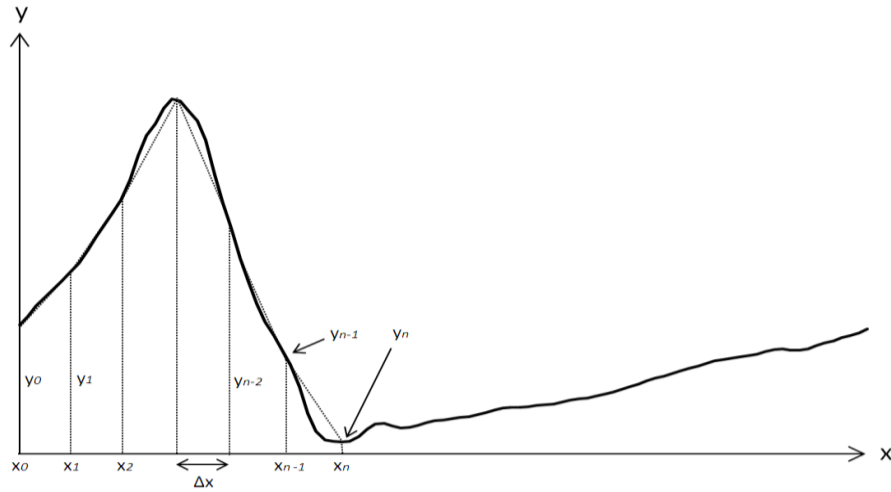


**Figure 5.2: Illustrative example of the calculation of impulse (i.e. area under the curve) using the trapezoidal method.**

Time was converted from stroke cycle (%) back to seconds for the purpose of calculating impulse. This was possible because stroke time was one of the extracted foot force parameters. Figure 5.3 also depicts how peak forces and the timing of peak forces were identified.

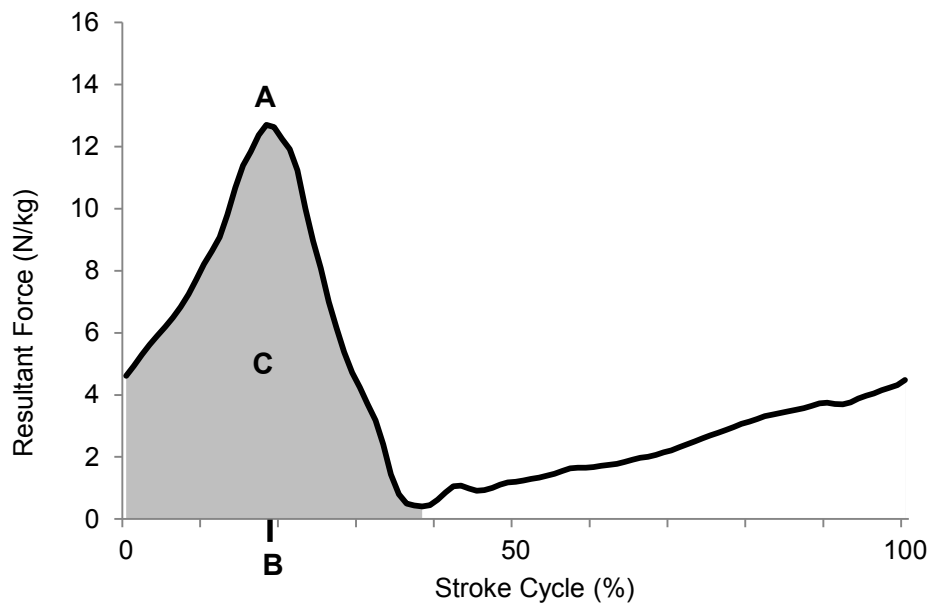


**Figure 5.3: Illustrative example of parameters calculated within a stroke: A is value of peak vertical force, B is the timing of peak vertical force, and C is the vertical impulse i.e. area under the curve above between 0% and minimum force. Parameters for the horizontal force component and resultant force were calculated in the same way.**

#### 5.2.4.5 *Asymmetry Index*

Bilateral asymmetry values for derived foot force parameters were quantified using the absolute version of the symmetry index, originally proposed by Robinson et al. (1987). The traditional symmetry index indicates the direction of symmetry, for example positive value indicates right side dominance and negative value indicates left side dominance. However, for the purpose of this study, it was necessary to calculate absolute values so that the problem of zero mean asymmetry values could be avoided i.e. where negative asymmetries and positive asymmetries would average out to be zero. Consequently, ASI of each rower with respect to the parameters listed above was calculated using Equation 5.3.

$$ASI (\%) = \frac{2|X_{right} - X_{left}|}{(X_{right} + X_{left})} \cdot 100 \quad \text{Equation 5.3}$$

$X_{right}$  is the value of the right limb and  $X_{left}$  is the value of the left limb. An ASI value of zero indicates perfect symmetry, and increasingly positive values indicate increasing bilateral asymmetries between the left and right sides.

#### 5.2.5 **Statistical Analysis**

Coefficient of multiple determination (CMD) (Kadaba et al., 1989) was calculated for the ten normalised force traces to quantify each rower's inter-cycle consistency. CMD was also used as a measure of reliability of the footplates as a force measuring device. Coefficient of variance (CV) was employed to examine the variability in peak force and impulse values. All statistical analyses were performed using SPSS (version 19, IBM Corporation, New York, USA). Group means and standard deviations were computed.

After testing for normality using the Shapiro-Wilk test, a two-way mixed model ANOVA was run to determine whether differences in outcome variables between and within groups were statistically significant. Significance level was set at  $P < 0.05$ , and where an overall significance was seen for the within groups main effect, Bonferroni post-hoc tests were conducted to locate differences.

## **5.3 Results**

### **5.3.1 Reliability**

CMD was very high within 10 strokes, averaging  $0.98 \pm 0.02$ ,  $0.98 \pm 0.01$ , and  $0.98 \pm 0.02$ , for resultant, vertical and horizontal force traces respectively (Table 5.1). These results support the use of COP as a reliable means of identifying a consistent point in new strokes, as it indicates ability of the footplates to measure force with high consistency and repeatability.

**Table 5.1: Coefficient of multiple determination (CMD) values for bilaterally summed foot force traces, across all four rates and all three groups.**

<b>Rate</b>	<b>Group</b>	<b>Peak resultant force</b>	<b>Peak vertical force</b>	<b>Peak horizontal force</b>
<b>18</b>	<b>LWM</b>	0.96 ± 0.03	0.97 ± 0.03	0.95 ± 0.05
<b>18</b>	<b>SCULL</b>	0.98 ± 0.01	0.99 ± 0.01	0.98 ± 0.02
<b>18</b>	<b>SWEEP</b>	0.98 ± 0.02	0.98 ± 0.01	0.97 ± 0.03
<b>24</b>	<b>LWM</b>	0.98 ± 0.01	0.98 ± 0.01	0.98 ± 0.02
<b>24</b>	<b>SCULL</b>	0.98 ± 0.01	0.98 ± 0.01	0.97 ± 0.02
<b>24</b>	<b>SWEEP</b>	0.99 ± 0.01	0.99 ± 0.01	0.98 ± 0.01
<b>28</b>	<b>LWM</b>	0.99 ± 0.01	0.99 ± 0.01	0.98 ± 0.01
<b>28</b>	<b>SCULL</b>	0.99 ± 0.01	0.99 ± 0.01	0.99 ± 0.01
<b>28</b>	<b>SWEEP</b>	0.98 ± 0.02	0.98 ± 0.02	0.97 ± 0.03
<b>Free</b>	<b>LWM</b>	0.98 ± 0.01	0.99 ± 0.01	0.98 ± 0.01
<b>Free</b>	<b>SCULL</b>	0.98 ± 0.02	0.98 ± 0.01	0.98 ± 0.02
<b>Free</b>	<b>SWEEP</b>	0.98 ± 0.02	0.99 ± 0.01	0.99 ± 0.01
	<b>Average</b>	<b>0.98 ± 0.02</b>	<b>0.98 ± 0.01</b>	<b>0.98 ± 0.02</b>

Additionally, it suggests that elite rowers tested in this study exhibited a high level of consistency in foot force production. There was no significant difference in CMD across different stroke rates or between groups, indicating that these groups of elite rowers all exhibited a similar level of consistency in force production, independent of stroke rate.

Coefficient of variance was calculated for peak force and impulse values (Table 5.2). The parameter with the greatest variance was peak horizontal force at 3.33%. However, all other parameters had CV values of less than 2.57% which is indicative of little variation in calculated parameters amongst ten consecutive strokes. Again there was no change in CV with respect to stroke rate for any of the measured parameters, thus highlighting the ability of the foot-stretchers to measure force reliably, as well as the rowers' high level of consistency across incremental stroke rates.

Table 5.2: Coefficient of variance values (average  $\pm$  SD) for foot force parameters for all three groups across all four rates.

Rate	Group	Peak resultant force (%)	Peak vertical force (%)	Peak horizontal force (%)	Peak resultant impulse (%)	Peak vertical impulse (%)	Peak horizontal impulse (%)
18	LWM	3.5 $\pm$ 1.7	3.93 $\pm$ 2.2	4.4 $\pm$ 3.0	3.2 $\pm$ 2.9	4.2 $\pm$ 4.0	2.8 $\pm$ 1.2
18	SCULL	1.6 $\pm$ 0.7	2.16 $\pm$ 0.6	3.2 $\pm$ 1.0	1.6 $\pm$ 0.5	2.1 $\pm$ 0.6	1.9 $\pm$ 0.4
18	SWEEP	1.54 $\pm$ 0.8	3.16 $\pm$ 0.8	3.4 $\pm$ 0.9	1.8 $\pm$ 0.5	2.8 $\pm$ 1.3	1.8 $\pm$ 0.4
24	LWM	2.3 $\pm$ 2.0	2.76 $\pm$ 2.0	3.9 $\pm$ 2.4	1.7 $\pm$ 0.5	2.4 $\pm$ 1.1	2.1 $\pm$ 1.3
24	SCULL	1.4 $\pm$ 0.5	1.84 $\pm$ 0.6	3.5 $\pm$ 2.3	1.9 $\pm$ 0.6	2.3 $\pm$ 0.8	1.9 $\pm$ 0.9
24	SWEEP	1.3 $\pm$ 0.3	2.65 $\pm$ 0.5	2.6 $\pm$ 0.4	1.8 $\pm$ 0.6	2.4 $\pm$ 1.0	1.7 $\pm$ 0.6
28	LWM	2.0 $\pm$ 0.8	3.02 $\pm$ 1.6	4.3 $\pm$ 1.9	1.4 $\pm$ 0.7	1.9 $\pm$ 0.7	2.1 $\pm$ 1.0
28	SCULL	1.4 $\pm$ 0.1	1.85 $\pm$ 0.2	2.4 $\pm$ 0.5	1.6 $\pm$ 0.6	1.5 $\pm$ 0.8	2.0 $\pm$ 0.9
28	SWEEP	1.6 $\pm$ 0.6	2.09 $\pm$ 0.8	2.3 $\pm$ 0.7	2.8 $\pm$ 1.9	3.3 $\pm$ 2.0	2.4 $\pm$ 1.3
Free	LWM	2.3 $\pm$ 1.0	2.52 $\pm$ 1.4	5.1 $\pm$ 1.9	1.8 $\pm$ 0.8	2.4 $\pm$ 1.0	2.1 $\pm$ 0.8
Free	SCULL	1.4 $\pm$ 0.6	1.80 $\pm$ 1.0	2.6 $\pm$ 1.0	2.4 $\pm$ 1.8	2.9 $\pm$ 2.5	2.12 $\pm$ 1.2
Free	SWEEP	1.1 $\pm$ 0.3	1.66 $\pm$ 0.8	2.3 $\pm$ 0.8	2.2 $\pm$ 1.6	2.6 $\pm$ 1.9	2.1 $\pm$ 1.5
<b>Average</b>		<b>1.8 <math>\pm</math> 0.8</b>	<b>2.5 <math>\pm</math> 1.1</b>	<b>3.3 <math>\pm</math> 1.4</b>	<b>2.0 <math>\pm</math> 1.1</b>	<b>2.6 <math>\pm</math> 1.5</b>	<b>2.1 <math>\pm</math> 1.0</b>

### 5.3.2 Total foot force

LWM had greater peak resultant foot force than SCULL and SWEEP ( $P<0.01$ ) and greater peak vertical force than SWEEP ( $P<0.05$ ; Figure 5.4).

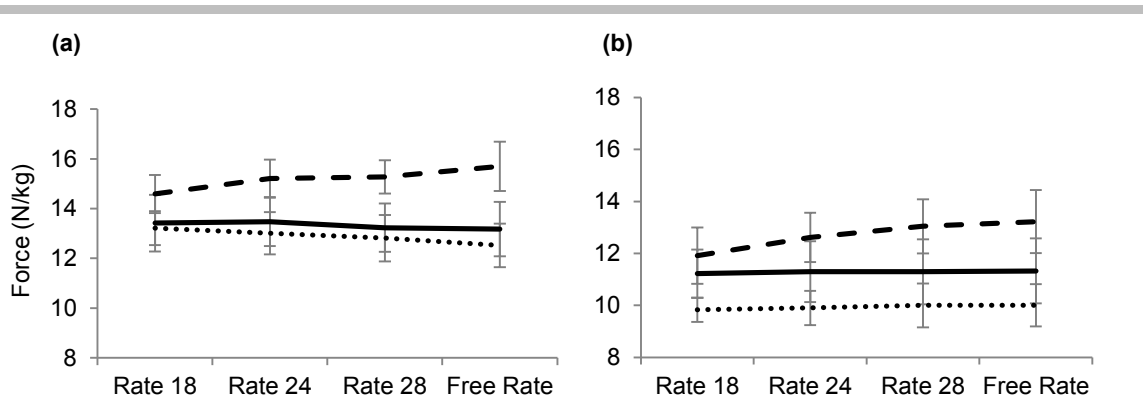


Figure 5.4: (a) Change in peak resultant force and (b) change in peak vertical force with respect to stroke rate. Thick dashed line is LWM, solid line is SCULL and dotted line is SWEEP. Error bars are  $\pm$  SD.

Resultant and vertical impulse followed a similar trend to the peak values, with LWM exhibiting significantly greater resultant impulse compared to SCULL and SWEEP, and significantly greater vertical impulse than SWEEP ( $P<0.05$ ; Figure 5.5).

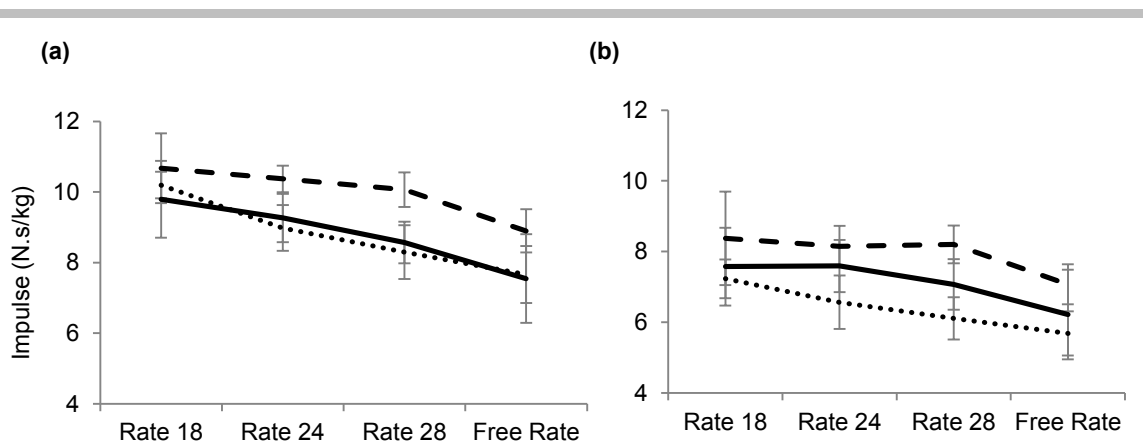
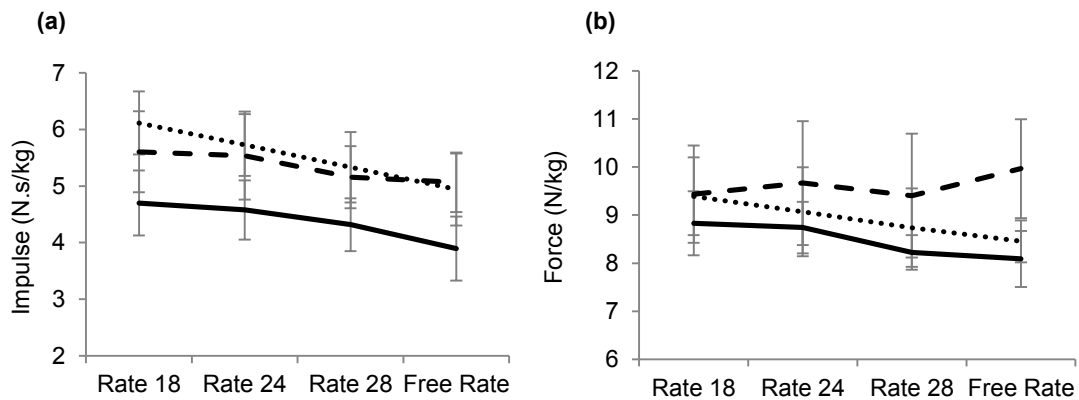


Figure 5.5: (a) Change in resultant impulse and (b) change in vertical impulse with respect to stroke rate. Thick dashed line is LWM, solid line is SCULL and dotted line is SWEEP. Error bars are  $\pm$  SD.



There were no significant differences in peak horizontal force between groups, except where horizontal impulse was significantly greater in SWEEP compared to SCULL ( $P<0.05$ ; Figure 5.6).



**Figure 5.6: (a) Change in horizontal impulse and (b) change in peak horizontal force with respect to stroke rate. Thick dashed line is LWM, solid line is SCULL and dotted line is SWEEP. Error bars are  $\pm$  SD.**

When examining data at progressive stroke rates, no change was observed in peak resultant or vertical forces in response to an increase in stroke rate. However, there was a significant reduction in peak horizontal force between Steps 1 and 3 and Steps 2 and 3 ( $P<0.01$ ). There were reductions in resultant, horizontal and vertical impulse as a function of rate due to stroke time decreasing at higher rates ( $P<0.001$ ). Timing of peak forces also changed with respect to rate, with peak horizontal force occurring later at higher stroke rates ( $P<0.05$ ). Furthermore, the timing of peak horizontal force occurred later in LWM compared to SCULL and SWEEP ( $P<0.01$ ). These occurrences are evident in the bilaterally summed resultant, horizontal and vertical foot force traces shown in Figure 5.7

There were significant interaction effects for peak resultant force ( $P<0.05$ ) and peak vertical force ( $P<0.05$ ). These parameters increased with respect to rate for LWM. However, SCULL and SWEEP had reductions in peak resultant force with respect to rate, and no change in peak vertical force with respect to rate (Figure 5.7).

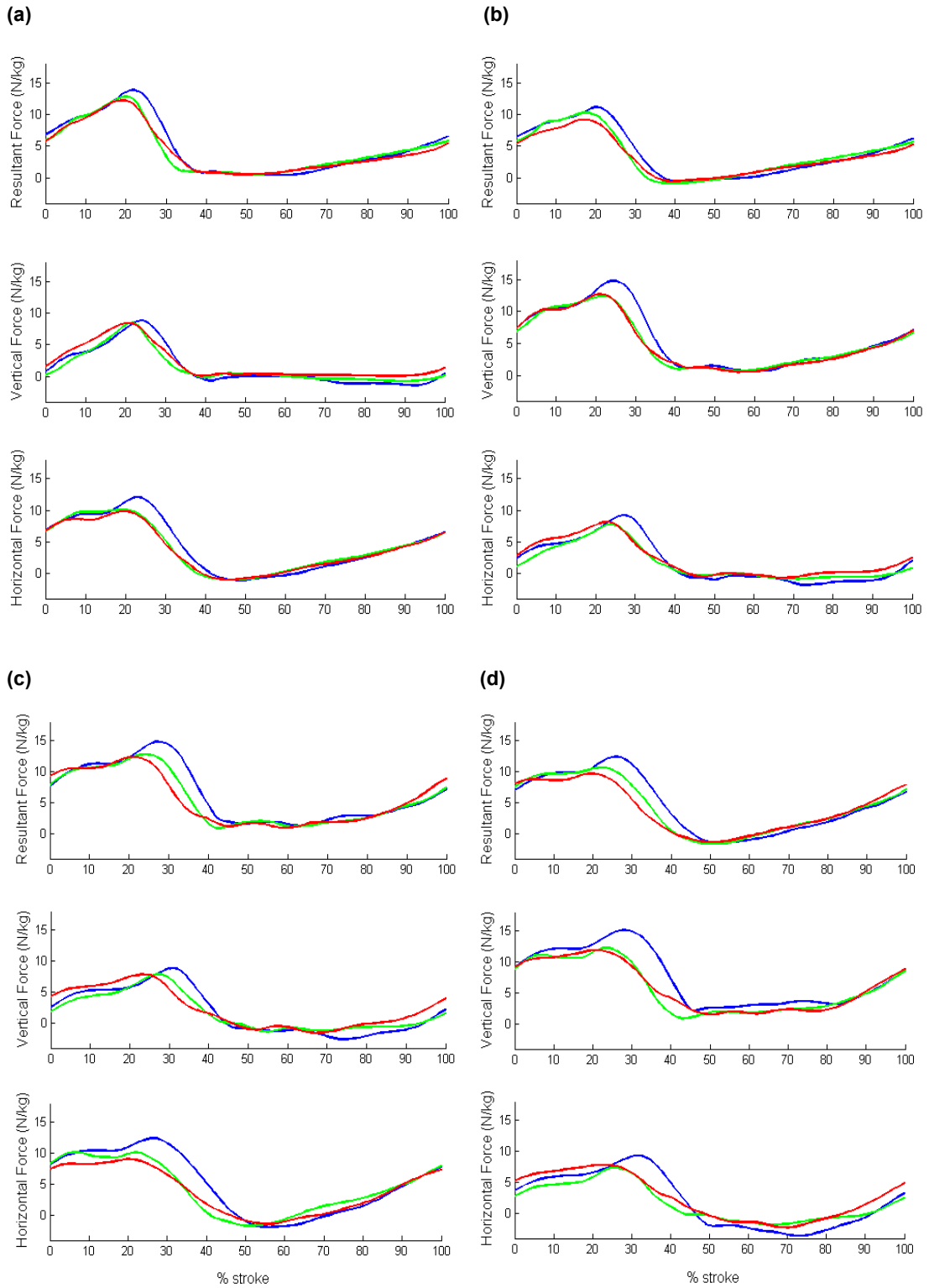


**Figure 5.7: Resultant, vertical and horizontal foot force traces at (a) Rate 18, (b) Rate 24, (c) Rate 28 and (d) Free Rate. Blue lines are LWM, green lines are SCULL and red lines are SWEEP. Standard deviations for this data ranged from  $\pm 0.2$  to  $\pm 4.0$  N/kg for Rate 18,  $\pm 0.2$  to  $\pm 3.6$  N/kg for Rate 24,  $\pm 0.2$  to  $\pm 3.8$  N/kg for Rate 28 and  $\pm 0.5$  to  $\pm 2.6$  N/kg for Free Rate.**

### 5.3.3 Foot force asymmetry

Group averages of ASI are shown in Table 5.3. Values ranged from 6.4% for resultant impulse in SCULL, up to 28.9% for timing of peak vertical force in SWEEP. There was large variability within groups as indicated by the ASI standard deviation values, which was on average, 77.1% of its mean. ASI values in Table 5.3 show resultant impulse to exhibit the least asymmetries compared to their vertical ( $P<0.01$ ) and horizontal ( $P<0.01$ ) components, whilst vertical impulse exhibits less asymmetry than horizontal impulse ( $P<0.05$ ). In terms of peak foot forces, resultant force again exhibited a smaller degree of asymmetry than its vertical ( $P<0.01$ ) and horizontal ( $P<0.01$ ) components, whilst peak vertical force was more asymmetrical than peak horizontal force ( $P<0.05$ ). None of the ASI values pertaining to foot force values or timings of peak force were significantly different between groups or at different stroke rates, although there was a trend for ASI of peak vertical force to increase at higher stroke rates ( $P=0.06$ ).

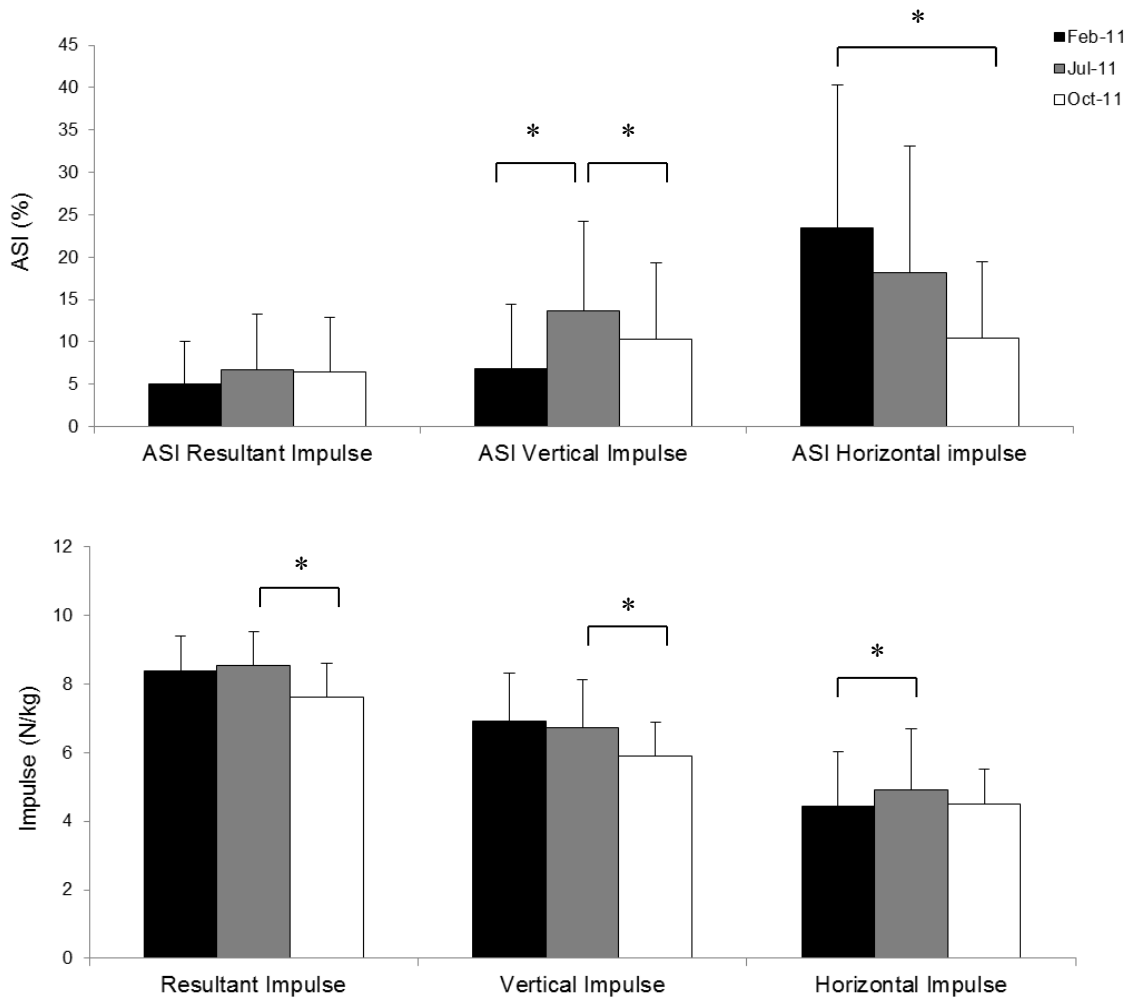
Although not a direct aim of this study, bow side rowers and stroke side rowers within the SWEEP and LWM groups were assessed to see if patterns in asymmetry related to the position of their inside leg. In total, the combined groups consisted of six bow side rowers where the inside leg is the left leg and four stroke side rowers. All bow side rowers exhibited greater resultant impulse on the right foot-stretcher, which is the outside leg. On the other hand, two stroke side rowers exhibited greater resultant impulse on their right side and two exhibited greater resultant impulse on their left side. In terms of the vertical and horizontal force components of the leg drive, there was no consistency in whether bilateral asymmetry favoured the inside leg or outside leg.

Table 5.3: Asymmetry index values (average  $\pm$  SD) for foot force parameters for all three groups across all four stroke rates. All values are % ASI.

Rate	Group	Resultant impulse (%)	Vertical impulse (%)	Horizontal impulse (%)	Peak resultant force (%)	Peak vertical force (%)	Peak horizontal force (%)	Timing peak vertical force (%)	Timing peak horizontal force (%)
18	LWM	13.3 $\pm$ 23.1	21.4 $\pm$ 23.7	14.1 $\pm$ 27.2	11.4 $\pm$ 9.1	28.2 $\pm$ 10.3	17.2 $\pm$ 10.0	13.1 $\pm$ 7.5	8.7 $\pm$ 6.0
18	SCULL	6.4 $\pm$ 6.2	12.9 $\pm$ 8.8	12.0 $\pm$ 12.0	9.7 $\pm$ 3.7	17.0 $\pm$ 7.1	12.1 $\pm$ 6.3	9.6 $\pm$ 3.6	8.4 $\pm$ 7.7
18	SWEEP	10.9 $\pm$ 3.8	11.1 $\pm$ 6.6	17.5 $\pm$ 9.7	6.8 $\pm$ 7.5	15.5 $\pm$ 6.7	9.5 $\pm$ 11.3	14.8 $\pm$ 8.7	6.8 $\pm$ 5.2
24	LWM	13.4 $\pm$ 5.4	21.5 $\pm$ 10.0	13.6 $\pm$ 14.2	6.7 $\pm$ 6.0	20.2 $\pm$ 11.5	16.8 $\pm$ 8.1	16.8 $\pm$ 20.5	9.0 $\pm$ 5.8
24	SCULL	7.3 $\pm$ 6.8	14.9 $\pm$ 9.7	13.6 $\pm$ 14.9	8.2 $\pm$ 3.5	16.4 $\pm$ 7.2	13.5 $\pm$ 11.0	13.7 $\pm$ 6.4	9.8 $\pm$ 6.2
24	SWEEP	10.9 $\pm$ 4.3	13.3 $\pm$ 6.1	17.3 $\pm$ 17.5	6.9 $\pm$ 7.6	16.0 $\pm$ 8.5	10.7 $\pm$ 13.3	17.9 $\pm$ 15.2	7.3 $\pm$ 15.3
28	LWM	14.4 $\pm$ 5.9	21.6 $\pm$ 7.1	14.0 $\pm$ 14.9	8.4 $\pm$ 5.2	19.8 $\pm$ 10.2	15.5 $\pm$ 7.9	28.1 $\pm$ 30.6	7.7 $\pm$ 6.0
28	SCULL	6.5 $\pm$ 5.7	14.9 $\pm$ 8.6	14.1 $\pm$ 12.5	8.0 $\pm$ 3.1	12.7 $\pm$ 7.1	12.5 $\pm$ 11.4	16.0 $\pm$ 21.7	6.4 $\pm$ 6.8
28	SWEEP	11.0 $\pm$ 4.8	14.4 $\pm$ 7.1	15.4 $\pm$ 12.2	6.7 $\pm$ 6.2	14.1 $\pm$ 8.0	10.1 $\pm$ 10.3	25.6 $\pm$ 27.3	7.3 $\pm$ 13.6
Free	LWM	9.9 $\pm$ 5.3	17.7 $\pm$ 8.4	8.1 $\pm$ 12.6	7.0 $\pm$ 7.0	16.0 $\pm$ 10.2	13.0 $\pm$ 5.5	20.9 $\pm$ 16.6	11.4 $\pm$ 9.5
Free	SCULL	8.2 $\pm$ 5.9	15.5 $\pm$ 8.6	11.9 $\pm$ 8.6	9.6 $\pm$ 3.7	12.0 $\pm$ 6.0	14.2 $\pm$ 9.8	18.6 $\pm$ 15.7	11.2 $\pm$ 7.4
Free	SWEEP	11.5 $\pm$ 5.8	14.2 $\pm$ 8.8	19.0 $\pm$ 18.7	8.8 $\pm$ 6.1	16.3 $\pm$ 9.2	13.0 $\pm$ 15.4	28.9 $\pm$ 23.8	25.1 $\pm$ 29.2
	<b>Average</b>	<b>10.3 <math>\pm</math> 6.9</b>	<b>16.1 <math>\pm</math> 9.5</b>	<b>14.2 <math>\pm</math> 14.6</b>	<b>8.2 <math>\pm</math> 5.7</b>	<b>17.0 <math>\pm</math> 8.5</b>	<b>13.2 <math>\pm</math> 10.0</b>	<b>18.7 <math>\pm</math> 16.5</b>	<b>9.9 <math>\pm</math> 9.9</b>

#### **5.3.4 Longitudinal foot force and asymmetry**

For the longitudinal analysis, data was analysed using a two way mixed model ANOVA with Session Month as an additional factor. There were no interaction effects between factors. In terms of force applied bilaterally to the foot-stretchers, there was no change in peak foot force values over the three testing sessions. However, regarding area under the force curves, resultant and vertical impulse was significantly higher in July compared to October ( $P<0.05$ ), whilst horizontal impulse was higher in July than February ( $P<0.05$ ) (Figure 5.8). In terms of asymmetry, changes over the year were again observed for impulse rather than peak forces. Vertical impulse ASI was significantly greater in July compared to February and October ( $P<0.05$ ), while there were progressive reductions in horizontal impulse ASI over the three sessions ( $P<0.05$ ) (Figure 5.8).



**Figure 5.8:** Average (error bars SD) resultant, vertical and horizontal impulse ASI (top graph) and magnitude (bottom graph) at Free Rate during three testing sessions. \* denotes significant difference where  $P < 0.05$ .

### 5.3.5 Summary of results

- Foot plates demonstrated high reliability in recording vertical and horizontal force outputs, where CMD were  $0.98 \pm 0.01$  and  $0.98 \pm 0.02$  respectively.
- LWM had significantly greater vertical and resultant foot force outputs compared to SCULL and SWEEP, whereas horizontal foot force was significantly greater in SWEEP compared to SCULL.
- Stroke rate affected only the magnitude of peak horizontal foot force.

- Asymmetries were smallest for resultant force traces (6.4%) and largest for timing of peak vertical forces (28.9%).
- Asymmetry values did not significantly differ between groups or between stroke rates.
- Changes in foot force magnitudes and asymmetries could be identified over successive testing sessions over the course of a season.

## **5.4 Discussion**

The purpose of this chapter was the application of custom footplates developed in Chapter 4 to quantify elite rowers' foot forces and asymmetries on an ergometer. Further aims were to examine changes in these parameters between groups of rowers, at different stroke rates, over multiple testing sessions. To summarise, this work noted that the footplates can measure foot force with a high level of reliability ( $CMD > 0.98$ ), and can identify bilateral foot force asymmetries in elite rowers and changes in these parameters over multiple testing sessions.

The instrumented footplates were able to distinguish between groups of rowers in terms of their overall foot force production. Resultant foot force was largest in LWM, so they were able to generate a greater magnitude of force per stroke, relative to body mass, compared to heavyweight female rowers. Large foot forces are favourable, because these forces are generated by powerful leg extensor muscles and transferred to the handle via the hips, trunk and arms (Hofmijster et al., 2008). However, it has been suggested that large resultant foot forces are only considered a positive characteristic of the leg drive when this increase in force arises from the horizontal component i.e. the force vector which directly contributes to boat propulsion (Caplan and Gardner, 2005).

Interestingly there were no significant differences between the three groups in terms of their horizontal force production. Therefore, whilst LWM exhibited the greatest magnitudes of resultant force, this may not positively influence their leg drive, due to the vertical component being the substantial contributor to their large resultant force. Additionally, horizontal impulse was significantly greater in SWEEP compared to SCULL. Therefore, whilst SWEEP exhibited the smallest resultant foot forces, they had the largest proportion of propulsive force, resulting in a more mechanically effective production of force. It is possible that the differences between the groups' leg drive kinetics in this study arose from long term training effects, due to their different training programmes and coaching environments. This study examined only foot forces so it was not possible to speculate from this data set alone, the biomechanical contributions to SWEEP rowers' kinetic outputs. Previous research has shown that female sweep rowers minimise flexion of the lumbar spine and maintain a strong trunk position from the catch through the critical drive phase (Murphy, 2009), thus are able to achieve better quality lumbar-pelvic kinematics on the ergometer than female scullers and lightweight men. It is thought that by exhibiting lumbar flexion at the start of the stroke, the vertical component of foot force would be greater, by creating a steeper angle of force application to the foot-stretcher (Caplan and Gardner, 2010). As such, kinematics of the trunk may play a substantial role in influencing the quality of foot force application.

It was expected that there would be an increase in both vertical and horizontal force at higher stroke rates, causing a corresponding increase in resultant force. Halliday et al. (2004) found a small increase in resultant force, along with corresponding increases in vertical and horizontal force of approximately 50 N, as stroke rate increased from 20 to 35 strokes per minute. However, the current study demonstrated increases in resultant



force for LWM only, whilst SCULL and SWEEP's resultant force decreased. In fact, overall there was a significant reduction in horizontal foot force, and the increase in LWM resultant force was largely due to corresponding increases in vertical force. This suggests that at higher stroke rates, forces applied to the foot-stretchers become mechanically less effective, because for the same resultant force, a smaller proportion of it is applied in the horizontal direction. Again, the mechanisms contributing to increases in vertical force at incremental stroke rates could be attributed to the quality of lumbar kinematics at higher stroke rates, which has previously been shown to diminish at higher stroke rates (McGregor et al., 2004). Greater anterior rotation of the rowers' thoracic and lumbar segments at the catch could theoretically result in a greater proportion of their trunk mass over their feet, thus contributing to a greater vertical foot force component. Additionally, changes in the degree of weight suspension from the seat during the critical drive at higher rates may directly influence the vertical component of foot force. However, to test these theories, kinematic analyses of lower limb joint angles and synchronised measures of seat and handle forces would be necessary, which was not possible in this study. Synchronised force and motion data would enable a detailed analysis of rowers' joint co-ordination, as well as their impact on foot-stretcher forces, consequent movement patterns and quality of force production through the drive phase. These will be addressed in Chapter 6.

Bilateral asymmetry was evident for numerous foot force parameters. Resultant foot force exhibited the least asymmetry. However, when examining resultant foot force components, much greater asymmetries were evident where one side generates larger horizontal forces at the expense of vertical forces, and vice versa for the contra-lateral side, exhibiting asymmetries up to 28.2%. As supplementary analysis, sweep rowers (i.e. SWEEP and four out of six LWM) were examined further to find out whether their

foot force asymmetries corresponded to their rowing side. Statistical analysis was not performed, as this supplementary work was not adequately powered. Eight out of ten rowers generated greater resultant impulses on their right side, with two remaining stroke side rowers exhibiting greater left side resultant impulses. Therefore, it was not possible to conclude from this group of rowers that a relationship exists between foot force asymmetries on a rowing machine, and preferred rowing side on-water. Leg dominance may have some influence on foot force asymmetries on an ergometer, but further research with a greater number of sweep rowers is necessary to validate this idea.

With an increase in stroke rate, it was anticipated that ASI values would increase due to deteriorations in technique that occurs with increased rowing intensity (McGregor et al., 2004). However, this theory was not supported in this study. Therefore, whilst it appears that higher stroke rates negatively affect technique in the sagittal plane (McGregor et al., 2004, Murphy, 2009) there is less impact of this on bilateral asymmetry of rowers' foot forces. Stroke rate had no effect on asymmetry of peak foot forces or impulse, suggesting that bilateral force asymmetries within rowers could be inherent and are not influenced by rowing intensity. However, this study did not test the rowers at their absolute maximum capacity, therefore, it would be necessary to quantify bilateral asymmetry of rowers at maximum effort to infer that bilateral asymmetry is independent of stroke rate.

The results of this study support findings from studies which found foot force asymmetries in elite sweep rowers (Janshen et al., 2009) and scullers (Colloud et al., 2001), as all three groups of elite rowers in this study demonstrated some degree of foot force asymmetry. Thus, despite ergometer rowing being theoretically symmetrical, unilateral analyses of the lower limbs should perhaps be re-considered. This is

especially pertinent for analysis of ergometer rowing, as greater levels of asymmetry have been observed for fixed head ergometer rowing compared to a floating head ergometer, which is thought to mimic the mechanics of on-water rowing (Colloud et al., 2001). This may be because ergometer rowing is thought to result in adverse body mechanics compared to rowing on-water in an attempt to maximise power output (Torres-Moreno et al., 2000). Therefore, it is clear that the different technical requirements of on-water and ergometer rowing will exhibit variable foot force symmetries, and as such must be explored further.

Examination of foot forces and asymmetries over multiple sessions showed that there are statistically significant changes in foot force patterns throughout the year. However, it is possible to achieve statistical significance, where the difference is real rather than due to chance, and for it to have little impact on performance or injury due to the small magnitude of the difference. Eta-squared ( $\eta^2$ ) is a measure of effect size for group mean differences. Only values greater than 0.5 were observed in this study, thus demonstrating a large effect size and implying clinical relevance of this data. Therefore, significant changes in foot force parameters over the season may be important in terms of identifying fluctuations in performance. For example, vertical, horizontal and resultant impulses were greatest in July, at a time when rowers are competing in the world cup series and preparing for the World Championships. This greater production of foot force likely reflects their cumulative training effects, which serves to optimise their technique and power output for the racing season. July was also when both vertical and horizontal impulse asymmetries were significantly inflated compared to February and October. Although it was purported that rowers' honing of their technique would mean a reduction in asymmetries, there is no evidence to demonstrate such links between technique, performance and symmetry. Greater ASI in July may be

a result of the greater foot force application that also occurred in that month, because previous research in cycling showed that increases in pedal reaction forces are accompanied by increases in bilateral asymmetries at the pedals (Carpes et al., 2006). The link between force output and asymmetry may be further supported through findings that both bilateral asymmetry and foot force magnitudes were found to be steady within each testing session, with respect to progressive stroke rates. Yet, examination of foot force over the calendar year shows that subtle changes in asymmetries and foot force productions are observable when analysed over multiple sessions.

In terms of the relevance of foot force asymmetries on the subsequent rowing stroke, there is no evidence to suggest that increasing asymmetry values are related to factors such as technique and performance. Nor is it possible to infer the influence of foot force asymmetries on those factors without a more comprehensive biomechanical analysis of rowing. The current data set incorporates reaction forces from the foot-stretchers only, but it is evident that a more detailed kinematic and inverse dynamic analysis of the lower limbs, in conjunction with external force measurements at the seat and handle, are necessary to understand and interpret how foot reaction forces and asymmetries affect subsequent body segment kinematics, joint loading and, ultimately, their impact on rowing performance.

## **5.5 Conclusion**

The newly developed instrumented foot-stretchers are an effective tool for accurately and reliably examining foot forces of elite rowers. They were able to distinguish foot force patterns between groups of rowers, and are valuable in determining the degree to

which rowers' exhibit kinetic asymmetries. Given the large variability in asymmetries between rowers, they would be useful for individual analysis of elite rowers' foot force production. They are also effective in identifying fluctuations in these parameters over a season, as they are sensitive to differences in foot force patterns and asymmetry that occur over multiple sessions.

The subsequent chapter will integrate the footplates with the instrumented ergometer and motion capture systems. This is done with the intention of gaining a greater and more complete understanding of how foot force characteristics and asymmetries influence subsequent performance and technique of the rowing stroke.

## **Chapter 6:**

# **Modelling the Relationship between Rowing Technique, Asymmetry and Performance**

The previous two chapters focused on the development and application of instrumented foot-stretchers. These were operated as standalone instruments that measured foot force across groups of elite rowers, whilst assessing their reliability and quantifying bilateral force asymmetries. Therefore, key aspects of the leg drive were examined independently, without consideration of their influence on rowers' kinematics, or their interactions with other contact forces between the athlete and rowing machine. In this chapter, kinematic data of the rower is synchronized with all external contact forces (i.e. those at the feet, seat and handle) in order to examine the relationship between force production, joint kinematics, asymmetries and performance. This was done with the intention of advising coaches and athletes on how technique can be altered to optimize force production. Furthermore, force asymmetries were investigated to see how they might impact the rower further along the kinematic chain, specifically at the lumbar spine, as asymmetrical rowing may be linked with increased risk of injury and LBP.

### **6.1 Introduction**

Given the cyclical nature of rowing many aspects of the rowing stroke are interdependent, making it difficult to isolate one element of the stroke from another. Therefore, it is important to assess interactions between magnitudes and asymmetries of rowers' foot forces, with lower limb and lumbar-pelvic kinematics, in addition to

subsequent key performance parameters. The previous chapter investigated foot forces and asymmetries in groups of elite rowers without looking into the associated movement patterns of the rower. In this chapter, foot force measurements are synchronized with kinematic data from the rower and external contact forces at the handle and seat, to gain greater insights into the factors which influence rowing performance.

### **6.1.1 How does technique influence force application?**

Rowing is a cyclical activity which involves a very specific sequence of motions to optimise boat speed. Therefore, whilst rowing requires extreme physical strength and endurance, a high level of skill and technique is also essential to enable an effective transfer of power through the rowing sequence (Nolte, 2004). In order to produce a large mean velocity of the boat, large forces must be produced, particularly by powerful leg extensors such as the quadriceps, and delivered to the handle/oars (Hofmijster et al., 2008). The importance of a powerful leg drive as a fundamental requirement of a successful stroke was expressed in the previous chapter (Section 5.1.1). Furthermore, in order to optimise the power generated during the leg drive and its transfer to the handle, excellent technique with accurate sequencing of knee extension, hip extension and stable trunk rotations are crucial. Suboptimal technique through inaccurate sequencing of body segment motion negatively affects the forces applied to the foot-stretcher, and impacts the efficiency of transfer to the handle/oar, thus reducing mean boat velocity (Baudouin and Hawkins, 2002). For example, ‘shooting the slide’ is when the legs extend to move the seat posteriorly, but the motion is disconnected from the trunk and handle, thus resulting in a miss-timed trunk rotation that wastes energy from the leg drive (McNeely and Royle, 2002). Other common technical faults include

taking the catch with the shoulders and upper body instead of engaging the leg drive, and over extending at the finish thus weakening lumbar-pelvic posture, to gain stroke length (Bull and McGregor, 2000). These faults are common in novice rowers, and highlight the crucial link between technical soundness and improved performance. Consequently, the movement patterns which occur during and after the leg drive are clearly important in optimising mean external power per stroke.

Key aspects of performance are the ability to generate large forces and to maintain a good kinematic sequence through the drive. More recently, there has been an emphasis on examining the horizontal component of force relative to the resultant force i.e. the ability to apply mechanically effective forces (Caplan and Gardner, 2010, Morin et al., 2011). Although the following studies did not directly measure foot force, it has previously been found that raising foot-stretcher heights compared to a standard height results in a more posterior trunk motion and improved power output (Caplan and Gardner, 2005, Caplan and Gardner, 2010). It was suggested that the height of the foot-stretchers placed the rower in a more mechanically effective position to generate horizontal foot force, which subsequently improved power output. Furthermore, research into sprinting has found a key performance predictor to be horizontal impulse during the stance phase (Hunter et al., 2005). In agreement, Morin et al. (2011) suggested that it was not the total force applied during the stance phase of a sprint, but rather the proportion of horizontal force with respect to the resultant force, which determined sprint performance. This was termed the foot force ratio (RF). Thus, for the same resultant force, different strategies of force application may be employed that result in larger horizontal force output and thus, net forward accelerations. Much like in sprinting, rowing requires acceleration in the horizontal plane to be maximised. Chapter 5 showed that lightweight men produced the largest resultant forces, but their



horizontal force output was the same as the other two groups, suggesting their RF values were lower.

In this chapter, the footplate system will be integrated with the FOB and instrumented ergometer systems, so that synchronised kinematic and kinetic data can be acquired. This will make it possible to quantify RF at key timings during the stroke, such as the catch and MHF. Consequently, it will be possible to examine discrete aspects of technique which positively influence RF. Regarding foot force and kinematics, the first aim of this chapter will be to identify aspects of technique that make significant contributions to large resultant foot force. A subsequent aim will be to further identify aspects of technique that elicit large RF at key points during the stroke.

### **6.1.2 Do asymmetries at the feet increase injury risk?**

Kinematic asymmetries have been identified at the hips and knees, with those at the hips proving to be a moderate predictor of lumbar-pelvic kinematics at the catch and MHF (see Chapter 3). Knowledge of kinematic asymmetries is important, but it is possible for these asymmetries to have occurred as a result of bilateral asymmetries in foot force production, as force is the driver of motion. Asymmetrical loading on the footplates has received limited attention to date. Furthermore, its influence on lumbar-pelvic kinematics and other aspects of asymmetry such as pelvic twist and ML drift has not been examined. Given that rowers are constrained at the hands, seat and feet and are performing a closed chain activity, asymmetrical loading of the foot-stretchers must be balanced through compensatory movement patterns or stabilizing co-contractions in order to keep the motion in the sagittal plane. For example asymmetrical lifting has been shown to cause asymmetrical torques at the lower back, which resulted in

increased spinal loading through stabilizing co-contractions of the lumbar spine (Kingma et al., 1998). However, Plamondon et al. (1995) did not find 3D moments at L5/S1 that significantly differed between asymmetrical and symmetrical lifting. They suggested that subjects may have minimized lateral flexion and torsional moments through compensatory twisting of their pelvis and lower limbs. Movements of the pelvis which counteract asymmetries will, in theory, impact the action of the lumbar spine and also create out of plane motion artefacts on the seat that are deleterious to performance. Consequently, further aims of this study were to examine whether asymmetries at the feet could influence: L5/S1 flexion during the critical drive period ( $\Delta$ L5/S1), pelvic twist and ML drift on the seat.

### **6.1.3 Investigating the kinetic chain in rowing**

The production of large foot forces are a key component of the leg drive (McArthur, 1997). However, these forces must be effectively transferred through the kinetic chain if the force generated by pulling at the handle is to be maximized, and translated to a power output that enhances the boat's velocity (Baudouin and Hawkins, 2002). One of the ways in which foot forces are effectively translated to the handle is through effective suspension from the seat (Murphy et al., 2010). This concept of the athlete suspending their weight between the foot-stretchers and handle during the critical drive phase is a key coaching point and is achieved by the legs engaging with the foot-stretcher and the trunk and shoulder muscles being activated to facilitate suspension (Thompson, 2005). Therefore, in order to achieve effective seat suspension, it is clear that large forces must be applied to the foot-stretchers. Validating this theory, it was found that strapping rowers' to their seat for the purpose of improving seat suspension resulted in significantly larger foot forces, in addition to significantly larger handle

force (van Soest and Hofmijster, 2009). As such, a greater ability to suspend from the seat may enhance the forces that are applied to the foot-stretchers, and consequently expressed at the handle.

The relationship between force outputs at the three external contact points on the rowing machine has not been comprehensively investigated in elite rowing. Examining the relationship between these outputs will provide a greater detail of information regarding the transfer of forces through the kinetic chain, and more specifically how an athlete's technique optimizes these forces. Furthermore, if peak handle force and peak foot force exhibits a highly linear relationship, it may be possible to instrument simply one part of the boat in order to achieve a basic measure of 'performance' on water.

#### **6.1.4 Statistical modelling of performance**

Statistical modelling of kinetic and kinematic data is extremely useful for identifying aspects of technique which influence pertinent performance parameters. It is the interrelation between variables for which it is hard to provide a mechanistic description, and therefore statistical techniques allow these relations to be explored. The previous sections clearly suggest that there are aspects of rowing performance which are inherently influenced by technique, and vice versa. By identifying discrete aspects of technique which may improve foot force, and by quantifying the influence of asymmetries on joint and segmental kinematics, it would be possible to provide an evidence based guide to coaches and athletes which aids performance optimisation and technique refinement.

In a detailed investigation of rowers' technique, performance and injury risk, Murphy (2009) employed correlation and multiple regression analyses to model performance

and injury based on 3D kinematic and kinetic predictors. Important variables which contributed to greater performance were: ability to suspend bodyweight from the seat during the critical drive, minimal medio-lateral motion on the seat, large mean power output per stroke, large peak handle force, lengthening the stroke, and rapid rate of force development. Kinematic variables which strongly influence the above measures of performance were all found to occur in the sagittal plane, with AP trajectory of the knee joint centre flagged as a key predictor. In terms of injury, Murphy flagged sagittal plane changes in L5/S1 angle between the catch and MHF, i.e.  $\Delta L5/S1$ , as a key variable which is strongly predicted by lower limb kinematics.

With the development of instrumented footplates, it is now possible to model the effect of foot force and their asymmetries on performance and lumbar-pelvic kinematics. This will provide a more complete picture of the effect of foot force on performance; in turn the influence of technique on foot forces; and whether asymmetries at the feet affect subsequent kinematics of the rowing stroke. Consequently, some of the key performance and injury variables previously identified will be investigated in this study, thus enabling the additional influence of foot force on these variables to be examined.

The ability to measure intricate details of performance, such as 3D kinematics and contact forces are rare outside of a laboratory environment, and even when possible in a field setting, it is unlikely that measures will offer the same precision and accuracy (Potvin et al., 1992). Consequently, it is desirable to determine the degree to which variables co-vary or influence one another, so that simpler measures can be taken on-water as pseudo-measures of variables that are difficult to quantify using custom instrumentation. No previous study has extensively examined the interaction between rower kinematics and forces at all three contact points on the rowing machine (handle,

seat and foot-stretchers), with respect to key technical features which may lead to improvements in performance. Therefore the aims of this study were to (a) investigate the key kinematic variables which influence foot force application, (b) investigate the effect of foot force asymmetries on ML drift, pelvic twist and  $\Delta L5/S1$ , and (c) investigate the interaction between the three external contact forces on the rowing machine. This might allow the use of foot force and other force variables as a surrogate measure for the kinematic performance variables.

## **6.2 Methodology**

### **6.2.1 Participants**

The study received ethical approval from the Imperial College Research Ethics Committee, and informed consent was obtained from all subjects (Appendix B). Twenty elite heavyweight female rowers participated in this study (mass  $76.6 \pm 5.1$  kg, age  $26.8 \pm 3.0$ ) in October 2011. Of these, six were scullers and 14 were sweep rowers. Six lightweight male rowers were also tested during this session. However, only three fully completed all stages of the protocol, therefore, the lightweight men's data were excluded from the study. Nevertheless, just seven subjects were required to achieve the desired moderate effect size of 0.5 and statistical power of 95% with an alpha significance level of 0.05. Therefore, this study was adequately powered to detect the given effect size. All participants were right leg dominant as defined by their preferred kicking leg. Subjects with a leg difference of more than 1 cm were excluded from this study because anatomical asymmetries may influence the results of this study. Additionally, rowers with a current episode of LBP or any other serious illness or injury were excluded from this study.

### **6.2.2 Experimental set-up**

All rowers performed their trials on a modified Concept II model D ergometer (Figure 6.1). The ergometer was instrumented at the handle with a uniaxial load cell (ELHS model, Entran, Lexington, Kentucky, USA) to measure pulling force on the handle (2.5 kN range, 0.5% combined non-linearity and hysteresis). The flywheel was instrumented with a linear encoder with 5000 increments per revolution (ERN120, Heidenhain Ltd., Traunreut, Germany) to enable measurements of stroke length. The seat was instrumented with four uniaxial load cells (ELPM model, Entran, Lexington, Kentucky, USA) to measure COP and vertical forces on the seat (1.25 kN range,  $\pm 0.15\%$  hysteresis, 0.15% non-linearity) (Murphy et al., 2010). Foot-stretchers were replaced with the strain gauge instrumented footplates described in Chapter 4 to bilaterally measure vertical, horizontal and resultant foot forces, as well as COP along the longitudinal axis of the footplates.

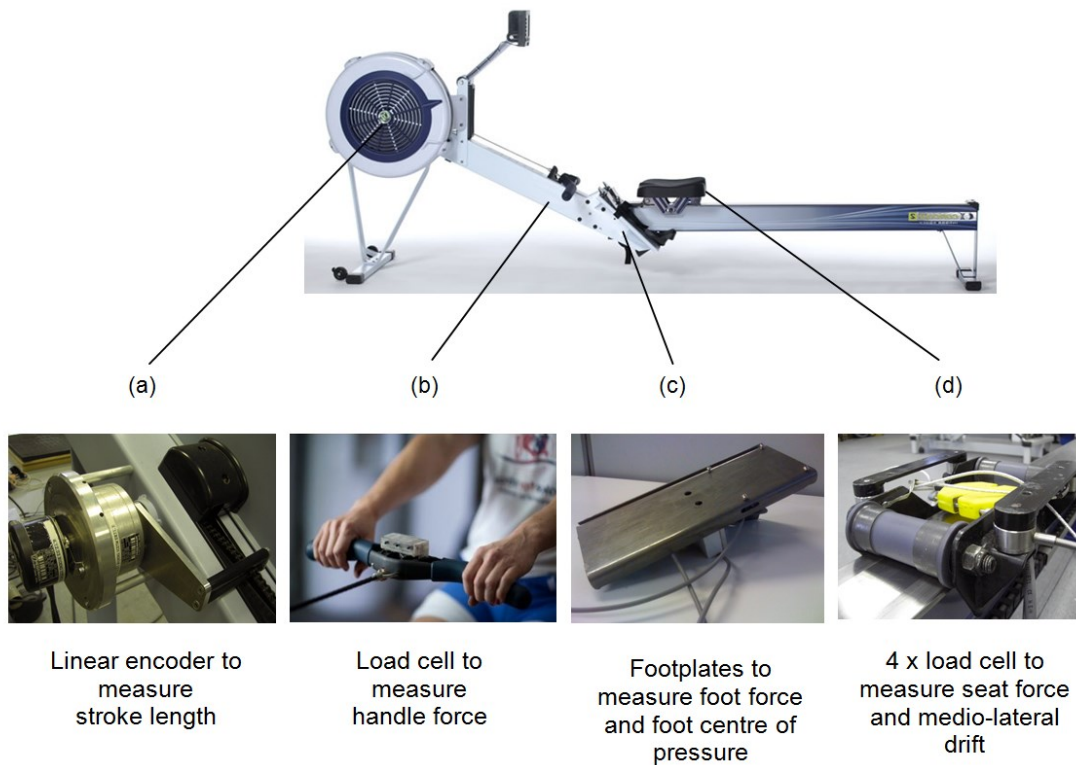


**Figure 6.1: Instrumentation of the Concept II ergometer at the flywheel (a), handle (b), feet (c) and seat (d).**

Rower kinematics were recorded using the FOB motion capture system (Ascension Technology, Burlington, USA). The system consists of an extended range electromagnetic transmitter, situated at a location that would optimise measurement accuracy (Murphy et al., 2011), and four receivers (S1 – S4) whose 3D translations ( $x$ ,  $y$ ,  $z$ ) and rotations ( $\alpha$ ,  $\beta$ ,  $\gamma$ ) could be quantified within the electromagnetic field.  $x$  represents the medio-lateral axis,  $y$  represents the vertical axis and  $z$  represents the anterior-posterior axis.  $\alpha$ ,  $\beta$  and  $\gamma$  are rotations about the  $x$ ,  $z$  and  $y$  axes respectively (i.e. flexion-extension, abduction-adduction and internal-external rotation). Previous work has validated this system's suitability for measuring spinal and lower limb motion (Bull et al., 1998, Bull and McGregor, 2000, Bull et al., 2004, Murphy, 2009).

### 6.2.3 Subject Preparation and Digitization

In order to comply with the testing procedure established with GB Rowing, the previously unilateral motion sensor set-up (Murphy, 2009) was utilized for this study. As such the sensor placement order differs from that of the bilateral set-up described in Chapter 3. Table 6.1 describes the placement of each sensor, the segment it represents, and the bony landmark local offsets that are stored relative to it.

**Table 6.1: Anatomical placement of FOB sensors.**

<b>Sensor</b>	<b>Fixed to:</b>	<b>Segment representation:</b>
S1	T12-L1 junction	Lumbar spine
S2	L5-S1 junction	Pelvis
S3	Mid way along lateral aspect of thigh	Thigh
S4	Mid way along anterior aspect of shank	Shank

Adhesive pads (PALstickies™, PAL Technologies Ltd, Glasgow, Scotland) were used to secure S1 and S2 to the skin, whilst S4 was attached to a foam cuff and strapped to the subjects' right shank. S3 was employed as a digitisation stylus (Figure 3.3) prior to being fixed to the thigh with Velcro straps. Whilst the rower was seated on the ergometer, the tip of the stylus was placed on landmarks of interest and rotated about that point in order to create a cloud of 3D position data. A sphere fitting procedure was then used to work out the 3D vector offset of that point relative to the sensors already attached to the body segments, so that the trajectories of the landmarks could be tracked at all points during the rowing stroke. Table 6.2 shows the bony landmarks that are digitised, and indicates the sensors that they are stored as offsets from.



**Table 6.2: Anatomical landmarks digitized during static recordings.**

<b>Anatomical Landmark</b>	<b>Stores as vector offset from:</b>
Right posterior superior iliac spine (RPSIS)	S2
Left posterior superior iliac spine (LPSIS)	S2
Right anterior superior iliac spine (RASIS)	S2
Left anterior superior iliac spine (LASIS)	S2
Lateral femoral epicondyle (LEPI)	S4
Medial femoral epicondyle (MEPI)	S4
Distal apex of the lateral malleolus (LMAL)	S4
Distal apex of the medial malleolus (MMAL)	S4
Dorsal aspect of the fifth metatarsal head (MET5)	Global origin
Hip joint centre (HJC)	S2

The hip joint centre was determined through a functional test. This involved strapping the S3 digitising stylus to the subject's thigh, and in a standing position, the subject rotated their thigh to capture their full range of motion about the hip, enabling a sphere fitting procedure to find the centre of rotation. S3 subsequently remained on the subjects' thigh for the dynamic trials purely to aid the visual biofeedback, where S3 completes the rowers' stick figure animation by representing the thigh segment (Figure 6.2).

#### **6.2.4 Experimental protocol**

The same rowing protocol as described in Section 5.2.2 is employed for this study.

#### **6.2.5 Data acquisition**

Signals from the load cells were hardware synchronized and connected to a PC through a multi-channel signal conditioning unit (SC-2345, National Instruments, Austin, Texas,

USA). Signals from the footplates were software synchronized with the load cells using timed synchronization loops in LabView (version 2009, National Instruments, Austin, Texas, USA). The load cells, footplates and FOB were initialized in separate timed loops, and a timed loop synchronization function (i.e. ‘Synchronised Times Structure Starts.vi’) ensured that the acquisition loops started at the same time in order to produce synchronized measurement data. By achieving data acquisition synchronization, the rowing biofeedback interface could be updated by enabling the stand-alone footplate interface (Figure 4.17) to be embedded as a graphical feature in the main biofeedback program (Figure 6.2).

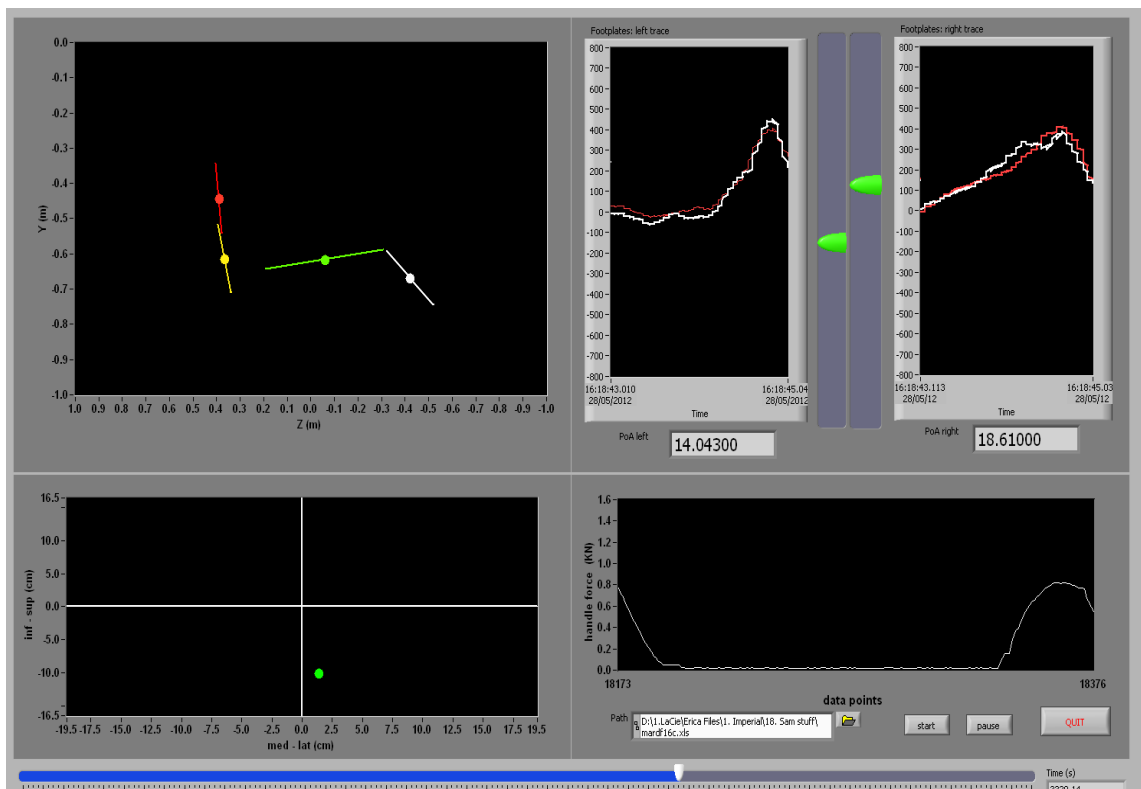


**Figure 6.2:** Screenshot of the integrated rowing biofeedback and acquisition program. Top left graphic displays 2D motion of rowers’ lower back and lower limbs; bottom left graphic is COP applied to the rowing seat (depicted by green dot); top right are the footplate biofeedback graphs; and bottom right is the handle force trace.

Custom Labview software (Version 7.1, National Instruments, Austin, Texas, USA) was used to initialise and synchronise all signals from the instrumented rowing machine and FOB, to acquire measurement data from all force and motion sensors at a rate of 75 Hz, and to write the data to an ASCII file. The raw output file consisted of the arrays of data shown in Table 6.3.

**Table 6.3: Headers of the raw output file consisting of force, length and kinematic data.**

<b>Column Number</b>	<b>Measured Parameter</b>	<b>Column Number</b>	<b>Measured Parameter</b>
1	Handle Force (N)	26	S3 x position (mm)
2	Chain Length (mm)	27	S3 y position (mm)
3	Chain Angle (°)	28	S3 z position (mm)
4	Stroke Marker	29	S3 $\alpha$ angle (°)
5	Front left seat force (N)	30	S3 $\beta$ angle (°)
6	Front right seat force (N)	31	S3 $\gamma$ angle (°)
7	Rear left seat force (N)	32	S3 Binary marker
8	Rear right seat force (N)	33	S4 x position (mm)
9	ML seat coordinate (cm)	34	S4 y position (mm)
10	AP seat coordinate (cm)	35	S4 z position (mm)
11	Seat Force (N)	36	S4 $\alpha$ angle (°)
12	S1 x position (mm)	37	S4 $\beta$ angle (°)
13	S1 y position (mm)	38	S4 $\gamma$ angle (°)
14	S1 z position (mm)	39	S4 Binary marker
15	S1 $\alpha$ angle (°)	40	Time stamp (ms)
16	S1 $\beta$ angle	41	Start AP handle (mm)
17	S1 $\gamma$ angle (°)	42	Start IS handle (mm)
18	S1 Binary marker	43	AP handle coordinate (mm)
19	S2 x position (mm)	44	IS handle coordinate (mm)
20	S2 y position (mm)	45	Right footplate vertical force (N)
21	S2 z position (mm)	46	Left footplate vertical force (N)
22	S2 $\alpha$ angle (°)	47	Right footplate horizontal force (N)
23	S2 $\beta$ angle (°)	48	Left footplate horizontal force (N)
24	S2 $\gamma$ angle (°)	49	Right footplate centre of pressure (cm)
25	S2 Binary marker	50	Left footplate centre of pressure (cm)

### 6.2.6 Data analysis

Data analysis was split into two main phases: calculation of 3D kinematics using a Labview program (which will be referred to as the kinematics program), and extraction of key performance and kinematic parameters using a Matlab program (which will be referred to as the data extraction program).

### 6.2.6.1 Kinematics program

A unilateral lower limb and lumbar-pelvic kinematic model was previously developed in Labview by Chee (2006) and subsequently used by Murphy (2009) to calculate 3D kinematics of elite rowers. This model employs the Grood and Suntay (1983) JCS approach to quantify 3D joint kinematics, and will be referred to as the *kinematics program* in this thesis. A detailed description of joint kinematic calculations using the current FOB set-up and kinematics program is given in Murphy (2009). This section will provide just a brief outline of the process.

The kinematics program first looked at the ten digitisation files and used the S3 sensor position and orientation data from each of those files to calculate local offsets of each digitised anatomical point to their reference FOB sensor (Table 6.2). These calculated local offsets were then combined with FOB sensor position and orientation information contained within the Step files, in order to calculate the 3D global positions of the bony landmarks and HJC during the dynamic rowing trials.

$$X_S = X_B + X_0 * M(1,1) + Y_0 * M(2,1) + Z_0 * M(3,1) \quad \text{Equation 6.1}$$

$$Y_S = Y_B + X_0 * M(1,2) + Y_0 * M(2,2) + Z_0 * M(3,2) \quad \text{Equation 6.2}$$

$$Z_S = Z_B + X_0 * M(1,3) + Y_0 * M(2,3) + Z_0 * M(3,3) \quad \text{Equation 6.3}$$

$X_B$ ,  $Y_B$  and  $Z_B$  are the XYZ position outputs from the sensor, that is, the location of the sensor's centre with respect to the transmitter's centre.  $X_0$ ,  $Y_0$  and  $Z_0$  are the local offset distances from the sensor's centre to the digitized bony landmarks.  $X_S$ ,  $Y_S$  and  $Z_S$  are the coordinates of the stylus's tip with respect to the transmitter's centre.  $M$  is a 3x3

matrix describing the sensors orientation.  $X_S, Y_S$  and  $Z_S$  data from dynamic trials were used as the basis for deriving joint centre positions and joint angles in 3D.

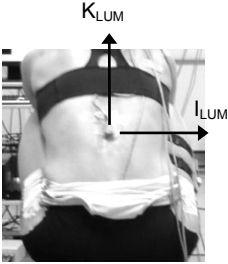
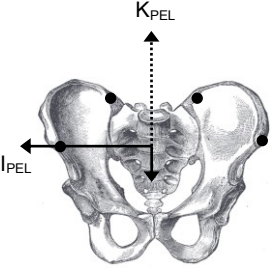
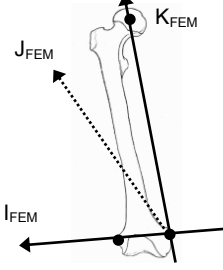
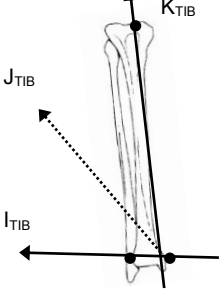
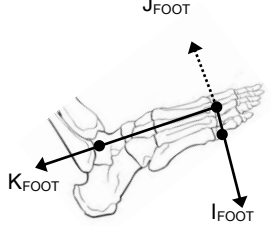
(i) *Joint Centre and Segment Definitions*

The kinematics model includes five joints: (1) Lumbar-pelvic joint; (2) hip joint; (3) knee joint; (4) ankle joint; (5) foot joint; the following table describes how the joint centres for each of these joints are located.

**Table 6.4: Method of determining joint centre locations.**

<b>Joint</b>	<b>Method of joint centre location</b>
Lumbar-pelvic joint (L5/S1)	Directly tracked as an offset from S2
Right Hip joint (HJC)	Functional digitisation method
Right Knee joint (KJC)	Mid-point between the MEPI and LEPI, which are located through stylus-digitisation.
Right Ankle joint (AJC)	Mid-point between the MMAL and LMAL, which are located through stylus-digitisation.
Right Foot joint (FJC)	Offset from the dorsal aspect of the fifth metatarsal head, coincident with the global X axis.

Local co-ordinate systems of five segments are defined in the model, based on vectors connecting digitised landmarks. These included the lumbar spine segment (LUM), pelvis segment (PEL), thigh segment (FEM), shank segment (TIB) and foot segment (FOOT). Each segment's local co-ordinate system is defined as follows:

Segment	Definition of local co-ordinate system
<p style="text-align: center;"><b>LUM</b></p> 	<p><i>Defined by SI orientation:</i></p> <p><math>\mathbf{I}_{LUM}</math> = medio-lateral axis of lumbar segment, positive towards the right</p> <p><math>\mathbf{J}_{LUM}</math> = anterior-posterior axis of lumbar segment, positive in anterior direction</p> <p><math>\mathbf{K}_{LUM}</math> = vertical axis of lumbar segment, positive in superior direction</p>
<p style="text-align: center;"><b>PEL</b></p> 	<p><i>Defined by vectors created from RASIS, LASIS, RPSIS and LPSIS:</i></p> <p><math>\mathbf{I}_{PEL}</math> = vector joining midpoint of RASIS and RPSIS to the midpoint of LASIS and LPSIS, positive towards the right</p> <p><math>\mathbf{J}_{PEL}</math> = perpendicular to <math>\mathbf{I}_{PEL}</math> where it intersects the midpoint of RASIS and LASIS</p> <p><math>\mathbf{K}_{PEL}</math> = Cross product of <math>\mathbf{I}_{PEL}</math> and <math>\mathbf{J}_{PEL}</math></p>
<p style="text-align: center;"><b>FEM</b></p> 	<p><i>Defined by vectors created from HJC, MEPI and LEPI:</i></p> <p><math>\mathbf{I}_{FEM}</math> = vector joining MEPI to LEPI, positive towards the right (LEPI)</p> <p><math>\mathbf{J}_{FEM}</math> = Cross product of <math>\mathbf{I}_{FEM}</math> and <math>\mathbf{K}_{FEM}</math></p> <p><math>\mathbf{K}_{FEM}</math> = perpendicular to <math>\mathbf{I}_{FEM}</math> where it intersects HJC, positive in proximal direction</p>
<p style="text-align: center;"><b>TIB</b></p> 	<p><i>Defined by vectors created from MEPI, LEPI, MMAL and LMAL:</i></p> <p><math>\mathbf{I}_{TIB}</math> = vector joining MMAL to LMAL, positive towards the right (LMAL)</p> <p><math>\mathbf{J}_{TIB}</math> = Cross product of <math>\mathbf{I}_{TIB}</math> and <math>\mathbf{K}_{TIB}</math></p> <p><math>\mathbf{K}_{TIB}</math> = perpendicular to <math>\mathbf{I}_{TIB}</math> where it intersects the KJC, positive in proximal direction</p>
<p style="text-align: center;"><b>FOOT</b></p> 	<p><i>Defined by vectors created from MMAL, LMAL and MET5:</i></p> <p><math>\mathbf{I}_{FOOT}</math> = vector joining MET5 to FJC (where FJC is an offset along global X axis), positive towards the right (MET5)</p> <p><math>\mathbf{J}_{FOOT}</math> = Cross product of <math>\mathbf{I}_{FOOT}</math> and <math>\mathbf{K}_{FOOT}</math></p> <p><math>\mathbf{K}_{FOOT}</math> = Positive from FJC to midpoint of MMAL and LMAL (coincident with the global Z axis)</p>

(ii) *Joint Co-ordinate System for the definition of joint angles*

A co-ordinate system was defined for the four joints below based on their proximal and distal segments.

L5/S1: proximal segment is LUM, distal segment is PEL

HJC: proximal segment is PEL, distal segment is FEM

KJC: proximal segment is FEM, distal segment is TIB

AJC: proximal segment is TIB, distal segment is FOOT

The joint coordinate system is formed from  $I_{proximal}$ ,  $K_{distal}$  and a floating axis (FA).

$$FA = \frac{K_{distal} \times I_{proximal}}{|K_{distal} \times I_{proximal}|} \quad \text{Equation 6.4}$$

Flexion/extension of the joint occurred about  $I_{proximal}$  and was the angle between  $K_{proximal}$  and FA.

$$\alpha = 90 - \cos^{-1}(K_{proximal} \cdot FA) \quad \text{Equation 6.5}$$

Abduction/adduction of the joint occurred about FA and was the angle between the  $I_{proximal}$  and  $K_{distal}$ .

$$\beta = -90 - \cos^{-1}(K_{distal} \cdot I_{proximal}) \quad \text{Equation 6.6}$$

Internal/external rotation of the joint occurred about  $K_{distal}$  and was the angle between  $I_{distal}$  and FA.

$$\gamma = 90 - \cos^{-1}(I_{distal} \cdot FA) \quad \text{Equation 6.7}$$



#### *6.2.6.2 Data extraction program*

Once all relevant Step files containing the relevant 3D kinematic data were derived, a subsequent custom Matlab program was written to calculate additional variables and extract key parameters from the dataset.

##### *(i) Time normalisation and Stroke Extraction*

All 50 columns of data in Table 6.3 were time normalized based on handle force thresholds, with every stroke represented as 101 data points, with 0% representing the catch of the stroke and 100% representing the completion of the stroke prior to the subsequent catch point (see Section 3.2.6.6). Of all the normalised strokes recorded within a Step, ten strokes in the middle of each trial were extracted for statistical analysis. This is so that any acceleration or deceleration phases at the start and end of each piece are discarded, and ten highly repeatable and consistent strokes could be analysed (Appendix D).

##### *(ii) Force Normalisation*

All measured forces, i.e. those at the foot-stretcher, seat and handle were recorded in Newtons (N), thus subsequently normalised to the rowers' BM in kilograms.

##### *(iii) Deriving additional foot force parameters*

Resultant foot force is bilaterally calculated from the vertical and horizontal components of force (see Section 5.2.4.3). Resultant, vertical and horizontal foot forces

are then bilaterally summed to provide measures of right, left and total resultant foot forces, for ten normalised strokes. Furthermore, based on vertical and horizontal components of force, a column of RF data, which represents the effectiveness of force application in the horizontal plane, is derived (Morin et al., 2011).

$$RF = \frac{F_{horiz}}{F_{res}} \times 100 \quad \text{Equation 6.8}$$

Where RF is foot force ratio,  $F_{horiz}$  is horizontal foot force and  $F_{res}$  is resultant foot force.

(iv) *Determine key timings of stroke*

In order to extract data at key timings within each stroke and to calculate new variables, such as those that occur in the drive phase, the index for the catch, MHF and finish positions were determined for every stroke.

(v) *Data extraction*

All kinetic and kinematic variables from Table 6.3 were extracted at catch, MHF and finish, thus producing ten values per trial, at each stroke position. For the kinetic variables, peak values within the drive phase were also extracted. Additionally, joint ROM in the sagittal plane was calculated at each joint, with ROM representing the motion that occurred between maximum and minimum values that occurred per stroke. A key variable extracted from the script was  $\Delta L5/S1$  i.e. change in sagittal plane angle of L5/S1 between catch and MHF. Pelvic twist and ML drift were further variables calculated from the data set, and the derivations of these values are given in Section 3.2.6.5.

(vi) *Quantifying Asymmetry*

The absolute version of the symmetry index (ASI) proposed by Robinson et al. (1987) was used to assess the degree of asymmetry of all foot force parameters. This was calculated using Equation 6.9:

$$\text{ASI (\%)} = \frac{2|X_{right} - X_{left}|}{(X_{right} + X_{left})} \cdot 100 \quad \text{Equation 6.9}$$

$X_{right}$  is the value of the right limb and  $X_{left}$  is the value of the left limb. An ASI value of zero indicates perfect symmetry, and increasingly positive values indicate increasing magnitudes of bilateral asymmetry.

### 6.2.7 Statistical Analysis

Using SPSS (version 19, IBM Corporation, New York, USA), multiple regression models were generated to quantify the contributions of (i) kinematics on foot force application, (ii) foot force ASI on ML drift, pelvic twist and  $\Delta L5/S1$ , and (iii) foot force on seat and handle force.

The quality of a regression model is often evaluated through post-test assessments of  $R^2$  and adjusted  $R^2$  values.  $R^2$  gives a measure of the goodness of fit of a regression model on the outcome variance. An adjusted  $R^2$  value quantifies the variance in the dependent variable that would be accounted for if the model had been derived from the population. Therefore the latter value must be used to compare models with different numbers of explanatory variables. When  $R^2$  is equal to 1, there is a perfect match between the line of least squares and the experimental data points, whilst a value of 0 suggests there is no relationship between the predictor and dependent variables.

### 6.2.7.1 Data reduction

Popular opinion when constructing a regression model is that the number of observations in the dataset should be at least ten times the number of explanatory variables inputted into a single regression model. Given the vast amount of kinematic and kinetic data outputted from the Data Extraction Program (recall that all data was extracted at multiple time points in the stroke), it was necessary to reduce the number of input explanatory variables into each model.

First, Pearson's correlation analysis was performed in Matlab to determine the variables that were significantly correlated ( $P < 0.05$ ) with each dependent variable. A new reduced set of predictor variables which were significantly correlated with each dependent variable could then be constructed. With this new dataset, a Stepwise multiple regression was performed to generate several regression equations of varying quality, by incorporating a different selection of explanatory variables derived from the reduced dataset. An optimal model was selected from the Stepwise regression which produced the highest adjusted  $R^2$  and a significant F-test in the ANOVA output.

A forced entry method of regression (i.e. *Enter* variable selection method) was subsequently employed, and the multiple regression was run again using the selected explanatory variables from the optimum Stepwise entry model. Therefore, all predictors were forced into the model simultaneously as there was no theoretical evidence which suggests one variable could be a stronger predictor of the outcome than another.

### 6.2.7.2 Diagnostics

Diagnostics were performed to test two important suppositions. First, that the model fits the observed data well, and second, that the model can be generalized to a larger sample.

#### (i) Influential Cases

It is necessary to establish whether the regression model accurately represents the actual dataset. Therefore, outliers and influential cases must be examined to see if the model is influenced by a small number of cases. Standardized residuals with z-scores of  $>3.0$  will be treated as outliers and dropped from the model as it indicates that the level of error within the model is unacceptable. Influential cases are when a certain case exerts unwarranted influence over the model parameters. To examine the effect of individual cases on the whole model, values for Cook's distance, leverage and Mahalanobis distance were assessed.

#### (ii) Generalizability

To enable generalizable conclusions to be drawn from this model, the following assumptions were not to be violated:

- *Homoscedasticity*: at each level of observation the variance of residuals should be constant. Unequal variance implies heteroscedasticity thus a scatterplot depicting this information should demonstrate no funneling effect.

- *Normally distributed errors*: residuals should be random, therefore normally distributed with a zero mean.
- *Independent errors*: for any two observations, residual terms should be uncorrelated. The Durbin Watson statistic tests for auto-correlation within the residuals of a regression analysis. The statistic is always a value between zero and four, with a value of two indicating no auto-correlation.
- *Multicollinearity*: There should be no strong correlation between two predictors as it becomes difficult to obtain unique estimates of regression coefficients. A variance inflation factor (VIF) provides a value of how much the variance in the model is influenced by multicollinearity. A value of 10 or above is considered problematic.

## **6.3 Results**

### **6.3.1 Does technique influence force application?**

The first general aim was to look at the relationship between lower limb kinematics and the application of foot force. Firstly, the kinematic variables which influence peak resultant foot force were examined. Secondly, the variables which influence RF were examined.

#### *6.3.1.1 Resultant foot force at maximum handle force*

Resultant force at MHF was selected as the dependent variable rather than resultant impulse, as impulse covaries with stroke rate, whereas Chapter 4 showed that peak foot force values are stable across incremental stroke rates. Peak resultant foot force

correlates highly with resultant foot force at MHF (Figure 6.3;  $R = 0.91$ ), therefore the latter was selected as the dependent variable as the occurrence of MHF is a meaningful time point in the stroke cycle which key kinematic variables are referenced against.

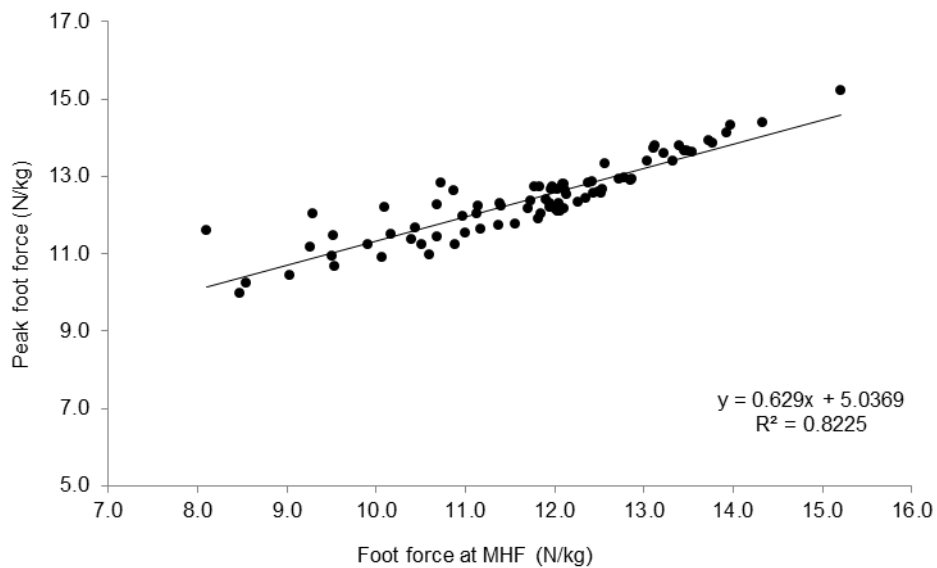


**Figure 6.3: Scatterplot depicting a linear relationship between peak resultant foot force and resultant foot force at MHF.**

---

A Pearson's product moment correlation coefficient was derived for the 41 kinematic variables that were correlated against resultant foot force at MHF. Of these 41 variables, those with significant p-values ( $P < 0.05$ ) are shown in Table 6.5.

**Table 6.5: Kinematic variables that are significantly correlated with resultant foot force at MHF. Variables subsequently extracted by Stepwise Regression are highlighted in grey.**

<b>Kinematic variable</b>	<b>R value</b>	<b>P value</b>
Hip $\alpha$ at catch	-0.38	0.00
Hip $\alpha$ at MHF	-0.49	0.00
Hip ROM	0.46	0.00
Hip $\beta$ at catch	-0.24	0.03
Hip $\beta$ at MHF	-0.32	0.00
Hip $\gamma$ at MHF	-0.24	0.04
Hip $\gamma$ at finish	-0.29	0.01
knee $\alpha$ at MHF	0.23	0.04
knee $\alpha$ at finish	-0.31	0.00
Ankle $\alpha$ at catch	-0.26	0.02
Ankle $\gamma$ at catch	-0.24	0.03

A stepwise regression was run after removing the non-sagittal plane kinematic variables. This was done because previous research has shown out-of-plane rotations to have low impact on technique, with only 0.53% of all out-of-plane rotations demonstrating significant changes with respect to rowing intensity and longitudinal training (Murphy, 2009). Furthermore, it was thought that implementing training interventions based on modifications in movement about the frontal and coronal planes (for example, changing the degree of external hip rotation during the mid-drive) would be difficult, particularly as these aspects of performance are not easily detected by eye. As such, those variables were excluded from the dataset used in the current chapter.

The optimal stepwise regression model extracted four variables which best explained the variance in peak resultant foot force. These were hip  $\alpha$  at MHF, Hip ROM, hip  $\alpha$  at the catch, and ankle  $\alpha$  at the catch. Athletes' mean  $\pm$  SD scores for these variables are in Table 6.6.



**Table 6.6: Descriptive statistics of the multiple regression model's dependent variable (top) and predictor variables.**

	<b>Variable</b>	<b>Mean</b>	<b>Standard Deviation</b>
Dependent	Resultant foot force at MHF	11.67	1.52
Predictor	Hip $\alpha$ at MHF	-102.15	9.40
Predictor	Hip ROM	103.00	12.30
Predictor	Ankle $\alpha$ at catch	-75.90	10.61
Predictor	Hip $\alpha$ at catch	-131.18	11.09

The four predictors had moderately good correlation with peak resultant force, as indicated by the highlighted R values in Table 6.5. The model achieved an  $R^2$  and adjusted  $R^2$  value of 0.48 and 0.46 respectively. This accounts for almost 50% of the outcome variance, indicating a moderately good ability of the model to predict resultant foot force at MHF. The F-value of the model was 17.46, which makes the results highly significant ( $P < 0.001$ ), indicating a good predictive ability where the results were not due to random variance.

### *Diagnostics*

In terms of influential cases no outliers (i.e. with a standard residual of  $> 3.00$ ) were detected in the data set. Cook's distance, which measures the overall influence of a case on the model, had a maximum value of 0.11 which is substantially less than the problematic value of 1.00. Mean leverage and Mahalanobis values were small (0.05 and 3.95 respectively), suggesting that overall, individual cases had only a small influence on the regression line.

In terms of the generalizability of the model, residuals in the model were random with a mean value of  $-9.21E^{-15}$  (i.e. almost zero mean). This means that error variables are

normally distributed, and that differences between the model and observed data happen only occasionally.

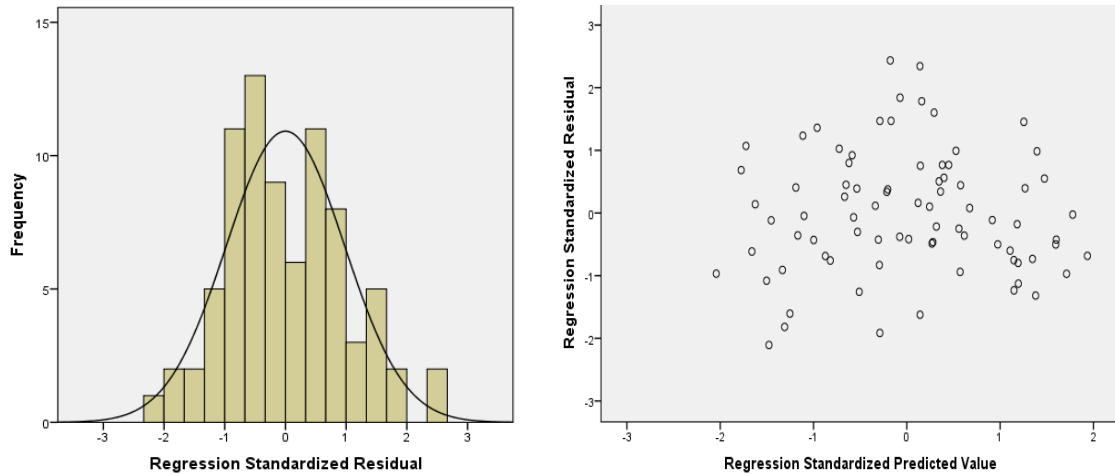


**Figure 6.4: Assessment of the assumptions of normality and constant variance with respect to resultant foot force at MHF.**

Figure 6.4 shows that the assumptions of normality and homoscedasticity were adhered to in the current model. There is no funnelling effect present in the standardised residual scatter plot, thus the assumption of constant variance is met. The Durbin-Watson test gave a value of 2.07 which is very close to the uncorrelated value of 2.00. This suggests that in any two observations, errors are independent of one another. Multicollinearity between predictor variables was investigated and it was found to be violated, where hip  $\alpha$  at MHF and hip  $\alpha$  at catch were strongly correlated ( $R=0.81$ ). As such, hip  $\alpha$  at catch was removed from the model (it was responsible for a smaller proportion of the variance in foot force compared to hip  $\alpha$  at MHF) and the regression analysis was performed with three predictor variables. In this situation the model achieved an  $R^2$  and adjusted  $R^2$  value of 0.40 and 0.37 respectively. Consequently, in this data set, 40% of the total variation in resultant foot force at MHF can be explained by its linear relationship with Hip  $\alpha$  at MHF, Hip ROM and Ankle  $\alpha$  at Catch.

### 6.3.1.2 Foot force orientation at maximum handle force

A Pearson's product moment correlation coefficient was derived for the 41 kinematic variables that were correlated against RF at MHF. Force ratio at MHF, in particular, was of interest because during a period of large force production such as the mid-drive, force should be orientated horizontally. Of these 41 variables, those with significant p-values ( $P < 0.05$ ) are shown in Table 6.7.

**Table 6.7: Kinematic variables that are significantly correlated with RF at MHF. Variables subsequently extracted by Stepwise Regression are highlighted in grey.**

Kinematic variable	R value	P value
$\Delta L5/S1$	0.38	0.00
L5/S1 $\beta$ at catch	0.41	0.00
L5/S1 $\beta$ at MHF	0.40	0.00
L5/S1 $\beta$ at finish	0.48	0.00
Hip $\beta$ at MHF	0.28	0.01
Hip $\gamma$ at catch	-0.28	0.01
Hip $\gamma$ at MHF	-0.29	0.01
knee $\alpha$ at MHF	-0.52	0.00
knee $\alpha$ at finish	-0.23	0.04
Ankle $\alpha$ at MHF	0.32	0.00
Ankle $\gamma$ at catch	0.23	0.04
Ankle $\gamma$ at MHF	0.37	0.00

A stepwise regression was run, again after removing the non-sagittal plane variables, as these are difficult to adjust through coaching. The optimal stepwise regression model extracted two variables which best explained the variance in RF at MHF. These were knee  $\alpha$  at MHF and  $\Delta L5/S1$ . Athletes' mean  $\pm$  SD scores for these variables are in Table 6.8.

**Table 6.8: Descriptive statistics of the multiple regression model's dependent variable (top) and predictor variables.**

	<b>Variable</b>	<b>Mean</b>	<b>Standard Deviation</b>
Dependent	RF at MHF	81.33	6.86
Predictor	$\Delta L5/S1$	-1.16	2.97
Predictor	Knee $\alpha$ at MHF	75.88	9.55

The two predictors had moderately good correlation with peak resultant force, as indicated by the highlighted R values in Table 6.7. The model achieved an  $R^2$  and adjusted  $R^2$  value of 0.41 and 0.39 respectively. This accounts for 41% of the outcome variance, indicating a moderately good ability of the model to predict RF at MHF. The F-value of the model was 26.61, which makes the results highly significant ( $P < 0.001$ ), indicating a good predictive ability where the results were not due to random variance.

### *Diagnostics*

In terms of influential cases no outliers were detected in the data set. Cook's distance, which measures the overall influence of a case on the model, had a maximum value of 0.07 which is substantially less than the problematic value of 1.00. Mean leverage and Mahalanobis values were small (0.01 and 0.03 respectively), suggesting that overall, individual cases had only a small influence on the regression line.

In terms of the generalizability of the model, residuals in the model were random with a mean value of  $-6.88E^{-15}$  (i.e. almost zero mean). This means that error variables are normally distributed, and that differences between the model and observed data happen only occasionally.

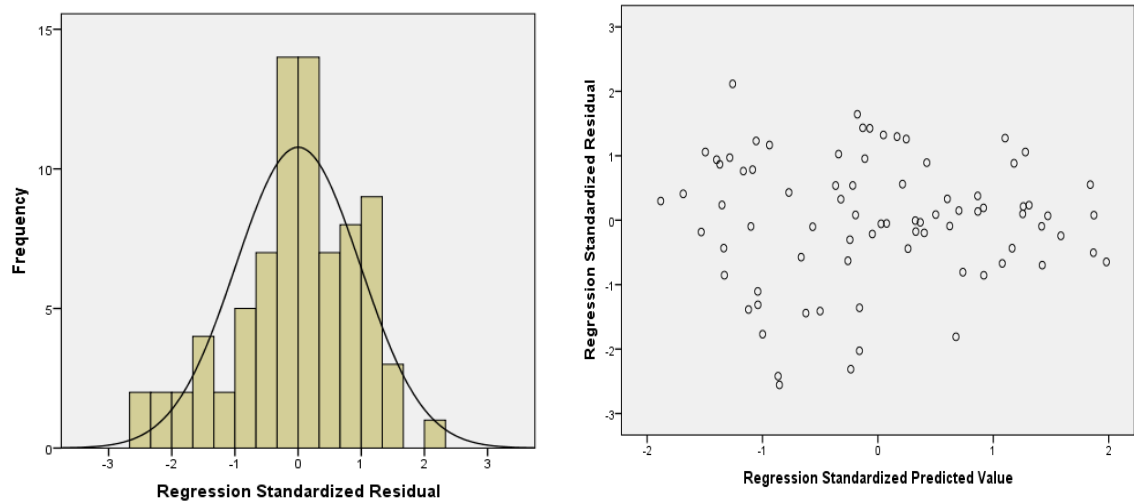


**Figure 6.5: Assessment of the assumptions of normality and constant variance with respect to RF at MHF.**

Figure 6.5 shows that the assumptions of normality and homoscedasticity were adhered to in the current model. There is no funnelling effect present in the standardised residual scatter plot, thus the assumption of constant variance is met. The Durbin-Watson test gave a value of 2.69 which suggests that errors are likely to be independent of one another. Finally, multicollinearity was avoided as the correlation matrix showed that the highest correlation between two predictor variables were 0.06, whilst VIF was 1.00. The model achieved an  $R^2$  or adjusted  $R^2$  value of 0.41 and 0.39 respectively. Consequently, in this data set, 41% of the total variation in RF at MHF can be explained by its linear relationship with  $\Delta L5/S1$  and Knee  $\alpha$  at MHF.

### **6.3.2 Do foot force asymmetries influence performance?**

The second aim of this study was to investigate whether asymmetries at the footplate influence, and could thus be used as a surrogate measure, for kinematics of the lumbar-pelvic region, ML drift on the seat and/or pelvic twist.

### 6.3.2.1 Lumbar-pelvic kinematics

A Pearson's product moment correlation coefficient was derived for the 22 foot force asymmetry variables that were correlated against  $\Delta L5/S1$ . Murphy (2009) found  $\Delta L5/S1$  to be the most pertinent variable in prediction of lower back injuries in rowing. Hence this variable was selected as the most appropriate dependent variable for this model, which represents changes in lumbar-pelvic motion during the loading phase of the rowing stroke. Those variables relating to foot force asymmetry that were significantly ( $P < 0.05$ ) correlated with  $\Delta L5/S1$  are shown in Table 6.9.

**Table 6.9: Aspects of foot force asymmetry that are significantly correlated with  $\Delta L5/S1$ . Variables subsequently extracted by Stepwise Regression are highlighted in grey.**

Asymmetry variable	R value	P value
ASI peak resultant force	-0.21	0.06
ASI horizontal force at catch	0.19	0.08
ASI vertical force at MHF	-0.37	0.00
ASI resultant impulse	-0.43	0.00
ASI efficiency	0.27	0.02
ASI COP at MHF	-0.25	0.02
ASI timing of heels down	0.27	0.01
ASI peak resultant force index	0.20	0.08

These variables were entered into a stepwise regression and the optimal model extracted three variables which best predict  $\Delta L5/S1$ . These were ASI resultant impulse, ASI vertical force at MHF and ASI heels down. Athletes' mean  $\pm$  SD scores for these variables are in Table 6.10.

**Table 6.10: Descriptive statistics of the multiple regression model's dependent variable (top) and predictor variables.**

	<b>Variable</b>	<b>Mean</b>	<b>Standard Deviation</b>
Dependent	$\Delta L5/S1$	-1.16	2.97
Predictor	ASI resultant impulse	6.26	4.60
Predictor	ASI vertical force at MHF	24.25	15.90
Predictor	ASI timing of heels down	22.44	15.34

The three predictors only had moderately good correlation with  $\Delta L5/S1$ , as indicated by the highlighted R values in Table 6.9. The model achieved an  $R^2$  and adjusted  $R^2$  value of 0.43 and 0.41 respectively. This accounts 43% of the outcome variance, indicating a moderate ability of the model to predict  $\Delta L5/S1$ . The F-value of the model was 18.96, which makes the results highly significant ( $P < 0.001$ ), indicating a good predictive ability where the results were not due to random variance.

### *Diagnostics*

Two cases had a standard residual of  $>3.00$  so these were removed and the model run again. After removing outliers, the model explained 46% of the outcome variation (adjusted  $R^2 = 0.46$ ). Cook's distance, which measures the overall influence of a case on the model, had a maximum value of 0.22 which is substantially less than the problematic value of  $>1.00$ . Mean leverage and Mahalanobis values were small (0.04 and 2.96 respectively). Following the removal of two cases, the remaining cases had only a small influence on the regression line. Therefore, the resulting regression model contained an acceptable level of error.

In terms of the generalizability of the model, residuals in the model were random with a mean value of  $1.91E^{-16}$  (i.e. almost zero mean). This means that error variables are

normally distributed, and that differences between the model and observed data happen only occasionally.

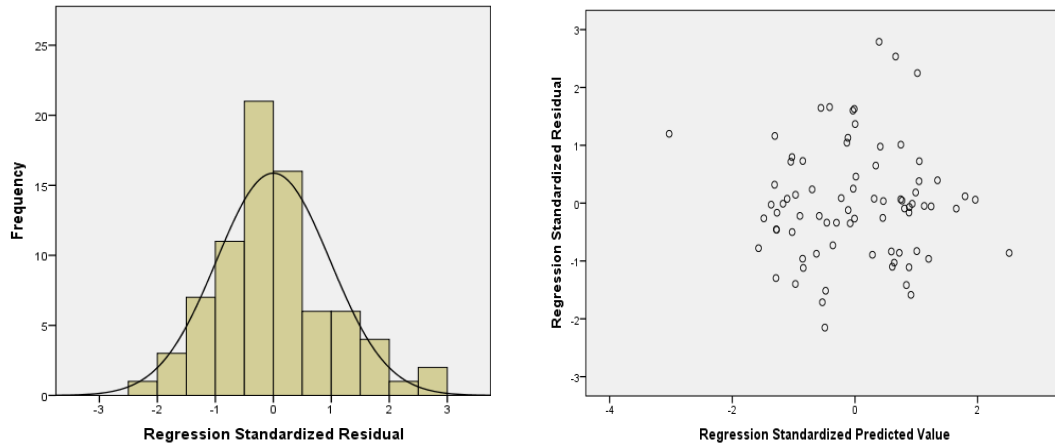


**Figure 6.6: Assessment of the assumptions of normality and constant variance with respect to  $\Delta L5/S1$ .**

Table 6.6 shows that the assumptions of normality and homoscedasticity were adhered to in the current model. There is no funnelling effect present in the standardised residual scatter plot, thus the assumption of constant variance is met. The Durbin-Watson test gave a value of 1.87 which is close to the uncorrelated value of 2.00. This suggests that in any two observations, errors are independent of one another. Finally, multicollinearity was avoided as the correlation matrix showed that the highest correlation between two predictor variables were 0.32, whilst VIF were all less than 1.00.

The model achieved an  $R^2$  and adjusted  $R^2$  value of 0.43 and 0.41 respectively. Consequently, in this data set, 43% of the total variation in  $\Delta L5/S1$  can be explained by its linear relationship with ASI resultant impulse, ASI vertical force at MHF and ASI timing of heels down.



### 6.3.2.2 Medio-lateral seat drift

A Pearson's product moment correlation coefficient was derived for the 22 foot force asymmetry variables that were correlated against ML drift. It is postulated that asymmetries in foot force application influences asymmetries at the seat, thus ML drift was input as a dependent variable to see if asymmetries at the feet translate to those at the seat. The variables relating to foot force asymmetry that were significantly ( $P < 0.05$ ) correlated with ML drift are shown in Table 6.11.

**Table 6.11: Aspects of foot force asymmetry that are significantly correlated with ML drift. Variables subsequently extracted by Stepwise Regression are highlighted in grey.**

Asymmetry variable	R value	P value
ASI vertical force at MHF	0.34	0.00
ASI horizontal impulse	0.23	0.04
ASI COP at MHF	0.25	0.03
ASI peak resultant force index	0.28	0.01
ASI peak horizontal force index	0.34	0.00

These variables were entered into a stepwise regression and the optimal model extracted two variables which best predict ML drift. These were ASI horizontal force index and ASI vertical force at MHF. Athletes' mean  $\pm$  SD scores for these variables are in Table 6.12.

**Table 6.12: Descriptive statistics of the multiple regression model's dependent variable (top) and predictor variables.**

	Variable	Mean	Standard Deviation
Dependent	ML drift	30.73	13.06
Predictor	ASI peak horizontal force index	10.83	7.21
Predictor	ASI vertical force at MHF	24.25	15.90

The two predictors only had moderately good correlation with ML drift, as indicated by the highlighted R values in Table 6.11. The model achieved an  $R^2$  and adjusted  $R^2$

value of 0.21 and 0.19 respectively. This accounts for approximately 21% of the outcome variance, indicating a poor ability of the model to predict level of knowledge of policy details. There were no outlier cases which strongly influenced the model, therefore the model was not run again and this variable was not considered any further.

### 6.3.2.3 Pelvic twist

A Pearson's product moment correlation coefficient was derived for the 22 foot force asymmetry variables that were correlated against pelvic twist during the drive phase. Asymmetries in foot force application may cause kinematic alterations further along the kinematic chain, and this may possibly be characterized by rotation of the pelvis in the axial plane. Thus, pelvic twist was used as a dependent variable to see if asymmetries at the feet translate to a rotation of the pelvis. The variables relating to foot force asymmetry that were significantly ( $P < 0.05$ ) correlated with pelvic twist are shown in Table 6.13.

**Table 6.13: Aspects of foot force asymmetry that are significantly correlated with pelvic twist. Variables subsequently extracted by Stepwise Regression are highlighted in grey.**

Asymmetry variable	R value	P value
ASI horizontal force at MHF	0.24	0.03
ASI peak horizontal force	0.30	0.01
ASI vertical force at finish	0.27	0.02
ASI resultant impulse	-0.29	0.01
ASI horizontal impulse	0.29	0.01
ASI heels down	0.36	0.00

These variables were entered into a stepwise regression and the optimal model extracted four variables which best predict pelvic twist. These were ASI heels down, ASI vertical

force at finish and ASI resultant impulse. Athletes' mean  $\pm$  SD scores for these variables are in Table 6.14.

**Table 6.14: Descriptive statistics of the multiple regression model's dependent variable (top) and predictor variables.**

	<b>Variable</b>	<b>Mean</b>	<b>Standard Deviation</b>
Dependent	Pelvic twist	-2.56	3.55
Predictor	ASI heels down	22.44	15.34
Predictor	ASI vertical force at finish	16.65	12.98
Predictor	ASI resultant impulse	6.26	4.60

The four predictors only had moderately good correlation with ML drift, as indicated by the highlighted R values in Table 6.13. The model achieved an  $R^2$  and adjusted  $R^2$  value of 0.32 and 0.29 respectively. This accounts for approximately 32% of the outcome variance, indicating a poor ability of the model to predict level pelvis twist. There were no outlier cases which strongly influenced the model, therefore the model was not run again and the variable was not considered any further.

### **6.3.3 How do forces at the feet influence the kinetic chain?**

It was clear from the start that there were to be three variables investigated in this section - MHF, seat force at MHF and foot force at MHF – as these are where the three external contact forces occur during an important part of the rowing stroke. For this analysis, it was decided that a simple linear regression would be utilized where variables would be assessed individually against resultant foot force at MHF, so that the direct relationship between forces at those points of contact could be established. Consequently, this section will not conduct any multicollinearity diagnostics. Firstly, all three variables were subjected to a Pearson's product moment correlation, and strong

coefficient R-values were present between all variables (Table 6.15), particularly between resultant foot force at MHF and seat force at MHF.

**Table 6.15: Pearson’s product moment correlation coefficients (R-value) between maximum handle force, resultant foot force at MHF and seat force at MHF**

	<b>Resultant foot force at MHF</b>	<b>Seat force at MHF</b>	<b>Maximum Handle force</b>
<b>Resultant foot force at MHF</b>	1.00	0.84	0.76
<b>Seat force at MHF</b>	0.84	1.00	0.77
<b>Maximum Handle force</b>	0.76	0.77	1.00

Subjects’ mean  $\pm$  SD scores for these variables are in Table 6.16.

**Table 6.16: Descriptive statistics of the multiple regression model’s dependent variable (top) and predictor variables.**

<b>Variable</b>	<b>Mean</b>	<b>Standard Deviation</b>
Resultant foot force at MHF	11.67	1.52
Seat force at MHF	-3.24	0.91
Maximum Handle force	9.22	1.22

### *6.3.3.1 Effect of foot force on seat force*

Seat force was entered into the model as the dependent variable, with foot force as a predictor. This was due to the sequence of the rowing stroke, where the leg drive initiates the drive phase and therefore has some influence over seat suspension and handle force.

The regression model achieved an  $R^2$  and adjusted  $R^2$  value of 0.70 and 0.70 respectively (Figure 6.7). This accounts for a large proportion of the outcome variance, indicating a good ability of foot force to predict seat force. The F-value of the model

was 184.06, which makes the results highly significant ( $P < 0.001$ ), indicating a good predictive ability where the results were not due to random variance.

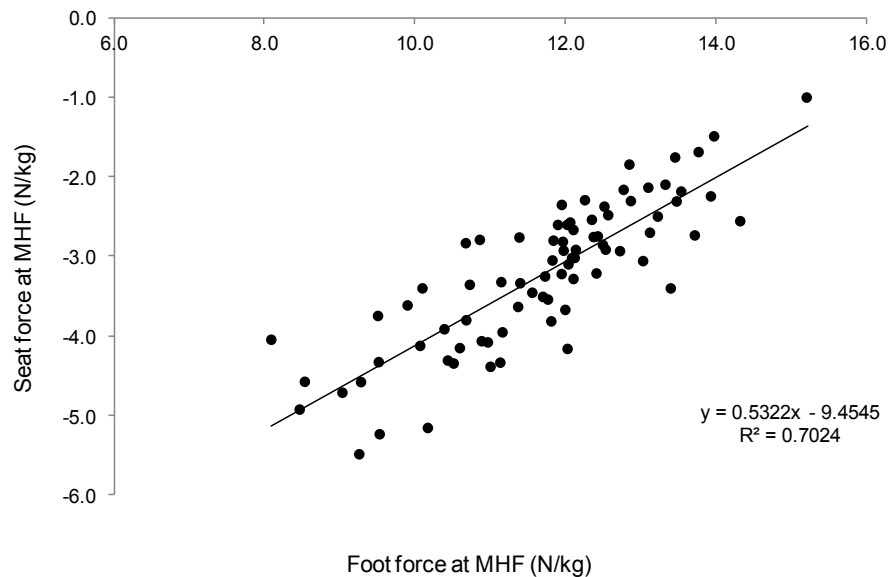


**Figure 6.7:** Scatterplot depicting a linear relationship between resultant foot force at MHF and seat force at MHF.

---

### *Diagnostics*

In terms of influential cases no outliers were detected in the data set. Cook's distance, which measures the overall influence of a case on the model, had a maximum value of 0.27 which is substantially less than the problematic value of  $>1.00$ . Mean leverage and Mahalanobis values were small (0.01 and 0.99 respectively), suggesting that overall, individual cases had only a small influence on the regression line.

In terms of the generalizability of the model, residuals in the model were random with a mean value of  $2.05E^{-15}$  (i.e. almost zero mean). This means that error variables are normally distributed, and that differences between the model and observed data happen only occasionally.

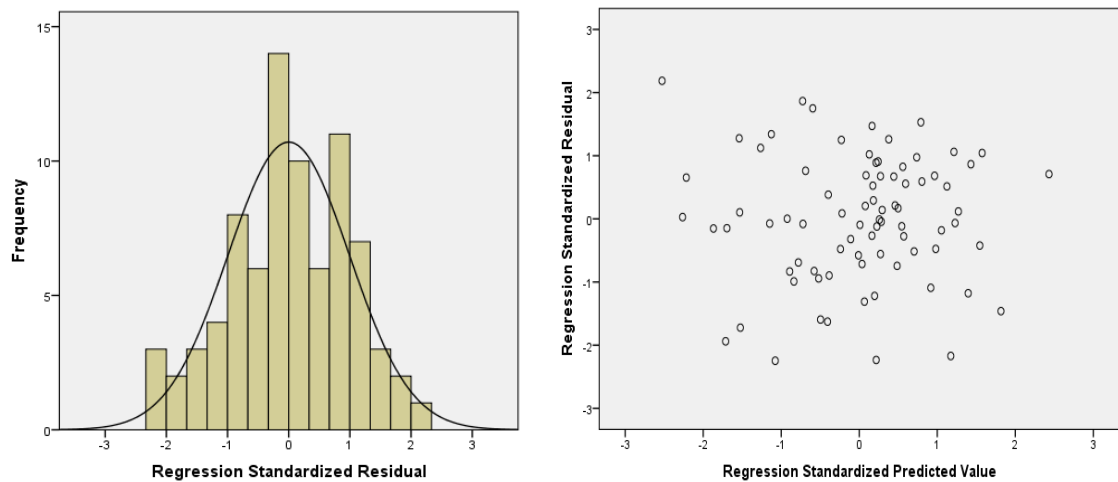


**Figure 6.8: Assessment of the assumptions of normality and constant variance with respect to seat force at MHF.**

Figure 6.8 shows that the assumptions of normality and homoscedasticity were adhered to in the current model. There is no funnelling effect present in the standardised residual scatter plot, thus the assumption of constant variance is met. The Durbin-Watson test gave a value of 2.24 which is close to the uncorrelated value of 2. This suggests that in any two observations, errors are independent of one another.

The large  $R^2$  value achieved by the model suggests that a large amount of the variability of seat force could be explained by the best model offered by the multiple regression analysis.

### *6.3.3.2 Effect of foot force on maximum handle force*

Maximum handle force was entered into the model as the dependent variable, with foot force as a predictor, due to the perceived influence of foot force on handle force in the kinetic chain of a rowing stroke.

The regression model achieved an  $R^2$  and adjusted  $R^2$  value of 0.58 and 0.58 respectively (Figure 6.9). This model accounts for a large proportion of the outcome

variance, indicating a good ability of foot force to predict handle force. The F-value of the model was 108.46, which makes the results highly significant ( $P < 0.001$ ), indicating a good predictive ability where the results were not due to random variance.

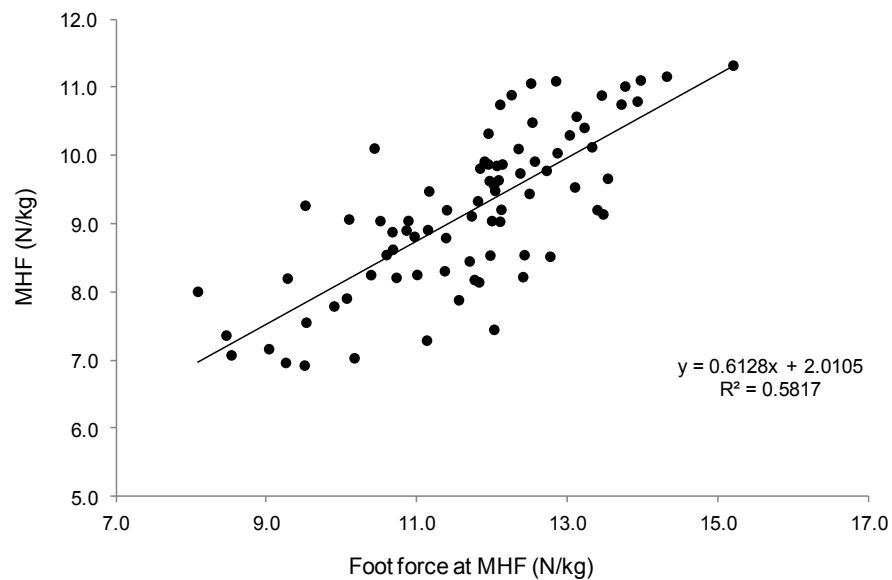


**Figure 6.9:** Scatterplot depicting a linear relationship between resultant foot force at MHF and MHF.

### *Diagnostics*

In terms of influential cases no outliers were detected in the data set. Cook's distance, which measures the overall influence of a case on the model, had a maximum value of 0.107 which is substantially less than the problematic value of  $>1.00$ . Mean leverage and Mahalanobis values were small (0.01 and 0.99 respectively), suggesting that overall, individual cases had only a small influence on the regression line.

In terms of the generalizability of the model, residuals in the model were random with a mean value of  $5.76E^{-16}$  (i.e. almost zero mean). This means that error variables are normally distributed, and that differences between the model and observed data happen only occasionally.

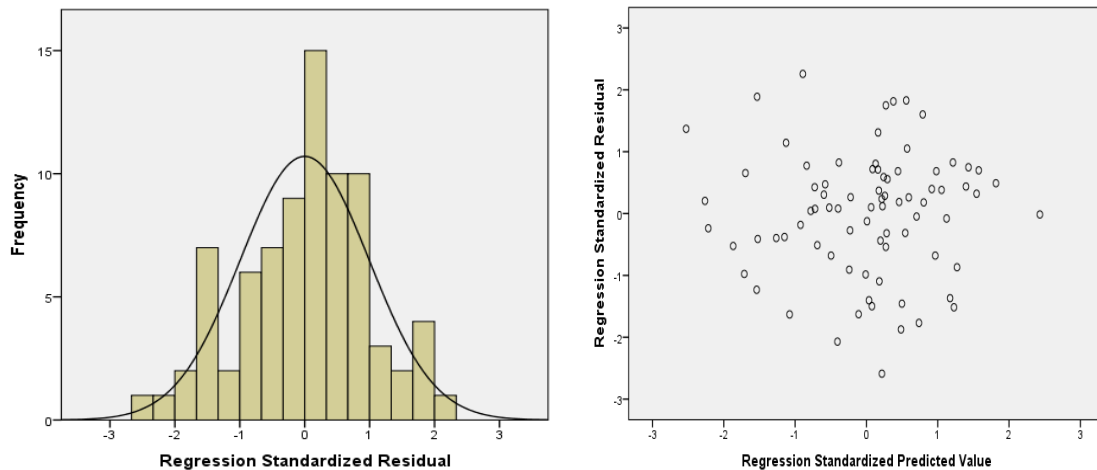


**Figure 6.10: Assessment of the assumptions of normality and constant variance with respect to peak handle force.**

Figure 6.10 shows that the assumptions of normality and homoscedasticity were adhered to in the current model. There is no funnelling effect present in the standardised residual scatter plot, thus the assumption of constant variance is met. The Durbin-Watson test gave a value of 2.09 which is very close to the uncorrelated value of 2. This suggests that in any two observations, errors are independent of one another.

The moderately large  $R^2$  value achieved by the model suggests that much of the variability in handle force could be explained by the best model offered by the multiple regression analysis.

#### **6.3.4 Summary of results**

- 43% of changes in L5/S1 angle during the critical drive can be predicted by foot force asymmetries.
- 21% of ML seat drift and 32% of pelvic twist can be predicted by foot force asymmetries.
- 40% of variance in peak resultant foot force is predicted by kinematics of the hip.



- 26% of foot force orientation is influenced by knee kinematics. When a stable lumbar-pelvic joint is maintained from catch to MHF, an additional 15% of variance in RF can be explained.
- Foot force at MHF explains 70% of variance in suspension at MHF and almost 58% of variance in peak handle force.

## **6.4 Discussion**

Following the synchronization of foot force data with kinematic data from the rower, and handle and seat force data from the rowing machine, it became possible to study in greater detail the interactions between movement of the rower and their force outputs. As such there were three main aims to this study. Firstly, to investigate which kinematic aspects of performance largely contribute to resultant and horizontal foot force. Secondly, to examine whether asymmetries at the feet influence subsequent motions of the rower which relate to risk of injury. Thirdly, to determine whether there is a linear relationship between forces applied to the foot-stretchers, and forces applied to the seat and handle.

The first aim investigated discrete aspects of technique which strongly influenced resultant forces applied to the foot-stretchers. The multiple regression model suggested that 40% of variance in foot force at MHF could be explained by sagittal plane hip and ankle kinematics. However, nearly 35% of variance in peak resultant foot force could be explained by kinematics of the hip alone. As such, in terms of producing large magnitudes of resultant foot force, hip kinematics appear to have a greater influence over foot force than knee or ankle kinematics. This idea is reflected in other activities with similar lower limb ROM, such as flywheel resisted squats and chair squats, where

significantly greater contribution of the hip joints have been demonstrated, over ankle and knee joint moments (Chiu and Salem, 2006, Flanagan et al., 2003). Greater hip ROM during the stroke and greater degrees of hip flexion at both the catch and MHF are suggested as key variables which contribute to greater resultant foot forces. As such, larger hip ROM seems to have been achieved in this data set through greater compression of the hips at the front end of the stroke.

Additional regression analyses showed that greater levels of hip flexion are associated with a smaller L5/S1 angle at the catch (Appendix I). Both these kinematic characteristics are considered beneficial in terms of performance and injury (Murphy, 2009). This is because hip flexibility at the catch enables the rower to gain length without having to compensate through flexion of the lower back to gain additional stroke length. Furthermore, greater hip flexion at MHF suggests that the hips (and consequently the trunk) do not open too early and that the legs remain engaged during the critical phase of the stroke (McArthur, 1997). The ability to apply high forces is dependent on maintaining postural position. Therefore, by opening up the body too early by posteriorly rotating the trunk before the legs have reached full extension, mechanical advantage is lost and greater reliance is placed on body mass rather than the leg drive to continue increasing velocity of the boat. Therefore, hip flexibility is important in rowing as it enables the rower to get into an optimal position at the catch, in order to achieve a long and powerful stroke (Kaehler, 2011).

Hip kinematics explain the greatest proportion of variance in resultant foot force. However, locomotive studies have shown that it is mainly propulsive ground reaction forces which contribute to large horizontal accelerations (Roberts and Scales, 2002, Hunter et al., 2005). In rowing, the goal is to achieve a large mean velocity of the boat

in the horizontal direction. However, the rowers' feet are constrained at the metatarsals, and the foot-stretchers against which forces are applied are orientated at  $42^\circ$ , thus making it difficult to apply purely horizontal forces. Consequently, in order to maximize the horizontal force ratio, technical application of foot force becomes very important. Investigations of individual force components have been done in cycling, where the effectiveness of force application has been defined as the ratio of propulsive force to the total force applied onto the pedal (Davis and Hull, 1981a, Ericson and Nisell, 1988). Similarly, in sprinting a runner is considered to have good force application technique by exhibiting a high force ratio which favours the horizontal component (Morin et al., 2011). In that situation, for a given magnitude of resultant force output, different strategies of force application which result in different RF may be used, thus increasing both the horizontal component of force and net forward acceleration. Given the direction in which the boat moves along the water, the same is true in the case of rowing. As such, it was necessary to consider the importance of foot force orientation, rather than simply the resultant force vector. The predictive kinematic variables which explained the greatest proportion of variance in RF at MHF were knee  $\alpha$  at MHF and  $\Delta L5/S1$ . Examination of the relationship between knee angle at MHF and RF show that the smaller the knee flexion at MHF the greater their RF. This means that a more rapid extension of the knees encourages a greater horizontal force output at the foot-stretchers, thus improving foot force application technique. However, knee kinematics were responsible for just 25% of the variance in RF at MHF. When a stable L5/S1 is maintained from catch to MHF, an additional 15% of variance in RF can be explained. Exhibiting as little flexion of L5/S1 as possible at the catch, and maintaining a strong posture through the critical drive were two key variables which were associated with improved performance (Murphy, 2009). By keeping a

strong connection between the lumbar spine and pelvis during the drive phase, the lumbar segment will be prevented from rotating anteriorly beyond the pelvis during the critical drive, thus putting the rower in a much stronger position to generate power (Strahan et al., 2011). Consequently, a strong posture and rapid extension of the knees during the critical drive phase are two key kinematic characteristics that explain some of the variance in force application technique in elite rowers. This notion is supported by Jones and Miller (2002) who stated that vertical movement in rowing is caused by flexion of the legs and swing of the upper body. Clearly the idea of optimizing the horizontal component of force is complicated by the requirement to provide a vertical force vector at the feet to dynamically maintain suspension during the drive. As such, some vertical force at the foot-stretchers is required to execute the most mechanically effective rowing stroke. However, the optimal relative magnitudes the two of foot force components are not known, and will be considered later in the discussion.

Further aims of this study were to examine the impact of asymmetries on discrete aspects of rowing technique. The previous chapter showed evidence of asymmetries at the foot-stretchers, however, their influence on subsequent aspects of rowing technique – namely; ML drift, pelvic twist and L5/S1 flexion during the critical drive and performance were not investigated.

The multiple regression model showed that 40% of variance in  $\Delta L5/S1$  could be accounted for by multiple aspects of foot force asymmetry. Specifically, these were ASI resultant impulse, ASI vertical force at MHF and ASI timing of heels down. ASI resultant impulse was responsible for explaining the greatest proportion of variance in  $\Delta L5/S1$ . This variable quantifies asymmetry of resultant foot force over the entire drive phase, thus is a key measure of asymmetry and may be useful in predicting kinematics

of the lumbar-pelvic region during the rowing stroke. In addition to the magnitude of forces produced, the synchronicity in timing the leg drive was also highlighted as a possible contributor to  $\Delta L5/S1$ . Timing differences in engaging the heels during the drive may result in kinematic asymmetries at the hips and knees. Kinematic asymmetries of the lower limbs were identified in Chapter 3, with those at the hip proving to be a moderate predictor of L5/S1 flexion at the catch and MHF. Whilst little research has investigated asymmetries and their impact on the lumbar-pelvic region in rowing, clinical studies have shown that bilateral leg power asymmetries affect trunk stability (Chung et al., 2008). Interestingly, the asymmetry variables which explained 31% of the variance in pelvic twist were similar to the explanatory variables for  $\Delta L5/S1$  i.e. ASI resultant impulse, ASI timing of heels down and ASI vertical force at the finish. Asymmetrical lifting has been shown to cause asymmetrical torques at the lower back, which resulted in increased spinal loading through stabilizing co-contractions of the lumbar spine (Kingma et al., 1998). However, Plamondon (1995) did not find 3D moments at L5/S1 that significantly differed between asymmetrical and symmetrical lifting. They suggested that subjects may have minimized lateral flexion and torsional moments through compensatory twisting of their pelvis and lower limbs. Even in seated activities (such as rowing) pelvic asymmetry has been shown to cause a significant increase in motion of the lumbar and thoracic spine (Al-Eisa et al., 2006a). Biomechanically, there is a clear influence of pelvic twisting on spinal kinematics, and in this study it may have been instigated by bilateral asymmetries of foot force. Consequently, foot force asymmetries may weakly influence both pelvic twist and  $\Delta L5/S1$ . As such, measures of asymmetry at the footplates may give some indication as to their effect on kinematics further along the chain of motion.

In the current dataset, less than 20% of ML drift was accounted for by the many aspects of asymmetry measured at the feet. Twisting actions of the pelvis which counteract asymmetries are thought to create out of plane motion artefacts on the seat that are deleterious to performance. There is evidence which shows that individuals with pelvic asymmetries demonstrate greater variability in pressure distribution on the seat when sitting, compared to control subjects (Al-Eisa et al., 2004a). However, rowing involves rapid anterior-posterior translations of the seat, rather than just quiet sitting, and there are also many confounding factors which may result in this out of plane seat motion. These include, initial positioning on the seat being off centre, leg length differences (which are accounted for through subject exclusion), and subtle swaying of the upper body (which are not measured) during the rapid drive phase. When the trajectory of COP on the seat was quantified it was found that in 65% of cases a larger resultant impulse on the right footplate would stimulate movement towards the left side of the seat. Therefore, there is no consistent compensatory mechanism where greater foot force on a given side results in seat motion towards the contra-lateral side, or vice-versa. This observation was simply made on an individual basis. However, regression analysis did not indicate any co-variance between foot force asymmetries and ML seat drift.

There were weak correlations between foot force asymmetries and both pelvic twist and ML drift to corroborate the link between asymmetries at the feet and seat. Clearly, there are other compensatory mechanisms that occur between the action of foot force application and what occurs at the seat and lumbar-pelvic segments that account for the majority of variance in this dataset. It would be extremely useful to collect bilateral lower limb kinematic data. However, due to the experimental limitations of the bilateral set-up indicated in Chapter 3, and the limitations imposed by elite athlete data

collection sessions, it was not possible to perform a bilateral kinematic analysis of the rowers' lower limbs.

The final aim of this chapter was to examine the interrelationships between forces expressed at the footplates, seat and handle. Regression analysis indicated that resultant foot force at MHF explains 70% of variance in seat force, where larger resultant foot forces exerted against the foot-stretchers were coupled with reduced force on the seat at MHF. There was also a strong positive relationship between foot force and handle force, where larger resultant foot force at MHF elicited greater peak handle force, explaining 58% of this variance. Therefore, rowers who apply greater forces to the foot-stretchers and exhibit large handle force relative to their bodyweight, demonstrate a greater ability to suspend from the seat during the critical drive phase. Very little research has focused specifically on seat suspension in rowing. However, a study by van Soest and Hofmijster (2009) found that strapping rowers to their seat resulted in significantly greater seat suspension, in addition to significantly greater force outputs at the foot-stretchers and handle. This implies an optimised closed kinetic chain effect where greater ability to suspend from the seat enhances force output at the foot-stretchers and handle.

From a static analysis perspective, when there is no force on the handle or movement of the athlete centre of mass (CM), force at the seat can be reduced (i.e. suspension improved) through a redistribution of vertical force from the seat to the foot-stretchers (Figure 6.11). Therefore, it is generally considered that large vertical foot forces must be produced at the catch in order to optimize seat suspension, presuming that seat suspension optimisation is a beneficial effect.

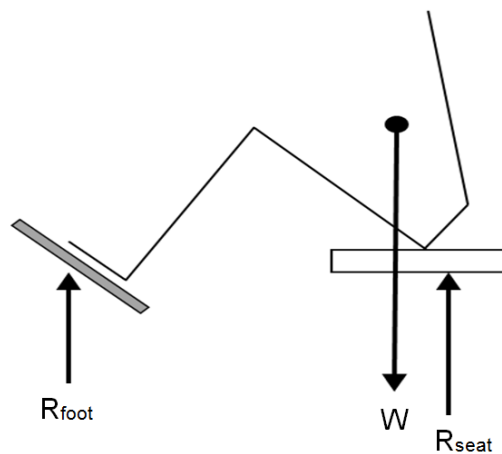


Figure 6.11: Free body diagram of the trunk and lower limbs of a rower in a static condition. No propulsive forces are generated at the handle and foot-stretchers, and the weight of the rower is balanced by vertical reaction forces at the seat and foot-stretchers.

However, resultant foot force actually had a greater  $R^2$  value for seat force at MHF ( $R^2 = 0.70$ ) compared to vertical foot force ( $R^2 = 0.39$ ) and horizontal foot force ( $R^2 = 0.44$ ). Therefore, the data from this study suggests that it is not purely vertical foot forces which influence seat suspension during the critical drive. In fact the resultant foot force must be applied at a certain angle for seat suspension to be optimised. This idea is demonstrated below by modelling the forces acting on the boat.

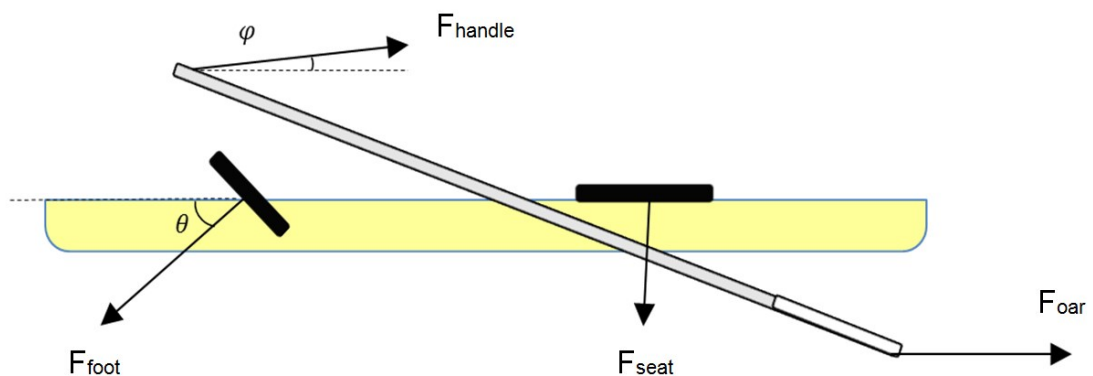


Figure 6.12: Forces acting on the rowing system at the foot-stretchers ( $F_{\text{foot}}$ ), handle ( $F_{\text{handle}}$ ), seat ( $F_{\text{seat}}$ ) and oars ( $F_{\text{oar}}$ ). Drag forces were not considered in this diagram.



A key aim in rowing is to maximise horizontal acceleration of the boat ( $a_{\text{boatH}}$ ) and to keep the vertical accelerations as low as possible. Both  $F_{\text{foot}}$  and  $F_{\text{handle}}$  are applied at an angle to the horizontal so the forces acting on the boat can be summed in the vertical and horizontal axes (Equation 6.10 – 6.11). An optimized scenario is presented below where horizontal acceleration is maximal and vertical acceleration is zero.

$$\sum F_H = F_{\text{handle}} \cdot \cos\varphi - F_{\text{foot}} \cdot \cos\theta + F_{\text{oar}} = m \cdot a_{\text{boatH}} \quad \text{Equation 6.10}$$

$$\sum F_V = F_{\text{handle}} \cdot \sin\varphi - F_{\text{foot}} \cdot \sin\theta - F_{\text{seat}} = 0 \quad \text{Equation 6.11}$$

When Equation 6.10 and Equation 6.11 are summed the following equation can be obtained.

$$F_{\text{handle}}(\sin\varphi + \cos\varphi) - F_{\text{foot}}(\sin\theta + \cos\theta) + F_{\text{oar}} - F_{\text{seat}} = m \cdot a_{\text{boatH}}$$

$$\text{Equation 6.12}$$

It can be seen from Equation 6.12 that  $F_{\text{seat}}$  must be zero in order to achieve a theoretical maximum of the boat's horizontal acceleration. Furthermore, the foot force application which contributes to this acceleration is an optimized ratio of both vertical and horizontal components of force.

Based on the optimized boat acceleration where seat force was zero, the forces acting on the rower can be analysed to examine the mechanism of seat suspension in situ. Forces act on the rower at the handle, foot-stretcher and CM, and the seat force is zero. The moment acting on the rower which serves to increase vertical seat contact is considered to be zero when the lines of action of the handle, foot-stretcher and gravity components all intersect through the same point (Figure 6.13). The line of action of the handle and gravity are fixed at each point in time and will intersect each other, whereas

that of the foot-stretcher can be modified due to technique. As the rower progresses through the drive phase, the intersection point between the handle and CM line of action becomes posteriorly displaced, thus the application of foot force must become more horizontally orientated to maintain equilibrium. Therefore, the foot force angle which allows the resultant foot force vector to intersect the lines of action of the handle force and weight component is the angle of force which is optimal for seat suspension. As such, it cannot be considered that pure vertical reaction forces at the foot-stretchers are required to optimize seat suspension.

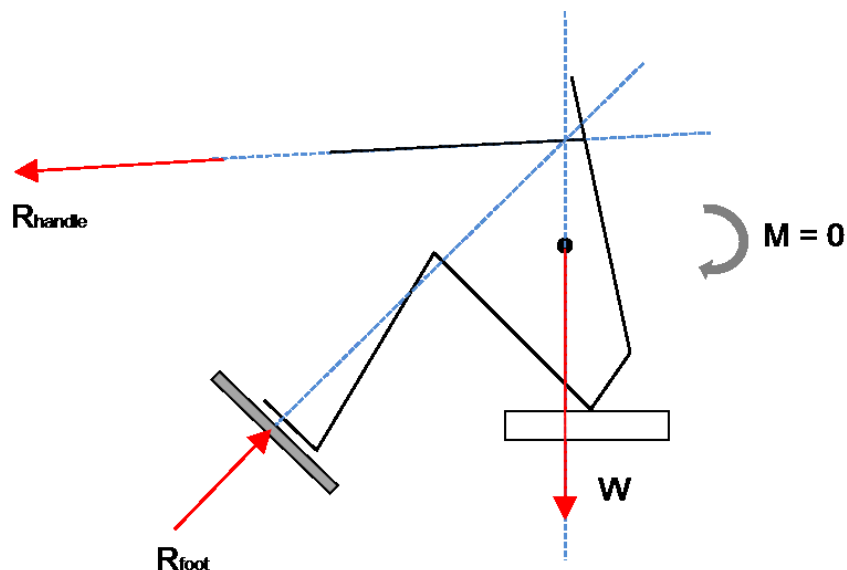


Figure 6.13: An optimised free body diagram where reaction force at the seat is zero, and lines of action for the weight of the rower acting through the centre of mass ( $W$ ), handle reaction force ( $R_{\text{handle}}$ ) and resultant foot reaction force ( $R_{\text{foot}}$ ) all intersect at a single point to provide zero moment about the rower. Dashed blue lines are the lines of action of the force vectors (presuming no acceleration for simplicity).

In the regression analysis, foot force at MHF explained 70% of variance in suspension at MHF and 58% of variance in peak handle force. An  $R^2$  value of 58% implies that resultant foot force strongly influences peak handle force, yet it explains less of the variance in handle force compared to seat force. Rowing is a sequential activity where large forces are initiated at the foot-stretchers through a rapid extension of the knees,

during which the trunk muscles must be engaged in order to provide a strong link for the transfer of force between the legs and the handle (McArthur, 1997). If the trunk muscles are not engaged, there will be a break in the link between the muscles which provide the power, meaning that some energy from the leg drive will be dissipated through poor suspension from the seat. For example, in javelin throwing where the aim is to achieve maximum release speed of the javelin, there is a very distinct sequence of delivery which is initiated by motion of the lower limbs, followed by forward rotations of the pelvis, trunk and upper limbs, prior to release (Liu et al., 2010). Without this progressive proximal-to-distal sequence of power transfer it is not possible to reach maximum release velocities (Mero et al., 1994). Due to the sequence of power transfer in rowing, forces at the feet cannot directly influence force output at the handle, without being mediated by the by the rowers' acceleration, muscle activation and interaction with the seat during the critical drive phase. As such, resultant foot force was shown to be a stronger predictor of seat force rather than handle force. Nevertheless, the strong linear relationship between all variables suggests that the majority of elite rowers are effectively able to use the force applied to the foot-stretchers to suspend from the seat and transfer this force to the handle.

Seat suspension and MHF have both previously been flagged as variables which predict good performance (Murphy, 2009). The results of this study show that both these variables can be improved through enhanced foot force production, and in turn foot force was shown to be influence by kinematics of the hips and knees. Therefore, statistical modeling of elite athlete data can provide an evidence based guide to coaches and athletes for the improvement technique which ultimately impacts on performance.

## 6.5 Conclusion

Measuring foot force in conjunction with rower kinematics and external contact forces have established that many aspects of the rowing stroke, including force application and movement patterns, are inherently dependent on one another. The results suggest hip kinematics are important in generating large resultant foot forces. However, there is a greater emphasis on a rapid drive through the knees and maintaining a strong lumbar-pelvic posture when aiming to maximize the horizontal component of foot force. In terms of the impact of foot force asymmetries on variables that may influence injury risk, there was a moderate effect of asymmetries on  $\Delta L5/S1$  during the critical drive, whereas they had little influence over pelvic twist and ML seat drift. Finally, there was a linear relationship between resultant foot force at MHF and both MHF and seat suspension at MHF. It was theoretically demonstrated that seat suspension is optimized when large foot forces are applied at an angle to the foot-stretcher. The influence of foot force on seat suspension was greater than on peak handle force. This reinforced the idea that large foot forces allow the athlete to suspend effectively from the seat, in turn enabling force production at the handle to be optimised.

In this chapter, all force data from the ergometer contact points were measured in conjunction with motion data of the rower, making it possible to look at interactions between force application and joint kinematics. This gave greater insight into aspects of technique that can be modified and improved to optimize force output and performance. The subsequent chapter will take a further step towards linking the forces generated in rowing with kinematics, by estimating the loading that occurs at the contributing joints.

## **Chapter 7:**

# **The effect of incremental training intensities on joint dynamics in elite rowers**

The previous chapter statistically examined the relationship between force production, joint kinematics, asymmetries and performance. This was achieved through synchronization of foot force data with all other kinematic and performance measures, thus enabling the relationship between force production and movement patterns to be experimentally examined. This chapter will go one step further in bridging the gap between kinetics and kinematics by quantifying inter-segmental loads at specific joints which influence the observed movement patterns. A five segment inverse dynamic model will be developed, which enables inter-segmental forces and moments at the ankle, knee, hip and L5/S1 to be estimated during ergometer rowing. Elite rowers' data recorded during incremental step tests are presented, and the implication of high intensity rowing on joint kinetics is discussed in terms of injury potential, joint loading and performance.

### **7.1 Introduction**

#### **7.1.1 Prevalence and aetiology of lower back injuries in rowing**

Rowing is a non-contact low-impact sport, and as such the injury rates amongst rowers have previously been reported as being relatively low (Weightman and Browne, 1975). However, recent epidemiological studies have reported an increasing incidence of

overuse injuries amongst senior rowers (Teitz et al., 2002, Rumball et al., 2005, Wilson et al., 2010). The most frequent site of injury was the lower back, with over one third of all injuries located there, followed by the knee (~20%) and forearm (~12%) (Smoljanovic et al., 2009). The majority of rowing injuries result from overuse and overloading of biological structures in combination with poor mechanics and technique. This is particularly true for the lower back where a study reported 93% of injuries over the course of a season to result from overuse rather than acute trauma (Smoljanovic et al., 2009). Furthermore, high volume of training on the indoor ergometer has been identified as having the most significant impact on lower back injury risk (Wilson et al., 2010).

Due to its wide prevalence and implications, rowing injuries to the lumbar spine have been extensively researched, however, the aetiology remains poorly understood. Lower back pain is not an injury in itself, but it is considered a symptom that can arise from damage or injury to the surrounding muscles and/or ligaments, or damage to the vertebrae or intervertebral discs of the lumbar spine. Other causes of LBP in rowers can include; degenerative disc disease, isthmic spondylolisthesis, facet joint syndrome, ring apophyseal injury, and sacral stress fracture (Bono, 2004).

The motion of the rowing stroke is conducive to injuries surrounding the lower back due to the repeated large rotations and high loadings that are possible there. Within the spinal column the lumbar spine has the largest capacity for sagittal plane range of motion, with approximately 70° of flexion and 35° of extension possible there. Within the lumbar spine the L4/L5 and L5/S1 joints can attain the greatest range of motion, and as mentioned in Section 1.2, they are the most frequently injured locations of the spine. Rowers spend 70% of the stroke in a flexed posture, and repeatedly achieve a large

proportion of their maximum flexion capacity. Caldwell et al. (2003) showed that rowers attain high levels of lumbar flexion during the rowing stroke, and these levels increased during the course of a 2000 m ergometer test, increasing from 75% to 90% of their maximum ROM. Flexion above 75% maximum ROM considerably increases stress on the intervertebral disc (Adams et al., 1994), and as such combined flexion and compressive loading has been identified as a mechanism for injury to the lumbar spine structures (Gallagher et al., 2005). Peak loads at the lumbar spine during a rowing stroke were estimated in the region of 6000 N and 5000 N for men and women respectively (Reid and McNair, 2000). In addition, *repetitive* compressive loading of the lumbar spine has been found to considerably increase the risk of back pain (Parkinson and Callaghan, 2007a, Parkinson and Callaghan, 2007b). It is therefore not surprising that a 90 minute rowing session where approximately 1800 cycles of trunk flexion occur may have a negative impact on spinal health.

The nature of overuse injuries of the lumbar spine in rowing would suggest that the cause is mechanical and directly linked to the degree and frequency of forces exerted through the lumbar spine (Wilson et al., 2010). However, there are currently no practical methods robust enough to directly measure joint forces and moments in rowers. As such, a non-invasive mathematical approach will be undertaken to estimate forces and moments across key joints of interest, based on external forces, anthropometric measurements and kinematic measures of the rower.

### **7.1.2 Inter-segmental inverse dynamic modelling**

The study of inter-segmental dynamics is important because it provides insight into the mechanisms which actuate human movement. Mathematical models have been

developed as a means of estimating biomechanical loading in lieu of direct invasive measures of force which present ethical issues. They are frequently used to analyse joint kinetics with respect to sports performance (Sørensen et al., 1996, Hase et al., 2004, Bezodis et al., 2008) loading strategies following surgery (Salem et al., 2003), or potential for injury during occupational or sporting tasks (Kowalk et al., 1996, Fry et al., 2003).

Inter-segmental inverse dynamic analysis (IDA) is a fundamental biomechanical procedure for the analysis of human movement. Net forces and moments from muscular contractions that span each joint are estimated by representing the skeleton as a series of joints connected by rigid uniform segments. Such simplifications are met with limitations, and these will be discussed in the following section. The Newton-Euler approach to IDA uses the principle of Newton's second law, where indeterminate unknown forces are combined to form *net* forces and moments at a segment's end point that can be solved based on known forces, as well as accelerations and inertial properties of moving bodies. Consequently, model inputs for the calculation of net forces and moments during closed chain dynamic activities include: externally measured reaction forces, kinematic data (i.e. segment position and acceleration), segment mass, segment CM positions, joint centres, and mass moment of inertia. Linear and angular equations of motion are used to derive model outputs which include net forces and moments across a joint. Therefore, IDA bridges the gap between kinematics and kinetics, by calculating inter-segmental dynamics which influence the experimentally acquired motion data. Multi-segmental analysis of human motion is possible using IDA, where unknown forces and moments are first derived for the proximal end of the most distal segment. Newton's third law is then employed where the negative *reaction* force is applied as an input to the distal end of the proximal



segment. Consequently, IDA can be applied to multiple segments using a sequential distal-to-proximal procedure where unknown forces and moments estimated at the distal segment is input as a known forces and moments to the proximal segment. As such, IDA modelling can take either a *bottom-up* approach, where kinetic data is acquired from the feet contacting a force plate, or a *top-down* approach, where external force at the hands are the distal segments' known force inputs.

### **7.1.3 Limitations of inter-segmental modelling**

Despite widespread use of IDA, it is well recognized that its solutions are prone to errors. Errors can arise from: inaccuracies from using generalized segmental parameters (i.e. mass, moment of inertia, and CM position), surface marker movements, and inaccurate location of joint centres (Riemer and Hsiao-Wecksler, 2008). Collectively, these errors were found to result in 6-232% uncertainty of peak moment values estimated during gait (Riemer et al., 2008). Given the indeterminacy problem of analysing muscle forces within the body (i.e. there are more unknowns than equations), a simplification procedure must occur, whereby segments and muscles are represented as rigid links allowing only minimal *net* moments to be quantified (Winter, 1990). When simplifications that limit the model's accuracy occur, certain assumptions are made, such as constant inertial property values, frictionless joints and uniformly rigid segments.

Errors in measuring human motion will always be present due to soft tissue artefacts, which are particularly problematic during activities that involve large accelerations. All measurement techniques which employ skin mounted sensors are prone to errors that arise from movement of the sensor relative to the underlying bone, which result from

skin and muscle deformations, and contractions that occur during limb movement. Non-rigid segments attenuate the forces applied to it, as such, the assumption of segment rigidity can potentially result in erroneous outputs, particularly with respect to flexible segments such as the trunk and foot (Robertson and Winter, 1980).

In addition to the assumption of rigid segments, the joints which connect the segments are often presumed to be frictionless. Frictional joint forces can be considered to be very low for young, small subjects. However, larger subjects, diseased joints, or modelling of joints under heavy external loads will substantially increase friction within a joint. Joint moments are required to overcome frictional forces, thus net moments calculated by models with frictionless joints are likely to underestimate true joint loading. Other characteristics of inter-segmental IDA models which attenuate joint loading is the inability to determine individual muscle activity, as muscle actions are simply represented as net moments about joints. Therefore, co-contractions that occur in human movement, particularly antagonistic co-contraction of trunk muscles to achieve spinal stability, are not accounted for. For example, it is not known whether a reduction in knee extensor moments results from reduced quadriceps activity, or increased antagonistic hamstring activity (Whittlesey and Robertson, 2004). These limitations do not invalidate IDA model data. However, efforts must be made to reduce measurement errors during data acquisition, and interpretation of model outputs and comparison of data against other studies must be made with caution.

#### **7.1.4 Applications of inter-segmental inverse dynamic modelling**

Researchers seek to quantify human joint loading because it provides useful information on fundamental mechanics of human movement, for example differences in

lower limb function between males and females, or between older and younger subjects. DeVita and Hortobagyi (2000) quantified lower limb joint moments in young and elder subjects during gait using a simple linked-segment model. Age was seen to cause a redistribution of joint moments, where older participants used their hip extensors more, and their knee and ankle extensors less than young adults. They suggested that consequences of aging are not just in reduced function, but also in neuromuscular adaptations that occur with age. Furthermore, females have been noted to have a higher incidence of running injuries. Using a 3D inverse dynamics model it has been demonstrated that females exhibit significantly different lower limb kinematics and joint moments compared to men during running, particularly at the hip, which may put them at greater risk of injuries and explain their higher incidence of injury (Ferber et al., 2003). Consequently, through the application of IDA models, the mechanisms that underlie human function can be better understood.

Quantifying joint kinetics can also be useful in identifying the loads that are required to execute certain sporting actions, and how changes in technique affects these loading patterns and distributions. Squatting is an activity for which the biomechanical mechanisms are commonly investigated. It is a closed chain activity which does not involve large CM translations, and as such the movement pattern is relatively easy to replicate and capture in a laboratory environment. (Dionisio et al., 2008) used a simple 2D model to investigate sagittal plane lower limb joint loading strategies during squatting and identified that knee flexion moments before and during the downwards acceleration phase switch to extension moments during the deceleration phase. The ankle consistently generated a plantarflexion moment throughout the motion. However, (Escamilla et al., 2001) found significant differences in joint moments during squatting in the sagittal plane when using 2D and 3D inverse dynamics techniques. These

differences were exacerbated when stance width of the squat was increased, thus highlighting the limitations of 2D inverse dynamic modelling.

In terms of technique, Escamilla et al. (2001) found from 3D modelling that increasing stance width during weighted squatting elicited significant increases in peak knee and hip moments, whereas at the ankle plantarflexion moments during the narrow stance transformed into dorsiflexion moments during wider stance squatting. Furthermore, Hwang et al. (2009) compared lumbar joint moments during squat and stoop lifting using the standard Vicon Plug-in-Gait model. Squatting is advocated in order to relieve pressure and loads at the lumbar spine, and the study by Hwang showed that lumbar joint moments do not significantly differ between squat and stoop lifting, despite lower limb joint loading patterns being different between the two styles. These are examples of differences in joint loading patterns and strategies that result from technique modifications.

In terms of rowing, a number studies have estimated joint loading during ergometer rowing. Halliday et al. (2004) combined a triaxial load cell at the foot-stretcher with optical motion tracking and a five segment lower body model to quantify ankle, knee and hip moments in university level heavyweight male rowers. Peak extensor moments about the ankle, knee and hip were 100 Nm, 320 Nm and 420 Nm, respectively. Models have been developed further to quantify loading of the lumbar spine, although the main methods have been to use a bottom-up approach for the ankle, knee and hip, and a top down approach for the lumbar spine, where the trunk is a single segment connecting the shoulder to the pelvis (Hase et al., 2004, Cerne et al., 2011). Morris et al. (2000) modelled spinal loading at L4/L5 in the sagittal plane during ergometer rowing and showed that compressive and shear force reached 2700 N and 660 N, respectively.

During on-water rowing Munro and Yanai (2000) found L5/S1 compressive loads to reach almost 5500 N. This was notably higher than the 3433 N recommended by the National Institute for Occupational Safety and Health (Mcgill, 1995). To investigate the differences in joint mechanics elicited by ergometer rowing and on-water rowing, a bottom up Newton-Euler IDA approach was employed to quantify joint kinetics whilst rowing on fixed versus sliding ergometers (Greene et al., 2011). The fixed ergometer has greater inertial forces that the rower must overcome at the start of the stroke, and this was seen to increase the moment and power output at the knee, compared to the sliding ergometer. Consequently, kinetic modelling of the rower provides useful information pertaining to loads experienced by the rower, and how these loads are influenced by various rowing conditions.

Despite the research outlined above, it seems there are no studies which have quantified ankle, knee, hip and lumbar-pelvic loading during rowing using a bottom-up approach, where the lumbar spine and pelvis are modelled as separate segments. It is extremely important to investigate loading about the lumbar-pelvic joint, because this is where the majority of rowing injuries occur. Particularly with lower back injuries being chronic in nature, the investigation of repeated loads in that region is imperative. Furthermore, no study has investigated the implications of rowing intensity on joint kinetics and examined these in terms of injury and performance. Rowers train at a range of intensities in order to develop aerobic fitness as well as explosive leg power and strength. Changes in lumbar-pelvic kinematics and lower limb ranges of motion have been noted when rowing at higher intensities (McGregor et al., 2004, Murphy, 2009). However, little is known about the changes in joint loading patterns that occur at increasing work rates. For example, joint loading strategies, particularly the contributions of hip and knee joint powers may be altered by stroke rate, where the

rowing action becomes more hip dominant due to reductions in knee ROM at higher stroke rates. In addition, the most commonly injured locations of the lumbar spine are the L4/L5 and L5/S1 discs (Humphreys and Eck, 1999), owing to the large range of motion and compressive forces that are possible there. Deteriorations in posture, characterized by greater degrees of lumbar-pelvic rotations, have been observed as stroke rate increased (McGregor et al., 2004), and this is thought to influence changes in the magnitude of loading occurring in that region. As such, the lumbar-pelvic joint (L5/S1) will be a key feature in the model developed for this study, as rotations and compressive loads of L5/S1 are associated with LBP in rowers (Reid and McNair, 2000).

Consequently, the aims of this study are to (i) develop a bottom-up 3D inter-segmental model to quantify 3D forces and moments at the ankle, knee, hip and L5/S1, and (ii) examine the effects of incremental stroke rates on joint kinematics and loading strategies during ergometer rowing, with a view to understanding the varying demands that incremental training intensities place on the joints.

## **7.2 Methodology**

### **7.2.1 Participants**

The study received ethical approval from the Imperial College Research Ethics Committee, and informed consent was obtained from all subjects (Appendix B). Eighteen elite rowers, all of whom rowed as part of the GB rowing squad in the 2012 Summer Olympics participated in this study in March 2012. Five were heavyweight female scullers (SCULL; mass  $77.1 \pm 2.4$  kg, age  $29.0 \pm 3.1$ ), seven were heavyweight female rowers (SWEEP; mass  $74.0 \pm 3.8$  kg, age  $27.1 \pm 2.3$ ) and six were lightweight

men (LWM; mass  $75.1 \pm 1.5$  kg, age  $26.6 \pm 4.0$ ). The sample size of eighteen was greater than the required number of fifteen which was necessary to achieve a moderate effect size of 0.5 and statistical power of 95% with an alpha significance level of 0.05.

All participants were right leg dominant as defined by their preferred kicking leg. Subjects with a leg difference of more than 1 cm were excluded from this study because anatomical asymmetries may influence some outcome measures of this study. Additionally, rowers with a current episode of LBP or any other serious illness or injury were excluded from this study.

### **7.2.2 Data Collection**

Experimental setup, subject preparation and digitization, experimental protocol and data acquisition were identical to those described in Sections 6.2.2 – 6.2.5 of Chapter 6. These will be briefly described in the context of this chapter.

Subjects performed a four stage ergometer Step Test. Each step was 3 minutes in duration and was performed at the following stroke rates; 18, 24 and 28 strokes per minute, and free rate i.e. an arbitrary stroke rate that corresponds to rowing a 500 m split that corresponds to their 2000 m personal best (McGregor et al., 2008).

All rowers performed their trials on a modified Concept II model D ergometer (Figure 6.1). On this ergometer the flywheel was instrumented with a linear encoder to enable stroke length to be quantified. Force data could be captured from the handle (tensile force), seat (vertical force) and bilaterally from the foot-stretchers (vertical and horizontal forces). Centre of pressure data was available for the seat in both the ML and AP directions, as well as for the foot-stretchers along their longitudinal axes.

Kinematic data of the rower were recorded using the electromagnetic FOB motion capture system (Ascension Technology, Burlington, USA). Flock of Birds sensors were attached to the rower at T12/L1 junction, L5/S1 junction, midway along the lateral aspect of the thigh, and midway along the anterior aspect of the shank. These sensors recorded 3D position and orientation of rowers' lumbar spine, pelvis, thigh and shank segments relative to an extended range transmitter. 3D global landmark co-ordinates of RPSIS, LPSIS, RASIS, LASIS, LEPI, MEPI, LMAL, MMAL, MET5 and HJC were derived through the digitisation procedure described in Section 6.2.3. These digitised landmarks were used to construct local co-ordinate systems of the pelvis, thigh, shank and foot.

Data from the FOB and load cells were acquired from separate data acquisition units, and were subsequently software synchronised using a custom LabView program. This ensured that movement and force data were time synchronized upon writing to file.

### **7.2.3 Data Analysis**

A *Kinematics Program* (see Section 6.2.6.1) calculated global 3D joint centre positions of the ankle, knee, hip and L5/S1 based on digitised bony landmark positions. Three-dimensional joint angles were calculated using the JCS method of Grood and Suntay (1983).



### 7.2.3.1 *Inverse Dynamics Procedure*

Inverse dynamics is a method for computing joint forces and moments of rigid bodies, based on kinematics and inertial properties (mass and moment of inertia) of the segments in question.

A 3D inter-segmental model was written in Matlab which represented the foot, shank, thigh and pelvis and lumbar spine as a rigid, five segment system (Appendix J). In this model the foot was treated as a single rigid segment. Linear and angular Newtonian equations of motion were employed to calculate joint reaction forces and moments at the ankle, knee, hip and lumbar-pelvic joints throughout multiple rowing cycles. Anthropometric and inertial parameters of each segment are outlined in Table 7.1.

This study deals with 3D inverse dynamics, thus all kinetic and kinematic descriptors subsequently presented are treated as 3D row vectors. To solve for joint forces and moments the following inputs are required:

- Mass, moment of inertia and CM position of each segment
- Position, velocity and acceleration of each segment's CM.
- Angular position, angular velocity and angular acceleration about each segment's CM.
- External forces for all contact points (i.e. foot force and seat force)
- Centre of pressure or location of external forces acting on the body.

**Table 7.1: Anthropometric measures from Zatsiorsky et al. (1990).**

Segment	$I_{ml}$ (kg/cm <sup>2</sup> )	$I_{si}$ (kg/cm <sup>2</sup> )	$I_{ap}$ (kg/cm <sup>2</sup> )	$m$ (%)	CM (%)
Foot	40.0	10.3	44.0	1.370	55.85
Shank	371.0	64.6	385.0	4.330	40.47
Thigh	1999.4	413.4	1997.8	14.165	45.49
Pelvis	525.0	592.4	656.8	11.174	35.41

$I_{ml}$ ,  $I_{si}$ , and  $I_{ap}$  are the moments of inertia about the medio-lateral, superior-inferior and anterior-posterior axes of the segments;  $m$  (%) is the mass of the segment relative to body mass; CM (%) is the location of CM along the segment's longitudinal axis as a percentage of segment length.

### 7.2.3.2 Linear and Angular Kinematics

Three dimensional co-ordinates of FJC, AJC, KJC, HJC and L5/S1 were used to calculate segment lengths of the foot, shank, thigh and pelvis by subtracting each segment's proximal joint co-ordinates from their distal joint co-ordinates. Segment lengths were combined with anthropometric data from Table 7.1 to derive segment CM co-ordinates. Linear velocity and acceleration of each segment's CM were obtained through differentiation using the finite difference method (Equations 7.1 and 7.2, respectively). Differentiation results in noisy data, so these were smoothed in Matlab using a five point moving average.

$$v = \frac{(p_{i+1} + p_{i-1})}{2 \times dt} \quad \text{Equation 7.1}$$

Where  $v$  is linear velocity of the segment's CM,  $p$  is the global position of CM and  $dt$  is the time interval between successive data points.

$$a = \frac{(v_{i+1} + v_{i-1})}{2 \times dt} \quad \text{Equation 7.2}$$

Where  $a$  is linear velocity of the segment's CM,  $v$  is the global position of CM and  $dt$  is the time interval between successive data points.

Angular velocity of segments' CM was calculated as shown in Equation 7.3 and angular acceleration was obtained by differentiation of angular velocity (Equation 7.4).

$$\dot{\theta} = \frac{v \times r}{r^2} \quad \text{Equation 7.3}$$

Where  $r$  is the radius from the global origin to segment CM and  $\dot{\theta}$  is angular velocity.

$$\ddot{\theta} = \frac{(\dot{\theta}_{i+1} + \dot{\theta}_{i-1})}{2 \times dt} \quad \text{Equation 7.4}$$

Where  $\ddot{\theta}$  is angular acceleration,  $\dot{\theta}$  is angular velocity and  $dt$  is the time interval between successive data points.

### 7.2.3.3 Newton-Euler Calculations

Calculating linear accelerations allows forces at the segment's CM to be derived based on Newton's Second law (Equation 7.5).

$$\Sigma F = m \cdot a \quad \text{Equation 7.5}$$

Where  $F$  is force,  $m$  is segment mass, and  $a$  is linear acceleration of segment CM.

Forces at CM are then used to derive unknown reaction forces at the proximal joint ( $R_{prox}$ ) (Equation 7.6). For the foot segment in contact with the footplate, the distal joint reaction force ( $R_{dist}$ ) is given by the multi-axis output from the transducer. For subsequent segments such as the shank and thigh,  $R_{dist}$  of the shank will be equal and opposite to  $R_{prox}$  of the foot (Figure 7.1). Consequently, in a bottom-up inverse dynamics procedure  $R_{dist}$  is always a known quantity, and  $R_{prox}$  can be derived sequentially for each segment using the equation below.

$$R_{prox} = m \cdot a - R_{dist} - m \cdot g \quad \text{Equation 7.6}$$

Where  $R_{prox}$  and  $R_{dist}$  are reaction forces at the proximal and distal ends of a segment,  $m$  is segment mass,  $a$  is segment CM acceleration, and  $g$  is a gravity component (i.e. -9.81).

Calculating angular accelerations allows moments about the proximal end of a segment to be derived based Euler's equation of rigid body motion (Equation 7.7). Moment of inertia about a segment's CM is taken from values established by Zatsiorsky et al. (1990) (Table 7.1).

$$\Sigma M = I \cdot \ddot{\theta} \quad \text{Equation 7.7}$$

Where  $M$  is net joint moment,  $I$  is moment of inertia and  $\alpha$  is angular acceleration.

Reaction forces at each joint contribute to the sum of muscle moments about a joint, given by laws established by the following equation:

$$M = R \cdot d \quad \text{Equation 7.8}$$

Where  $M$  is a moment about the centre of mass,  $R$  is joint reaction force and  $d$  is moment arm.

As such, it was necessary to calculate moment arms corresponding to each joint reaction force. For the foot segment in contact with the footplate, the distal moment arm ( $d_{dist}$ ) was the vector between the footplate's global COP and the foot's CM. It was possible to convert COP from the footplate's local co-ordinate frame to the global kinematic reference frame, based on the digitized location of the right footplate. For subsequent segments in the free body diagram, proximal and distal moment arms were derived based on the distance between joint centre positions and CM locations.

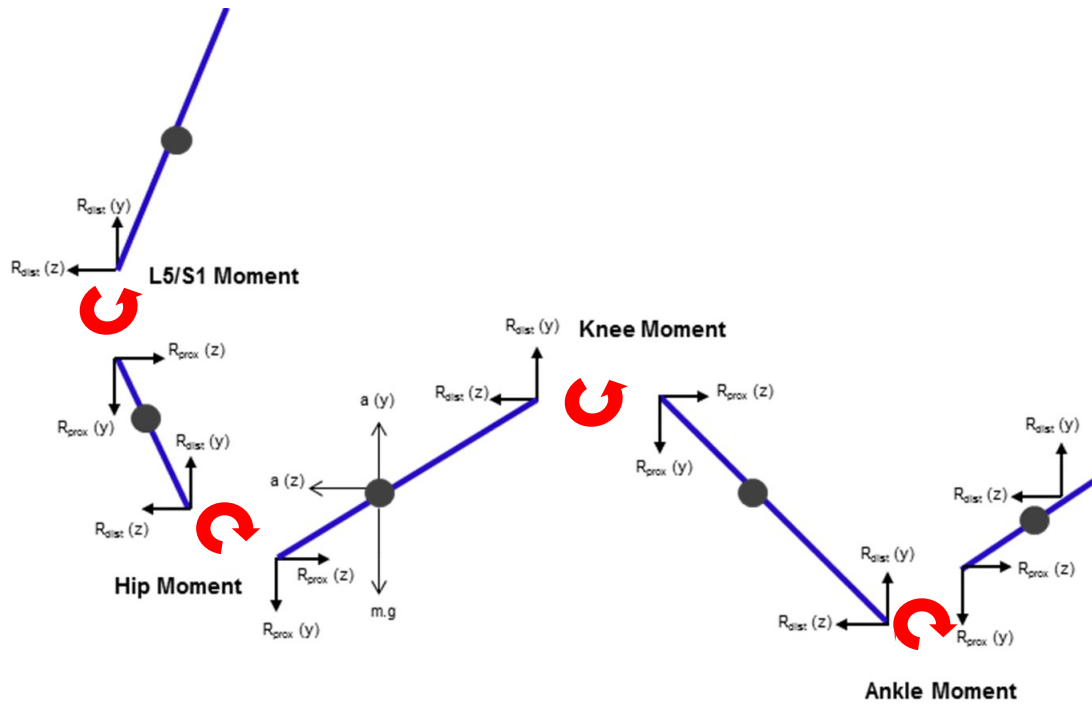


Figure 7.1: Two-dimensional representation of a five segment closed-chain link-segment model of the foot, shank and thigh, pelvis and lumbar spine, with forces and moments acting on all segments. Grey circles represent the location of each segments' centre of mass, and the accelerations acting at the centre of mass is shown for just the thigh. Red arrows represent extension moments at each joint.

Based on the construction of the link-segment model (Figure 7.1) and inputs including linear and angular accelerations, proximal and distal reaction forces and moment arms, segmental masses and inertial properties, net moments about a segment's proximal joint can be calculated:

$$M_{prox} = I \cdot \ddot{\theta} - (R_{dist} \cdot d_{dist}) - (R_{prox} \cdot d_{prox}) - M_{dist} \quad \text{Equation 7.9}$$

Where  $M_{prox}$  and  $M_{dist}$  are net joint moments,  $R_{prox}$  and  $R_{dist}$  are joint reaction forces,  $d_{prox}$  and  $d_{dist}$  are moment arms about the proximal and distal ends of a segment,  $I$  is moment of inertia, and  $\alpha$  is angular acceleration.

The value of the foot's  $M_{prox}$  (i.e. ankle moment) is the equal and opposite of the shank's  $M_{dist}$ . Knowing this value enables the shank's  $M_{prox}$  (i.e. knee moment) to be calculated, and thus joint moments at progressively proximal joints can be obtained, in a similar manner to proximal joint reaction forces.

Due to the FOB system enabling just a unilateral kinematic analysis, distal moments at the pelvis were derived by assuming perfect lower limb symmetry. Therefore, joint moments and forces from the right hip were doubled for the sagittal plane and mirrored in the frontal and transverse planes (Figure 7.2). Seat force was then included as an additional force input in order to derive  $R_{prox}$  and  $M_{prox}$  at the pelvis. It was not possible to derive seat COP trajectories in the global frame as the position of the seat was not known. Consequently, it had to be assumed that seat force always acted through the pelvis CM. This was deemed an acceptable assumption as there is little motion of the pelvis relative to the seat during rowing, and because seat COP and pelvis CM trajectories did not greatly differ during rowing trials (Appendix K).

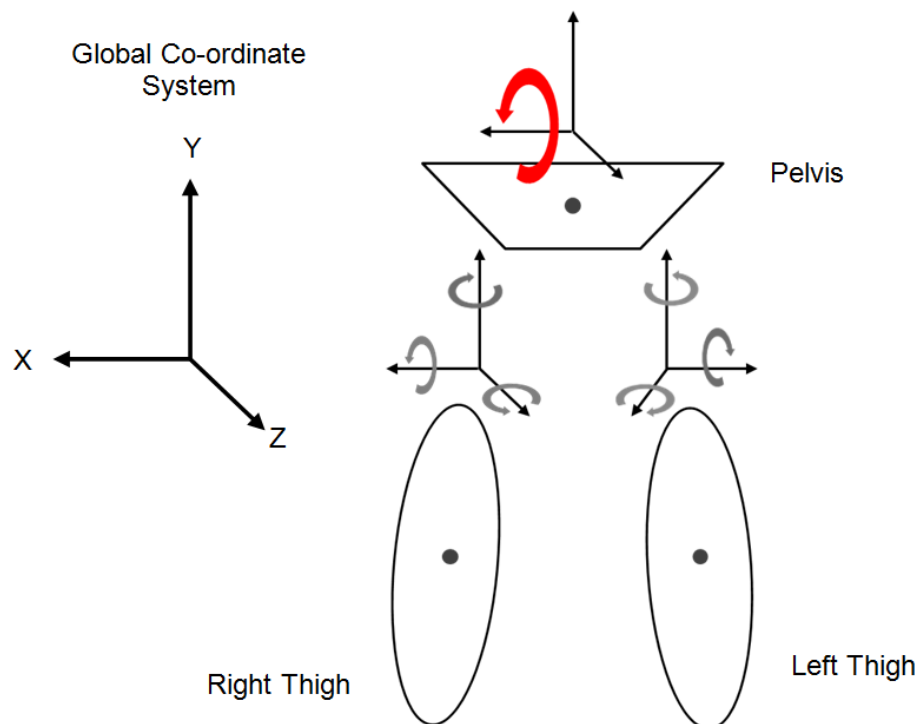


**Figure 7.2: Three dimensional moments acting about the L5/S1 and bilateral hip co-ordinate systems. The left thigh is assumed to mirror the right thigh, thus negating pelvis moments about the Y and Z axis, whilst doubling moments about the X axis.**

#### 7.2.3.4 Joint Work and Power

Joint power at the ankle, knee, hip, and L5/S1 joints was the product of the instantaneous joint moment and instantaneous joint angular velocity.

$$P = M \times \dot{\theta} \quad \text{Equation 7.10}$$

Where  $P$  is joint power and  $M$  is net joint moments, and  $\omega$  is angular velocity.

Work done was calculated as the time integral of joint power production between specified time points. Using this data, contribution of work done in the sagittal plane by each of the joints during the drive phase was quantified as a percentage of the sum of work done by all joints (Equation 7.11). The percentage contribution of joint work gives a measure of the relative targeting of joint extensors' musculature during the drive phase of the rowing stroke.

$$W_{ankle} = \frac{W_{ankle}}{W_{ankle} + W_{knee} + W_{hip} + W_{L5/S1}} \times 100 \quad \text{Equation 7.11}$$

Where  $W_{ankle}$  is work done at the ankle,  $W_{knee}$  is work done at the knee,  $W_{hip}$  is work done at the hip, and  $W_{L5/S1}$  is work done at L5/S1.

#### 7.2.3.5 Global to Local Transformation

The inverse dynamics model generated all joint reaction forces and moments in the global co-ordinate frame. As such, local co-ordinate frames for the lumbar spine, pelvis, thigh, shank and foot were constructed using digitised landmark positions, in the same way as in Chapter 6 (Section 6.2.6.1). These co-ordinate frames were subsequently unitised and added to the joint centre of each segment so that a four by four transformation matrix could be constructed at each new time frame. These were used to enable transformations of joint forces and moments calculated in the global co-ordinate

frame, to those in the anatomical co-ordinate frames. For L5/S1, moments were defined as positive for: extension, right side abduction and clockwise rotation moments. For the other joints, moments were defined as positive for: extensor moments, abduction moments and external rotation moments. All forces were defined as positive in the anterior, lateral and inferior directions.

#### 7.2.3.6 *Data Extraction*

All relevant Step files from the dynamic rowing trials were entered into the inverse dynamics model described above, and generated 3D kinetic and kinematic data from the raw FOB and force data. All forces and moments were quantified in Newtons (N) and Newton meters (Nm) respectively, but to enable comparison of data between athletes and between groups, these values were normalised to the rowers' BM. In addition to this data, vertical, horizontal and resultant foot force, seat force and handle force were also extracted for subsequent analysis with respect to 3D joint loading. Table 7.2 lists all the parameters that were derived for the purpose of this study. A Matlab program was custom written to time normalise the data, and represent every stroke as 0-100% based on handle force thresholds, where 0% is considered the catch position (see Section 3.2.6.6). Of all the normalised strokes recorded within a Step, ten strokes in the middle of each trial were extracted for statistical analysis. This was so that any acceleration or deceleration phase at the start and end of each piece are discarded, and ten highly repeatable and consistent strokes could be analysed (Appendix D).

All kinetic and kinematic variables from Table 7.2 were extracted at catch, MHF, finish and 10% in the recovery phase, thus producing ten values per trial, at each stroke position. For the kinetic variables, maximum/minimum values within the drive phase



were also extracted. Additionally, joint ROM in the sagittal plane was calculated at each joint, with ROM representing the motion that occurred between maximum and minimum values within a stroke.

**Table 7.2: Kinetic, kinematic and performance parameters derived from the Step files.**

<b>Joint Kinetics</b>	<b>Joint Kinematics</b>	<b>Performance</b>
3D L5/S1 normalised moment (Nm/kg)	3D L5/S1 angle (°)	Resultant foot force (N/kg)
3D HJC normalised moment (Nm/kg)	3D HJC angle (°)	Vertical foot force (N/kg)
3D KJC normalised moment (Nm/kg)	1D KJC angle (°)	Horizontal foot force (N/kg)
3D AJC normalised moment (Nm/kg)	3D AJC angle (°)	Seat force (N/kg)
3D L5/S1 normalised force (N/kg)		Handle force (N/kg)
3D HJC normalised force (N/kg)		
3D KJC normalised force (N/kg)		
3D AJC normalised force (N/kg)		

#### **7.2.4 Statistical Analysis**

All statistical analyses were performed using SPSS (version 19, IBM Corporation, New York, USA). Group means and standard deviations from ten strokes of each trial were computed, and normality of the data set was tested using the Shapiro-Wilk test. A two-way mixed model ANOVA was run with Step (i.e. Rate 18, Rate 24, Rate 28, Free Rate) as the repeated measure and Group (i.e. SWEEP, SCULL, LWM) as the independent measure. This test was employed to determine whether 3D kinetics, 3D kinematics, and associated performance measures change with respect to Step, and whether these changes are consistent between different groups of rowers. Where an overall significance was seen, Bonferroni post-hoc tests were conducted to locate differences. Significance level for all tests was set at  $P < 0.05$ .

## 7.3 Results

Inter-segmental 3D moments and forces can be seen in

Table 7.3 and

Table 7.4 respectively. These show that forces and moments in the sagittal plane are far greater than in the transverse or coronal planes. As such, the results in this chapter will largely focus on those in the sagittal plane.

### 7.3.1 Influence of stroke rate on joint dynamics and performance

Stroke rate generally had a large effect on inter-segmental forces and moments at the catch, finish and recovery positions, and this was most notable for sagittal plane dynamics.

With respect to stroke rate, all joints exhibited significantly increasing extension moments at the catch ( $P<0.05$ ), and increasing flexion moments at the finish and during the recovery phase ( $P<0.05$ ). Compressive and shear forces increased with respect to stroke rate for all joints at the catch and finish. This was with the exception of hip compression at the catch and L5/S1 shear force at the finish, both of which were stable across all four stroke rates. However, compressive forces at L5/S1 were very large, increasing from  $-12.91\pm 2.24$  Nm/kg at Rate 18 to  $-17.85\pm 3.37$  Nm/kg at Free Rate.

With regards to non-sagittal plane joint dynamics, it was predominately values at the catch and finish that were sensitive to stroke rate. Only peak external hip rotation moments and L5/S1 peak abduction moments increased with stroke rate. Additionally, values for peak external hip rotation and peak L5/S1 abduction moments had some of

the highest relative out-of-plane moment values, at 16% and 14% of their respective joints' peak extensor moment values.

Regarding peak joint moments in the sagittal plane, ankle extension moments increased from  $1.26 \pm 0.23$  Nm/kg to  $1.37 \pm 0.29$  Nm/kg from Rate 18 to Free Rate ( $P < 0.05$ ), whilst no significant change was noted for peak knee or peak hip extension moments during the drive phase. Peak L5/S1 extension moments increased from  $12.99 \pm 1.25$  Nm/kg to  $13.67 \pm 1.46$  Nm/kg ( $P < 0.05$ ). This was coupled by concurrent increases in: peak L5/S1 compressive forces from  $12.91 \pm 2.24$  to  $17.85 \pm 3.37$  N/kg, peak L5/S1 shear forces from  $11.91 \pm 1.69$  to  $12.25 \pm 1.89$  N/kg, and L5/S1 ROM from  $15.62 \pm 5.23^\circ$  to  $18.15 \pm 5.10^\circ$ , with respect to stroke rate. Conversely, ankle and knee ROM were significantly reduced, and no change in hip ROM was seen as stroke rate increased. There was no overall effect of stroke rate on the contribution of knee or hip work as a proportion of the sum of all measured joint work. However, contribution of the ankle to the sum of work done decreased, whilst L5/S1 contribution increased with respect to stroke rate ( $P < 0.05$ ). However, when work done at Rate 24, Rate 28 and Free Rate were normalised to work done at Rate 18, a considerable increase in work done across all joints were seen as stroke rate increased ( $P < 0.01$ ). With regards to performance, there was no change in foot force parameters across different stroke rates, although both MHF and peak seat force values increased at higher stroke rates ( $P < 0.01$ ).

**Table 7.3: Three dimensional inter-segmental moment values (average  $\pm$  SD) at key positions in the stroke are shown for Rate 18 and Free Rate. All values are in Nm/kg where kg is the rowers' body mass. \* is where there is an overall significant difference ( $P<0.05$ ) for the parameters with respect to stroke rate.**

Segment	Stroke Position	Extension (+)	Flexion (-)	Abduction (+)	Adduction (-)	External Rotation (+)	Internal Rotation (-)
		Rate 18	Free Rate	Rate 18	Free Rate	Rate 18	Free Rate
Ankle	CATCH	0.90 $\pm$ 0.18	1.17 $\pm$ 0.21*	0.01 $\pm$ 0.07	-0.05 $\pm$ 0.09*	0.29 $\pm$ 0.08	0.37 $\pm$ 0.09*
	MHF	1.14 $\pm$ 0.25	1.23 $\pm$ 0.36	-0.22 $\pm$ 0.08	-0.21 $\pm$ 0.07	0.33 $\pm$ 0.10	0.35 $\pm$ 0.14
	FIN	-0.03 $\pm$ 0.16	-0.20 $\pm$ 0.20*	0.00 $\pm$ 0.04	0.03 $\pm$ 0.05*	-0.02 $\pm$ 0.03	-0.04 $\pm$ 0.04*
	PEAK	1.26 $\pm$ 0.23	1.37 $\pm$ 0.29*	0.08 $\pm$ 0.07	0.10 $\pm$ 0.04	0.39 $\pm$ 0.10	0.44 $\pm$ 0.13
	REC	-0.04 $\pm$ 0.10	-0.31 $\pm$ 0.13*	0.01 $\pm$ 0.03	0.06 $\pm$ 0.03	-0.02 $\pm$ 0.02	-0.06 $\pm$ 0.02
Knee	CATCH	1.41 $\pm$ 0.36	2.45 $\pm$ 0.52*	0.09 $\pm$ 0.18	0.22 $\pm$ 0.25	-0.01 $\pm$ 0.09	-0.03 $\pm$ 0.11
	MHF	3.74 $\pm$ 0.61	3.79 $\pm$ 0.59	-0.07 $\pm$ 0.40	0.01 $\pm$ 0.32	0.11 $\pm$ 0.17	0.10 $\pm$ 0.17
	FIN	-0.15 $\pm$ 0.35	-0.67 $\pm$ 0.45*	-0.04 $\pm$ 0.08	-0.02 $\pm$ 0.12	0.01 $\pm$ 0.02	0.04 $\pm$ 0.04*
	PEAK	3.99 $\pm$ 0.41	3.98 $\pm$ 0.55	0.27 $\pm$ 0.24	0.35 $\pm$ 0.22	0.18 $\pm$ 0.13	0.18 $\pm$ 0.11
	REC	-0.10 $\pm$ 0.21	-0.78 $\pm$ 0.30*	0.01 $\pm$ 0.04	-0.01 $\pm$ 0.09	-0.01 $\pm$ 0.01	0.02 $\pm$ 0.04
Hip	CATCH	2.93 $\pm$ 0.43	4.43 $\pm$ 0.45*	-0.11 $\pm$ 0.51	0.20 $\pm$ 0.64*	0.36 $\pm$ 0.21	0.64 $\pm$ 0.27*
	MHF	5.36 $\pm$ 0.99	5.52 $\pm$ 1.12	0.20 $\pm$ 0.69	0.26 $\pm$ 0.54	0.21 $\pm$ 0.42	0.29 $\pm$ 0.41
	FIN	-0.80 $\pm$ 0.59	-1.98 $\pm$ 0.80*	-0.26 $\pm$ 0.19	-0.53 $\pm$ 0.47	0.11 $\pm$ 0.07	0.21 $\pm$ 0.12*
	PEAK	5.80 $\pm$ 0.62	5.93 $\pm$ 0.84	0.59 $\pm$ 0.40	0.63 $\pm$ 0.42	0.56 $\pm$ 0.34	0.73 $\pm$ 0.29*
	REC	-0.40 $\pm$ 0.33	-1.67 $\pm$ 0.54*	-0.03 $\pm$ 0.08	-0.37 $\pm$ 0.38	0.01 $\pm$ 0.02	0.10 $\pm$ 0.09
L5/S1	CATCH	7.82 $\pm$ 1.13	11.87 $\pm$ 1.06*	0.95 $\pm$ 0.46	1.45 $\pm$ 0.75*	-0.02 $\pm$ 0.43	0.02 $\pm$ 0.70
	MHF	11.92 $\pm$ 2.16	12.17 $\pm$ 2.40	1.35 $\pm$ 0.75	1.47 $\pm$ 0.82	1.01 $\pm$ 0.62	0.90 $\pm$ 0.66
	FIN	-1.21 $\pm$ 1.30	-3.82 $\pm$ 1.82*	0.31 $\pm$ 0.15	0.46 $\pm$ 0.25*	0.28 $\pm$ 0.16	0.06 $\pm$ 0.26*
	PEAK	12.99 $\pm$ 1.25	13.67 $\pm$ 1.46*	1.58 $\pm$ 0.68	1.87 $\pm$ 0.82*	1.26 $\pm$ 0.52	1.23 $\pm$ 0.51
	REC	-0.19 $\pm$ 0.70	-3.07 $\pm$ 1.25*	0.31 $\pm$ 0.09	0.49 $\pm$ 0.24	0.31 $\pm$ 0.10	0.03 $\pm$ 0.22

**Table 7.4: Three dimensional inter-segmental force values (average  $\pm$  SD) at key positions in the stroke are shown for Rate 18 and Free Rate. All values are in Nm/kg where kg is the rowers' body mass. \* is where there is an overall significant difference ( $P<0.05$ ) for the parameters with respect to stroke rate.**

Segment	Stroke Position	Lateral (+) Medial (-)		Tension (+) Compression (-)		Anterior shear (+) Posterior shear (-)	
		Rate 18	Free Rate	Rate 18	Free Rate	Rate 18	Free Rate
Ankle	CATCH	-0.03 $\pm$ 0.12	0.00 $\pm$ 0.12	-4.45 $\pm$ 0.70	-5.59 $\pm$ 0.65*	-0.03 $\pm$ 1.10	-0.85 $\pm$ 1.36*
	MHF	0.23 $\pm$ 0.34	0.16 $\pm$ 1.25	-4.87 $\pm$ 1.24	-5.23 $\pm$ 1.46	-4.40 $\pm$ 1.21	-4.00 $\pm$ 1.14
	FIN	0.03 $\pm$ 0.09	-0.02 $\pm$ 0.07	0.38 $\pm$ 0.43	0.81 $\pm$ 0.54*	-0.28 $\pm$ 0.78	0.52 $\pm$ 0.90*
	PEAK	0.31 $\pm$ 0.33	0.25 $\pm$ 0.23	-5.84 $\pm$ 0.86	-6.37 $\pm$ 1.03*	-4.82 $\pm$ 1.00	-4.46 $\pm$ 1.15
	REC	0.01 $\pm$ 0.05	-0.07 $\pm$ 0.06	0.41 $\pm$ 0.25	0.91 $\pm$ 0.33	-0.11 $\pm$ 0.48	1.06 $\pm$ 0.60
Knee	CATCH	-0.16 $\pm$ 0.42	0.12 $\pm$ 0.41	-1.16 $\pm$ 0.77	-2.88 $\pm$ 1.12 *	4.98 $\pm$ 0.85	5.79 $\pm$ 0.78*
	MHF	-0.19 $\pm$ 0.69	-0.10 $\pm$ 0.55	-6.43 $\pm$ 1.06	-6.29 $\pm$ 0.86	2.24 $\pm$ 1.66	2.79 $\pm$ 1.79
	FIN	-0.02 $\pm$ 0.09	0.06 $\pm$ 0.15*	0.02 $\pm$ 0.52	0.74 $\pm$ 0.65 *	-0.13 $\pm$ 0.72	0.60 $\pm$ 0.83*
	PEAK	-0.81 $\pm$ 0.33	-0.68 $\pm$ 0.22	-6.85 $\pm$ 0.74	-6.67 $\pm$ 0.84	5.65 $\pm$ 0.96	6.09 $\pm$ 0.92
	REC	-0.02 $\pm$ 0.04	0.02 $\pm$ 0.11	-0.02 $\pm$ 0.29	0.82 $\pm$ 0.40 *	-0.07 $\pm$ 0.45	0.97 $\pm$ 0.53
Hip	CATCH	0.07 $\pm$ 0.44	0.49 $\pm$ 0.48*	-1.04 $\pm$ 0.87	-1.04 $\pm$ 1.33	-5.00 $\pm$ 1.19	-7.53 $\pm$ 0.94*
	MHF	0.40 $\pm$ 0.73	0.41 $\pm$ 0.59	-3.56 $\pm$ 1.07	-3.67 $\pm$ 1.24	-4.58 $\pm$ 1.23	-4.60 $\pm$ 1.04
	FIN	-0.11 $\pm$ 0.26	-0.09 $\pm$ 0.46	1.78 $\pm$ 0.58	2.93 $\pm$ 0.79 *	-0.28 $\pm$ 0.78	0.98 $\pm$ 1.20*
	PEAK	0.84 $\pm$ 0.44	0.81 $\pm$ 0.44	-3.96 $\pm$ 0.89	-4.23 $\pm$ 0.88	-5.89 $\pm$ 0.78	-7.72 $\pm$ 0.84
	REC	-0.13 $\pm$ 0.22	-0.22 $\pm$ 0.40	1.22 $\pm$ 0.30	2.26 $\pm$ 0.50	-0.50 $\pm$ 0.49	0.81 $\pm$ 0.77*
L5/S1	CATCH	0.23 $\pm$ 0.54	0.71 $\pm$ 0.95*	-8.00 $\pm$ 2.80	-13.26 $\pm$ 3.38*	5.87 $\pm$ 1.97	9.22 $\pm$ 1.84*
	MHF	0.26 $\pm$ 0.56	0.30 $\pm$ 0.57	-7.26 $\pm$ 2.65	-6.84 $\pm$ 2.53	4.86 $\pm$ 3.56	5.56 $\pm$ 4.10
	FIN	0.82 $\pm$ 0.91	1.14 $\pm$ 1.01*	11.29 $\pm$ 3.01	16.45 $\pm$ 3.99*	-10.97 $\pm$ 1.90	-9.98 $\pm$ 3.18
	PEAK	1.36 $\pm$ 0.46	1.76 $\pm$ 0.66*	-12.91 $\pm$ 2.24	-17.85 $\pm$ 3.37*	11.91 $\pm$ 1.69	12.25 $\pm$ 1.89
	REC	0.68 $\pm$ 0.84	0.95 $\pm$ 0.94	9.34 $\pm$ 2.14	13.02 $\pm$ 2.59	-10.17 $\pm$ 1.59	-9.47 $\pm$ 2.50

### 7.3.2 Gender Differences

No significant differences were noted between SCULL and SWEEP for any parameter, and LWM always demonstrated differences against both SCULL and SWEEP. Consequently, in this section SCULL AND SWEEP data will be grouped together and referred to as HWW.

Compared to HWW, LWM demonstrated significantly greater peak extension moments, extension moments at MHF, and greater peak compressive forces at all joints ( $P<0.05$ ). They also exhibited larger shear forces at the catch and finish positions in all joints ( $P<0.05$ ). Figure 7.3 displays joint torque patterns in the sagittal plane for LWM and HWW at Rate 18 and Free Rate. These show that LWM generate much larger joint flexion and extension moments during the rowing stroke. Furthermore, their peak joint moments are larger at Free Rate compared to Rate 18 for all joints, whereas in HWW this was only the case for the ankle and L5/S1. Interestingly, there were no gender differences for out-of-plane moments, with the exception of HWW exhibiting greater hip external rotation moments at the finish ( $P<0.05$ ).

No differences in joint ROM were observed between HWW and LWM. However, LWM exhibited significantly greater foot forces than HWW ( $P<0.01$ ). In terms of joint work, knee contributions were significantly greater for HWW (44%) than LWM (41%), whereas LWM demonstrated significantly greater hip joint contribution during the drive phase (46%) than HWW (44%) ( $P<0.01$ ).

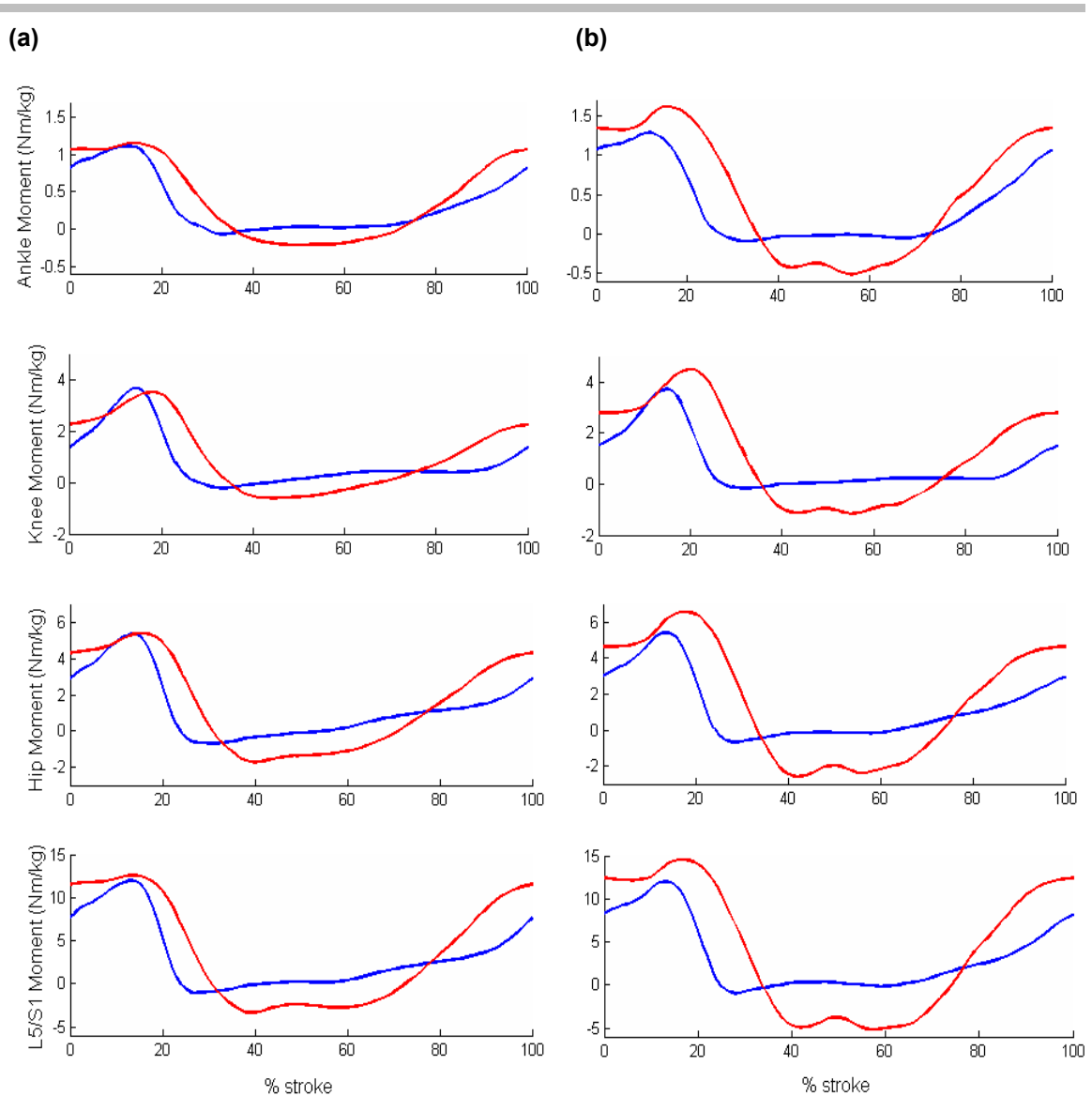


**Figure 7.3:** Ankle, knee, hip and L5/S1 joint moment traces in the sagittal plane at Rate 18 (blue) and Free Rate (red) for (a) HWW and (b) LWM. Standard deviations for this data ranged from  $\pm 0.03$  to  $\pm 0.32$  Nm/kg for ankle moments,  $\pm 0.15$  to  $\pm 1.13$  Nm/kg for knee moments,  $\pm 0.09$  to  $\pm 1.61$  Nm/kg for hip moments and  $\pm 0.36$  to  $\pm 3.63$  Nm/kg for L5/S1 moments.

### 7.3.3 Interaction effects

Significant interaction effects (crew x stroke rate) for joint moments were identified only in the sagittal plane, for peak knee extensor moments ( $P < 0.05$ ) and peak hip extensor moments ( $P < 0.05$ ). For the knee, interaction effects were characterised by LWM exhibiting progressively greater knee extensor moments, and HWW exhibiting

progressive reductions for this parameter (Figure 7.4). Peak shear and peak compressive forces at the knee also exhibited the same interaction effect, with LWM increasing, and HWW decreasing with respect to stroke rate. At the hip, LWM exhibited progressively greater extensor moments, and HWW demonstrated no change in this parameter with respect to stroke rate.

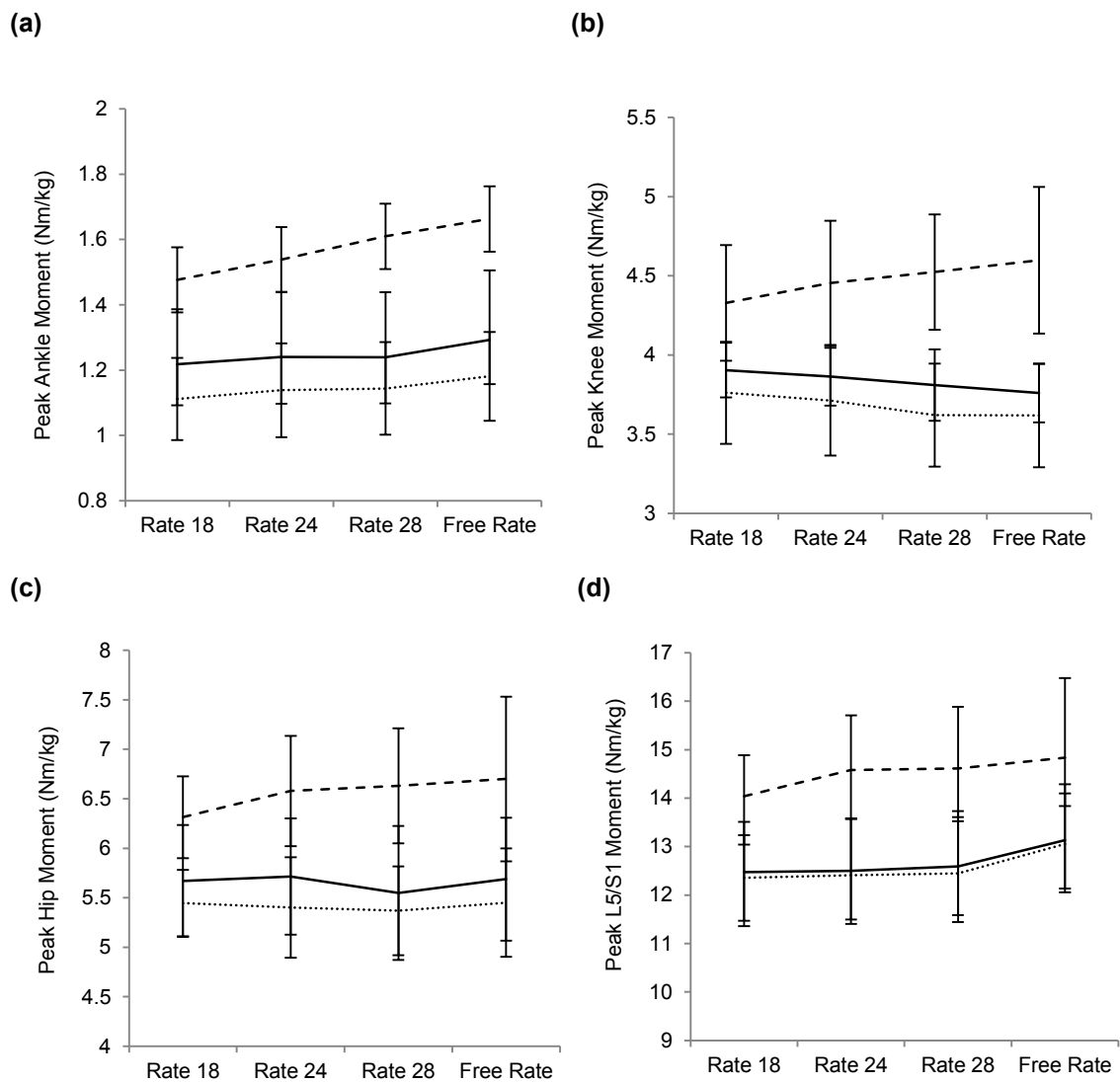


**Figure 7.4:** Changes in (a) Peak Ankle Moment, (b) Peak Knee Moment, (c) Peak Hip Moment, and (d) Peak L5/S1 Moment with respect to stroke rate. Thick dashed line is LWM, solid line is HWW. Error bars are  $\pm$  SD.



Interaction effects for joint work were most evident at the hip and knee. HWW demonstrated no changes in proportions of either hip or knee joint work, whereas LWM significantly reduced their knee contribution and increased their hip contributions as stroke rate increased (Figure 7.5). Additionally, there was also a significant interaction effect for knee ROM where LWM demonstrated a more rapid decline in ROM compared to HWW. When work done at Rate 24, Rate 28 and Free Rate was normalised to work done at Rate 18 there was a clear interaction effect where LWM exhibited a much greater increase in total work done at progressive work rates compared to HWW ( $P<0.01$ ) (Figure 7.6) At Free Rate, LWM exhibited 304% of total joint work done at Rate 18, whilst HWW exhibited 189% of total joint work done at Rate 18 when rowing at Rate 28. The same pattern was evident when looking at individual joints, where values at the ankle, knee, hip and L5/S1 all increased with respect to rate, but again, LWM exhibited more pronounced increases in work done at progressive work rates ( $P<0.05$ ).

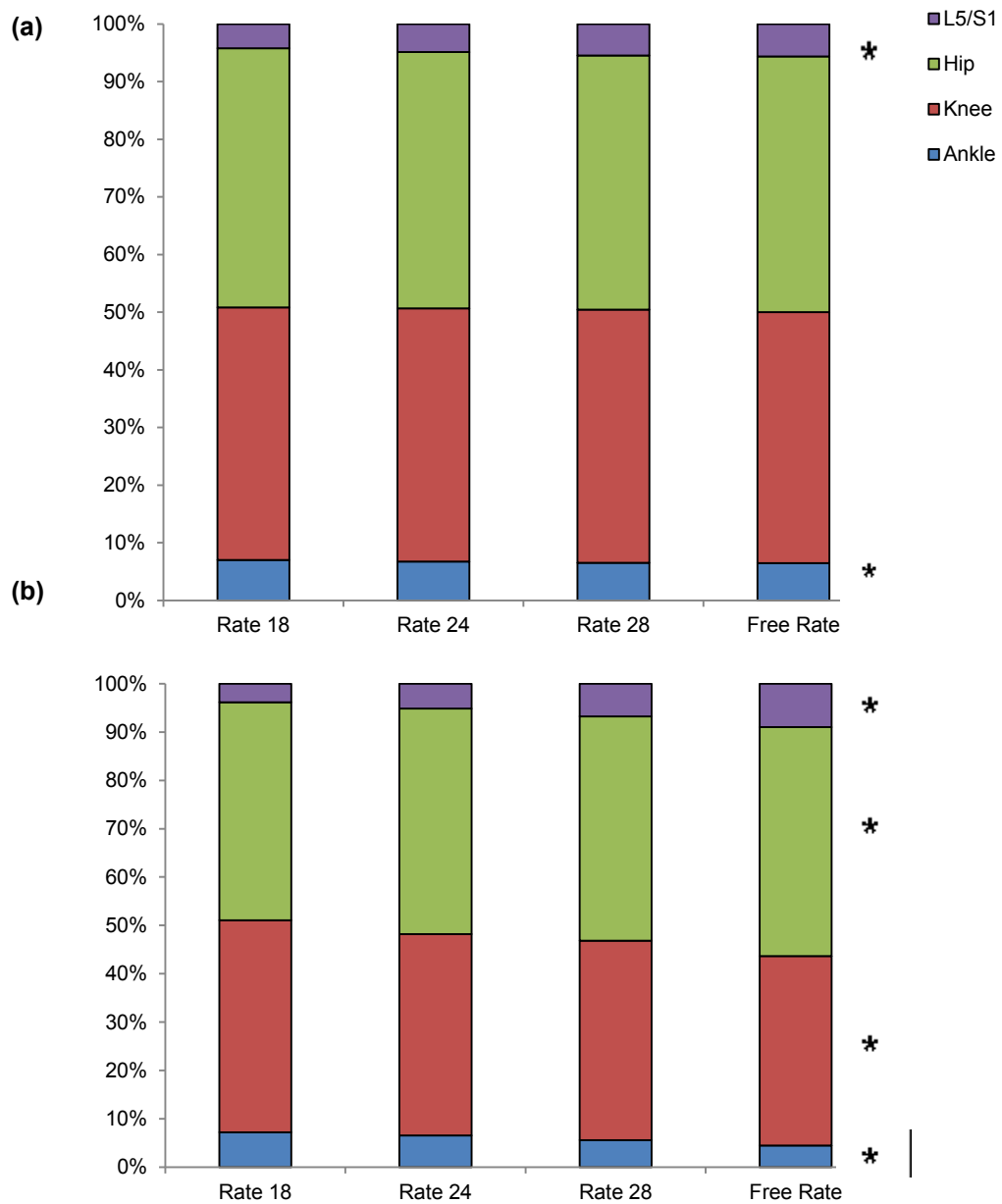


**Figure 7.5: Change in proportion of joint work done with respect to stroke rate for (a) HWW and (b) LWM. \* represent an overall change in % Work done for that joint with respect to stroke rate ( $P < 0.05$ )**

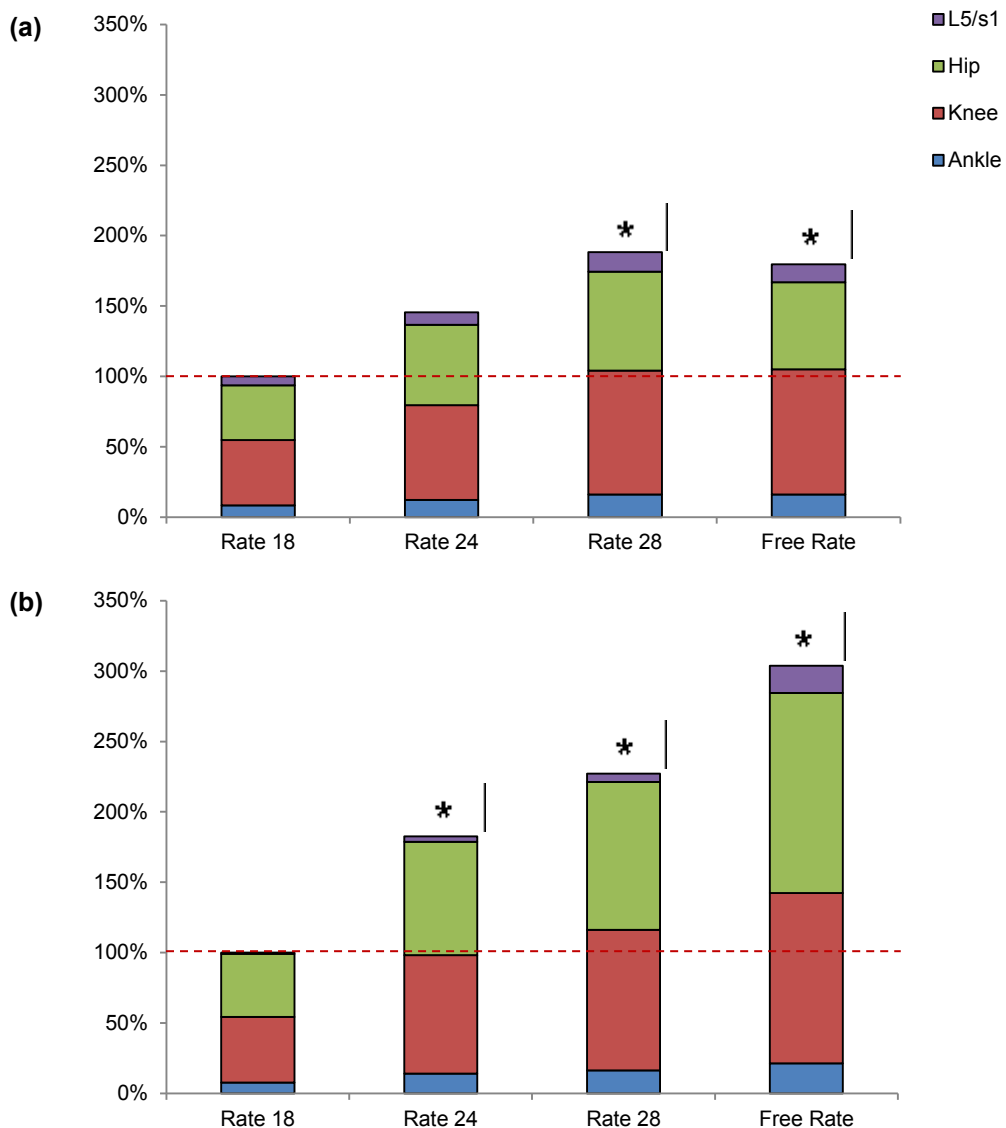


Figure 7.6: Change in joint work done relative to work done at Rate 18, for (a) HWW and (b) LWM. Red dotted line represents 100% of work done at Rate 18. \* represent an overall change in % Work done for that joint relative to Rate 18 ( $P < 0.01$ ).

In terms of rowing performance, there were significant interaction effects for MHF ( $P < 0.05$ ) and peak seat force ( $P < 0.01$ ). For LWM there was a progressive increase in MHF as stroke rate increased, whereas MHF was not sensitive to stroke rate in HWW (Figure 7.7). In terms of peak seat force, all groups exhibited an increase in this parameter with respect to stroke rate, but LWM demonstrated a more pronounced increase compared to HWW (Figure 7.7).

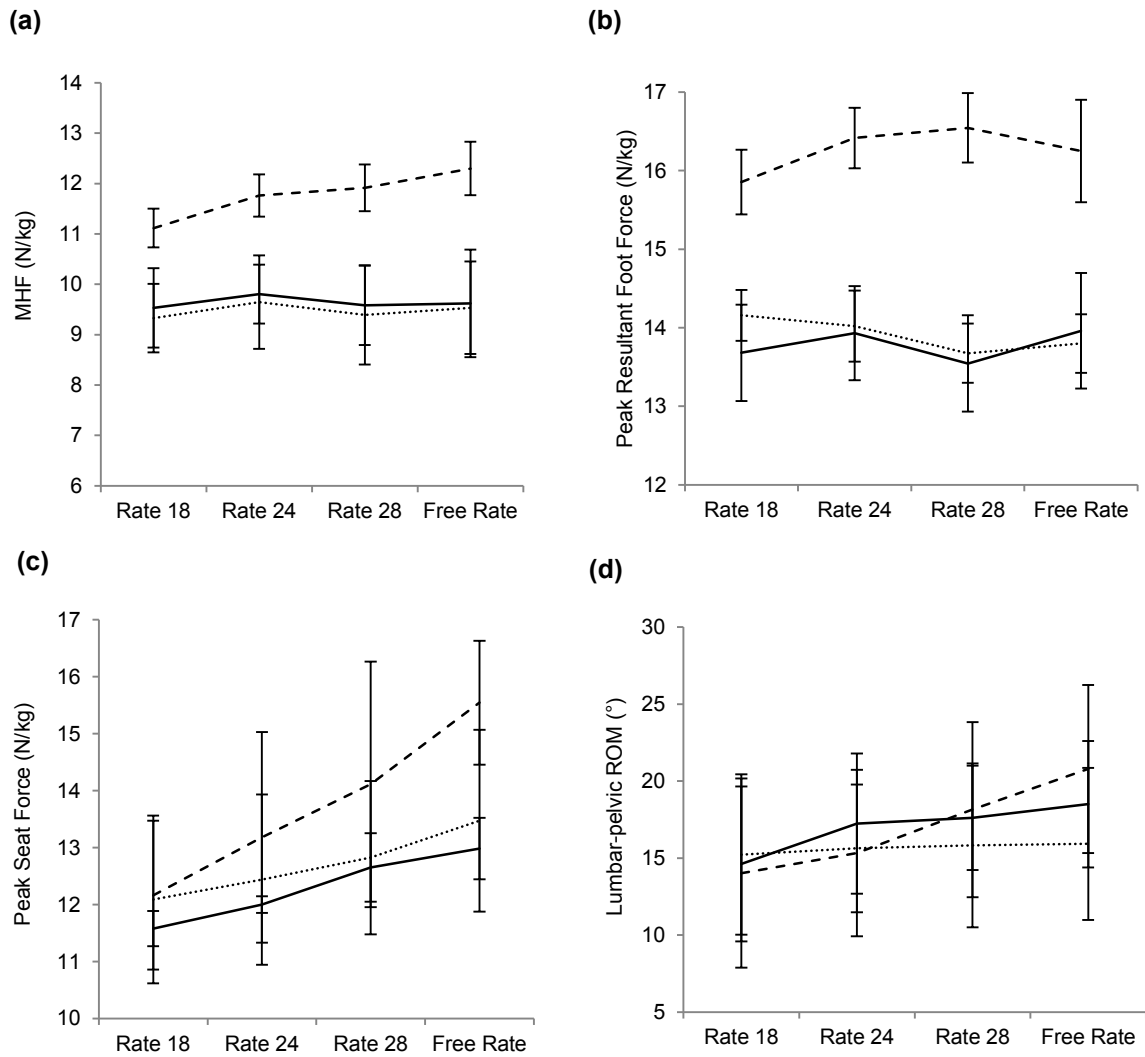


Figure 7.7: Changes in (a) MHF, (b) Peak Resultant Foot Force, (c) Peak Seat Force, and (d) Peak L5/S1 ROM with respect to stroke rate. Thick dashed line is LWM, solid line is HWW. Error bars are  $\pm$  SD.

### 7.3.4 Summary of Results

- Inter-segmental forces and moments in the sagittal plane were sensitive to changes in rowing intensity, particularly at the catch, finish and recovery portions of the stroke.
- Notable non-sagittal plane moments were seen for external hip rotation moments and L5/S1 abduction moments, both of whose peak values increased with respect to stroke rate.

- No gender differences in non-sagittal plane moments were seen for peak values or at the catch and MHF positions.
- HWW demonstrated increases in peak ankle and L5/S1 extensor moments, but also reductions in peak knee moments and no change in peak hip moments, with respect to stroke rate. On the other hand, all joints' peak extensor moments increased for LWM. This was reflected in the changes observed in joint work with respect to stroke rate.
- There was an increase in L5/S1 ROM and reductions in ankle and knee ROM as stroke rate increased.
- Peak seat force increased for both LWM and HWW, whilst contribution of hip work and MHF increased with stroke rate for LWM only, and were consistent across stroke rates for HWW.

## **7.4 Discussion**

In this study an inverse dynamics model was developed which quantifies 3D inter-segmental forces and moments, in order to examine the effect of incremental intensities of ergometer rowing on dynamics of the lower limb and lower back.

The results of this study reveal that loading across the ankle, knee, hip and L5/S1 changed with respect to stroke rate, and the way in which they changed differed between HWW and LWM. Overall, the results showed that as stroke rate increased, there were concurrent increases in peak ankle and peak L5/S1 extensor moments, whilst peak hip and knee extensor moments were stable throughout the Step Test. However, interaction effects of joint forces and moments in the sagittal plane revealed that HWW and LWM modify their joint loading in different ways over the course of a Step Test.

LWM showed pronounced increases in peak extensor joint moments for all joints investigated (Figure 7.3). On the other hand, HWW exhibited increased joint moments at just the ankle and L5/S1, with the knee demonstrating reductions in peak moments, and the hip remaining stable across all stroke rates. Along with peak L5/S1 moments, L5/S1 ROM progressively increased in all groups of rowers, which suggests that changes in joint loading may occur in relation to modifications in technique that occur at increasing stroke rates.

Changes in joint loading patterns were expected as stroke rate increased, but the differences in these changes between groups were not anticipated. However, it is well established that due to anatomical traits such as large pelvis width and quadriceps angle, females tend to exhibit different kinematics compared to men during locomotion. These differences include, greater peak hip adduction, hip internal rotation and knee abduction angles (Arendt and Dick, 1995, Ferber et al., 2003). These altered knee motion patterns are thought to affect joint loading around the knee, thus making females more susceptible to anterior cruciate ligament injuries (Malinzak et al., 2001). When investigating cutting manoeuvres, female athletes demonstrated significantly greater hip adductor moments as well as decreased hip extensor moments compared to males (Pollard et al., 2007). Cutting manoeuvres are clearly very different from rowing, for which the majority of movement occurs in the sagittal plane. However, hip rotation angles during rowing have been found to increase with respect to stroke rate in women only (Murphy, 2009). Therefore, at higher stroke rates women may increase loading about the coronal and transverse planes, thus restricting increases in sagittal plane dynamics in comparison to LWM. In fact, peak external hip rotation moments at the finish position were greater for HWW compared to LWM, with this parameter being the only gender difference in all measured non-sagittal plane moments.

All extensor moments significantly increased in value at the catch position, and there were consistent increases in flexor moments and tensile forces at all joints for the finish position and during the recovery phase. These findings were consistent across genders and no interaction effects were observed, so clearly there is a consistently strong effect of stroke rate on sagittal plane joint loading at the finish and catch positions. These positions mark the start and end of the recovery phase, so there are marked dynamic differences in the recovery slide as stroke rate increases. At Rate 18 the rower slides naturally back to the catch position exerting little effort, whereas higher stroke rates requires the rower to progressively increase the speed of their recovery, thus generating negative work through greater joint flexion moments. The dynamic differences between high and low rowing intensities have previously been highlighted for on-water rowing. In 28 elite Canadian rowers, total kinetic energy during the recovery phase was approximately six times greater during high intensity rowing and approximately equal to the kinetic energy required during the drive phase (Bechard et al., 2009). As the results from this study also suggests, high intensity rowing places greater demands on the body during the recovery phase, compared to rowing at a lower intensity. These are important considerations when constructing training plans and analysing the rowing stroke, where the importance of the non-propulsive phase should not be overlooked.

In addition to the differences in mechanical demands during the recovery phase, those during the drive phase were also subject to change with increasing stroke rate. In terms of work done at the joints, contributions from the hip and knee were almost equal at Rate 18, but gradually became more hip dominant in LWM as stroke rate increased. Both peak hip and knee extensor moments notably increased with stroke rate for LWM, so their greater hip contribution at higher stroke rates may be due to their concurrent rapid decline in knee ROM. Most of this loss in knee ROM occurred at the front of the

stroke, where the shins became progressively less vertical at the catch. In a study of barbell squatting, it was found that restricting knee ROM minimized stress on the knees and redistributed those forces to the hips and low-back region (Fry et al., 2003). Similarly, LWM experienced a significant reduction in proportion of knee work, but significant increases in the proportions of hip and L5/S1 work, with respect to stroke rate.

For HWW there was no significant change in hip or knee work contributions, but a significant increase in L5/S1 contribution and decrease in ankle contribution was seen across stroke rates. HWW did not exhibit as large a drop in knee ROM as LWM which may have helped maintain the contributions of hip and knee work. However, they exhibited a reduction in peak knee extensor moments and no change in peak hip extensor moments across stroke rates, which suggest that when stroke rate increases, there is reduced effort from the lower limbs, which is compensated by increased effort at the lower back. For example, in stoop lifting there is much greater dynamic contribution from the lumbar spine and hip compared to the knees, whereas squat lifting requires greater loading of the lower limbs (Hwang et al., 2009). Therefore, previously identified differences in rowing technique between HWW and LWM (Murphy, 2009) may have contributed to this result. However, when work done at each joint was normalised to those at Rate 18, all joints for both LWM and HWW significantly increased work done with respect to stroke rate. In spite of this there was a significant interaction effect where the increase in work done at each joint was found to be far greater in LWM compared to HWW, and this is reflected in LWM's progressive increase in peak extensor moments for all joints.

Whilst there were no significant gender differences in anterior shear forces at the knee,



Table 7.4 shows that large peak values were recorded for this parameter. During knee extension, contractions of the quadriceps causes anterior tibial displacement (relative to the femur), thus resulting in anterior shear forces at the knee (Shimokochi and Schultz, 2008). The hamstrings are thought to have the potential to counteract anterior shear forces at the knee through antagonistic contractions during knee extension (Kingma et al., 2004). Powerful knee extensor muscles such as the vastus lateralis and vastus medialis have been shown to exhibit high levels of muscle activity during the early portion of the drive phase (Janshen et al., 2009, Nowicky et al., 2005). Additionally, Koutedakis et al. (1997) observed a low knee flexor to extensor ratio in a population of rowers, thus indicating relative hamstring weakness. As such, large anterior shear forces may arise from deficits in antagonistic co-contractions during knee extension. Furthermore, these deficits in hamstring strength are believed to be associated with back pain in rowing, due to its effect on pelvic mobility (Koutedakis et al., 1997). As such, it is possible that loading at the knee may influence kinematics and loading at the lumbar-pelvic region.

Loading across L5/S1 was found to be extremely high during ergometer rowing, with peak compressive forces of nearly 18 N/kg and extension moments of up to 14 Nm/kg measured at Free Rate. Additionally, abduction and external rotation moments about L5/S1 were also found to be relatively large, with peak values of 1.87 Nm/kg and 1.26 Nm/kg, respectively. L5/S1 adduction moments tended to remain high throughout the critical drive phase, whereas their external rotation moments tended to increase as MHF approached. The presence of kinematic asymmetry has been shown to increase lateral flexion and twisting loads of the lumbar spine during lifting movements (Kingma et al., 1998). Murphy (2009) has shown that significant lateral flexion of L5/S1 is present during the drive phase of rowing, thus there is evidence that instability at the lumbar-

pelvic region during the drive phase leads to compensatory loadings about the lumbar spine.

A 2000 m rowing race will involve over 200 stroke cycles, so a high magnitude of lumbar loading will be experienced over several hundred strokes. Injuries to the intervertebral discs may result from cumulative trauma produced by repeated application of load, or from an application of a very high magnitude of load (McGill, 1998). Additionally, the compressive tolerance of the spine is reduced in the final stages of full spinal flexion (Adams and Dolan, 1995). Increases in peak L5/S1 loading occurred alongside increased L5/S1 ROM for both LWM and HWW, suggesting that deteriorations in posture and technique at higher work rates may contribute to increased loading of the lower back. Therefore, it is possible that posture and lumbar-pelvic motion throughout the rowing stroke are related to the forces which occur there, so this is an area which requires further investigation. Furthermore, L5/S1 loading at higher work rates is unlikely to be a measure of greater performance, as corresponding increases in external force production at the foot-stretchers were not observed. Although MHF increased with respect to stroke rate for LWM, this did not result from an increase in foot forces, which should theoretically influence forces and moments along the kinetic chain to the handle. The large increase in peak seat force and L5/S1 ROM suggests that an increase in MHF comes from a greater use of the back during the drive phase, where extending the hips (and thus posteriorly rotating the trunk) too early after the catch causes the mechanical advantage in the lower limbs' kinetic chain to be lost. Consequently, some of the power at the handle must be generated through posterior acceleration of body mass, rather than transfer of forces through the kinetic chain. As such, increases in L5/S1 loading at higher stroke rates may be an indicator of technique decline, as larger peak L5/S1 moments occurred alongside increases in L5/S1

flexion and increased loading of the seat, both of which are considered deleterious to performance (McGregor et al., 2004, Murphy, 2009). Therefore, rowers may be at greater risk of developing LBP when training at high intensities.

Large L5/S1 extension moments were present during the rowing stroke and increased with respect to work rate. The highest compressive forces in this study were just under 2000 N, which were lower than values presented in previous studies of 2700 N (Morris et al., 2000) and 5500 N (Munro and Yanai, 2000). Limitations of the model used in this study are that loads can be underestimated due to *net* joint moments, rather than individual muscle forces being quantified through the activity. Furthermore, errors can accumulate through kinematic data collection and differentiation of noisy data. In addition, the generalisation of anthropometric data collected from a non-athletic population may not be appropriate for a group of elite rowers, and may again lead to under-estimation of values. Nevertheless, it was possible to draw important conclusions regarding inter-segmental loading during ergometer rowing by observing the change in the joint loads between progressive Steps.

## **7.5 Conclusion**

To conclude, joint dynamics are sensitive to rowing intensity, particularly at the catch and finish positions, due to vastly different dynamic requirements at higher stroke rates. LWM and HWW used different joint loading strategies at the lower limbs in response to increasing rowing intensity. However, large L5/S1 extension moments were present during the rowing stroke, and these increased with respect to stroke rate for both groups of rowers. Increases in L5/S1 loading at higher work rates is unlikely to be a measure of greater performance, as corresponding increases in foot-stretcher forces were not

observed. In fact, it may be an indicator of technique decline at higher work rates, as larger peak L5/S1 moments occurred alongside increases in L5/S1 flexion and increased loading of the seat, which are considered deleterious to performance. Therefore, rowers may be at greater risk of developing LBP when training at high intensities.

In this chapter inter-segmental loading of the lower limbs and lumbar-pelvic region were estimated using a custom written inverse dynamics model. It was then possible to examine the degree of loading that occurs at progressive rowing intensities in different groups of rowers. The subsequent chapter will employ this model, in addition to kinematic and performance models, in order to investigate the effect of an intervention in ergometer set-up, on; technique, performance and biomechanical loading.

## **Chapter 8:**

### **Effect of changes in foot-stretcher height on rowing technique and performance**

The previous chapters in this thesis have outlined the development of novel technologies and scientific approaches to rowing biomechanics research.

The development of bilaterally instrumented footplates enabled loading patterns and asymmetries in foot force to be quantified and examined with respect to performance and injury risk (Chapter 5). Subsequent integration of this system with the instrumented ergometer and motion capture systems enabled key aspects of technique, which positively influence external force application, to be identified (Chapter 6). Finally, integrated force and motion data facilitated the development of an inter-segmental inverse dynamics model for the estimation of the loads that the lower limb and lumbar-pelvic joints are exposed to during varying intensities of ergometer training (Chapter 7).

With these progressive developments in biomechanical rowing models and feedback tools, the current chapter will apply these technologies to examine implications of foot-stretcher set-up on ergometer rowing performance and technique. More specifically, the impact of increasing foot-stretcher height on subsequent foot force application technique, lumbar-pelvic posture, lower limb joint kinematics and inter-segmental loading, will be investigated.

## 8.1 Introduction

The fundamental aim in competitive rowing is to drive the boat as fast as possible over an Olympic distance of 2000 m. To produce movement of the boat, a rower must repeatedly perform a rowing stroke – an action which is made up of two distinct phases: the drive and recovery (explained in detail in Section 1.1). The drive phase is a crucial part of the rowing stroke as this is when external forces are applied to the foot-stretchers, seat and handle, thus causing the boat to accelerate through the water. All components of the rowing stroke are intimately linked through a dynamic equilibrium, where the resultant force at the handle is highly dependent on the force applied to the foot-stretcher, with this transfer of force limited by how well the rower maintains a strong, stable core and posture throughout the stroke (Baudouin and Hawkins, 2004). Rowing performance is, therefore, fundamentally dependent on the rower's ability to develop large foot forces and to efficiently transmit these forces to the upper limbs.

From a two-dimensional perspective resultant foot forces can be broken down into their vertical and horizontal (anterior-posterior) vector components. Horizontal forces applied to the footplates are propulsive in nature, and act to drive the boat along the direction of travel (Caplan and Gardner, 2005). Conversely, the vertical component of foot force can contribute to pitching of the boat, causing the surface area of the boat in contact with the water to increase, thereby increasing drag forces (Caplan and Gardner, 2010). The orientation of the resultant force vector is dependent on the ratios of the vertical and horizontal foot force components, hence it is advantageous for this ratio to favour the horizontal component, such that propulsive force generation is maximised during the drive. This is because for the same amount of energy expended, the vertical component (which contributes to an ineffective transfer of energy) will be minimized

and a greater proportion of the energy expended by the rower will be transmitted directly into propelling the boat, thus improving mechanical effectiveness (Caplan and Gardner, 2005).

The effectiveness of force application has been investigated in sports that require large propulsive forces to be generated by the lower limbs. For example, the ratio of propulsive to total force application has been quantified in cycling (Davis and Hull, 1981b, Ericson and Nisell, 1988) and sprinting (Morin et al., 2011) in order to examine technical efficiency of the athlete. By doing so, Morin et al. (2011) found the horizontal orientation of the force applied to the ground during sprint acceleration to be more influential on performance than the total force. Consequently, it is important that athletes optimise their foot force orientation, in order to improve both their mechanical efficiency and performance. In Chapter 6 it was discovered that a rapid knee extension and steady lumbar-pelvic rhythm through the critical drive phase were aspects of rowing technique which positively influenced RF towards the horizontal axis. Consequently, there are aspects of rowing technique which can be modified in order to optimise the effectiveness of a rowers' force application through the stroke.

Footplates act as solid platforms against which a rower applies their foot force in order to produce forward acceleration of the boat. Therefore, in addition to technical modifications, external interventions where the athlete's foot-stretcher set-up is modified can also positively influence force application technique. It has previously been suggested that the vertical distance between the bottom edge of the foot-stretchers and seat should be minimised to achieve optimum application of power through the legs (Herberger, 1987). Soper and Hume (2005) placed the foot-stretchers in a more vertical position by increasing their inclination angle, and found that male rowers significantly

increased their power output and reduced their time to row 2000 m, in response to a steeper foot angle. Caplan et al. (2005) also manipulated athlete set-up by modifying the seat-to-heel distance of the ergometer. They found that raising the height of the foot-stretchers significantly attenuated the decline in power output per stroke that occurred during 3 and a half minutes of maximal effort rowing. It was suggested that this improvement was due to reductions in the downward forces applied to the foot-stretchers which do not contribute to forward propulsion, thereby reducing energy wasted with each stroke. However, foot forces were not directly measured in the previous study, therefore this theory requires validation using instrumented footplates.

From a purely mechanical perspective, vertical foot forces should be reduced when increasing the height of foot-stretchers, due to a reduction in the seat-to-heel distance resulting in a more horizontal orientation of resultant force. However, foot-stretchers are rarely positioned level with the seat due to anatomical limitations such as a rowers' hip and ankle flexibility preventing them from reaching an effective catch position that enables them to generate a strong leg drive (Kaehler, 2011). As previously mentioned, the trunk is a key link in the kinetic chain, transmitting forces from the lower to upper limbs (McArthur, 1997). Therefore, despite a more mechanically effective position at the feet, if the lower back and trunk cannot transfer these forces to the handle, performance will not improve and the rower may be at greater risk of developing back injuries. The lower back is the most commonly injured area of the body in rowers (Smoljanovic et al., 2009). A possible mechanism for this is a lack of anterior rotation of the pelvis (i.e. pelvic *rock-over*) at the catch position, as reduced pelvic rock-over is often compensated by increased lumbar and/or thoracic rotation at the catch in an attempt to maintain stroke length (McGregor et al., 2004). These compensatory actions



will result in large L5/S1 flexions which have previously been noted as deleterious to performance and increasing risk of injury (Murphy, 2009).

Common advice to rowers regarding choice of foot height position is to select a comfortable position based on their height and size of feet, where the balls of the feet are just below the level of the seat (McArthur, 1997). Competitive rowers have an extremely high volume of training, with sessions up to three times a day for six days a week at the height of the season (Caldwell et al., 2003). Given the training load, it is important that a sound technique is developed early in the rowing career so that the likelihood of injury is reduced throughout an individual's career. As such, it is especially important to determine a rower's optimal foot position, monitoring changes in performance and injury parameters and adapting the position as necessary. Ideally, the foot position must be a compromise between maximising mechanical effectiveness of the leg drive, without negatively affecting the athlete's kinematics and increasing injury risk.

Consequently, the first aim of this study will be to look at the effect of raising foot-stretcher heights on foot force application technique, by determining whether propulsive forces transmitted to the handle are increased through greater mechanical effectiveness of the leg drive. The subsequent effect on performance parameters such as stroke length, peak forces, mean power per stroke and seat suspension will also be examined. Further aims will be to investigate the effect of footplate height on joint kinetics and kinematics, specifically focussing on L5/S1 dynamics, where the influence of foot-stretcher height on injury potential can be assessed.

It was hypothesised that raising the height of the foot-stretchers (i.e. minimising the seat-to-heel distance) would alter the ratio of vertical to horizontal foot forces in favour

of the horizontal component, and consequently improve performance parameters, although this may adversely affect lumbar-pelvic rhythm.

## **8.2 Methodology**

### **8.2.1 Participants**

The study received ethical approval from the Imperial College Research Ethics Committee, and informed consent was obtained from all subjects (Appendix B). A sample size of seven was necessary to achieve a moderate effect size of 0.5 and statistical power of 95% with an alpha significance level of 0.05. As such, ten heavyweight male sweep rowers participated in this study (mass  $89.0 \pm 9.1$  kg, age  $26.0 \pm 4.1$ ) between June and November 2012. All ten rowers had previously rowed for the GB Under 23 team or their international equivalent. Their mean  $\pm$  SD personal best time for 2000 m on the ergometer was  $6:12.1 \pm 8.4$  s. All participants were right leg dominant as defined by their preferred kicking leg. Rowers with a current episode of LBP or any other serious illness or injury were excluded from this study.

### **8.2.2 Experimental set-up**

All rowers performed their trials on a modified Concept II model D ergometer (Figure 6.1). On this ergometer the flywheel was instrumented with a linear encoder to enable stroke length to be quantified. Force data was captured from the handle (tensile force), seat (vertical force) and bilaterally from the foot-stretchers (vertical and horizontal forces).

For this particular study, adjustable plates were developed which attached to the surface of the instrumented footplate (Weinert-Aplin, 2011). The plastic foot-stretcher and cradle could then be screwed to the surface of the adjustable plate at different locations, thus enabling the seat-to-heel distance to be adjusted (Figure 8.1).



**Figure 8.1: Foot-stretchers are fixed to the adjustable footplates to demonstrate two different heights. The left foot-stretcher depicts the lowest height (Position 1) and the right foot-stretcher depicts the highest height (Position 4).**

---

An adjustable plate was used to alter the seat-to-heel distance, rather than the traditional means of inserting the foot-stretcher into holes at incremental levels in order to alter the height of the foot cradle (Figure 8.2). This is because the latter will cause the foot-strap to be pulled across the foot at different locations (Figure 8.3). Placing the strap over the tarsals or toes as opposed to the mid dorsal aspect of the foot may affect the rower's comfort as well as foot and ankle range of motion.



**Figure 8.2:** Two different foot-stretcher heights adjusted in the traditional way by slotting the end of the foot-stretcher into holes arranged at incremental heights.



**Figure 8.3:** Feet constrained to the foot-stretchers at two different positions, showing the bilateral differences in placement of each strap relative to the foot.

---

Kinematic data of the rower was recorded using the FOB motion capture system (Ascension Technology, Burlington, USA). Flock of Birds sensors were attached to the rower at T12/L1 junction, L5/S1 junction, midway along the lateral aspect of the thigh, and midway along the anterior aspect of the shank. These sensors recorded 3D position and orientation of the rower's lumbar spine, pelvis, thigh and shank segments relative to an extended range transmitter. 3D global landmark co-ordinates of RPSIS, LPSIS,

RASIS, LASIS, LEPI, MEPI, LMAL, MMAL, MET5 and HJC were derived through the digitisation procedure described in Section 6.2.3. However, for this study MET5 was digitised every time foot-stretcher height was modified, because that particular landmark was stored as a global offset from the FOB transmitter. These digitised landmarks were used to construct local co-ordinate systems of the pelvis, thigh, shank and foot.

Data from the FOB and load cells were acquired from separate data acquisition units, and software synchronised using a custom LabView program.

### **8.2.3 Experimental protocol**

At the start of the session each rower was asked to set the foot-stretchers to their preferred position through the traditional means of adjusting the foot cradle. Each subject then performed a 10 minute warm up on the ergometer, followed by four separate rowing trials at free rate (i.e. a pace consistent with the athlete's personal best 2000 m pace). Each trial was performed for one minute with the foot-stretcher and cradle fixed to the adjustable plate at four distinct positions:

- Position 1 (P1): rowers' original foot-stretcher height
- Position 2 (P2):  $P1 + 1.7$  cm (in the vertical axis)
- Position 3 (P3):  $P1 + 3.4$  cm (in the vertical axis)
- Position 4 (P4):  $P1 + 5.1$  cm (in the vertical axis)

The order of P1 – P4 within the protocol was randomised for each subject. Seat-to-heel distances for P1 – P4 were relative to the rower's preferred foot-stretcher height, thus absolute seat-to-heel distance values may differ between rowers. For example, if a

rower usually slots their foot-stretchers into hole number 5 (i.e. one hole showing at the top), then all experimental trials will maintain the same position of the cradle within the foot-stretcher, with modifications in height being made purely through the adjustable plate. This meant that changes in performance and technique could be assessed when footplate height was raised above a rowers' usual set-up position. A break of at least 5 minutes was given between each trial to ensure that fatigue did not affect the results of the test. During every break, rowers were asked to mark on the scale below how they perceived their footplate position to impact their rowing performance (Figure 8.4). Each time the foot-stretcher height was modified, rowers were asked to familiarise themselves with the new set-up by performing their usual warm-up, prior to the 1 minute free rate trial.

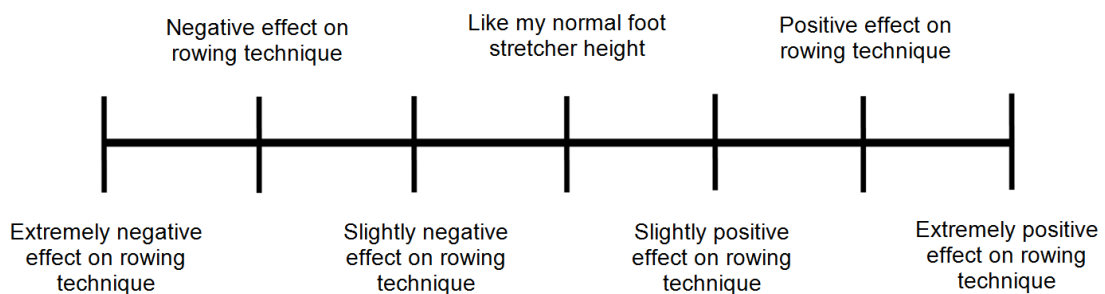


**Figure 8.4: Scale of perceived effect of footplate height on rowing performance, relative to the rowers' traditional foot-stretcher set-up.**

---

#### **8.2.4 Data analysis**

Global 3D joint centre positions of the ankle, knee, hip and L5/S1 were calculated based on digitised bony landmark positions (Section 6.2.6.1). Three-dimensional angles for each of those joints were calculated using the JCS method of Grood and Suntay (1983). The inverse dynamics model developed in Chapter 7 was used to derive

joint moments and forces using the bottom-up Newton-Euler approach. Although all joint kinetics and kinematics were derived in 3D, Chapter 7 and previous work by Murphy (2009) have shown that in rowing the most pertinent variables are those in the sagittal plane. Therefore, the majority of the analysis focussed on the sagittal plane values. In addition to joint kinetics and kinematics, rowing performance data were also derived (Table 8.1).

Ten consecutive strokes in the middle of each trial were analysed from each subject. This was so that any acceleration or deceleration phase at the start and end of each piece were discarded, and ten highly repeatable and consistent strokes could be analysed (Appendix D). All kinetic and kinematic variables from Table 8.1 were extracted at catch, MHF and finish, producing ten values per trial, at each stroke position. For kinetic variables, peak values within the drive phase were also extracted. Additionally, joint ROM in the sagittal plane was calculated for each joint.

**Table 8.1: Kinetic, kinematic, performance and asymmetry data derived from experimental trials at each footplate position.**

<b>3D Joint Kinetics</b>	<b>3D Joint Kinematics</b>	<b>Sagittal plane ROM</b>	<b>Performance</b>	<b>Asymmetry (%ASI)</b>
3D L5/S1 normalised moment (Nm/kg)	Lumbar orientation (°)	Lumbar ROM (°)	Seat COP (cm)	Resultant force (%)
3D HJC normalised moment (Nm/kg)	Pelvis orientation (°)	Pelvis ROM (°)	Seat Suspension	Horizontal force (%)
3D KJC normalised moment (Nm/kg)	Pelvic Twist (°)	L5/S1 ROM (°)	Seat Force (N/kg)	Vertical force (%)
AJC normalised moment (Nm/kg)	3D L5/S1 angle (°)	Hip ROM (°)	Handle force (N/kg)	Res. impulse (%)
3D L5/S1 normalised force (N/kg)	3D HJC angle (°)	Knee ROM (°)	Stroke length (mm)	Horiz. impulse (%)
3D HJC normalised force (N/kg)	KJC $\alpha$ angle (°)	Ankle ROM (°)	Power (W)	Vert. impulse (%)
3D KJC normalised force (N/kg)	3D AJC angle (°)		Res. foot force (N/kg)	ASI COP (%)
3D AJC normalised force (N/kg)	3D L5/S1 angle (°)		Horiz. foot force (N/kg)	
	3D HJC angle (°)		Vert. foot force (N/kg)	
	KJC $\alpha$ angle (°)		Res. Impulse (Ns/kg)	
	3D AJC angle (°)		Horiz. Impulse (Ns/kg)	
			Vert. impulse (Ns/kg)	
			Footplate COP (cm)	
			Foot force ratio	



### 8.2.5 Statistical analysis

All statistical analyses were performed using SPSS (version 19, IBM Corporation, New York, USA). Group means and standard deviations from ten strokes of each trial were computed, and normality of the data set was tested using the Shapiro-Wilk test. A repeated measures ANOVA was run, with foot-stretcher height (i.e. P1, P2, P3, P4) as the repeated measure, to determine whether biomechanical aspects of performance and technique are affected by changes in foot-stretcher height. Where an overall significance was seen, Bonferroni post-hoc tests were conducted to locate differences. Significance level for all tests was set at  $P < 0.05$ .

## 8.3 Results

All participants successfully completed all aspects of the protocol, with descriptive statistics of their performance for Positions 1-4 given below in Table 8.2. None of these parameters were found to be significantly different between the four footplate positions ( $P > 0.05$ ). All variables tested in this study were found to be normally distributed.

**Table 8.2: Descriptive data of rowing performance at each footplate position.**

	<b>500 m Projected Split (s)</b>	<b>Distance (m)</b>	<b>Stroke Rate (spm)</b>
<b>P1</b>	01:33.6 ± 3.9	320.4 ± 11.2	31.3 ± 2.0
<b>P2</b>	01:33.4 ± 3.8	321.3 ± 11.2	32.0 ± 2.4
<b>P3</b>	01:33.7 ± 3.9	320.1 ± 11.1	31.9 ± 2.1
<b>P4</b>	01:33.5 ± 3.7	320.9 ± 10.6	32.4 ± 2.1

Spm = strokes per minute

Regarding the ratings of rowers' perception of each footplate position, the number of responses to each description at the four positions can be seen in Table 8.3 below. There was no correlation between the height of the rower and their perception of footplate height on performance.

**Table 8.3: Distribution of rower responses to perceived effect of P1-P4 on rowing performance.**

	<b>Position 1</b>	<b>Position 2</b>	<b>Position 3</b>	<b>Position 4</b>
Extremely negative effect on rowing technique	0	0	0	1
Negative effect on rowing technique	0	0	3	5
Slightly negative effect on rowing technique	0	3	5	2
Like my normal foot-stretcher height	10	3	1	0
Slightly positive effect on rowing technique	0	4	1	2
Positive effect on rowing technique	0	0	0	0
Extremely positive effect on rowing technique	0	0	0	0

### **8.3.1 Foot force application technique**

In response to increasing footplate heights, no significant change in RF was seen at the catch ( $P=0.174$ ). However, it was shown to decrease significantly at MHF, where P1 exhibited significantly greater RF than P2, P3 and P4 ( $P<0.01$ ) (Figure 8.5). In accordance with the above result, peak resultant foot force significantly decreased at the highest two positions compared to the lowest two positions ( $P<0.01$ ), producing values of  $14.2\pm 1.2$  N/kg,  $13.9\pm 1.4$  N/kg,  $13.7\pm 1.4$  N/kg and  $13.5\pm 1.4$  N/kg for P1 - P4 respectively. Furthermore, peak horizontal foot force was significantly different between all footplate positions, decreasing from  $11.5\pm 1.0$  N/kg at P1 to  $10.2\pm 1.5$  N/kg

at P4 ( $P<0.01$ ). There was no change in resultant ( $P=0.09$ ), horizontal ( $P=0.30$ ) or vertical ( $P=0.09$ ) impulse with respect to foot-stretcher height.

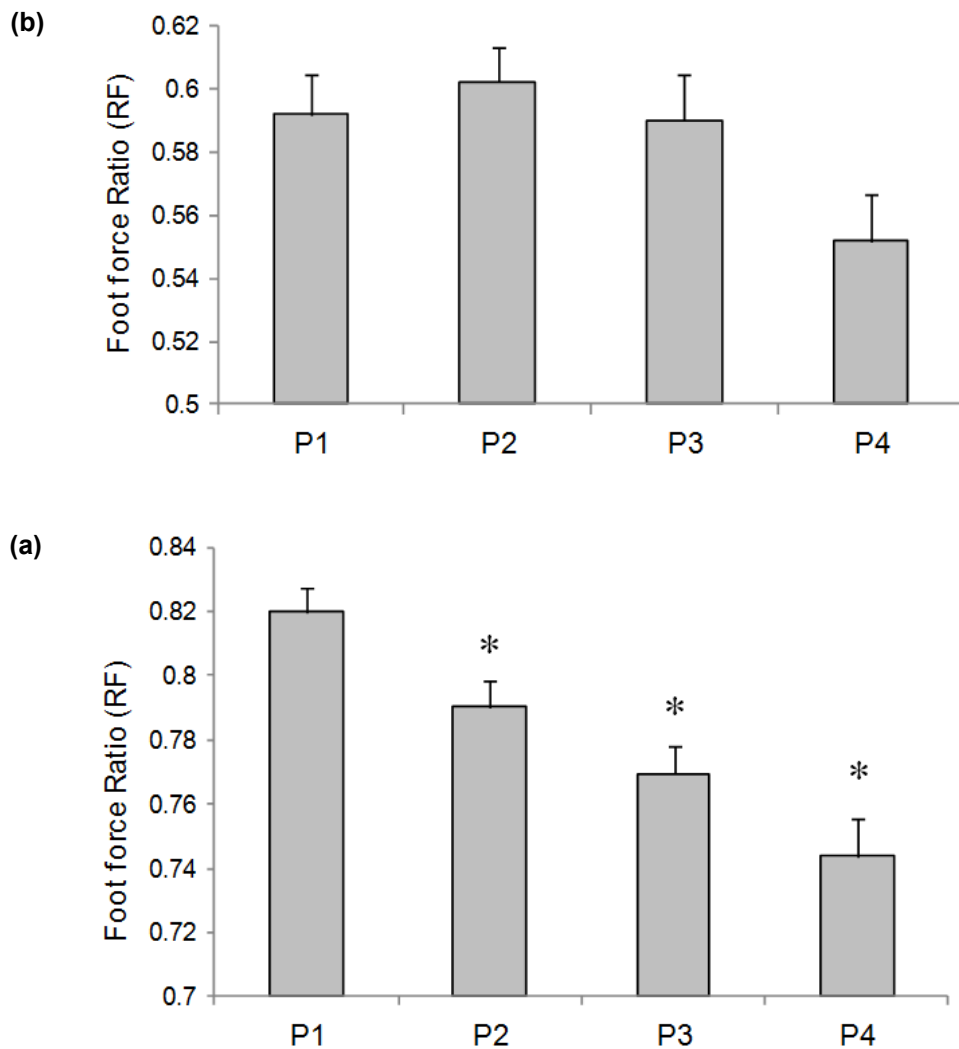


Figure 8.5: Mean + SD of (a) RF at the catch and (b) RF at MHF at P1, P2, P3 and P4. \* is a significant difference from P1 ( $P<0.01$ ).

When rowers' data were examined individually, it was discovered that just four out of the ten rowers exhibited an increase in RF at the catch between P1 and P3. These four also exhibited trends of increasing horizontal impulse with respect to footplate height. However, only one of the four rowers gave positive feedback at P2, whilst the other

three stated that P2 and P3 either felt *'like my normal stretcher height'* or had a *'Slightly negative effect on rowing technique'*.

### 8.3.2 Rowing performance

Both mean power output per stroke and MHF were consistent across all four positions, exhibiting no change in value as footplate height was raised ( $P=0.17$  and  $P=0.48$ , respectively). However, stroke length was sensitive to footplate height, demonstrating progressive reductions in length from P1 and P4 ( $P<0.01$ ) (Table 8.4).

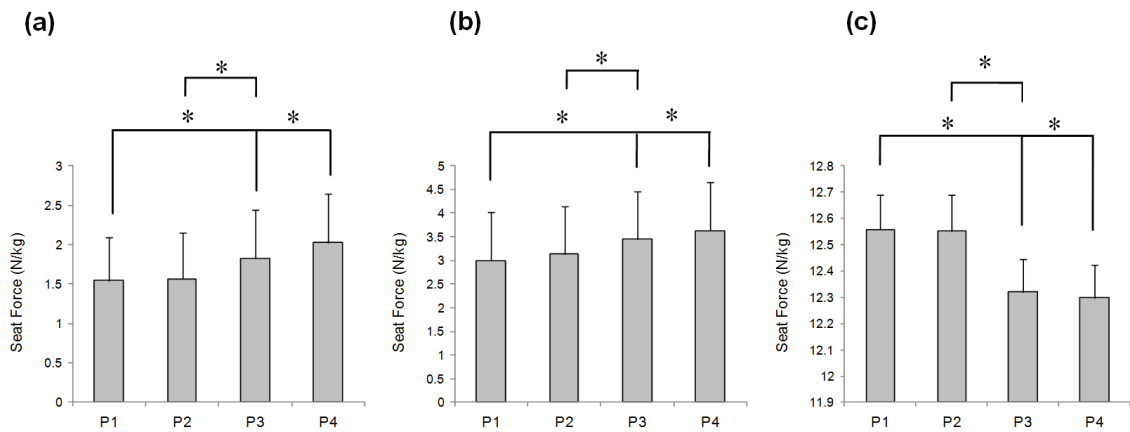
**Table 8.4: Mean power output, MHF and stroke length values (average  $\pm$  SD) are shown for P1 – P4.**

	<b>Mean Power Output (W)</b>	<b>MHF (N/kg)</b>	<b>Stroke Length (mm)</b>
<b>P1</b>	427.9 $\pm$ 60.0	10.6 $\pm$ 1.4	1492.8 $\pm$ 81.7
<b>P2</b>	430.1 $\pm$ 62.9	10.6 $\pm$ 1.2	1484.1 $\pm$ 88.7
<b>P3</b>	434.5 $\pm$ 61.9	10.5 $\pm$ 1.4	1466.6 $\pm$ 80.9*
<b>P4</b>	422.2 $\pm$ 12.6	10.6 $\pm$ 1.3	1456.6 $\pm$ 89.9*

\* significant difference from P1 ( $P<0.05$ )

None of the parameters pertaining to foot force asymmetries significantly differed as footplate height was modified, although both peak resultant foot force and resultant impulse showed trends of increasing asymmetry with respect to increasing height ( $P=0.09$  and  $P=0.08$ , respectively).

Seat force at the catch and MHF was greater (i.e. reduced seat suspension) with increasing footplate height ( $P<0.01$ ). However, there was a significant reduction in force applied to the seat at the finish position, with respect to footplate height ( $P<0.01$ ) (Figure 8.6).



**8.6: Mean  $\pm$  SD for seat force at (a) the catch, (b) MHF, and (c) the finish positions. Significant differences between footplate positions are given by square brackets. \*  $P < 0.01$ .**

### 8.3.3 Joint kinematics

Ankle dorsi-flexion progressively increased at the catch and MHF ( $P < 0.01$ ), whilst plantar-flexion was reduced at the finish ( $P < 0.01$ ), as the foot-stretchers were moved from P1 to P4 (Table 8.5). There was a reduction in knee flexion angle at the catch as footplate height was increased ( $P < 0.05$ ), whilst hip flexion increased at the catch with respect to foot-stretcher height ( $P < 0.05$ ). No change in L5/S1 angle was observed, but both the pelvis and lumbar segments' anterior rotation at the catch decreased as footplate height increased ( $P < 0.01$ ). In terms of joint and segment ROM (in the sagittal plane) during the rowing stroke, there was a significant increase in ankle ROM ( $P < 0.01$ ), and a significant reduction in pelvis ROM ( $P < 0.05$ ) between P1 and P4.

**Table 8.5: Sagittal plane angles (average  $\pm$  SD) at key positions in the stroke are shown for P1 – P4. All values are in degrees ( $^{\circ}$ ).  $0^{\circ}$  is full joint extension; ankle dorsi-flexion, knee hyper-extension, hip flexion and L5/S1 flexion are negative.**

		Catch	MHF	Finish	10% Recovery
Ankle	P1	$-65.3 \pm 17.7$	$-50.2 \pm 13.9$	$-8.8 \pm 8.7$	$-8.0 \pm 9.4$
	P2	$-79.4 \pm 12.5$	$-58.9 \pm 6.4$	$-14.5 \pm 6.4$	$-8.0 \pm 9.5$
	P3	$-86.0 \pm 19.5^*$	$-63.6 \pm 16.8$	$-17.6 \pm 10.0$	$-8.0 \pm 9.4$
	P4	$-92.5 \pm 11.9^{*\wedge}$	$-67.7 \pm 14.1^*$	$-19.2 \pm 10.0^*$	$-8.1 \pm 9.4$
Knee	P1	$125.7 \pm 7.4$	$79.7 \pm 10.8$	$1.2 \pm 7.8$	$2.2 \pm 7.7$
	P2	$125.3 \pm 6.7$	$78.7 \pm 8.2$	$0.7 \pm 8.2$	$2.2 \pm 7.7$
	P3	$124.6 \pm 7.7$	$79.3 \pm 10.3$	$0.9 \pm 8.5$	$2.2 \pm 7.7$
	P4	$123.6 \pm 7.0^{\#}$	$79.3 \pm 11.6$	$0.2 \pm 8.4$	$2.4 \pm 7.8$
Hip	P1	$-129.1 \pm 9.5$	$-103.4 \pm 12.1$	$-39.4 \pm 13.7$	$-36.4 \pm 14.6$
	P2	$-130.4 \pm 10.2$	$-103.7 \pm 21.2$	$-36.9 \pm 12.2$	$-36.8 \pm 14.4$
	P3	$-131.1 \pm 10.4^{\#}$	$-105.8 \pm 12.6$	$-41.8 \pm 14.7$	$-36.6 \pm 14.5$
	P4	$-131.7 \pm 10.7^{\#\wedge}$	$-106.7 \pm 13.7$	$-40.6 \pm 19.0$	$-36.8 \pm 14.5$
L5/S1	P1	$-17.1 \pm 11.4$	$-13.6 \pm 10.4$	$-3.6 \pm 10.6$	$-1.1 \pm 11.7$
	P2	$-16.4 \pm 11.7$	$-13.8 \pm 14.9$	$-5.4 \pm 10.9$	$-1.1 \pm 11.6$
	P3	$-16.1 \pm 11.7$	$-13.0 \pm 10.7$	$-2.8 \pm 11.2$	$-1.1 \pm 11.6$
	P4	$-16.7 \pm 12.3$	$-13.5 \pm 11.7$	$-5.1 \pm 11.5$	$-1.0 \pm 11.7$
Pelvis	P1	$7.7 \pm 7.3$	$-4.2 \pm 7.5$	$-35.7 \pm 10.4$	$-39.4 \pm 13.0$
	P2	$7.3 \pm 8.0$	$-4.7 \pm 8.1$	$-39.2 \pm 9.1$	$-39.1 \pm 12.7$
	P3	$5.8 \pm 8.3^{*\wedge}$	$-4.9 \pm 7.8$	$-36.3 \pm 9.8$	$-39.2 \pm 12.8$
	P4	$4.8 \pm 7.9^{*\wedge}$	$-5.3 \pm 7.4$	$-38.3 \pm 7.7$	$-39.3 \pm 12.7$
Lumbar	P1	$22.5 \pm 11.4$	$7.1 \pm 10.6$	$-34.5 \pm 10.4$	$-40.7 \pm 11.7$
	P2	$21.3 \pm 11.7$	$6.7 \pm 12.9$	$-36.2 \pm 10.9$	$-40.4 \pm 11.6$
	P3	$19.9 \pm 11.7^*$	$6.1 \pm 11.1$	$-35.5 \pm 10.7$	$-40.5 \pm 11.6$
	P4	$19.4 \pm 12.3^{*\wedge}$	$6.3 \pm 10.5$	$-35.2 \pm 11.3$	$-40.4 \pm 11.7$

\* significant difference from P1 ( $P < 0.05$ ), # significant difference from P1 ( $P < 0.01$ ),  $\wedge$  significant difference from P2 ( $P < 0.05$ )

### 8.3.4 Joint kinetics

At L5/S1, reductions in extension and flexion moments were observed at the catch and finish positions, respectively, as footplate height was raised ( $P < 0.01$ ) (Table 8.6).

Shear force at the joint was seen to increase at the finish but progressively decreased at

the catch ( $P<0.05$ ; Figure 8.7). Peak ankle and knee joint moments in the sagittal plane demonstrated progressive reductions as the footplates were raised from P1 - P4 ( $P<0.01$ ; Table 8.6). At the ankle, there were also reductions in peak compressive force, and compressive force at the catch and MHF ( $P<0.01$ ), whilst peak shear force, as well as shear force at the catch and MHF increased with respect to footplate height ( $P<0.05$ ; Figure 8.8). There was a reduction in hip flexion moments at the finish position ( $P<0.05$ ), however there were no corresponding changes in hip joint forces during the rowing stroke.

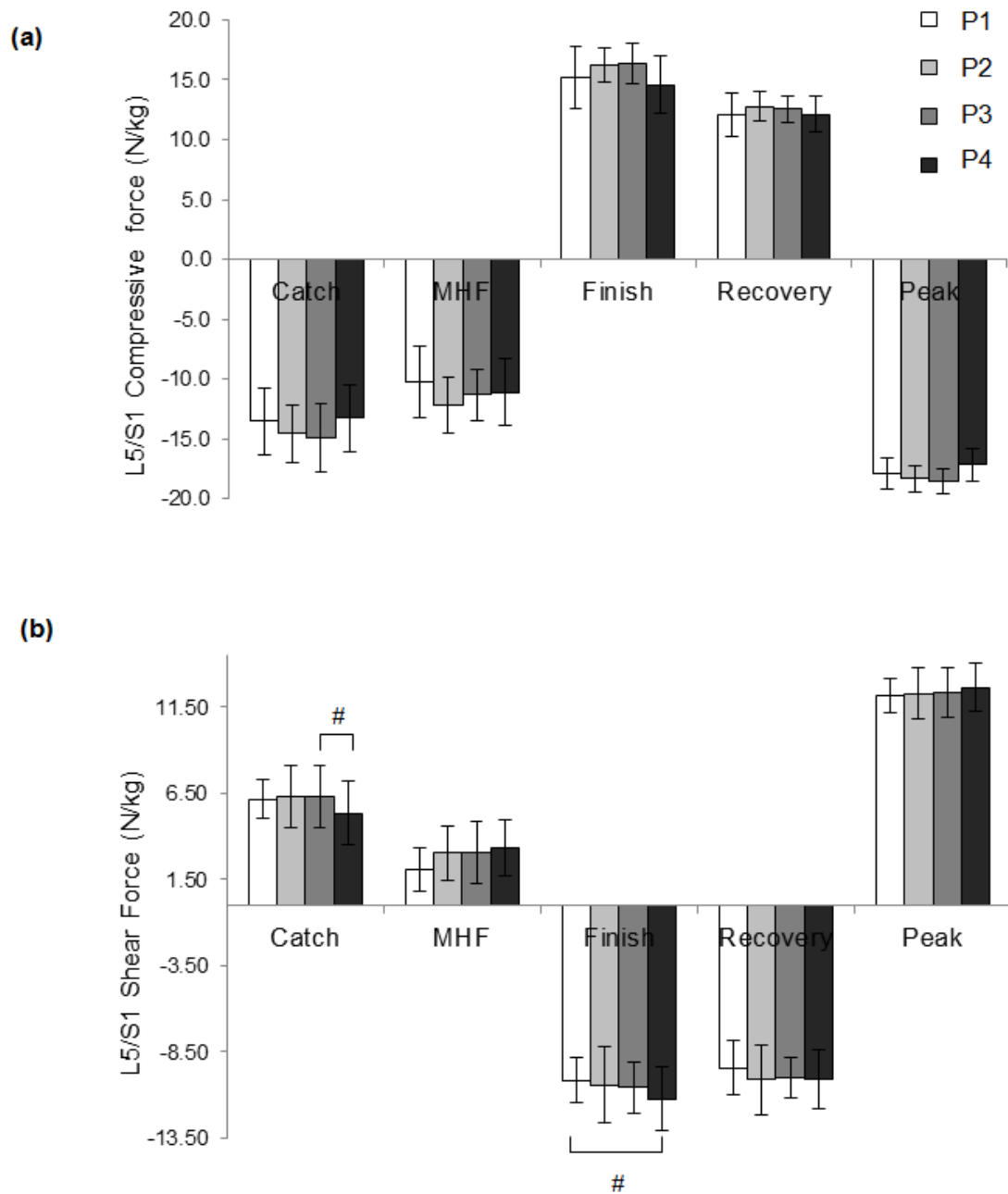
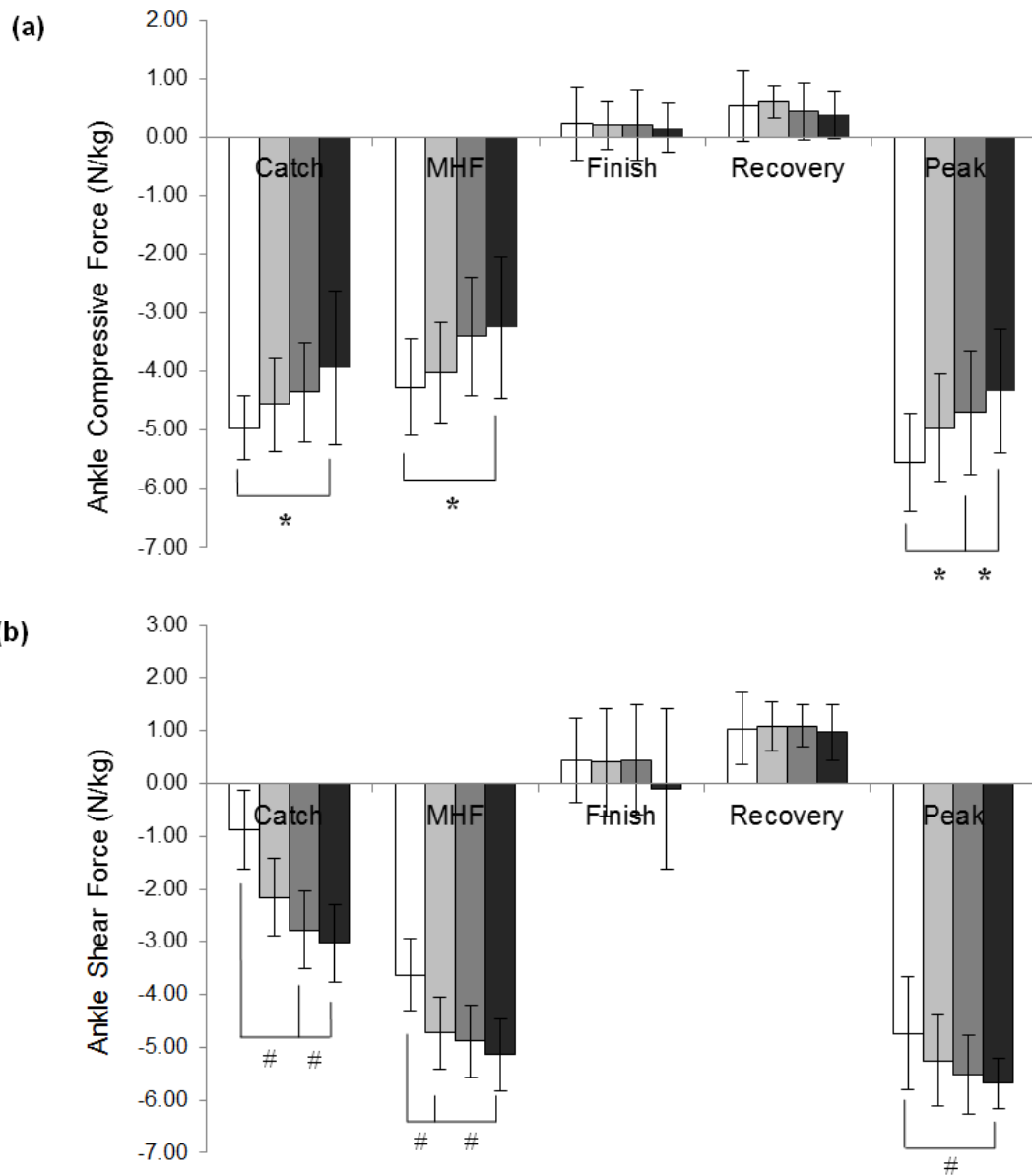


Figure 8.7: Mean  $\pm$  SD of (a) L5/S1 compressive force and (b) L5/S1 shear force with respect to footplate position. White, light grey, dark grey and black bars are P1, P2, P3 and P4 respectively. Significant differences between footplate positions are given by square brackets. #  $P < 0.05$ .





**Figure 8.8: Mean  $\pm$  SD of (a) ankle compressive force and (b) ankle shear force with respect to footplate position. White, light grey, dark grey and black bars are P1, P2, P3 and P4 respectively. Significant differences between footplate positions are given by square brackets. \*  $P < 0.01$ , #  $P < 0.05$ .**

**Table 8.6: Sagittal plane joint moment values (average  $\pm$  SD) at key positions in the stroke are shown for P1 – P4. All values are in Nm/kg where kg is the rowers' body mass.**

		Catch	MHF	Finish	10% Recovery	Peak
Ankle	P1	0.5 $\pm$ 0.2	0.7 $\pm$ 0.2	-0.2 $\pm$ 0.2	-0.3 $\pm$ 0.1	0.8 $\pm$ 0.2
	P2	0.5 $\pm$ 0.2	0.7 $\pm$ 0.2	-0.2 $\pm$ 0.2	-0.3 $\pm$ 0.1	0.7 $\pm$ 0.2
	P3	0.5 $\pm$ 0.2	0.7 $\pm$ 0.2	-0.2 $\pm$ 0.3	-0.3 $\pm$ 0.2	0.7 $\pm$ 0.2
	P4	0.4 $\pm$ 0.1	0.6 $\pm$ 0.2	-0.1 $\pm$ 0.4	-0.3 $\pm$ 0.2	0.6 $\pm$ 0.2#
Knee	P1	1.9 $\pm$ 0.5	3.4 $\pm$ 0.5	-0.5 $\pm$ 0.4	-0.6 $\pm$ 0.1	3.7 $\pm$ 0.4
	P2	1.9 $\pm$ 0.5	3.4 $\pm$ 0.5	-0.5 $\pm$ 0.4	-0.6 $\pm$ 0.2	3.5 $\pm$ 0.4
	P3	1.9 $\pm$ 0.5	3.3 $\pm$ 0.5	-0.5 $\pm$ 0.4	-0.6 $\pm$ 0.1	3.5 $\pm$ 0.4#
	P4	1.8 $\pm$ 0.4	3.3 $\pm$ 0.4	-0.2 $\pm$ 0.6	-0.5 $\pm$ 0.3	3.4 $\pm$ 0.4#
Hip	P1	3.2 $\pm$ 0.5	4.3 $\pm$ 0.6	-2.1 $\pm$ 0.9	-1.5 $\pm$ 0.3	4.7 $\pm$ 0.3
	P2	3.3 $\pm$ 0.4	4.5 $\pm$ 0.5	-2.0 $\pm$ 0.7	-1.5 $\pm$ 0.3	4.8 $\pm$ 0.3
	P3	3.3 $\pm$ 0.3	4.3 $\pm$ 0.6	-2.2 $\pm$ 0.8	-1.5 $\pm$ 0.3	4.7 $\pm$ 0.4
	P4	3.1 $\pm$ 0.5	4.4 $\pm$ 0.5	-1.6 $\pm$ 1.0^	-1.4 $\pm$ 0.6	4.6 $\pm$ 0.5
L5/S1	P1	9.2 $\pm$ 1.2	10.1 $\pm$ 1.5	-4.3 $\pm$ 1.8	-2.6 $\pm$ 0.8	11.6 $\pm$ 0.9
	P2	9.4 $\pm$ 1.1	10.4 $\pm$ 1.2	-4.3 $\pm$ 1.5	-2.8 $\pm$ 0.7	11.7 $\pm$ 1.0
	P3	9.6 $\pm$ 0.6	10.1 $\pm$ 1.6	-4.7 $\pm$ 1.6	-2.6 $\pm$ 0.7	11.6 $\pm$ 1.0
	P4	8.8 $\pm$ 1.1*	10.4 $\pm$ 1.3	-3.2 $\pm$ 2.1	-2.2 $\pm$ 1.2	11.3 $\pm$ 1.2*^

\* significant difference from P1 ( $P < 0.05$ ), # significant difference from P1 ( $P < 0.01$ ), ^ significant difference from P2 ( $P < 0.05$ )

### 8.3.5 Summary of results

The following biomechanical changes were observed as the position of the foot-stretchers were raised from P1 – P4:

- The majority of rowers subjectively reported a negative impact on their performance.
- Foot force ratio exhibited no change at the catch but progressively decreased at MHF.
- Progressive reductions occurred in stroke length and suspension of body weight from the seat at front of the stroke.

- Ankle dorsiflexion and hip flexion angle were increased, and knee flexion angle was reduced at the catch position.
- Anterior rotation of the lumbar spine and pelvis at the catch were reduced, as was pelvic ROM over a full stroke.
- L5/S1 shear force at catch and peak extensor moments at the ankle, knee and L5/S1 were diminished.

## 8.4 Discussion

The aim of this study was to investigate the impact of four foot-stretcher heights on biomechanical aspects of rowing technique and performance, particularly focussing on the resulting foot force ratio, performance outputs and inter-segmental dynamics of the lower limb joints and L5/S1.

Highly experienced rowers were recruited for this study to ensure that a consistent performance could be accomplished across the four foot-stretcher positions, and that the results would be transferrable to elite rowers. Table 8.1 shows that descriptors of performance (i.e. 500 m split, distance rowed in one minute, and stroke rates) were consistent across foot-stretcher positions ( $P>0.1$ ), and differed between conditions by just 0.2 s, 1.2 m and 1.1 strokes per minute, respectively. This suggests that rowing performance was repeatable across conditions, and was not influenced by fatigue during the test.

An important finding in this study was the change in RF that was observed during the drive phase as foot-stretcher heights were raised. At the catch position there was no significant change in RF, but at MHF there were clear reductions in this variable,

indicating that foot force became significantly more vertically orientated at MHF as foot-stretcher heights were raised ( $P<0.01$ ). Closer inspection of the foot force components show that reductions in RF at MHF were due to reductions in horizontal foot force ( $P<0.01$ ), with a non-significant increase in vertical foot force at MHF as stretcher heights were raised. In sprinting, a major determinant of performance was found to be the force application technique (i.e. proportion of horizontal force), as opposed to the magnitude of the resultant force (Morin et al., 2011). Rowing also requires large propulsive forces to accelerate the boat horizontally (Baudouin and Hawkins, 2004). However this study found that raising foot-stretcher heights in fact negatively affects foot force application. These results were not expected, as Caplan and Gardner (2005) had theoretically demonstrated that decreasing seat-to-heel distance on the rowing machine would result in reduced vertical foot force, thus optimising the ratio of foot force components. However, they did not experimentally test this idea. Therefore, they did not consider the possible negative effects that changes in foot-stretcher set-up might have on rowers' posture and joint kinematics, which could prevent them from reaching an effective catch position from which to execute a powerful leg drive.

The current study investigated both inter-segmental kinetics and kinematics, to enable the effect of stretcher height modification on the biomechanics of the rower to be assessed. The results revealed that raising foot-stretcher height induced substantial changes in ankle dynamics. Table 8.5 shows large increases in ankle dorsi-flexion at the catch and MHF, and reduced plantar-flexion at the finish, compared to when the footplate was positioned lower. These changes in ankle kinematics have previously been noted by Soper and Hume (2005), who suggested that a commonly employed strategy to cope with more vertically orientated foot-stretchers were to manipulate the

heel position with respect to the toes - enabling knee, hip and trunk angles to be maintained as closely as possible across all foot-stretcher conditions. Likewise, in this study, rowers had to significantly increase ankle dorsi-flexion at the catch in order to maintain their shank orientation. This subsequently led to a re-distribution of shear and compressive forces at the ankle, where shear force significantly increased ( $P<0.05$ ) and compressive force decreased ( $P<0.01$ ), with a subsequent reduction in peak ankle extensor moments. When the shank is anteriorly rotated relative to the foot, the vertical force component from the foot becomes a more posterior force at the shank, causing greater shear force to go through it, for the same force output at the foot. Whilst there was no change in ankle dorsi-flexor moment at the catch, and in fact a reduction in peak dorsi-flexor moment, the re-distribution of compressive and shear forces at the ankle will place greater stress on the ankle plantar-flexors, which may work to pull the foot backwards to provide posterior shear (Rodgers, 1988).

Significant changes in hip and knee dynamics at the catch were also seen ( $P<0.01$ ), although to a much smaller degree than the ankle, with a reduction in knee flexion of  $2.0^\circ$  and an increase in hip flexion of  $2.5^\circ$ , between P1 and P4. Changes in hip flexion has previously been noted, where an increase in height of 3.4 cm above the standard Concept II foot-stretcher position saw an increase in hip flexion at the catch by  $2.3^\circ$  (Caplan et al., 2010). The equivalent increase in height in this study (i.e. P1 - P3) saw a similar significant increase in hip flexion of  $2.0^\circ$ . However, both the pelvis and lumbar spine lost  $3.0^\circ$  of anterior rotation at the catch from P1 to P4, suggesting rowers achieved greater hip flexion through a more posterior orientation of their thigh, as opposed to anteriorly rotating their pelvis. Raising foot height will naturally alter thigh orientation posteriorly and consequently increase hip flexion if the pelvis is held in a

neutral position. This results in a lengthening of the hip extensor muscles and could lead to pelvic tilt, particularly if hamstring flexibility is insufficient (Milner, 2010).

Although seven out of 10 rowers stated that P2 either felt natural, or slightly improved their rowing technique, eight and nine out of ten rowers stated that P3 and P4 had a negative effect on rowing technique to a certain extent. Associated comments generally indicated that foot positions above P2 restricted ROM of the pelvis at the front end of the stroke, with limitations in hip flexibility making it difficult to slide into an effective catch position to initiate a powerful leg drive. Consequently, despite the rowers being in a more mechanically advantageous position to generate horizontal foot forces at P4, anatomical restrictions, such as hamstring and hip joint inflexibility meant that rowers could not effectively rock-over with their trunk and pelvis into a powerful catch position. As a result, raising the foot-stretchers from P1 to P4 prevented them from initiating a powerful leg drive and from transferring those forces to through the kinetic chain. Consequently, there were reductions in resultant foot force, horizontal foot force (and thus RF) and extensor moments at the ankle and knee, indicating reduced capabilities in foot force production as foot-stretcher height was raised.

Reduction in anterior pelvic tilt, occurring as a function of increasing rowing intensity, is a common technical finding in rowing (McGregor et al., 2004). Male rowers have been shown to compensate for a lack of pelvic rock-over with greater anterior lumbar rotations, in order to maintain stroke length (McGregor et al., 2008). In this study L5/S1 flexion angle did not significantly change with respect to foot-stretcher height. As such, the orientation of the lumbar spine relative to the pelvis was consistent across foot-stretcher positions, despite both segments' greater posterior orientation in the global frame. This reduction in anterior rotation of the trunk caused a progressive

decline in stroke length, dropping by 3.6 cm between P1 and P4. Previously, stroke length was seen to be maintained during higher intensities of rowing because the lumbar and thoracic spine is thought to compensate for the reduced pelvic rock-over which occurs with high intensity rowing (McGregor et al., 2004, Murphy, 2009). However, in this study there were no increases in L5/S1 flexion at the catch, thus the trunk became progressively more posterior as foot-stretcher height was raised, causing stroke length to be compromised. Furthermore, L5/S1 anterior shear forces at the catch, and peak L5/S1 extensor moments were significantly smaller at P4 compared to P1 ( $P < 0.05$ ). The erector spinae does not contribute to shear force of lumbar discs when its line of action is parallel to the long axis of the vertebrae. Therefore, anterior shear force at L5/S1 tends to increase with respect to flexion of the lumbar spine (McGill and Kippers, 1994). In addition, this study showed that the pelvis became progressively more vertical at the catch (i.e. losing anterior rotation), meaning that vertical forces from the seat will contribute less to the shear component of force at L5/S1. A large scale epidemiological study investigating predictors of back pain found that workers exposed to higher peak lumbar shear forces and higher cumulative joint loads were at greater risk of developing back injuries (Norman et al., 1998). As such, the reductions in L5/S1 and lower limb loads that were observed at higher stretcher positions may be beneficial in terms of reducing joint stress and preventing injuries. This conclusion may be strengthened as higher foot positions did not induce greater L5/S1 flexion at the catch, which is another key contributor to injuries in rowing (Murphy, 2009).

A key aim of this study was to examine the effect of modifying foot-stretcher height on RF and to determine how this influences resulting performance of the rower. Previous research has indicated that the following variables are considered positive influences towards rowing performance: large MHF, large power output, long stroke length,

suspension from the seat during the critical drive phase, returning bodyweight to the seat at the finish position, high RF and horizontal foot force (Caplan and Gardner, 2005, Murphy, 2009). It was speculated by (Caplan and Gardner, 2005) that raising foot-stretcher height would improve mechanical effectiveness of the stroke by reducing the unwanted vertical foot force component which does not contribute to boat propulsion. However, as mentioned previously, raising foot-stretcher height negatively affected RF in this study, through progressive reductions in the proportion of horizontal foot force application. In fact there was a significant reduction in both the absolute horizontal and resultant foot forces ( $P < 0.05$ ). In addition, there were distinct negative effects of increased foot-stretcher height on the previously mentioned parameters of rowing performance, which included progressive reductions in stroke length, and seat suspension at the catch and MHF. Chapter 6 showed that a negative linear correlation exists between resultant foot force and seat force at MHF ( $R^2 = 0.70$ ), where rowers with larger resultant foot forces at MHF had better suspension during the critical drive. In accordance, progressive reductions in resultant foot force was seen to negatively affect seat suspension, as a greater magnitude of force was applied to the seat at the catch and MHF positions, as foot-stretcher height was raised. Furthermore, a reduced seat-to-heel distance when foot-stretchers are raised causes the line of leg extension during the drive phase to be more horizontal, thus reducing the upwards reaction force of the rower from the seat, and consequently diminishing suspension.

Force applied to the seat at the finish position decreased from P1 to P4 ( $P < 0.01$ ). However, it has previously been shown that it is beneficial to return bodyweight to the seat during the latter part of the drive phase, as an increase in rowers' base of support on the seat helps to avoid motion that is thought to be associated with spinal injury (Murphy, 2009). It is also speculated that reduced suspension from the seat during the



critical drive prevents the rower from dropping their weight vertically onto the seat following the release of suspension. Despite progressive reductions in performance parameters such as RF, stroke length, resultant foot force and seat suspension, it was found that both MHF and power output were maintained across all four foot-stretcher positions. The key aim in rowing is to maximise horizontal acceleration of the boat by generating large propulsive forces at the handle and oars (Baudouin and Hawkins, 2002), and raising the foot-stretchers was seen to result in a smaller loss in force between the foot-stretchers and the handle. This suggests that the overall mechanical efficiency of the system was improved i.e. for the same magnitude of force expressed at the handle, a less powerful leg drive was required. Improved efficiency of the system may therefore reduce the effects of fatigue and attenuate the drop in power output that occurs during a 2000 m rowing test (Caplan and Gardner, 2005).

This study focussed on the effect of modifying just the height of the foot-stretchers, on rowing performance and technique. Foot-stretchers on a boat can be modified in a number of ways through adaptations in height, width, splay and angle. However, height was selected for this study as that is the only way in which rowers are able to adapt their foot position on an ergometer. The best foot-stretcher position is conceivably the highest position which does not induce unfavourable trunk posture and lower limb kinematics. However, if the rower suffers from substantial lack of flexibility around the hip muscles, their limits of ROM may be reached with very little increase in foot-stretcher height. Therefore, an important consideration would be to influence RF alternative changes in foot-stretcher set-up. For example, changes in the inclination of the foot-stretchers may enable a rower to maintain an effective trunk posture, whilst enhancing their horizontal foot force component.

All rowers who participated in this study stated that they selected their Concept II foot-stretcher height at which they train, largely based on the size of their feet and their ankle and hip flexibility, rather than a position which is proven to enhance their technique or performance. However, the results of this study would indicate that rowers generally selected an optimal foot-stretcher height at which the greatest anterior pelvic rock-over, stroke length and RF would occur. This was true even for a case by case analysis of all ten rowers, where these results were seen consistently across all individuals. However, it is important to note that rowers produced their best performance when employing a foot-stretcher position with which they had trained for many years, and this may have had a significant impact on the subsequent result of this study. Rowers were given at least five minutes to familiarise themselves with each new foot-stretcher position. However, the rowing trial itself lasted just one minute each, in order to prevent the onset of fatigue affecting subsequent trials. It has previously been shown that higher foot-stretchers attenuated the drop in power output per stroke during the latter part of a 2000 m rowing test (Caplan and Gardner, 2005). However, the present study examined instantaneous changes in foot force with respect to foot-stretcher height, rather than investigating changes that occur over the course of a longer rowing trial. Furthermore, Caplan and Gardner (2008) showed that four minutes of familiarisation at a new stretcher height was inadequate for a rower to overcome their level of familiarisation at their usual stretcher height. In fact, they found that for foot-stretchers raised 6.8 cm vertically, three weeks of familiarisation training was necessary in order to see gains in stroke power output. Therefore it is possible that a longer rowing trial following several weeks of familiarisation at each height would have seen a more positive effect on performance, with respect to raised foot-stretcher positions.

However, in this study it is considered that randomisation of the order of trials was able to mitigate this effect to some degree.

## **8.5 Conclusion**

To conclude, the male rowers tested in this study exhibited distinct alterations in the biomechanics of their rowing technique and performance as foot-stretcher heights were raised. There were reductions in horizontal foot force, which caused the resultant foot force to be more vertically orientated. This may be associated with kinematic changes in the rower, particularly at the lumbar-pelvic region where a reduced anterior rotation of the lumbar spine and pelvis segments were observed in the catch position. Thus, whilst there was no change in L5/S1 flexion, there was a posterior shift of the rowers' body in the sagittal plane. Raising the foot-stretchers generally had a negative impact on parameters which influence good performance, namely reducing stroke length, resultant and horizontal foot force and quality of suspension from the seat. However, these reductions did not influence key performance indicators, namely, MHF and power output. Therefore, it is suggested that mechanical efficiency of the rower is enhanced when foot-stretchers are raised, because the same magnitude of handle force and power was expressed for a less powerful leg drive. Additionally, reduced loading at L5/S1 and the lower limb joints suggest that raising foot-stretcher height may be beneficial in reducing joint stress. From a coaching perspective these results provide useful information regarding the implications of foot-stretcher heights on rowing performance, and may be particularly useful for considerations of athlete set-up on an individual basis.

## **Chapter 9:**

### **Summary and Future Work**

The primary aims of this research were to develop methods for assessing biomechanical asymmetries of the lower limbs, in addition to inter-segmental loading at the ankle, knee hip and L5/S1, so that these occurrences could be investigated in elite rowers. This was done with a view to advancing the previous work carried out in the field of elite rowing biomechanics, but also with the purpose of informing future rowing research.

This chapter summarises the work that was sequentially carried out between the first and last studies (i.e. Chapters 3-8), whilst discussing some key issues regarding the methodologies that were developed. A summary of the key results are presented, and suggestions for future work are offered. The aims of this thesis were addressed in six separate studies as follows:

1. Investigation of kinematic lower limb asymmetries and their impact on the quality of lumbar-pelvic kinematics (Chapter 3).
2. Development of bilateral force measuring footplates (Chapter 4).
3. Application of instrumented footplates to assess reliability, asymmetry and magnitudes of foot force in elite rowers (Chapter 5).
4. Examination of the influence of foot force magnitude and asymmetries on previously identified indicators of good performance and technique (Chapter 6).
5. Development of an inter-segmental inverse dynamics model to examine the impact of high intensity rowing on joint loading (Chapter 7).

6. Examination of the effect of modifications of foot stretcher height on rowing technique and performance (Chapter 8).

## **9.1 Summary of work**

The analysis of asymmetry has proved to be useful from perspectives of performance (Herzog et al., 1989), injury (Jacobs et al., 2005) and sports technology (Buckley, 2000). However, only a small number of studies have investigated asymmetries during rowing (Janshen et al., 2009), with the majority of biomechanical rowing models taking a unilateral approach (Bull and McGregor, 2000, Halliday et al., 2004, Greene et al., 2011). As such, the first study modified the traditional unilateral FOB sensor set-up, to track bilateral lower limb motion of elite, club and novice rowers on an ergometer. Interestingly both hip and knee angles in the sagittal plane demonstrated some degree of asymmetry in rowers at all levels of experience. Furthermore, hip ROM was significantly more asymmetrical than knee ROM when the full stroke cycle was assessed.

It is speculated that causes of hip asymmetry may be due to unilateral anatomical abnormalities such as cam or pincer deformities at the femoral head and acetabulum, respectively (Pfirrmann et al., 2006). Such unilateral deformities can restrict hip ROM in the sagittal plane, and this would be particularly detrimental for rowers where deep hip flexion is necessary to reach an effective catch position. Furthermore, gluteal muscle contractures and inflexibilities of muscles surrounding the hip joints are additional factors which could limit unilateral hip movement, thus contributing to bilateral ROM asymmetries (Godges et al., 1993, Zhao et al., 2009). However, this study did not investigate the possible mechanisms which contribute to knee and hip

motion asymmetries, and additional imaging data (such as MRI), in addition to clinical hip ROM and flexibility tests, would be necessary to ascertain direct causes of hip asymmetry in rowers. Imbalances at the hips are often thought to contribute to LBP in athletes, as the hip musculature is crucial in the effective transfer of forces from the lower extremities to the spine (Nadler et al., 2002). Interestingly, hip ROM asymmetry was found to be a moderate predictor of L5/S1 kinematics during the drive phase, explaining nearly 40% of the variance in L5/S1 flexion that occurred at the catch and MHF. Whilst there are clearly other variables which influence quality of the lumbar-pelvic rhythm during rowing, the moderate influence of hip ROM asymmetry on L5/S1 kinematics is a clinically relevant one with important implications. This is because sub-optimal L5/S1 kinematics are thought to be associated with LBP in rowers, where repeated loading combined with sub-optimal posture increases stress on the intervertebral discs (Reid and McNair, 2000). Therefore, given the relationship between L5/S1 flexion and hip ROM asymmetry, a simple measure of hip asymmetry through measurement tools such as goniometers may give insight into the quality of the lumbar-pelvic rhythm, and possible potential for lower back pain. Furthermore, this idea of hip asymmetries influencing lumbar-pelvic kinematics is a novel result which gives insight into a possible mechanism that contributes to lower back injuries in rowers.

The above study provided new information regarding asymmetry in rowing, as no previous research had quantified asymmetries of lower limb movement patterns during rowing in relation to its impact on lumbar-pelvic kinematics. Whilst these results are important, it was necessary to consider sources of asymmetry other than kinematics. For example, it is possible for a rower to achieve symmetrical lower limb motion and yet exhibit asymmetrical loading of the lumbar spine, if uneven pressure is exerted onto the foot stretchers. Therefore, there is a need to investigate kinetic asymmetries exerted

against the foot stretchers, in addition to just movement asymmetries. Consequently instrumented footplates which measure the forces exerted onto each foot stretcher were developed for the Concept II ergometer. The footplates consisted of stainless steel and aluminium beams which were both instrumented with full Wheatstone bridge configured strain gauges to quantify forces applied to each beam. Instrumenting two beams meant that forces in two axes could be quantified i.e. those in the vertical (SI) and horizontal (AP) axes. The third ML axis has been shown to be minimal during rowing (Halliday et al., 2004, Pudlo et al., 2005), so it was considered acceptable to quantify just the two main axes of force.

The footplates were deemed to have good accuracy, with mean system errors of 1.8%, 4.9% and 3.9 mm for normal force, shear force and COP respectively. The footplates could measure foot force of elite rowers' during a step test with high reliability (CMD>0.98). They were effective in distinguishing foot force patterns between different groups of rowers, indicating that LWM generate significantly greater resultant foot forces compared to SWEEP and SCULL rowers. They also showed that when the vertical and horizontal force vectors were assessed individually, force asymmetries appeared greater, than when comparing the resultant force outputs. Although there have been prior studies which developed instrumented footplates (Macfarlane et al., 1997, Baca et al., 2006b, Krumm et al., 2010), none had extensively tested their instruments on a large group of elite rowers over multiple rowing sessions. From the perspective of GB rowing coaches, foot force feedback was particularly useful for assessing loading asymmetries of individual athletes, as it gave an insight into possible mechanisms for injuries through the initial loading phase. For example, significantly greater loading of the right foot stretcher indicates some level of lower extremity imbalance which could propagate through the kinetic chain and cause negative changes

in spinal kinematics and imbalanced loading of the lumbar spine. Therefore, if asymmetries are a risk factor for LBP, then even healthy people with a certain degree of asymmetry may be predisposed to future LBP and injury. However, in order to investigate the effects of asymmetrical foot stretcher loading on subsequent kinematic patterns, it was imperative that force and motion data could be recorded in a synchronised manner.

Following the independent examination of foot forces patterns, the software for the footplates was synchronised with that of the motion capture and instrumented ergometer system so that the data acquisition program in Labview could record data from all systems simultaneously. This was so that considerations of the leg drive could be made with respect to rowers' movement patterns, and interactions with other contact forces on the rowing machine. However, the bilateral FOB motion capture set-up developed for Chapter 3 could not be employed in subsequent studies. Firstly, because the GB rowing testing sessions were set up for unilateral data collection and two-dimensional real-time biofeedback of rowers' lumbar-pelvic and lower limb motion. Secondly, problems had previously been encountered with FOB bilateral set-up where the left malleoli could not be accurately digitised due to interference from the adjacent shank sensor during digitisation. An investigation into the mal-tracking of the left malleoli was conducted and presented in Appendix C. Missing data from the left malleoli meant that ankle kinematics could not be captured, and the JCS approach could not be employed to calculate sagittal plane knee kinematics, resulting in less accurate knee flexion/extension values. As a result, bilateral foot force data was synchronised with a FOB system which utilised a unilateral kinematics model, to enable ankle, knee and hip kinematics on the right side and L5/S1 kinematics to be quantified.



The results of the statistical modelling in Chapter 6 suggest that greater hip flexion at the front of the stroke is important in generating large resultant foot forces. Additionally, rapid extension of the knees, in conjunction with maintaining a strong lumbar-pelvic posture was key when aiming to maximize the horizontal component of foot force. As with hip ROM asymmetry, there was a moderate effect of foot force asymmetry on L5/S1 kinematics, where larger foot force asymmetries were associated with a greater occurrence of L5/S1 flexion during the critical drive phase. Flexion of L5/S1 during the critical drive phase is associated with poor postural control and was identified by (Murphy, 2009) as increasing the risk of injury to the lumbar spine. This supports the supposition from Chapter 3 that lower limb asymmetries negatively influence L5/S1 kinematics, and consequently may increase the likelihood of attaining lower back injuries.

An investigation into the rowing kinetic chain highlighted strong correlations between MHF, seat force at MHF and foot force at MHF. This enforced the idea that a small lift of the bodyweight from the seat is an important link in the transfer of forces from the lower to the upper limbs. A static force analysis would suggest that reducing load applied to the seat would require greater vertical force to be applied to the foot stretchers. However, it was theoretically demonstrated that seat suspension is optimized when large foot forces are applied at an angle to the foot stretcher. The optimal condition for foot force to be orientated horizontally to generate large propulsive forces is met with constraints from the requirement of vertical foot force to aid seat suspension. As such, it is considered that there exists an optimal vertical to horizontal foot force ratio, and when that is combined with correct kinematic sequencing, a powerful and effective drive can be executed. An investigation into this optimal foot force ratio needs to be explored, and it would be particularly interesting to

examine how the optimum ratio is influenced by anthropometric characteristics such as thigh and shank length ratio, or flexibility of the ankle joint and hamstrings.

Instrumentation of the foot stretchers is important for assessments of foot force profiles and asymmetries in rowers, but also because these foot forces can act as an input into a model which enables inter-segmental forces and moments to be estimated, through a closed chain inverse-dynamics analysis. There had been some limited research investigating net joint moments during rowing, particularly focussing on the lower limbs i.e. ankle, knee and hip moments (Halliday et al., 2004, Cerne et al., 2011, Greene et al., 2011). However, no study had separated the lumbar spine and pelvis into separate segments to investigate loading which occurs at L5/S1. It is especially important to investigate loading in the lumbar-pelvic region because that is the most commonly injured area in rowers. The majority of these injuries are due to overuse, where the cause is mechanical and results from the high degree and frequency of loads exerted through the lumbar spine (Wilson et al., 2010). As such, a five segment inter-segmental model was developed where the foot, shank, thigh, pelvis and lumbar spine were represented as rigid linked segments. A bottom-up inverse dynamics approach was utilised where force outputs from the foot stretchers and seat were combined with kinematic data from the FOB to estimate inter-segmental forces and moments at the ankle, knee, hip and L5/S1. This model was then used to quantify inter-segmental loads during ergometer rowing at incremental intensities (Rate 18 – Free Rate).

In Chapter 7 different inter-segmental loads, particularly in the sagittal plane, were identified at the ankle and L5/S1 at higher stroke rates compared to lower rates. Furthermore, male and female rowers used different loading strategies through the lower limbs in response to increasing rowing intensity. For example, lightweight men

demonstrated an increase in peak extension moments through the hips and knees in response to higher stroke rates. However, heavyweight female rowers reduced knee loading and exhibited no change in hip loading as stroke rate increased. A key result was that large peak L5/S1 extension moments were present during the rowing stroke in both male and female rowers, and were seen to increase with respect to stroke rate for both groups. These increases in L5/S1 loading at incremental stroke rates were coupled with increases in L5/S1 flexion. Additionally no concurrent increases in foot or handle force were observed at higher stroke rates. As such, greater loading of L5/S1 during high intensity rowing is unlikely to be an indicator of greater performance and force transmission, but rather an effect of technique decline. Therefore rowers may be at greater risk of developing LBP when training at high intensities, particularly when combined with sub-optimal L5/S1 kinematics.

With regards to these results, it is important to be aware of the limitations of inverse dynamics models. For example anthropometric data often originates from cadaveric specimens that may have had very different inertial properties to elite rowers. Also, many simplifications which limit the model's accuracy are made when calculating *net* moments about a joint, where segments are represented as uniform rigid links, inertial values remain constant and joints are frictionless (Winter, 1990). Furthermore, footplates measure force in the sagittal plane only, whilst 3D kinematic data is acquired from FOB. This may explain why the majority of significant differences were seen in the sagittal plane, and as such the non-sagittal plane inter-segmental dynamics must be viewed with caution. In spite of these limitations, the results clearly show the changes in inter-segmental loading that occurs with incremental rowing intensities, and while the absolute values may be prone to some errors, the relative changes in values that occur at increasing stroke rates is an important consideration.

In a final study, new adjustable footplates were developed which enabled changes to be made in foot stretcher height with respect to the seat. Contrary to previously proposed theories, raising foot stretcher heights resulted in a mechanically less effective leg drive, where resultant foot force became more vertically orientated. This appeared to be caused by a more posterior orientation of the trunk as the foot-stretcher positions were raised, where reduced pelvic ROM prevented anterior pelvic rock-over from being achieved at the catch, thus limiting the delivery of a powerful leg drive. There was some evidence of reduced inter-segmental loading with raised foot stretchers, so despite some deteriorations in performance, it may be beneficial in reducing joint stress and injury potential.

The majority of rowers achieved their best foot force ratio, performance and lumbar-pelvic ratios when rowing at P1 i.e. their original foot stretcher position. However, this is the position for which they have the most experience, thus adaptations over many years may have resulted in P1 eliciting their maximal joint ROM and flexibility, as they would be rarely challenged beyond this position. As such, restrictions in flexibility and ROM which prevents anterior pelvic rotations at the catch may be a key obstacle in gaining benefits from raised foot stretcher heights. Training for flexibility should therefore be a long term objective so that performance gains can be realised from modifications in foot stretcher height set-up. An alternative method of overcoming ROM limitations may be to manipulate the foot stretcher angle rather than height, because the angle of the foot stretcher directly influences the orientation of foot force application. For example, placing the foot stretcher at a steeper angle would increase the foot force ratio in favour of the horizontal component, provided the greater requirement for ankle dorsi-flexion can be met. Alternatively reducing the foot stretcher angle when it is placed at a higher position may compensate for hip and ankle

ROM restrictions at the catch position. Therefore, it is speculated that improved hip and ankle flexibility may be important considerations for achieving extra gains in performance from external intervention such as the refinement of foot stretcher set-up.

Ideally, a longer period would have been given to the rower to familiarise themselves and train at each new foot stretcher height, with participants attending four different sessions, and performing a more fatiguing trial each time, as opposed to 1 minute at race pace. However, in the context of this study, it would not have been feasible to have high level rowers train with multiple different foot stretcher settings over several months, so a randomisation of the trials orders was ensured to mitigate the impact of this. It was also assumed that all rowers chose their original foot stretcher position based on the same criteria of comfort and foot size, and deviations from this foot position would have a similar effect on all participants. However, the rowers tested ranged in body size and height, and particularly anatomical differences in thigh to shank length ratio will have affected the way in which they responded to the interventions. As such, these variables should be monitored and controlled in the future, so that a greater understanding of subject specific set-up can be gained from these tests. Furthermore, this final study did not use elite GB rowers in the current Olympic squad, as with the previous studies in this thesis. Although it would have been ideal to use the same pool of rowers in each study, it was not possible to have elite rowers perform a free rate rowing trial at foot stretcher positions over 5 cm higher than which they normally train. Nevertheless, the rowers used in the study were at an extremely high standard, reaching national standard and competing at GB Under 23 trials or equivalent. This suggests that results from the study could be applied to elite GB rowers.

### **9.1.1 Research Contributions**

Given the collaborative nature of this research project, with Imperial College working in partnership with GB Rowing, the work conducted had direct application in terms of furthering knowledge of elite rowing biomechanics. The key contributions of the work contained in this thesis include:

- Kinematic and kinetic descriptions of lower limb asymmetries in elite rowers, and examining their influence on lumbar-pelvic kinematics.
- Development of instrumented footplates which were incorporated into GB Rowing's biomechanical testing and biofeedback delivery.
- Understanding the key kinematic variables and movement patterns which enable force production during the rowing stroke to be optimised.
- Description of the loads experienced at the lower extremity and lumbar-pelvic joints, and how these loads respond to changes in rowing intensity.
- Understanding how immediate changes in foot stretcher height influences lower limb, and particularly, lumbar-pelvic biomechanics.

### **9.2 Future recommendations**

It is suggested that future work could focus on using an optical motion tracking system such as Vicon to capture kinematic data on a rowing ergometer. With the FOB there is a limitation to the number of sensors that can be tracked at once due to the inherent constraints of the system, whereas optical markers are passive, and as such there would

be no limitation to the number of body segments that can be monitored and analysed. This means that once a suitable kinematic model has been written in programs such as BodyBuilder and/or Matlab, a more accurate set of bilateral kinematic data can be acquired for the purpose of describing bilateral asymmetry of the lower limbs. Furthermore, these new kinematic measures can be synchronised with footplate and seat force data to enable bilateral inter-segmental loading asymmetries to be examined, which was not possible in this project. Optical motion tracking would also allow movements of a greater number of body segments to be tracked; especially the thoracic spine and upper limbs all of which have to date received limited attention in relation to rowing performance. This would increase knowledge of how athletes could gain performance advantages, whilst providing insight into injury mechanisms over the whole of the spine.

The FOB sensor limitation also meant that the foot segment was defined relatively poorly, as it was not possible to track the motion of the calcaneus. Consequently, there was an offset in the calculated sagittal plane angles of the ankle joint centre. The use of optical tracking would also mean that the foot and ankle can be defined with greater accuracy, thus paving the way for detailed musculoskeletal modelling of the lower limbs where individual muscle forces can be estimated during rowing (Weinert-Aplin, 2011). However, the disadvantage of utilising optical motion tracking during elite athlete testing sessions is that athlete set-up, and in particular post-processing of data, would be far more time consuming. For example, three markers are required to define a single segment (as opposed to one FOB sensor), and these markers must be correctly labelled and tracked during data analysis. Furthermore, when the view of a marker is obstructed from the motion cameras, a gap filling process must be undertaken where the position of the marker for a single frame is estimated. This becomes particularly

cumbersome when numerous markers are tracked over a long period, as there is greater potential for markers to be labelled incorrectly and for gaps to appear in the marker trajectory. These issues are not encountered in electro-magnetic motion tracking, and thus it is possible to generate a more rapid turnaround of data feedback to the coaches and athletes.

Bilateral EMG data has been collected and analysed for the purpose of investigating muscle activation asymmetries of the lower limbs, lower back and abdominal muscles (Hardijzer, 2012). This type of data could also be useful for temporal analysis of muscle activation during a rowing stroke, to see which muscle groups are highly activated at specific portions of a stroke cycle. It would also enable frequency analyses to be performed, where muscle fatigue can be assessed through examining the ratio of fast to slow twitch fibre recruitment using wavelet transform analysis. By providing information on specific muscle recruitment patterns and changes in fibre type recruitment over the course of a fatiguing trial, physiological and strength training regimes can be adapted to target specific muscles that may not be used optimally during the rowing trial.

The work produced in this thesis has provided novel technological approaches enabling investigations of biomechanical asymmetries and inter-segmental loading to be conducted during ergometer rowing. Ergometers are considered an effective training tool that can be readily instrumented for biomechanical research purposes (Hawkins, 2000, Page and Hawkins, 2003, Soper and Hume, 2004). However, whilst they are considered to reproduce on-water kinematics to a good degree (Lamb, 1989, Elliott et al., 2002), the data derived from ergometer rowing cannot be directly inferred to on-water rowing performance. Nevertheless, current developments in wireless sensor



technologies and telemetry systems should permit limited instrumentation to be transferred to boats, where more meaningful on-water rowing data can be obtained during race simulations.

The information derived in an artificial laboratory setting will always enable more detailed biomechanical data to be acquired, compared to a racing environment on-water, as there are fewer limitations to the level of instrumentation that can be employed. However, simple biomechanical measures of on-water data can subsequently be correlated to more detailed data acquired from the laboratory, in order to infer greater meaning to the data derived from wireless sensors. Whilst the work in this thesis has contributed towards a wider understanding of elite rowing biomechanics with respect to ergometer performance, injury and coaching feedback, it is clear that new and developing technologies will dictate the direction of future on-water rowing biomechanics research.

## References

- ADAMS, M. A. & DOLAN, P. 1995. Recent advances in lumbar spinal mechanics and their clinical significance. *Clinical Biomechanics*, 10, 3-19.
- ADAMS, M. A., MCNALLY, D. S., CHINN, H. & DOLAN, P. 1994. Posture and the Compressive Strength of the Lumbar Spine. *Clinical Biomechanics*, 9, 5-14.
- AL-EISA, E., EGAN, D., DELUZIO, K. & WASSERSUG, R. 2006a. Effects of pelvic asymmetry and low back pain on trunk kinematics during sitting: a comparison with standing. *Spine (Phila Pa 1976)*, 31, E135-43.
- AL-EISA, E., EGAN, D., DELUZIO, K. & WASSERSUG, R. 2006b. Effects of pelvic skeletal asymmetry on trunk movement - Three-dimensional analysis in healthy individuals versus patients with mechanical low back pain. *Spine*, 31, E71-E79.
- AL-EISA, E., EGAN, D. & FENETY, A. 2004a. Association Between Lateral Pelvic Tilt and Asymmetry in Sitting Pressure Distribution. *The Journal of Manual & Manipulative Therapy*, 12, 133 -142.
- AL-EISA, E., EGAN, D. & WASSERSUG, R. 2004b. Fluctuating asymmetry and low back pain. *Evolution and Human Behavior*, 25, 31-37.
- ARELLANO, R., PARDILLO, S., DE LA FUENTE, B. & GARCÍA, F. 2000. A system to improve the swimming start technique using force recording, timing and kinematic analyses. *Proceedings of the 18th International Symposium of Biomechanics in Sports*. 609-613.
- ARENDT, E. & DICK, R. 1995. Knee Injury Patterns among Men and Women in Collegiate Basketball and Soccer - Ncaa Data and Review of Literature. *American Journal of Sports Medicine*, 23, 694-701.
- BACA, A., KORNFEIND, P. & HELLER, M. 2006a. Comparison of foot-stretcher force profiles between on-water and ergometer rowing. *Proceedings of 24th International Symposium of Biomechanics in Sports*. 347-350.
- BACA, A., KORNFEIND, P. & HELLER, M. 2006b. Feedback Systems in Rowing. In: MORITZ, E. F. & HAAKE, S. (eds.) *The engineering of sport 6. Vol. 1*. Heidelberg: Springer-Verlag.
- BAUDOUIN, A. & HAWKINS, D. 2002. A biomechanical review of factors affecting rowing performance. *British Journal of Sports Medicine*, 36, 396-402; discussion 402.
- BAUDOUIN, A. & HAWKINS, D. 2004. Investigation of biomechanical factors affecting rowing performance. *Journal of Biomechanics*, 37, 969-976.
- BECHARD, D. J., NOLTE, V., KEDGLEY, A. E. & JENKYN, T. R. 2009. Total kinetic energy production of body segments is different between racing and training paces in elite Olympic rowers. *Sports Biomechanics*, 8, 199-211.

- BEZODIS, I. N., KERWIN, D. G. & SALO, A. I. T. 2008. Lower-limb mechanics during the support phase of maximum-velocity sprint running. *Medicine and Science in Sports and Exercise*, 40, 707-715.
- BOBBERT, M. F. & SCHAMHARDT, H. C. 1990. Accuracy of Determining the Point of Force Application with Piezoelectric Force Plates. *Journal of Biomechanics*, 23, 705-710.
- BONO, C. M. 2004. Low-back pain in athletes. *Journal of Bone and Joint Surgery-American Volume*, 86A, 382-396.
- BUCKLEY, J. G. 2000. Biomechanical adaptations of transtibial amputee sprinting in athletes using dedicated prostheses. *Clinical Biomechanics*, 15, 352-358.
- BUCKTHORPE, M., MORRIS, J. & FOLLAND, J. P. 2012. Validity of vertical jump measurement devices. *Journal of Sports Sciences*, 30, 63-69.
- BULL, A. M. J., BERKSHIRE, F. H. & AMIS, A. A. 1998. Accuracy of an electromagnetic measurement device and application to the measurement and description of knee joint motion. *Proceedings of the Institution of Mechanical Engineers Part H-Journal of Engineering in Medicine*, 212, 347-355.
- BULL, A. M. J., HOLT, B., WRAGG, P. & MCGREGOR, A. H. 2004. Validation of the use of a skin-mounted device to measure out-of-plane rotations of the spine for a rowing activity. *Journal of Musculoskeletal Research*, 8, 129 –132.
- BULL, A. M. J., KESSLER, O., ALAM, M. & AMIS, A. A. 2008. Changes in knee kinematics reflect the articular geometry after arthroplasty. *Clinical Orthopaedics and Related Research*, 466, 2491-2499.
- BULL, A. M. J. & MCGREGOR, A. H. 2000. Measuring spinal motion in rowers: the use of an electromagnetic device. *Clinical Biomechanics*, 15, 772-776.
- BURNETT, D. R., CAMPBELL-KYUREGHYAN, N. H., CERRITO, P. B. & QUESADA, P. M. 2011. Symmetry of ground reaction forces and muscle activity in asymptomatic subjects during walking, sit-to-stand, and stand-to-sit tasks. *Journal of Electromyography and Kinesiology*, 21, 610-615.
- CALDWELL, J. S., MCNAIR, P. J. & WILLIAMS, M. 2003. The effects of repetitive motion on lumbar flexion and erector spinae muscle activity in rowers. *Clinical Biomechanics*, 18, 704-711.
- CAPLAN, N., COPPEL, A. & GARDNER, T. 2010. A review of propulsive mechanisms in rowing. *Proceedings of the Institution of Mechanical Engineers Part P-Journal of Sports Engineering and Technology*, 224, 1-8.
- CAPLAN, N. & GARDNER, T. 2008. The Influence of a Three Week Familiarisation Period on Rowing Mechanics at a New Stretcher Position. *International Journal of Sports Science and Engineering*, 2, 15-22.
- CAPLAN, N. & GARDNER, T. 2010. The influence of stretcher height on posture in ergometer rowing. *European Journal of Sport Science*, 10, 263-268.

- CAPLAN, N. & GARDNER, T. N. 2005. The influence of stretcher height on the mechanical effectiveness of rowing. *Journal of Applied Biomechanics*, 21, 286-96.
- CARPES, F. P., ROSSATO, M., MOTA, C. B. & FARIA, I. E. 2006. Bilateral Pedaling Asymmetry during a Simulated 40 km Cycling Time-Trial. *Medicine and Science in Sports and Exercise*, 38, S394-S394.
- CERNE, T., KAMNIK, R. & MUNIH, M. 2011. The measurement setup for real-time biomechanical analysis of rowing on an ergometer. *Measurement*, 44, 1819-1827.
- CHAFFIN, D. B. & ERIG, M. 1991. 3-Dimensional Biomechanical Static Strength Prediction Model Sensitivity to Postural and Anthropometric Inaccuracies. *Iie Transactions*, 23, 215-227.
- CHEE, S. 2006. *Biomechanical Modelling of Lumbar Spine Loading in Rowing*. MPhil, Imperial College London.
- CHIU, L. Z. F. & SALEM, G. J. 2006. Comparison of joint kinetics during free weight and flywheel resistance exercise. *Journal of Strength and Conditioning Research*, 20, 555-562.
- CHOCKLEY, C. 2008. Ground Reaction Force Comparison Between Jumps Landing on the Full Foot and Jumps Landing en Pointe in Ballet Dancers. *Journal of Dance Medicine and Science*, 12, 5-8.
- CHOLEWICKI, J., MCGILL, S. M. & NORMAN, R. W. 1991. Lumbar spine loads during the lifting of extremely heavy weights. *Medicine and Science in Sports and Exercise*, 23, 1179-86.
- CHUNG, L. H., REMELIUS, J. G., VAN EMMERIK, R. E. A. & KENT-BRAUN, J. A. 2008. Leg Power Asymmetry and Postural Control in Women with Multiple Sclerosis. *Medicine and Science in Sports and Exercise*, 40, 1717-1724.
- CLEATHER, D. J. & BULL, A. M. J. 2010. Influence of inverse dynamics methods on the calculation of inter-segmental moments in vertical jumping and weightlifting. *Biomedical Engineering Online*, 9, 74.
- COLLOUD, F., BAHUAUD, P., DORIOT, N., CHAMPELY, S. & CHEZE, L. 2006. Fixed versus free-floating stretcher mechanism in rowing ergometers: Mechanical aspects. *Journal of Sports Sciences*, 24, 479-493.
- COLLOUD, F., BAHUAUD, P., DORIOT, N., CHAMPELY, S., MONTEIL, K. M. & CHÈZE, L. 2001. Is force symmetry influenced by using a fixed versus a free-floating rowing ergometer mechanism? *Archives of Physiology and Biochemistry*, 109 (supplement), 65.
- DAVIS, R. R. & HULL, M. L. 1981a. Measurement of Pedal Loading in Bicycling. *Journal of Biomechanics*, 14, 496-496.

- DAVIS, R. R. & HULL, M. L. 1981b. Measurement of Pedal Loading in Bicycling .2. Analysis and Results. *Journal of Biomechanics*, 14, 857-872.
- DEVITA, P. & HORTOBAGYI, T. 2000. Age causes a redistribution of joint torques and powers during gait. *Journal of Applied Physiology*, 88, 1804-1811.
- DINGWELL, J. B., DAVIS, B. L. & FRAZIER, D. M. 1996. Use of an instrumented treadmill for real-time gait symmetry evaluation and feedback in normal and trans-tibial amputee subjects. *Prosthetics and Orthotics International*, 20, 101-110.
- DIONISIO, V. C., ALMEIDA, G. L., DUARTE, M. & HIRATA, R. P. 2008. Kinematic, kinetic and EMG patterns during downward squatting. *Journal of Electromyography and Kinesiology*, 18, 134-43.
- ELLIOTT, B., LYTTLE, A. & BIRKETT, O. 2002. The RowPerfect ergometer: a training aid for on-water single scull rowing. *Sports Biomechanics*, 1, 123-34.
- ELLISON, J. B., ROSE, S. J. & SAHRMANN, S. A. 1990. Patterns of Hip Rotation Range of Motion - a Comparison between Healthy-Subjects and Patients with Low-Back-Pain. *Physical Therapy*, 70, 537-541.
- ERICSON, M. O. & NISELL, R. 1988. Efficiency of Pedal Forces during Ergometer Cycling. *International Journal of Sports Medicine*, 9, 118-122.
- ESCAMILLA, R. F., FLEISIG, G. S., LOWRY, T. M., BARRENTINE, S. W. & ANDREWS, J. R. 2001. A three-dimensional biomechanical analysis of the squat during varying stance widths. *Medicine and Science in Sports and Exercise*, 33, 984-98.
- FARFAN, H., COSSETTE, J., ROBERTSON, G., WELLS, R. & KRAUS, H. 1970. The effects of torsion on the lumbar intervertebral joints: the role of torsion in the production of disc degeneration. *The Journal of Bone and Joint Surgery*, 52, 468.
- FERBER, R., DAVIS, I. M. & WILLIAMS, D. S. 2003. Gender differences in lower extremity mechanics during running. *Clinical Biomechanics*, 18, 350-357.
- FLANAGAN, S., SALEM, G. J., WANG, M. Y., SANKER, S. E. & GREENDALE, G. A. 2003. Squatting exercises in older adults: Kinematic and kinetic comparisons. *Medicine and Science in Sports and Exercise*, 35, 635-643.
- FLANAGAN, S. P. & SALEM, G. J. 2007. Bilateral differences in the net joint torques during the squat exercise. *Journal of Strength and Conditioning Research*, 21, 1220-6.
- FOTHERGILL, S. 2010. Examining the effect of real-time visual feedback on the quality of rowing technique. *Proceedings of the 8th Conference of the International Sports Engineering Association*.

- FRY, A. C., SMITH, J. C. & SCHILLING, B. K. 2003. Effect of knee position on hip and knee torques during the barbell squat. *Journal of Strength and Conditioning Research*, 17, 629-33.
- FUKUNAGA, T., MATSUO, A., YAMAMOTO, K. & ASAMI, T. 1986. Mechanical Efficiency in Rowing. *European Journal of Applied Physiology and Occupational Physiology*, 55, 471-475.
- GALLAGHER, S., MARRAS, W., LITSKY, A. & BURR, D. 2005. Torso flexion loads and the fatigue failure of human lumbosacral motion segments. *Spine*, 30, 2265.
- GANDER, R. E., MCCLEMENTS, J. D., SANDERSON, L. K., ROSTAD, B. A. & JOSEPHSON, K. E. 1994. Sprint Start Instrumentation. *IEEE Transactions on Instrumentation and Measurement*, 43, 637-643.
- GARHAMMER, J. & GREGOR, R. 1992. Propulsion forces as a function of intensity for weightlifting and vertical jumping. *Journal of Applied Sports Science Research*, 6, 129-134.
- GARHAMMER, J. & GREGOR, R. J. 1979. Force Plate Evaluations of Weightlifting and Vertical Jumping. *Medicine and Science in Sports and Exercise*, 11, 106-106.
- GODGES, J. J., MACRAE, P. G. & ENGELKE, K. A. 1993. Effects of Exercise on Hip Range of Motion, Trunk Muscle Performance, and Gait Economy. *Physical Therapy*, 73, 468-477.
- GORDON, S., YANG, K., MAYER, P., MACE JR, A., KISH, V. & RADIN, E. 1991. Mechanism of disc rupture: a preliminary report. *Spine*, 16, 450.
- GREENE, A. J., SINCLAIR, P. J., DICKSON, M. H., COLLOUD, F. & SMITH, R. M. 2011. The effect of ergometer design on rowing stroke mechanics. *Scand J Med Sci Sports*.
- GROOD, E. S. & SUNTAY, W. J. 1983. A joint coordinate system for the clinical description of three-dimensional motions: application to the knee. *Journal of Biomechanical Engineering*, 105, 136-144.
- HALL, M. G., FLEMING, H. E., DOLAN, M. J., MILLBANK, S. F. D. & PAUL, J. P. 1996. Static in situ calibration of force plates. *Journal of Biomechanics*, 29, 659-665.
- HALLIDAY, S. E., ZAVATSKY, A. B. & HASE, K. 2004. Can functional electric stimulation-assisted rowing reproduce a race-winning rowing stroke? *Archives of Physical Medicine and Rehabilitation*, 85, 1265-1272.
- HARDIJZER, A. 2012. *Bilateral Trunk and Lower Limb Muscle Activity during Rowing*. MRes, Imperial College, London.

- HARLAND, M. J., ANDREWS, M. H. & STEELE, J. R. 1995. Instrumented start blocks: A quantitative coaching aid. *Proceedings of the 13th International Symposium of Biomechanics in Sport*, 367-370.
- HASE, K., KAYA, M., ZAVATSKY, A. B. & HALLIDAY, S. E. 2004. Musculoskeletal loads in ergometer rowing. *Journal of Applied Biomechanics*, 20, 317-323.
- HAWKINS, D. 2000. A new instrumentation system for training rowers. *Journal of Biomechanics*, 33, 241-245.
- HERBERGER, E. 1987. Rowing/Rudern: The GDR Text of Oarsmanship Toronto: Sports Book Publisher.
- HERZOG, W., NIGG, B. M., READ, L. J. & OLSSON, E. 1989. Asymmetries in ground reaction force patterns in normal human gait. *Med Sci Sports Exerc*, 21, 110-4.
- HICKEY, G. J., FRICKER, P. A. & MCDONALD, W. A. 1997. Injuries to elite rowers over a 10-yr period. *Medicine and Science in Sports and Exercise*, 29, 1567-1572.
- HIGHSMITH, M. J., KAHLE, J. T., CAREY, S. L., LURA, D. J., DUBEY, R. V., CSAVINA, K. R. & QUILLEN, W. S. 2011. Kinetic asymmetry in transfemoral amputees while performing sit to stand and stand to sit movements. *Gait & Posture*, 34, 86-91.
- HISLOP, S. 2008. *Is ergometer rowing symmetrical? A focus on the legs*. MSc, Imperial College London.
- HOFMIJSTER, M. J., SOEST, A. J. & VAN KONING, J. J. D. 2008. Rowing skill affects power loss on a modified rowing ergometer. *Medicine and science in Sport and Exercise*, 40, 1101-1110.
- HOFMIJSTER, M. J., VAN SOEST, A. J. & DE KONING, J. J. 2009. Gross Efficiency during Rowing Is Not Affected by Stroke Rate. *Medicine and Science in Sports and Exercise*, 41, 1088-1095.
- HOLT, P. J., BULL, A. M., CASHMAN, P. M. & MCGREGOR, A. H. 2003. Kinematics of spinal motion during prolonged rowing. *International Journal of Sports Medicine*, 24, 597-602.
- HUMPHREYS, S. C. & ECK, J. C. 1999. Clinical evaluation and treatment options for herniated lumbar disc. *Am Fam Physician*, 59, 575-582.
- HUNTER, J. P., MARSHALL, R. N. & MCNAIR, P. 2004. Reliability of biomechanical variables of sprint running. *Medicine and Science in Sports and Exercise*, 36, 850-861.
- HUNTER, J. P., MARSHALL, R. N. & MCNAIR, P. 2005. Relationships between ground reaction force impulse and kinematics of sprint-running acceleration. *Journal of Applied Biomechanics*, 21, 31-43.

- HWANG, S., KIM, Y. & KIM, Y. 2009. Lower extremity joint kinetics and lumbar curvature during squat and stoop lifting. *Bmc Musculoskeletal Disorders*, 10.
- INGHAM, S. A., WHYTE, G. P., JONES, K. & NEVILL, A. M. 2002. Determinants of 2,000 m rowing ergometer performance in elite rowers. *European Journal of Applied Physiology*, 88, 243-246.
- JACOBS, C., UHL, T. L., SEELEY, M., STERLING, W. & GOODRICH, L. 2005. Strength and fatigability of the dominant and nondominant hip abductors. *Journal of Athletic Training*, 40, 203-206.
- JANSHEN, L., MATTES, K. & TIDOW, G. 2009. Muscular Coordination of the Lower Extremities of Oarsmen During Ergometer Rowing. *Journal of Applied Biomechanics*, 25, 156-164.
- JONES, C. & MILLER, C. 2002. *The mechanics and biomechanics of rowing*. [Online]. Available: <http://www.yorkshirerowing.co.uk/Files/Coaching%20+%20Training/Rowing%20Mechanics%20+%20Biomechanics.pdf> [Accessed].
- KADABA, M. P., RAMAKRISHNAN, H. K., WOOTTEN, M. E., GAINEY, J., GORTON, G. & COCHRAN, G. V. 1989. Repeatability of kinematic, kinetic, and electromyographic data in normal adult gait. *Journal of Orthopaedic Research*, 7, 849-60.
- KAEHLER, B. 2011. *Coach Kaehler: Ease Into The Catch*. [Online]. Available: <http://www.row2k.com/columns/index.cfm?action=read&ID=520&site=features> [Accessed 20/11/12].
- KARLSON, K. A. 2000. Rowing injuries: identifying and treating musculoskeletal and nonmusculoskeletal conditions. *Phys Sportsmed*, 28, 40-50.
- KIM, C. M. & ENG, J. J. 2003. Symmetry in vertical ground reaction force is accompanied by symmetry in temporal but not distance variables of gait in persons with stroke. *Gait & Posture*, 18, 23-28.
- KINGMA, I., AALBERSBERG, S. & VAN DIEEN, J. H. 2004. Are hamstrings activated to counteract shear forces during isometric knee extension efforts in healthy subjects? *Journal of Electromyography and Kinesiology*, 14, 307-15.
- KINGMA, I., VAN DIEEN, J. H., DE LOOZE, M., TOUSSAINT, H. M., DOLAN, P. & BATEN, C. T. M. 1998. Asymmetric low back loading in asymmetric lifting movements is not prevented by pelvic twist. *Journal of Biomechanics*, 31, 527-534.
- KOLLIAS, I., PANOUTSAKOPOULOS, V. & PAPAIAKOVOU, G. 2004. Comparing jumping ability among athletes of various sports: Vertical drop jumping from 60 centimeters. *Journal of Strength and Conditioning Research*, 18, 546-550.
- KOUTEDAKIS, Y., FRISCHKNECHT, R. & MURTHY, M. 1997. Knee flexion to extension peak torque ratios and low-back injuries in highly active individuals. *International Journal of Sports Medicine*, 18, 290-295.



- KOWALK, D. L., DUNCAN, J. A. & VAUGHAN, C. L. 1996. Abduction-adduction moments at the knee during stair ascent and descent. *Journal of Biomechanics*, 29, 383-388.
- KRUMM, D., SIMNACHER, M., RAUTER, G., BRUNSCHWEILER, A., ODENWALD, S., RIENER, R. & WOLF, P. 2010. High-Fidelity Device for Online Recording of Foot-Stretcher Forces During Rowing. *Proceedings of the 8th Conference of the International Sports Engineering Association*. 2721–2726.
- KUNTZE, G., SELLERS, W. I. & MANSFIELD, N. J. 2009. Bilateral ground reaction forces and joint moments for lateral sidestepping and crossover stepping tasks. *Journal of Sports Science and Medicine*, 8, 1-8.
- LAMB, D. H. 1989. Dynamic modeling of ergometer and on water rowing. *American Journal of Sports Medicine*, 17, 367-373.
- LIU, H., LEIGH, S. & YU, B. 2010. Sequences of upper and lower extremity motions in javelin throwing. *Journal of Sports Sciences*, 28, 1459-1467.
- LOH, J. H. H., BULL, A. M. J., MCGREGOR, A. H. & SCHROTER, R. C. Year. Instrumentation of a Concept II rowing ergometer for kinetic & kinematic data acquisition. *In: The Engineering of Sport 5*, 2004. Sheffield, 173-179.
- LUND, T., NYDEGGER, T., SCHLENZKA, D. & OXLAND, T. R. 2002. Three-dimensional motion patterns during active bending in patients with chronic low back pain. *Spine*, 27, 1865-74.
- MACFARLANE, D. J., EDMOND, I. M. & WALMSLEY, A. 1997. Instrumentation of an ergometer to monitor the reliability of rowing performance. *Journal of Sports Sciences*, 15, 167-73.
- MACKENZIE, H. A. M., BULL, A. M. J. & MCGREGOR, A. H. 2008. Changes in rowing technique over a routine one hour low intensity high volume training session. *Journal of Sports Science and Medicine*, 7, 486-491.
- MALINZAK, R. A., COLBY, S. M., KIRKENDALL, D. T., YU, B. & GARRETT, W. E. 2001. A comparison of knee joint motion patterns between men and women in selected athletic tasks. *Clinical Biomechanics*, 16, 438-45.
- MARRAS, W. S., FERGUSON, S. A., BURR, D., DAVIS, K. G. & GUPTA, P. 2004. Spine loading in patients with low back pain during asymmetric lifting exertions. *The Spine Journal*, 4, 64-75.
- MATTES, S. J., MARTIN, P. E. & ROYER, T. D. 2000. Walking symmetry and energy cost in persons with unilateral transtibial amputations: Matching prosthetic and intact limb inertial properties. *Archives of Physical Medicine and Rehabilitation*, 81, 561-568.
- MCARTHUR, J. 1997. *High Performance Rowing*, Marlborough., The Crowood Press Ltd.

- MCCRORY, J. L., WHITE, S. C. & LIFESO, R. M. 2001. Vertical ground reaction forces: objective measures of gait following hip arthroplasty. *Gait & Posture*, 14, 104-109.
- MCGILL, S. M. 1995. The Mechanics of Torso Flexion - Situps and Standing Dynamic Flexion Maneuvers. *Clinical Biomechanics*, 10, 184-192.
- MCGILL, S. M. 1998. Low back exercises: evidence for improving exercise regimens. *Physical Therapy*, 78, 754-65.
- MCGILL, S. M. & KIPPERS, V. 1994. Transfer of Loads between Lumbar Tissues during the Flexion-Relaxation Phenomenon. *Spine*, 19, 2190-2196.
- MCGREGOR, A. H., BULL, A. M. J. & BYNG-MADDICK, R. 2004. A comparison of rowing technique at different stroke rates: A description of sequencing, force production and kinematics. *International Journal of Sports Medicine*, 25, 465-470.
- MCGREGOR, A. H., PATANKAR, Z. S. & BULL, A. M. J. 2005. Spinal kinematics in elite oarswomen during a routine physiological "step test". *Medicine and Science in Sports and Exercise*, 37, 1014-1020.
- MCGREGOR, A. H., PATANKAR, Z. S. & BULL, A. M. J. 2007. Longitudinal changes in the spinal kinematics of oarswomen during step testing. *Journal of Sports Science and Medicine*, 6, 29-35.
- MCGREGOR, A. H., PATANKAR, Z. S. & BULL, A. M. J. 2008. Do men and women row differently? A spinal kinematic and force perspective. *Proceedings of the Institution of Mechanical Engineers Part P-Journal of Sports Engineering and Technology*, 222, 77-83.
- MCNEELY, E. & ROYLE, M. 2002. *Skillful Rowing*, UK, Meyer & Meyer Sport.
- MERO, A., KOMI, P. V., KORJUS, T., NAVARRO, E. & GREGOR, R. J. 1994. Body Segment Contributions to Javelin Throwing during Final Thrust Phases. *Journal of Applied Biomechanics*, 10, 166-177.
- MILNER, C. 2010. Joints of the Lumbar spine and Pelvic. In: BARTLETT, R., GRATTON, C. & ROLF, C. G. (eds.) *Encyclopedia of Internatinal Sports Studies*. Nw York: Routledge.
- MORIN, J. B., EDOUARD, P. & SAMOZINO, P. 2011. Technical Ability of Force Application as a Determinant Factor of Sprint Performance. *Medicine and Science in Sports and Exercise*, 43, 1680-1688.
- MORRIS, F. L., SMITH, R. M., PAYNE, W. R., GALLOWAY, M. A. & WARK, J. D. 2000. Compressive and shear force generated in the lumbar spine of female rowers. *International Journal of Sports Medicine*, 21, 518-523.
- MULLINEAUX, D. R., UNDERWOOD, S. M., SHAPIRO, R. & HALL, J. W. 2012. Real-time biomechanical biofeedback effects on top-level rifle shooters. *Applied Ergonomics*, 43, 109-14.

- MUNRO, C. & YANAI, T. 2000. Forces on the lower back during rowing performance in a single scull. *Proceedings of the 18th International Symposium of Biomechanics in Sports*. 186-189.
- MUNRO, C. F., MILLER, D. I. & FUGLEVAND, A. J. 1987. Ground Reaction Forces in Running - a Reexamination. *Journal of Biomechanics*, 20, 147-155.
- MURPHY, A. J. 2009. *Elite Rowing: Technique and Performance*. PhD, Imperial College London.
- MURPHY, A. J., BULL, A. M. J. & MCGREGOR, A. H. 2011. Optimizing and validating an electromagnetic tracker in a human performance laboratory. *Proceedings of the Institution of Mechanical Engineers Part H-Journal of Engineering in Medicine*, 225, 343-351.
- MURPHY, A. J., CHEE, S. T. H., BULL, A. M. J. & MCGREGOR, A. H. 2010. The calibration and application of a force-measuring apparatus on the seat of a rowing ergometer. *Proceedings of the Institution of Mechanical Engineers Part P-Journal of Sports Engineering and Technology*, 224, 109-116.
- NADLER, S. F., MALANGA, G. A., BARTOLI, L. A., FEINBERG, J. H., PRYBICIEN, M. & DEPRINCE, M. 2002. Hip muscle imbalance and low back pain in athletes: influence of core strengthening. *Medicine and Science in Sports and Exercise*, 34, 9-16.
- NAGANO, A., GERRITSEN, K. G. & FUKASHIRO, S. 2000. A sensitivity analysis of the calculation of mechanical output through inverse dynamics: a computer simulation study. *Journal of Biomechanics*, 33, 1313-8.
- NOLAN, L., WIT, A., DUDZINSKI, K., LEES, A., LAKE, M. & WYCHOWANSKI, M. 2003. Adjustments in gait symmetry with walking speed in trans-femoral and trans-tibial amputees. *Gait & Posture*, 17, 142-151.
- NOLTE, V. 2004. *Rowing Faster*, Champaign, IL, Human Kinetics.
- NORMAN, R., WELLS, R., NEUMANN, P., FRANK, J., SHANNON, H. & KERR, M. 1998. A comparison of peak vs cumulative physical work exposure risk factors for the reporting of low back pain in the automotive industry. *Clinical Biomechanics*, 13, 561-573.
- NOWICKY, A. V., BURDETT, R. & HORNE, S. 2005. The impact of ergometer design on hip and trunk muscle activity patterns in elite rowers: An electromyographic assessment. *Journal of Sports Science and Medicine*, 4, 18-28.
- ODDSSON, L. I. E. & DE LUCA, C. J. 2003. Activation imbalances in lumbar spine muscles in the presence of chronic low back pain. *Journal of Applied Physiology*, 94, 1410-1420.
- OKEN, O. F., OKEN, O., YILDIRIM, A. O., YAVUZER, G., GULCEK, M., UNAL, V. S. & UCANER, A. 2010. Gait symmetry in patients with unilateral partial hip

- arthroplasty. *Eklemler Hastalıkları Ve Cerrahisi-Joint Diseases and Related Surgery*, 21, 86-90.
- OZGUVEN, H. N. & BERME, N. 1988. An Experimental and Analytical Study of Impact Forces during Human Jumping. *Journal of Biomechanics*, 21, 1061-1066.
- PAGE, P. & HAWKINS, D. 2003. A real-time biomechanical feedback system for training rowers. *Sports Engineering*, 6, 67-79.
- PAIN, M. T. G. & HIBBS, A. 2007. Sprint starts and the minimum auditory reaction time. *Journal of Sports Sciences*, 25, 79-86.
- PANJKOTA, A., STANCIC, I. & SUPUK, T. 2009. Outline of a Qualitative Analysis for the Human Motion in Case of Ergometer Rowing. *Proceedings of the 9th Wseas International Conference on Simulation, Modelling and Optimization*. 182-186.
- PARKIN, S., NOWICKY, A. V., RUTHERFORD, O. M. & MCGREGOR, A. H. 2001. Do oarsmen have asymmetries in the strength of their back and leg muscles? *Journal of Sports Sciences*, 19, 521-526.
- PARKINSON, R. & CALLAGHAN, J. 2007a. Can periods of static loading be used to enhance the resistance of the spine to cumulative compression? *Journal of Biomechanics*, 40, 2944-2952.
- PARKINSON, R. & CALLAGHAN, J. 2007b. The role of load magnitude as a modifier of the cumulative load tolerance of porcine cervical spinal units: progress towards a force weighting approach. *Theoretical Issues in Ergonomics Science*, 8, 171-184.
- PFIRRMANN, C. W. A., MENGIARDI, B., DORA, C., KALBERER, F., ZANETTI, M. & HODLER, J. 2006. Cam and pincer femoroacetabular impingement: Characteristic MR arthrographic findings in 50 patients. *Radiology*, 240, 778-785.
- PLAMONDON, A., GAGNON, M. & GRAVEL, D. 1995. Moments at the L(5)/S-1 Joint during Asymmetrical Lifting - Effects of Different Load Trajectories and Initial Load Positions. *Clinical Biomechanics*, 10, 128-136.
- POLLARD, C. D., SIGWARD, S. M. & POWERS, C. M. 2007. Gender differences in hip joint kinematics and kinetics during side-step cutting maneuver. *Clinical Journal of Sports Medicine*, 17, 38-42.
- POLLOCK, C. L., JENKYN, T. R., JONES, I. C., IVANOVA, T. D. & GARLAND, S. J. 2009. Electromyography and Kinematics of the Trunk during Rowing in Elite Female Rowers. *Medicine and Science in Sports and Exercise*, 41, 628-636.
- POTVIN, J. R., NORMAN, R. W., ECKENRATH, M. E., MCGILL, S. M. & BENNETT, G. W. 1992. Regression-Models for the Prediction of Dynamic L4/L5 Compression Forces during Lifting. *Ergonomics*, 35, 187-201.

- PUDLO, P., PINTI, A. & LEPOUTRE, F. X. 2005. Experimental laboratory apparatus to analyze kinematics and 3D kinetics in rowing. *Sports Engineering*, 8, 39-46.
- REID, D. & MCNAIR, P. 2000. Factors contributing to low back pain in rowers. *British Medical Journal*, 34, 321.
- REISER, R. F., PETERSON, M. L. & BROKER, J. P. 2003. Instrumented bicycle pedals for dynamic measurement of propulsive cycling loads. *Sports Engineering*, 6, 41-48.
- RHEAULT, W., MILLER, M., NOTHNAGEL, P., STRAESSLE, J. & URBAN, D. 1988. Intertester Reliability and Concurrent Validity of Fluid-Based and Universal Goniometers for Active Knee Flexion. *Physical Therapy*, 68, 1676-1678.
- RIEMER, R. & HSIAO-WECKSLER, E. T. 2008. Improving joint torque calculations: optimization-based inverse dynamics to reduce the effect of motion errors. *Journal of Biomechanics*, 41, 1503-9.
- RIEMER, R., HSIAO-WECKSLER, E. T. & ZHANG, X. 2008. Uncertainties in inverse dynamics solutions: a comprehensive analysis and an application to gait. *Gait & Posture*, 27, 578-88.
- RITCHIE, A. C. 2008. Dynamic modeling of ergometer and on-water rowing. *Sports Technology*, 1, 110-116.
- ROBERTS, T. J. & SCALES, J. A. 2002. Mechanical power output during running accelerations in wild turkeys. *Journal of Experimental Biology*, 205, 1485-1494.
- ROBERTSON, D. G. & WINTER, D. A. 1980. Mechanical energy generation, absorption and transfer amongst segments during walking. *Journal of Biomechanics*, 13, 845-54.
- ROBERTSON, D. G. E. 2004. *Research methods in biomechanics*, Champaign, IL, Human Kinetics.
- ROBINSON, R. O., HERZOG, W. & NIGG, B. M. 1987. Use of Force Platform Variables to Quantify the Effects of Chiropractic Manipulation on Gait Symmetry. *Journal of manipulative and physiological therapeutics*, 10, 172-176.
- RODGERS, M. M. 1988. Dynamic biomechanics of the normal foot and ankle during walking and running. *Physical Therapy*, 68, 1822-30.
- RUMBALL, J. S., LEBRUN, C. M., DI CIACCA, S. R. & ORLANDO, K. 2005. Rowing injuries. *Sports Medicine*, 35, 537-555.
- SALEM, G. J., SALINAS, R. & HARDING, F. V. 2003. Bilateral kinematic and kinetic analysis of the squat exercise after anterior cruciate ligament reconstruction. *Archives of Physical Medicine and Rehabilitation*, 84, 1211-6.

- SCHACHE, A. G., BLANCH, P. D. & MURPHY, A. T. 2000. Relation of anterior pelvic tilt during running to clinical and kinematic measures of hip extension. *British Journal of Sports Medicine*, 34, 279–283.
- SEEGMILLER, J. G. & MCCAWE, S. T. 2003. Ground reaction forces among gymnasts and recreational athletes in drop landings. *Journal of Athletic Training*, 38, 311-314.
- SEELEY, M. K., UMBERGER, B. R., CLASEY, J. L. & SHAPIRO, R. 2010. The relation between mild leg-length inequality and able-bodied gait asymmetry. *Journal of Sports Science and Medicine*, 9, 572-579.
- SHIMOKOCHI, Y. & SCHULTZ, S. J. 2008. Mechanisms of Noncontact Anterior Cruciate Ligament Injury. *Journal of Athletic Training*, 43, 396-408.
- SMITH, H. K. 2000. Ergometer sprint performance and recovery with variations in training load in elite rowers. *International Journal of Sports Medicine*, 21, 573-578.
- SMITH, R. M. & LOSCHNER, C. 2002. Biomechanics feedback for rowing. *Journal of Sports Sciences*, 20, 783-791.
- SMOLJANOVIC, T., BOJANIC, I., HANNAFIN, J. A., HREN, D., DELIMAR, D. & PECINA, M. 2009. Traumatic and Overuse Injuries Among International Elite Junior Rowers. *American Journal of Sports Medicine*, 37, 1193-1199.
- SOPER, C. & HUME, P. 2005. Ergometer rowing performance improves over 2000 m when using a steeper foot stretcher angle. *23rd International Symposium on Biomechanics in Sports*. 326-329.
- SOPER, C. & HUME, P. A. 2004. Towards an ideal rowing technique for performance - The contributions from biomechanics. *Sports Medicine*, 34, 825-848.
- SØRENSEN, H., ZACHO, M., SIMONSEN, E. B., DYHRE-POULSEN, P. & LKLAUSEN, K. 1996. Dynamics of the martial arts high front kick. *Journal of Sports Sciences*, 14, 483.
- STACOFF, A., KRAMERS-DE QUERVAIN, I. A., LUDER, G., LIST, R. & STUSSI, E. 2007. Ground reaction forces on stairs - Part II: Knee implant patients versus normals. *Gait & Posture*, 26, 48-58.
- STALLARD, M. C. 1980. Backache in oarsmen. *British Journal of Sports Medicine*, 14, 105-8.
- STEER, R. R., MCGREGOR, A. H. & BULL, A. M. J. 2006. A comparison of kinematics and performance measures of two rowing ergometers. *Journal of Sports Science and Medicine*, 5, 52-59.
- STRAHAN, A. D., BURNETT, A. F., CANEIRO, J. P., DOYLE, M. M., O'SULLIVAN, P. B. & GOODMAN, C. 2011. Differences in Spinopelvic Kinematics in Sweep and Scull Ergometer Rowing. *Clinical Journal of Sport Medicine*, 21, 330-336.

- TEITZ, C. C., O' KANE, J., LIND, B. K. & HANNAFIN, J. A. 2002. Back pain in intercollegiate rowers. *American Journal of Sports Medicine*, 30, 674-679.
- THOMPSON, P. 2005. *Sculling. Training, technique and performance.*, Marlborough., The Crowood Press Ltd.,
- THOMPSON, P. 2010. *RE: Athlete Review Meeting.*
- TORRES-MORENO, R., TANAKA, C. & PENNEY, K. L. 2000. Joint excursion, handle velocity, and applied force: a biomechanical analysis of ergonomic rowing. *International Journal of Sports Medicine*, 21, 41-44.
- VAN SOEST, A. J. & HOFMIJSTER, M. 2009. Strapping rowers to their sliding seat improves performance during the start of ergometer rowing. *Journal of Sports Sciences*, 27, 283-289.
- VAVERKA, F., VODICKOVA, S. & ELFMARK, M. 2012. Kinetic analysis of ski turns based on measured ground reaction forces. *Journal of Applied Biomechanics*, 28, 41-7.
- WALKER, M. L., ROTHSTEIN, J. M., FINUCANE, S. D. & LAMB, R. L. 1987. Relationships between Lumbar Lordosis, Pelvic Tilt, and Abdominal Muscle Performance. *Physical Therapy*, 67, 512-516.
- WALSH, M. S., FORD, K. R., BANGEN, K. J., MYER, G. D. & HEWETT, T. E. 2006. The validation of a portable force plate for measuring force-time data during jumping and landing tasks. *Journal of Strength and Conditioning Research*, 20, 730-4.
- WEIGHTMAN, D. & BROWNE, R. C. 1975. Injuries in Eleven Selected Sports. *British Journal of Sports Medicine*, 9, 136-141.
- WEINERT-APLIN, R. 2011. *How do the biomechanics of the foot and ankle impact on rowing performance?* MPhil, Imperial College London.
- WHEELER, J. B., GREGOR, R. J. & BROKER, J. P. 1992. A Dual Piezoelectric Bicycle Pedal with Multiple Shoe Pedal Interface Compatibility. *International Journal of Sport Biomechanics*, 8, 251-258.
- WHITTLESEY, S. N. & ROBERTSON, D. G. E. 2004. Two Dimensional Inverse Dynamics. In: D.G.E., R., CALDWELL, G. E., HAMILL, J., KAMEN, G. & WHITTLESEY, S. N. (eds.) *Research Methods in Biomechanics*. Champaign; Illinois: Human Kinetics.
- WILSON, F., GISSANE, C., GORMLEY, J. & SIMMS, C. 2010. A 12-month prospective cohort study of injury in international rowers. *British Journal of Sports Medicine*, 44, 207-214.
- WINTER, D. A. 1990. *Biomechanics and Motor Control of Human Movement. 2nd ed.*, New York, Chichester: Wiley.

- WOOTTEN, D. & HULL, M. L. 1992. Design and Evaluation of a Multi-Degree-of-Freedom Foot Pedal Interface for Cycling. *International Journal of Sport Biomechanics*, 8, 152-164.
- ZATSIORSKY, V. M., SELUYANOV, V. N. & CHUGUNOVA, L. G. 1990. Methods of determining mass-inertial characteristics of human body segments. In: CHERNYI, G. G. & REGIRER, S. A. (eds.) *Contemporary Problems of Biomechanics*. USA: CRC Press.
- ZHAO, C. G., HE, X. J., LU, B., LI, H. P., WANG, D. & ZHU, Z. Z. 2009. Classification of gluteal muscle contracture in children and outcome of different treatments. *Bmc Musculoskeletal Disorders*, 10.
- ZIFCHOCK, R. A., DAVIS, I. & HAMILL, J. 2006. Kinetic asymmetry in female runners with and without retrospective tibial stress fractures. *Journal of Biomechanics*, 39, 2792-2797.



# **Appendix A:**

## **Model Sensitivity Analysis**

---

Table showing joint angles (in degrees) outputted from the 3D kinematic model (shaded grey), with '+ error' and '- error' representing output values derived when extreme sensor errors are added and subtracted from the raw sensor measurements.

	Catch			MHF			Finish		
	Alpha	Beta	Gamma	Alpha	Beta	Gamma	Alpha	Beta	Gamma
LSJ - error	-12.5	97.4	-3.8	-10.1	96.4	-5.8	-3.4	94.6	-8.1
LSJ	-12.8	95.9	-3.7	-10.2	95.0	-5.7	-3.4	93.9	-8.1
LSJ + error	-12.9	94.3	-3.5	-10.3	93.7	-5.6	-3.4	93.1	-8.1
HJC - error	-140.9	74.5	3.8	-109.5	89.9	-17.6	-33.0	108.7	2.4
HJC	-141.5	74.3	3.8	-114.0	88.7	-15.2	-37.9	106.6	1.6
HJC + error	-142.4	74.0	3.8	-118.2	87.9	-12.7	-42.9	104.5	1.1
KJC - error	137.0	-	-	72.5	-	-	-5.3	-	-
KJC	137.8	-	-	76.8	-	-	-0.9	-	-
KJC + error	138.8	-	-	80.8	-	-	3.8	-	-
AJC - error	81.5	74.5	-9.4	152.2	96.5	-14.1	-156.0	101.8	0.6
AJC	76.0	78.7	-4.0	148.8	95.7	-6.1	-163.4	98.1	7.6
AJC + error	69.0	83.5	0.7	142.8	95.7	1.5	-168.5	97.3	15.0

Table showing the difference in joint angles from the measured outputs, when maximum sensor measurement errors are taken into account.

	Catch			MHF			Finish		
	Alpha	Beta	Gamma	Alpha	Beta	Gamma	Alpha	Beta	Gamma
LSJ - error	-0.3	-1.5	0.1	-0.1	-1.4	0.1	0.0	-0.7	0.0
LSJ	0.0	0.0	0.0	0.0	0.0	0.0	0.0	0.0	0.0
LSJ + error	0.1	1.6	-0.2	0.1	1.3	-0.1	0.0	0.8	0.0
HJC - error	0.6	0.2	0.0	4.5	1.2	-2.4	4.9	2.1	0.8
HJC	0.0	0.0	0.0	0.0	0.0	0.0	0.0	0.0	0.0
HJC + error	-0.9	-0.3	0.0	-4.2	-0.8	2.5	-5.0	-2.1	-0.5
KJC - error	-0.8	-	-	-4.3	-	-	-4.4	-	-
KJC	0.0	-	-	0.0	-	-	0.0	-	-
KJC + error	1.0	-	-	4.0	-	-	4.7	-	-
AJC - error	5.5	-4.2	-5.4	3.4	0.8	-8.0	7.4	3.7	-7.0
AJC	0.0	0.0	0.0	0.0	0.0	0.0	0.0	0.0	0.0
AJC + error	-7.0	4.8	4.7	-6.0	0.0	7.6	-5.1	-0.8	7.4

The results of the sensitivity analysis show that when the input parameters to the model are modified to incorporate the extreme ranges of error possible at each sensor, the ankle joint was most sensitive to these changes.

- Ankle joint errors were up to  $8.0^\circ$  of the measured output in the transverse plane at MHF.
- Knee and hip angles were not sensitive at the catch position, but demonstrated output errors of less than  $\pm 5^\circ$  at MHF and Finish in the sagittal plane at these positions.
- Lumbar-pelvic joint was least sensitive to modifications in the input parameters for all three planes of motion.

Based on the model sensitivity, it is recommended that ankle angle outputs should be interpreted with caution. However, the key feature of this model i.e. the lumbar-pelvic joint, is a robust kinematic measure and demonstrated minimal error ( $<0.5^\circ$  in sagittal plane) when modifying input parameters.

# **Appendix B:**

## **Ethics**

---

## CONSENT FORM

### Kinetic and kinematic analysis of the lumbar spine and lower extremities during rowing

Name of Researcher:

*Please  
initial box*

1. I confirm that I have read and understood the information sheet dated March 2012 for the above study. I have had the opportunity to consider the information, ask questions and have had these answered satisfactorily.
2. I understand that my participation is voluntary and that I am free to withdraw at any time, without giving any reason, and without legal rights being affected.
3. I agree to my coach being informed of my participation in the study and having access to the results. This is in accordance with British International Rowing standard athlete coach disclosure agreement
4. I agree to take part in the above study.

\_\_\_\_\_  
Name of participant

\_\_\_\_\_  
Date

\_\_\_\_\_  
Signature

\_\_\_\_\_  
Name of person taking consent  
(if different from researcher)

\_\_\_\_\_  
Date

\_\_\_\_\_  
Signature

\_\_\_\_\_  
Researcher

\_\_\_\_\_  
Date

\_\_\_\_\_  
Signature

**Chief Investigator: Professor Alison McGregor**

**Co-Investigator(s): Erica Buckeridge, Robert Weinert-Aplin**

### **Information Sheet (version 2 05/9/11)**

#### **Analysis of the lumbar spine and lower extremities during rowing**

This sheet describes the purpose of the study, and explains what is involved. Please read the information below before deciding whether or not you would like to take part.

#### **Purpose of Research**

To date the impact of the way the body moves during rowing and its effect on performance and injury has been limited. We believe that the way the body moves during rowing is important and that this can be used to enhance performance and at the same time it may help us to understand why rowers frequently experience back problems. This study plans to build on existing knowledge which has focused on forward and backwards motions of the body and to investigate technique in terms of out of plane motion (rotations and side bends) and force generation symmetry (symmetric drive through seat and footplates). We propose that through an in-depth understanding of rowing technique we can find novel ways to enhance performance and prevent injury.

#### **What does it involve?**

A rowing test is performed on the rowing machine in the Biodynamics Lab at Charing Cross Hospital. Additionally, you will also be required to have four motion sensors fixed to you at different points on your back and leg, using non allergenic adhesives. To be able to perform the optical motion tracking, reflective markers will be attached using double-sided tape to your pelvis, thigh, calf and feet (on your shoes, over the respective landmarks of the foot).

#### **Do I have to take part?**

No, it is entirely up to you. If you would like to take part and have these additional measures performed, you will be asked to sign a consent form. Even after you have signed this consent form and agreed to the study, you are free to withdraw from the study at any time.

**Are there any risks or benefits?**

The assessment techniques are entirely safe and non-invasive and there are no known risks from having these test performed. All tests will be performed within your own limits.

**Confidentiality**

Any information you give us will be kept confidential. If the study is published in a book or scientific journal, no individual will be identified in any way.

**Further Information**

If you are unsure about this study and would like to consider further before you make your decision, please take your time to do so. Please contact Erica Buckeridge ([e.buckeridge09@imperial.ac.uk](mailto:e.buckeridge09@imperial.ac.uk)) or Robert Weinert-Aplin ([rob.aplin06@imperial.ac.uk](mailto:rob.aplin06@imperial.ac.uk)) for further information.

## **Rowing Biomechanics – Testing protocol**

### **AIM:**

The aim of this study will be to assess club and elite rowers' performance kinetics and kinematics in relation to performance parameters and injury risks.

### **METHODOLOGY:**

All rowers will be instrumented with electro-magnetic sensors and/or optical markers and asked to perform a physiological step test (see Protocol) on an ergometer which has been instrumented at the handle, seat, foot-stretchers and flywheel.

#### ***Instrumented ergometer and Motion analysis***

An electromagnetic system, the Flock of Birds™ (Ascension Technology, Vermont, USA) and/or an optical motion tracking system (Vicon) will be used to assess the kinematics of the lumbopelvic region of the spine and the lower extremities.

Flock of Birds™ quantifies the motion of sensors (which can be aligned to body segments) in an electromagnetic field in terms of rotations about and translations along an electromagnetic transmitter axis, and has been shown to have acceptable accuracy. The receivers of the system are attached to the skin at the thoraco-lumbar junction (T12) (to measure anterior-posterior lumbar rotation, more specifically back flexion and extension), the lumbo-sacral junction (S1) (to measure anterior-posterior sacral rotation i.e. pelvic tilt), 10 cm proximal to the lateral epicondyle of the right femur (to measure anterior-posterior femoral rotation i.e. thigh flexion-extension), and on the lower third of the anterior aspect of the tibia.

In addition to the electromagnetic system (Flock of Birds™), motion capture will be performed using a Vicon MX optical motion tracking system (Vicon Motion Systems Ltd, Oxford, UK), which uses small retro-reflective markers attached to the body using adhesive to track body segment motion in space. The use of optical tracking will provide data which can be reconstructed in a 3D model of the lower limb (pelvis, thigh, calf and foot) to determine the position and orientation of the body segments.

The motion capture systems will be synchronised with the instrumented ergometer which has load cells at the handle, seat and footplates. Using this configuration, athletes will undergo the physiological step test outlines in the following section.



**EXPERIMENTAL PROTOCOL:**

Baseline characteristics including age, height and weight will be recorded on all subjects.

Electro-magnetic sensors and retro-reflective markers will be attached to body segments and bony landmarks respectively, as stated 'Instrumented ergometer and motion analysis'.

Rowers will be required to perform the physiological Step Test on the instrumented rowing machine. The step test requires the rower to perform the following steps:

- (i) 3 mins rowing at 18 strokes per minute (i.e. effort corresponding to 55% of their 2 km personal best time)
- (ii) 3 mins rowing at 24 strokes per minute
- (iii) 3 mins rowing at 28 strokes per minute
- (iv) 3 mins rowing at Free rate (i.e. effort corresponding to 100% of their 2 km personal best time)

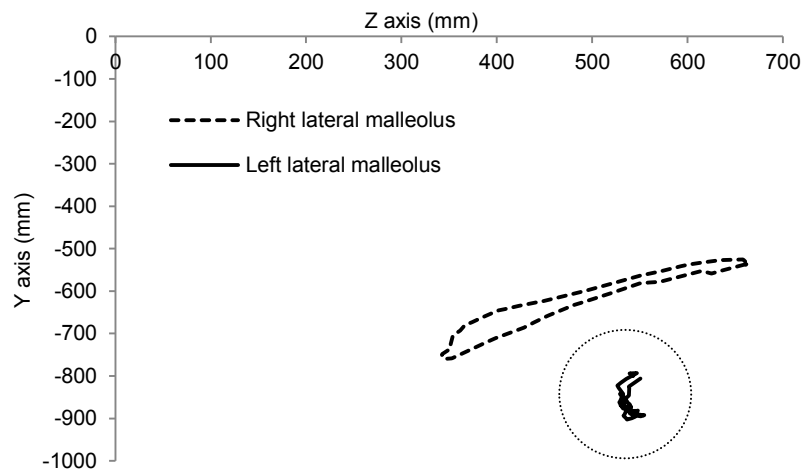
# **Appendix C:**

## **Bilateral bony landmark digitization**

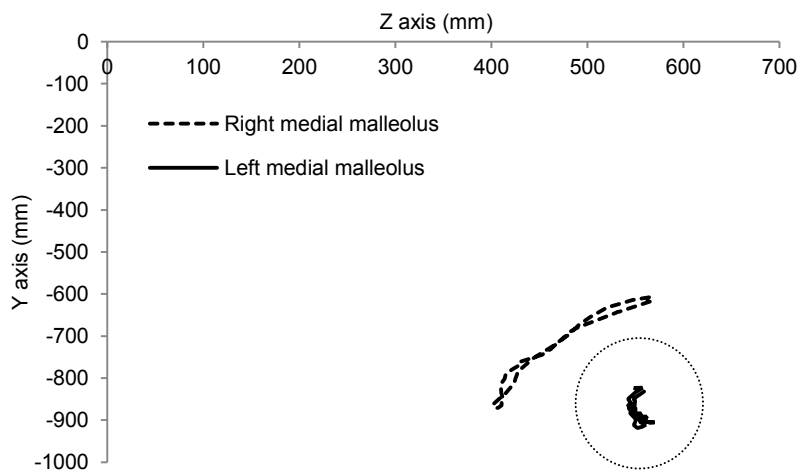
---

In Chapter 3, it was evident that there was a problem digitizing the medial and lateral malleolus on the left ankle when the adapted bilateral FOB motion capture set-up was employed.

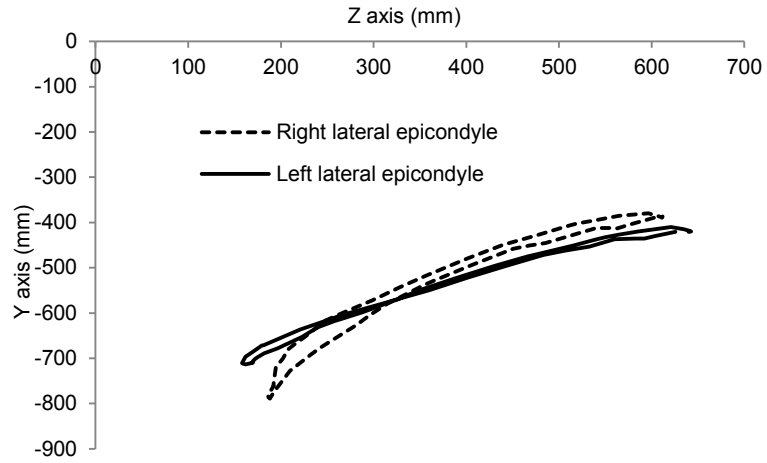
This problem can be seen in the graphs below where the trajectories of the left lateral malleolus and left medial malleolus (circled) during a single rowing stroke do not follow the trajectory of the right side. Whereas, the medial and lateral epicondyles, and HJC are follow a bilaterally similar trajectory (where deviations in symmetry likely arose from actual asymmetries and some measurement and digitisation errors).



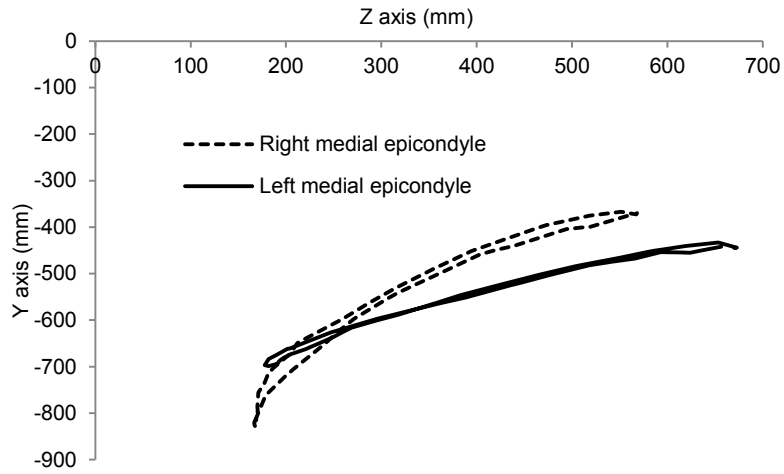
**Bilateral lateral malleolus trajectories during a single rowing stroke**



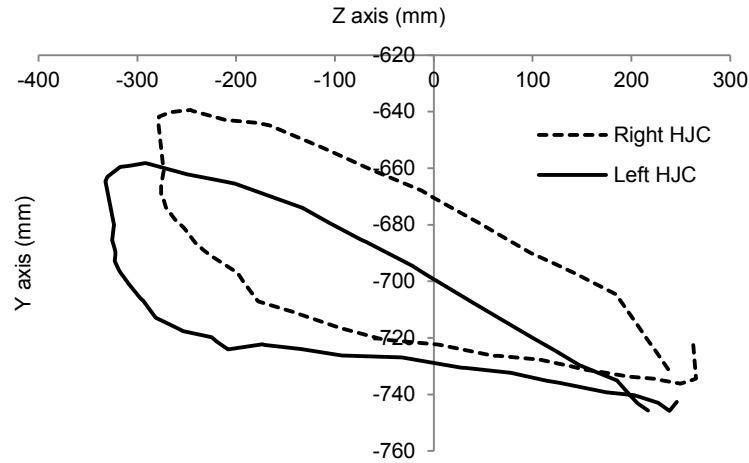
**Bilateral medial malleolus trajectories during a single rowing stroke**



**Bilateral lateral epicondyle trajectories during a single rowing stroke**



**Bilateral medial epicondyle trajectories during a single rowing stroke**



**Bilateral functionally determined HJC trajectories during a single rowing stroke**

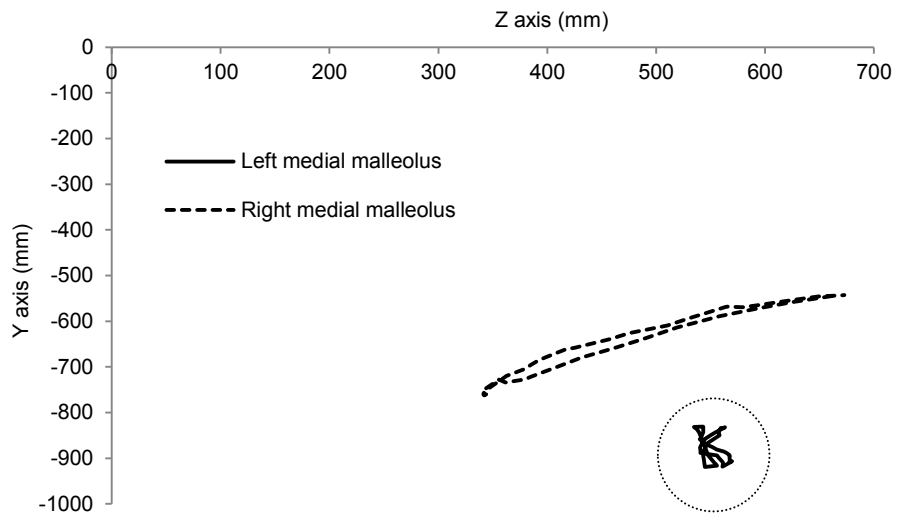
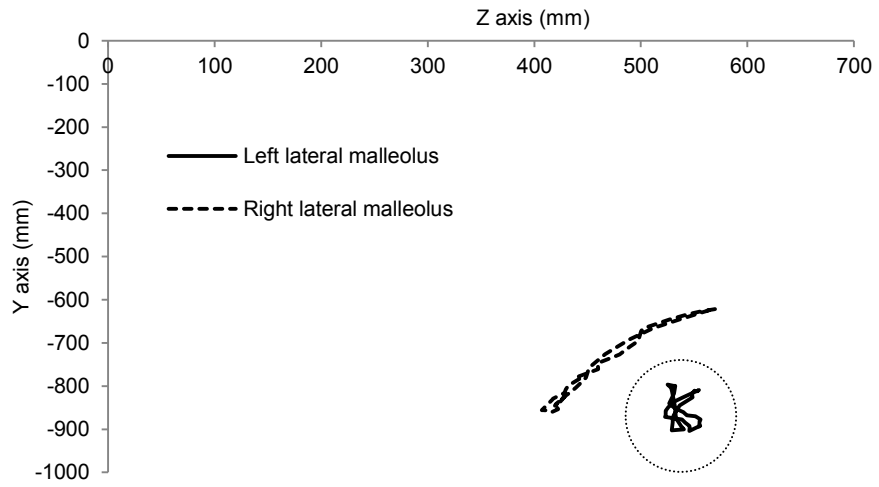
Anatomically, it is not possible for the left medial and lateral malleolus to follow the trajectory shown in the above graphs. The digitisation recordings are performed with the rower in a seated position with their digitised limb resting on the Concept II slide. It was thought that motion tracking errors arose due to the FOB sensor on the right shank causing interference through its proximity to the left shank's sensor during digitisation.

As such, two further malleoli digitisations were performed:

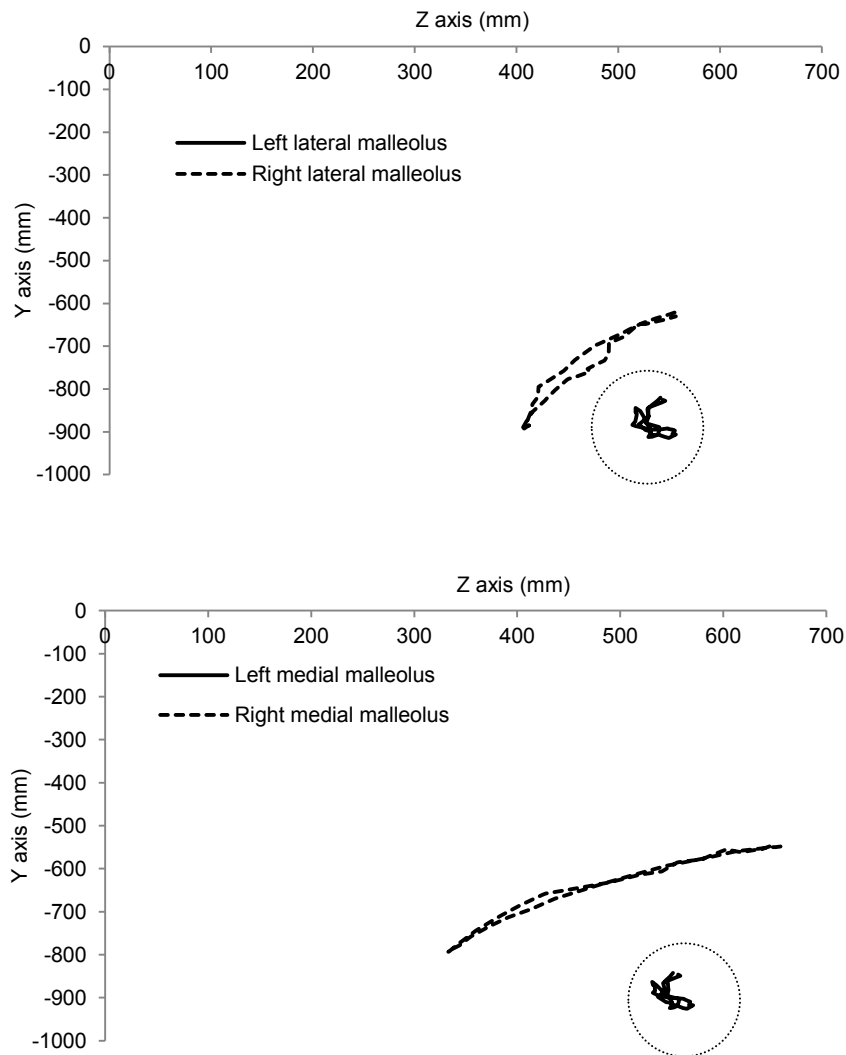
- (i) With the rower stood with their left knee flexed and foot raised.
- (ii) With the rower stood whilst resting their left foot on a wooden stool.

The above two scenarios ensured that the right shank sensor was not causing interference between the electro-magnetic transmitter and the left shank sensor.

(i) *Digitisation with raised foot*



**(ii) Digitisation with foot resting on stool**



The new digitisation set-up did not appear to improve motion tracking of the medial and lateral malleoli on the left ankle. As such, this led to a modified kinematic analysis technique for knee flexion-extension which was utilised and explained in Chapter 3.

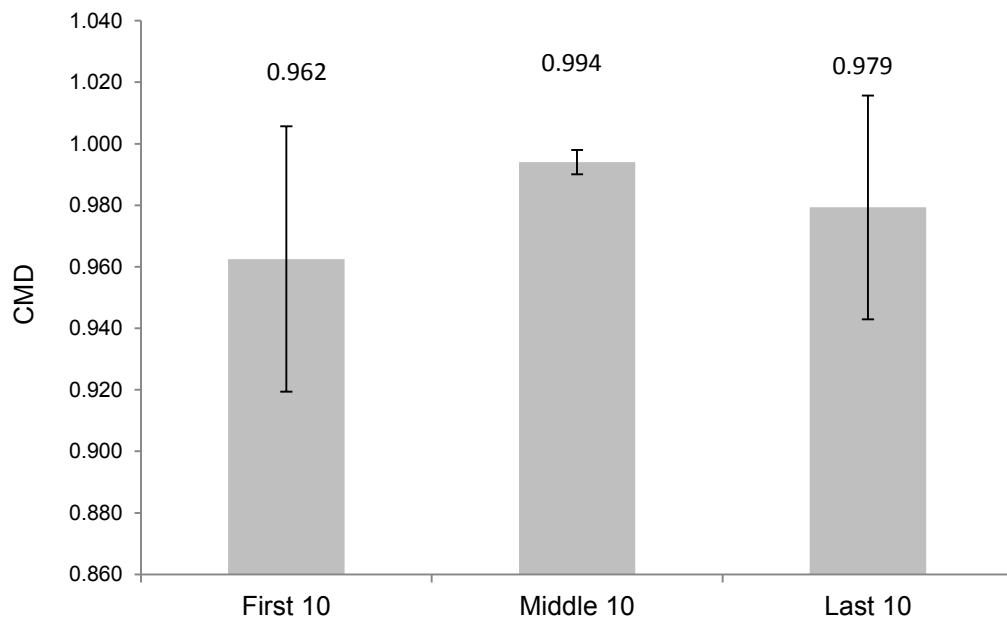
# **Appendix D:**

## **Assessing repeatability of handle force curves**

---



Ten time normalised handle force traces were extracted at the start (First 10), middle (Middle 10) and end (Last 10) of a 3 minute Free Rate step for 35 rowers that participated in the October 2009 testing sessions. For each rower, CMD values for each of the three portions of the Step were derived in Matlab, and the mean and standard deviations of these three values are represented in the bar chart below.



The above chart depicts the CMD values for ten strokes at the start, middle and finish of the Step.

The mean and standard deviation values of each rowers' ten strokes were analysed using a one way repeated measures ANOVA. It was found that CMD for Middle 10 strokes were significantly greater than the First 10 and Last 10 strokes ( $P < 0.05$ ), suggesting that the middle ten strokes of a Step exhibited the greatest level of consistency, thus making it a portion of the test that is suitable for further biomechanical analysis. Furthermore, the standard deviation values for Middle 10 were significantly less than at First 10 or Last 10 ( $P < 0.01$ ), again supporting the idea that the middle part of the Step generates the most consistent data.

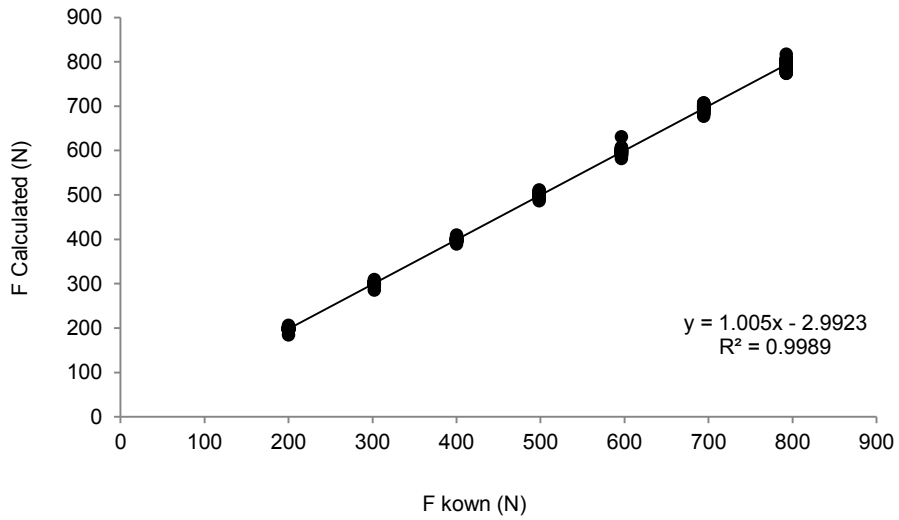
# **Appendix E:**

## **Calibration curves**

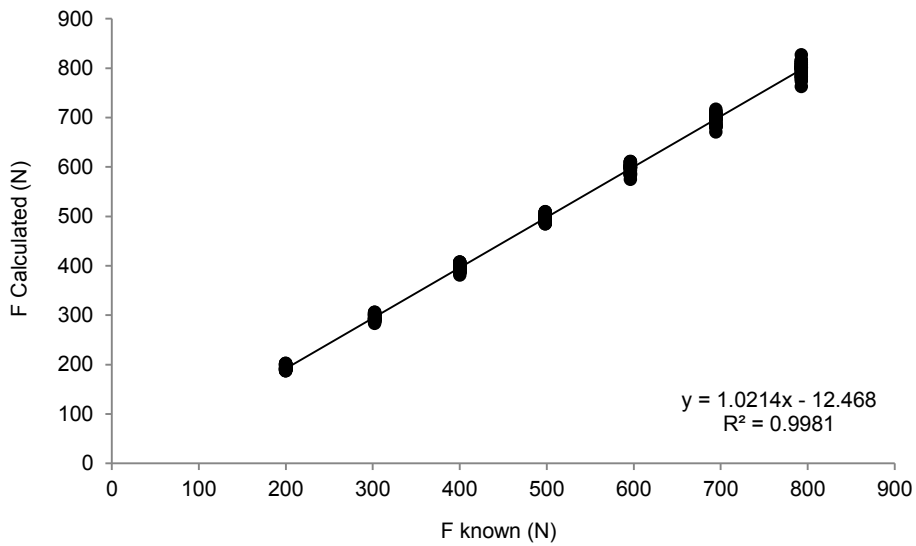
---

## Normal Calibration Results

### *Right Footplate*

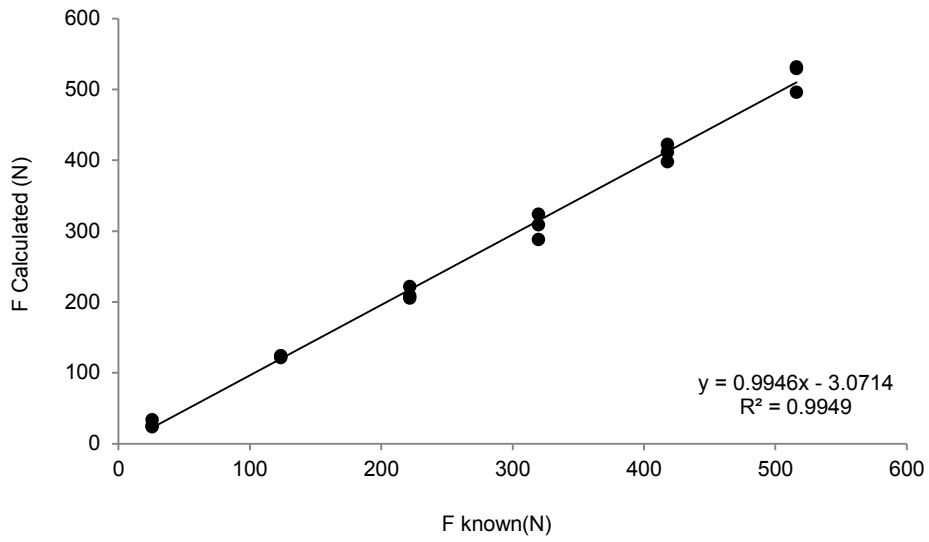


### *Left Footplate*

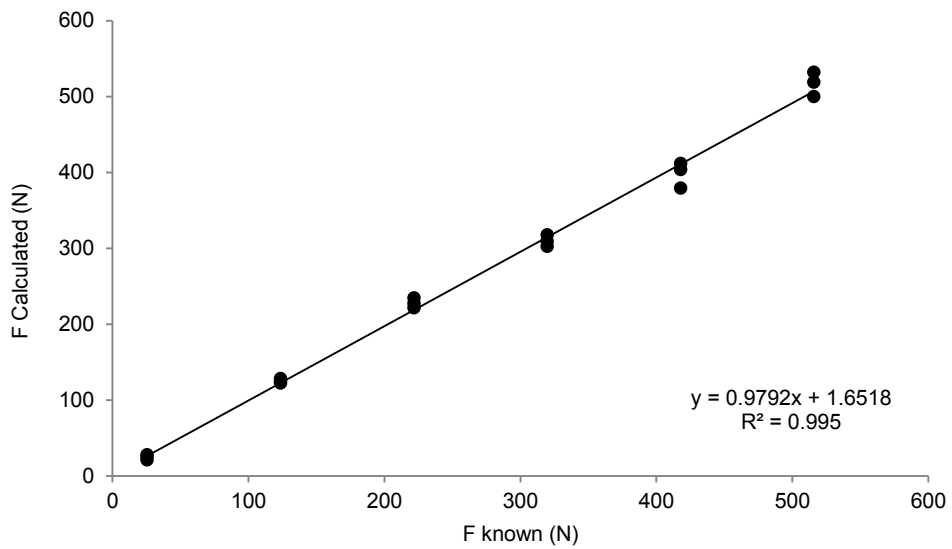


# Shear Calibration Results

## *Right Footplate*



## *Left Footplate*

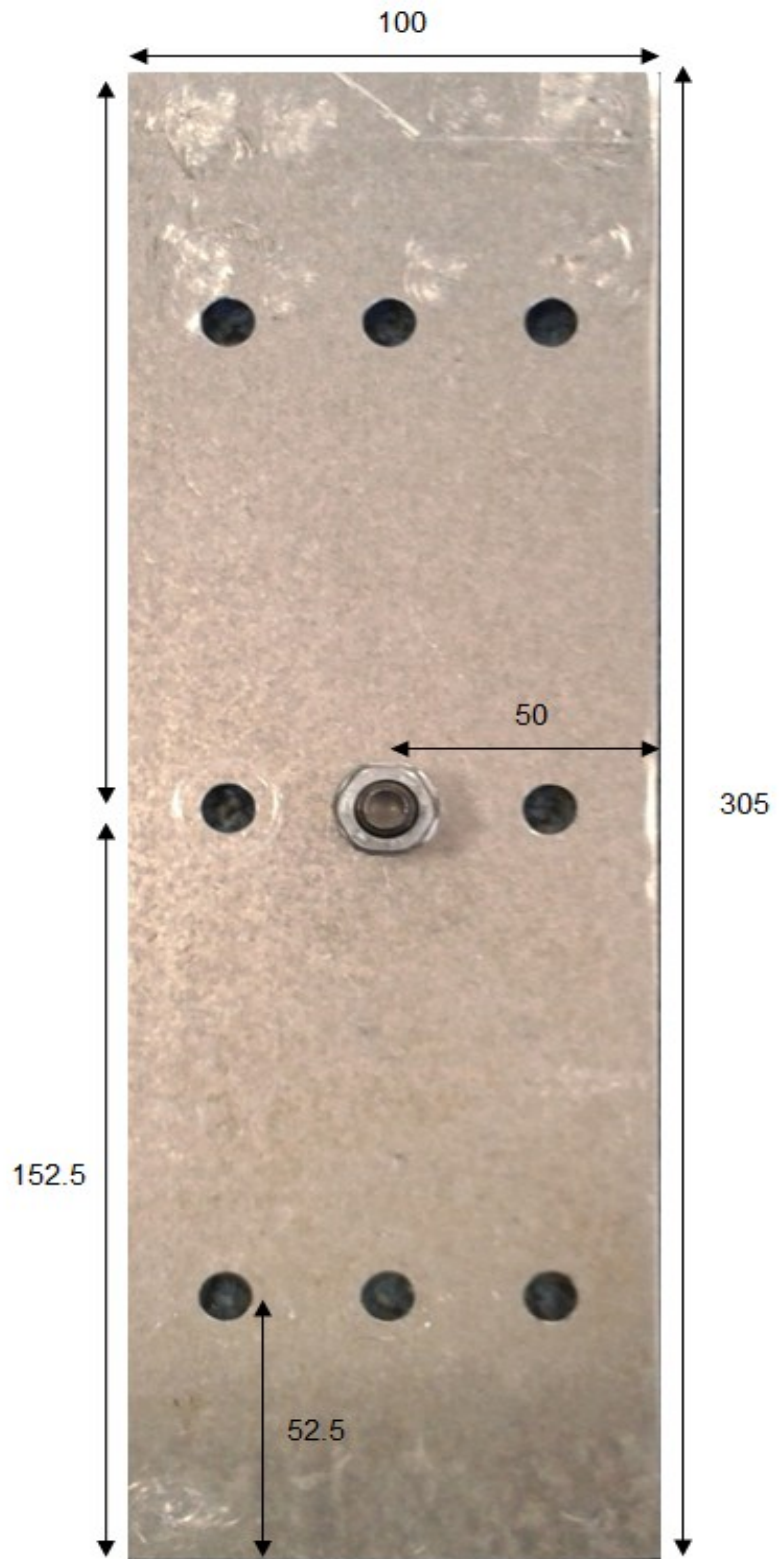


# **Appendix F:**

## **Side plate developed for shear force calibration**

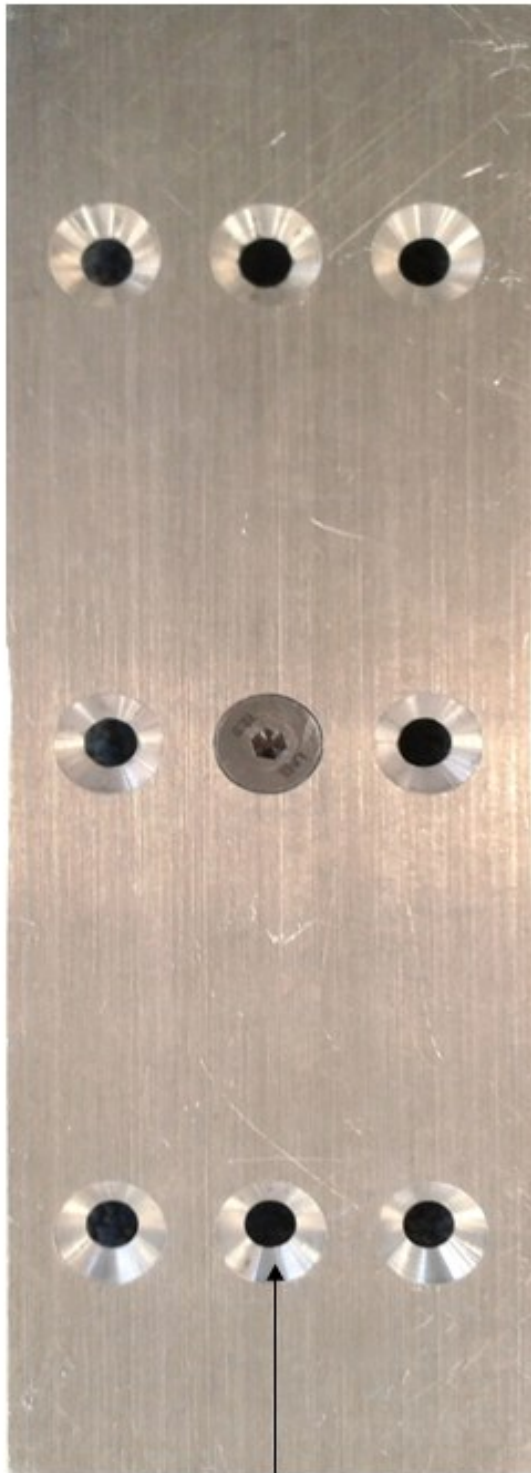
---

**Front View**



*Dimensions in mm*

**Rear View**



Countersunk holes enable the back of the calibration plate to be flush with the surface of the footplate

**Side View**



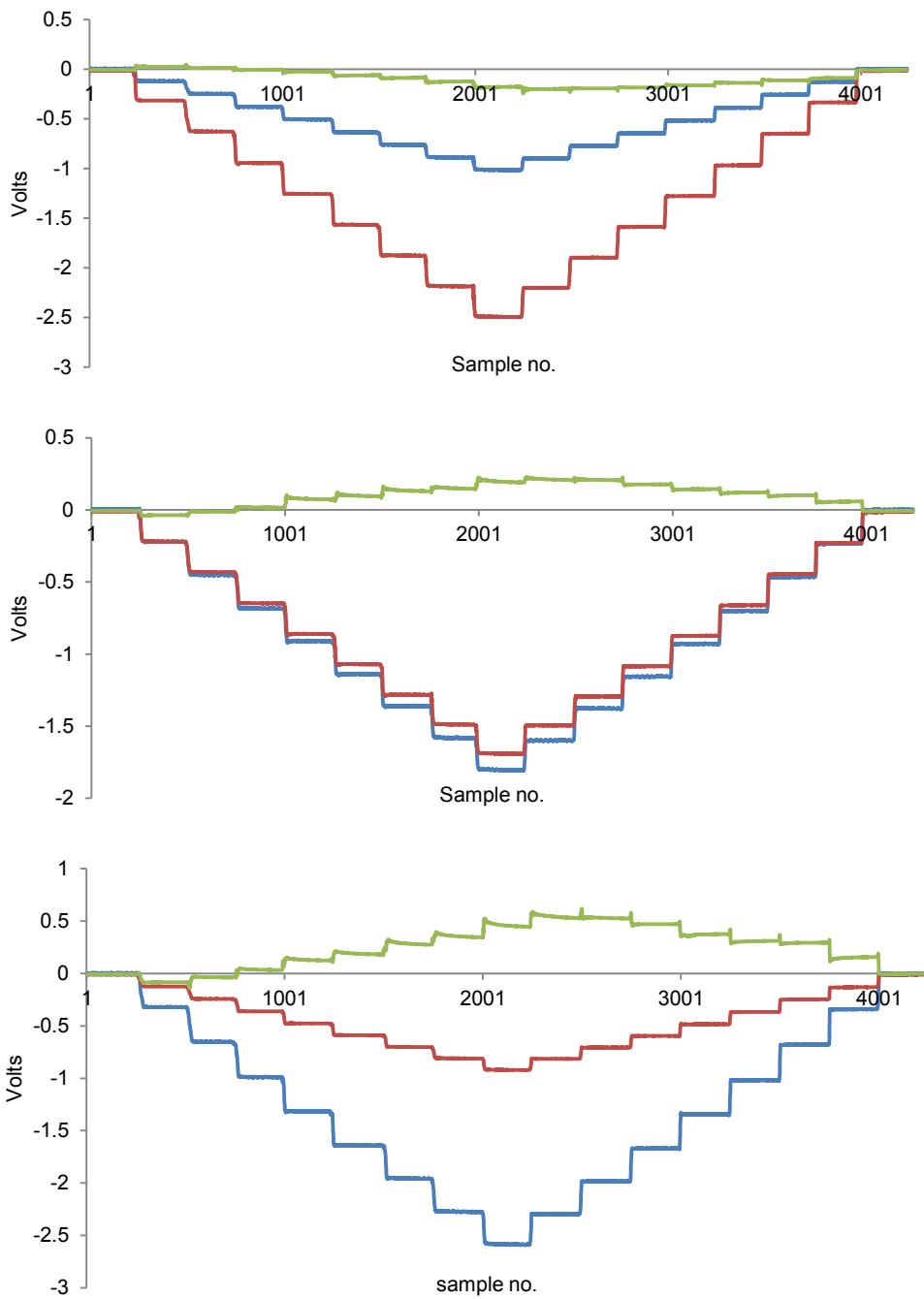
# **Appendix G:**

## **Cross talk during calibration**

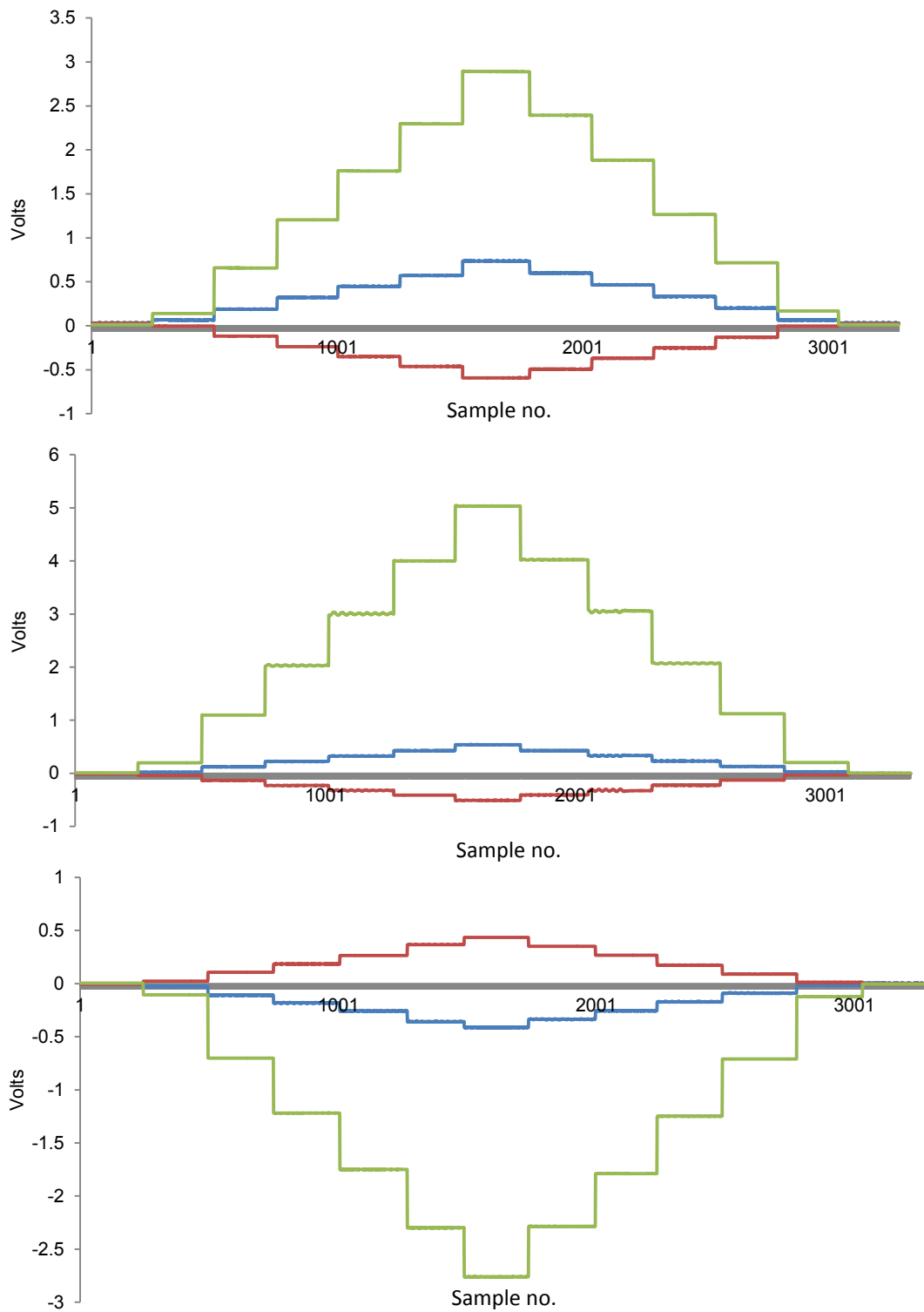
---



*Example of Cross Talk during normal calibration*



*Example of Cross Talk during shear calibration*



# **Appendix H:**

## **LabVIEW code for foot force data acquisition**

---

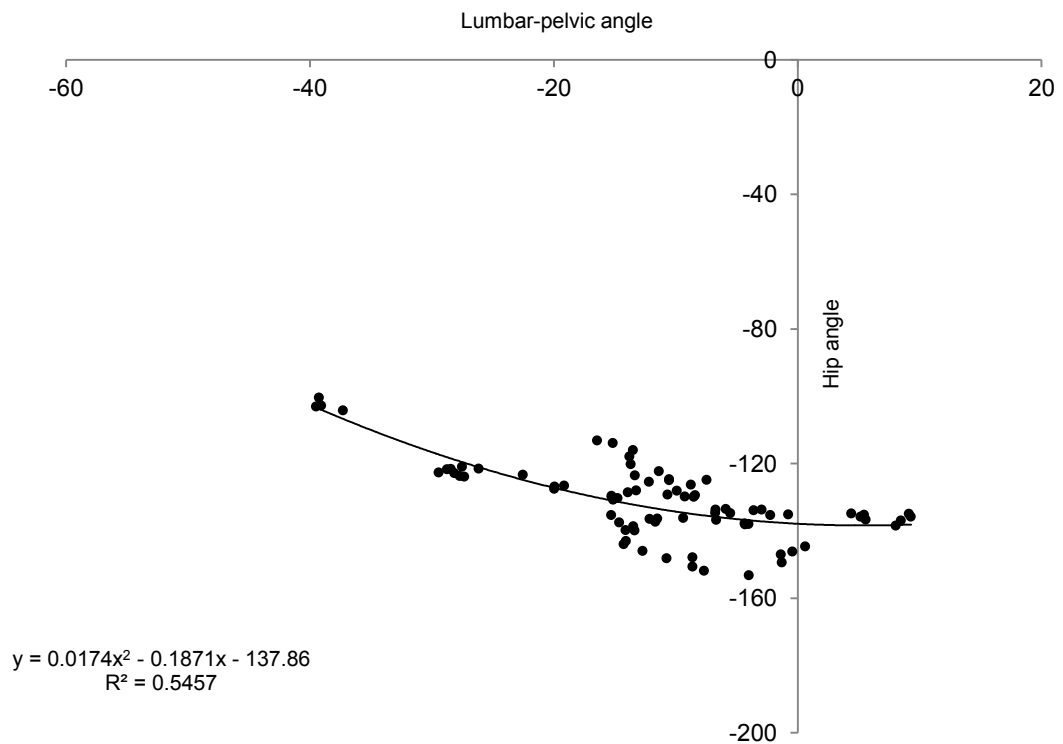


**Appendix I:**

**Relationship between hip angle and  
lumbar-pelvic angle**

---

## Sagittal plane hip angle plotted against lumbar-pelvic angle



Above is a regression model which shows that the largest hip flexion angles are associated with smaller lumbar-pelvic angles, and particularly those with large lumbar-pelvic flexion angles have small hip flexion angles at the catch.

**Appendix J:**

**Matlab function for 3D inter-segmental  
inverse dynamics calculations**

---

```

function [allforces,allmoments] = RNE_IDA(fobdata,mass)

% Number of rows in the data file
n = length(fobdata);

%Extract relevant data from the synchronised FOB and foot force data
file
%KINEMATICS
LSJ = fobdata(:,12:14)/1000;
HJC = fobdata(:,15:17)/1000;
KJC = fobdata(:,18:20)/1000;
AJC = fobdata(:,21:23) /1000;
FJC = fobdata(:,24:26) /1000;
RPSIS = fobdata(:,43:45) /1000;
LPSIS = fobdata(:,46:48) /1000;
RASIS = fobdata(:,49:51) /1000;
LASIS = fobdata(:,52:54) /1000;
Lepi = fobdata(:,55:57) /1000;
Mepi = fobdata(:,58:60) /1000;
Mmal = fobdata(:,61:63) /1000;
Lmal = fobdata(:,64:66) /1000;
MET5 = fobdata(:,67:69) /1000;

% Extract FORCES and Seat COP
Fvert = fobdata(:,70);
Fap = fobdata(:,72);
Footforce = [Fvert Fap];
zero = zeros(n,1);
Fgrf = [zero Footforce];
fseat = fobdata(:,8);
Fseat = [zero fseat zero];
SEATCOP = fobdata(:,6:7)/100;
seatcop = [zero SEATCOP];

%%%%%%%%%%%%%POSITION%%%%%%%%%%%%%
%%% COM of each segment %%%

for i=1:n

% Foot centre of mass from distal end GLOBAL
footcm(i,:) = AJC(i,:) + 0.5*((FJC(i,)-AJC(i,)));
% Shank centre of mass from distal end GLOBAL
shankcm(i,:) = KJC(i,) + 0.567*((AJC(i,)-KJC(i,)));
% Thigh centre of mass from distal end GLOBAL
thighcm(i,:) = HJC(i,) + 0.567*((KJC(i,)-HJC(i,)));
% Pelvis centre of mass from distal end GLOBAL
pelviscm(i,:) = LSJ(i,) + 0.895*((HJC(i,)-LSJ(i,)));

end

%Get rid of negative FP COP values and very large FP COP values (as
they are not
%a true reflection of where FP COP was)
COP = fobdata(:,74)/100;

for i=1:n
if COP(i)<0
    COP(i) = 0;
else COP(i);
end
end

```



```

if COP(i)>30
    COP(i) = COP(i-1);
else COP(i);
end

end

%Resolving COP into vertical and AP COP relative to rear of footplate
%(LOCAL)
COPvertLCS = sin(0.74)*COP; %0.74rads
COPapLCS = cos(0.74)*COP;

%Convert to GLOBAL

COPvert = COPvertLCS - 1.099;
COPap = COPapLCS + 0.5707;

COP=[];
for i=1:n
COP(i,:) = [0.9589 COPvert(i,:) COPap(i,:)];
end

%%%%%%%%%%%%%%%%%%%%%%%%%%%%%%%%%%%%%%%%%%%%%%%%%%%%%%%%%%%%%%%%%%%%%%%%
%%%%%%%%%%%%%%%%%%%%%%%%%%%%%%%%%%%%%%%%%%%%%%%%%%%%%%%%%%%%%%%%%%%%%%%%
%%%%%%%%%%%%LINEAR KINEMATICS SECTION%%%%%%%%%%%%
%%%%%%%%%%%%%%%%%%%%%%%%%%%%%%%%%%%%%%%%%%%%%%%%%%%%%%%%%%%%%%%%%%%%%%%%
%%%%%%%%%%%%%%%%%%%%%%%%%%%%%%%%%%%%%%%%%%%%%%%%%%%%%%%%%%%%%%%%%%%%%%%%

% Time interval between data points (this is average interval - make
sure I
% correct this and delete repeated data points later on....)
for i = 1:n-1
dt(i) = ((fobdata(i+1,79) - fobdata(i,79))/1000);
end
dt = dt';

R = [footcm shankcm thighcm pelviscm];

% calculate velocity using 3-point finite differences
Rd(1,:) = [0,0,0,0,0,0,0,0,0,0,0,0];
for i=2:n-1
    for k=1:length(dt)
        Rd(i,:) = (R(i+1,:) - R(i-1,:))/dt(k);
    end
end

Rd(n,:) = [0,0,0,0,0,0,0,0,0,0,0,0];
Rdfilt(:,1)=smooth(Rd(:,1));
Rdfilt(:,2)=smooth(Rd(:,2));
Rdfilt(:,3)=smooth(Rd(:,3));
Rdfilt(:,4)=smooth(Rd(:,4));
Rdfilt(:,5)=smooth(Rd(:,5));
Rdfilt(:,6)=smooth(Rd(:,6));
Rdfilt(:,7)=smooth(Rd(:,7));
Rdfilt(:,8)=smooth(Rd(:,8));
Rdfilt(:,9)=smooth(Rd(:,9));
Rdfilt(:,10)=smooth(Rd(:,10));
Rdfilt(:,11)=smooth(Rd(:,11));
Rdfilt(:,12)=smooth(Rd(:,12));

```

```

%Velocity
%Foot
  footLv =[Rdfilt(:,1) Rdfilt(:,2) Rdfilt(:,3)];%
%Shank
  shankLv =[Rdfilt(:,4) Rdfilt(:,5) Rdfilt(:,6)];
%Thigh
  thighLv = [Rdfilt(:,7) Rdfilt(:,8) Rdfilt(:,9)];
%Pelvis
  pelvisLv = [Rdfilt(:,10) Rdfilt(:,11) Rdfilt(:,12)];

  % calculate velocity using 3-point finite differences
Rdd(1,:) = [0,0,0,0,0,0,0,0,0,0,0,0];
for i=2:n-1
  for k=1:length(dt)
    Rdd(i,:) = (Rd(i+1,:) - Rd(i-1,:))/dt(k);
  end
end

Rdd(n,:) = [0,0,0,0,0,0,0,0,0,0,0,0];
Rddfilt(:,1)=smooth(Rdd(:,1));
Rddfilt(:,2)=smooth(Rdd(:,2));
Rddfilt(:,3)=smooth(Rdd(:,3));
Rddfilt(:,4)=smooth(Rdd(:,4));
Rddfilt(:,5)=smooth(Rdd(:,5));
Rddfilt(:,6)=smooth(Rdd(:,6));
Rddfilt(:,7)=smooth(Rdd(:,7));
Rddfilt(:,8)=smooth(Rdd(:,8));
Rddfilt(:,9)=smooth(Rdd(:,9));
Rddfilt(:,10)=smooth(Rdd(:,10));
Rddfilt(:,11)=smooth(Rdd(:,11));
Rddfilt(:,12)=smooth(Rdd(:,12));

%Velocity
%Foot
  footLa =[Rddfilt(:,1) Rddfilt(:,2) Rddfilt(:,3)];%
%Shank
  shankLa =[Rddfilt(:,4) Rddfilt(:,5) Rddfilt(:,6)];
%Thigh
  thighLa = [Rddfilt(:,7) Rddfilt(:,8) Rddfilt(:,9)];
%Pelvis
  pelvisLa = [Rddfilt(:,10) Rddfilt(:,11) Rddfilt(:,12)];

%%%%%%%%%%%%%%%%%%%%%%%%%%%%%%%%%%%%%%%%%%%%%%%%%%%%%%%%%%%%%%%%%%%%%%%%
%%%%%%%%%ANGULAR KINEMATICS SECTION%%%%%%%%%
%%%%%%%%%%%%%%%%%%%%%%%%%%%%%%%%%%%%%%%%%%%%%%%%%%%%%%%%%%%%%%%%%%%%%%%%

% Angular velocity can be found by  $r \times v/r^2$ 
%It is important to note that the pseudoscalar angular velocity of a
%particle depends upon the choice of the origin and upon the
orientation
%of the coordinate axes - here everything is based on the GCS

%Angular velocity foot relative to Global
  for i=1:size(footcm,1)
    footAv(i,1:3)=
cross(footcm(i,:),footLv(i,))/(norm(footcm(i,:),2)^2);
  end

```

```

%Angular velocity shank relative to Global
for i=1:size(shankcm,1)
    shankAv(i,1:3)=
cross(shankcm(i,:),shankLv(i,:))/(norm(shankcm(i,:),2)^2);
end
%Angular velocity thigh relative to Global
for i=1:size(thighcm,1)
    thighAv(i,1:3)=
cross(thighcm(i,:),thighLv(i,:))/(norm(thighcm(i,:),2)^2);
end
%Angular velocity foot relative to Global
for i=1:size(footcm,1)
    pelvisAv(i,1:3)=
cross(pelviscm(i,:),pelvisLv(i,:))/(norm(pelviscm(i,:),2)^2);
end

Ad = [footAv shankAv thighAv pelvisAv];

% calculate accelerations using 3-point finite differences
Add(1,:) = [0,0,0,0,0,0,0,0,0,0,0,0,0,0];
for i=2:n-1
    for k=1:length(dt)
        Add(i,:) = (Ad(i+1,:) - Ad(i-1,:))/dt(k);
    end
end

Add(n,:) = [0,0,0,0,0,0,0,0,0,0,0,0,0,0];
Addfilt(:,1)=smooth(Add(:,1));
Addfilt(:,2)=smooth(Add(:,2));
Addfilt(:,3)=smooth(Add(:,3));
Addfilt(:,4)=smooth(Add(:,4));
Addfilt(:,5)=smooth(Add(:,5));
Addfilt(:,6)=smooth(Add(:,6));
Addfilt(:,7)=smooth(Add(:,7));
Addfilt(:,8)=smooth(Add(:,8));
Addfilt(:,9)=smooth(Add(:,9));
Addfilt(:,10)=smooth(Add(:,10));
Addfilt(:,11)=smooth(Add(:,11));
Addfilt(:,12)=smooth(Add(:,12));

%Acceleration
%Foot
footAa =[Addfilt(:,1) Addfilt(:,2) Addfilt(:,3)];
%Shank
shankAa =[Addfilt(:,4) Addfilt(:,5) Addfilt(:,6)];
%Thigh
thighAa = [Addfilt(:,7) Addfilt(:,8) Addfilt(:,9)];
%Pelvis
pelvisAa = [Addfilt(:,10) Addfilt(:,11) Addfilt(:,12)];

%%%%%%%%%%%%%%%%%%%%%%%%%%%%%%%%%%%%%%%%%%%%%%%%%%%%%%%%%%%%%%%%%%%%%%%%
%%%%%%%%%%%%%%%%%%%%%%%%%%%%%%%%%%%%%%%%%%%%%%%%%%%%%%%%%%%%%%%%%%%%%%%% Newton Euler Calculation %%%%%%%%%%%%%%%%%%%%%%%%%%%%%%%%%%%%%%%%%%%%%%%%%%%%%%%%%%%%%%%%%%%%%%%%%
%%%%%%%%%%%%%%%%%%%%%%%%%%%%%%%%%%%%%%%%%%%%%%%%%%%%%%%%%%%%%%%%%%%%%%%%

% Working out the mass of each segemnt relative to the rower's body
mass
footm = (mass/100)*1.370;
shankm = (mass/100)*4.33;
thighm = (mass/100)*14.165;
pelvism = (mass/100)*11.174;

```

```

% This is the segment's Moment of Inertia about the centre of mass
(i.e. LCS of the segment)
inertiafoot1 = [0.004 0.00103 0.0044];
inertiashank1 = [0.0371 0.00646 0.0385];
inertiathigh1 = [0.1999 0.04134 0.1998];
inertiapelvis1 = [0.0525 0.0592 0.06568];

inertiafoot2 = repmat(inertiafoot1,n,1);
inertiashank2 = repmat(inertiashank1,n,1);
inertiathigh2 = repmat(inertiathigh1,n,1);
inertiapelvis2 = repmat(inertiapelvis1,n,1);

% We want MoI in the GCS (i.e. about the global origin) so we use the
% equation: Iglobal = Icm + m*r^2
inertiafoot = inertiafoot2 + footm*(footcm.*footcm);
inertiashank = inertiashank2 + shankm*(shankcm.*shankcm);
inertiathigh = inertiathigh2 + thighm*(thighcm.*thighcm);
inertiapelvis = inertiapelvis2 + pelvism*(pelviscm.*pelviscm);

%%%%%%%%%%%%%%%%%%%%%%%%%%%%%%%%%%%%%%%%%%%%%%%%%%%%%%%%%%%%%%%%%%%%%%%% Foot segment %%%%%%%%%%%%%%%%%%%%%%%%%%%%%%%%%%%%%%%%%%%%%%%%%%%%%%%%%%%%%%%%%%%%%%%%%

%Foot Force at ankle:
for i=1:size(footLa,1)
    Fankle(i,:) = (footm*footLa(i,:)) - Fgrf(i,:) - ([0 -9.81
0]*footm);% force applied by Forearm to Hand
end

%Foot Moments at ankle:
for i=1:size(footAa,1)
    Mankle(i,:) = (footAa(i,:).*inertiafoot(i,:)) - cross((COP(i,:)-
footcm(i,:)),Fgrf(i,:)) - cross((AJC(i,:)-footcm(i,:)),Fankle(i,:));
end

%%%%%%%%%%%%%%%%%%%%%%%%%%%%%%%%%%%%%%%%%%%%%%%%%%%%%%%%%%%%%%%%%%%%%%%% Shank segment %%%%%%%%%%%%%%%%%%%%%%%%%%%%%%%%%%%%%%%%%%%%%%%%%%%%%%%%%%%%%%%%%%%%%%%%%

%Shank Force at knee
for i=1:size(shankLa,1)
    Fknee(i,:) = (shankm*shankLa(i,:)) - (-Fankle(i,:)) + ([0 -9.8
0]*shankm);% force applied by thigh to knee
end

%Shank Moments at knee:
for i=1:size(shankAa,1)
    Mknee(i,)=(shankAa(i,:).*inertiashank(i,:)) - cross((AJC(i,:)-
shankcm(i,:)),-Fankle(i,:)) - cross((KJC(i,:)-
shankcm(i,:)),Fknee(i,:)) - (-Mankle(i,:));
end

%%%%%%%%%%%%%%%%%%%%%%%%%%%%%%%%%%%%%%%%%%%%%%%%%%%%%%%%%%%%%%%%%%%%%%%% Thigh Segment %%%%%%%%%%%%%%%%%%%%%%%%%%%%%%%%%%%%%%%%%%%%%%%%%%%%%%%%%%%%%%%%%%%%%%%%%

%Thigh Force at hip:
for i=1:size(thighLa,1)
    Fhip(i,)=(thighm*thighLa(i,:))-(-Fknee(i,:))+[0 -9.8 0]*thighm);%
force applied by pelvis to hip
end

```

```

%Thigh Moments at hip:
for i=1:size(thighAa,1)
    Mhip(i,:)=(thighAa(i,:).*inertiathigh(i,:)) - cross((KJC(i,:)-
thighcm(i,:)),-Fknee(i,:)) - cross((HJC(i,:)-thighcm(i,:)),Fhip(i,:))
- (-Mknee(i,:));
end

%%%%%%%%%%%%%%%%%%%%%%%%%%%%%%%%%%%%%%%%%%%%%%%%%%%%%%%%%%%%%%%%%%%%%%%% Pelvis Segment %%%%%%%%%%%%%%%%%%%%%%%%%%%%%%%%%%%%%%%%%%%%%%%%%%%%%%%%%%%%%%%%%%%%%%%%%

%Pelvis Force at LSJ:
for i=1:size(pelvisLa,1)
    Flsj(i,:)=(pelvism*pelvisLa(i,:))-([0 2*Fhip(i,2) 2*Fhip(i,3)]+[0
-9.8 0]*pelvism) - Fseat(i,:);% force applied by Lumbar spine to
pelvis
end

% Distance from hip to pelvis COM (DISTAL)
CMdist = HJC - pelviscm;
% Distance from hip to pelvis COM (PROXIMAL)
CMprox = pelviscm - LSJ;

%Pelvis moments at LSJ:
for i=1:size(pelvisAa,1)
    Mlsj(i,:)=(pelvisAa(i,:).*inertiapelvis(i,:)) - cross((HJC(i,:)-
pelviscm(i,:)),-[0 2*Fhip(i,2) 2*Fhip(i,3)]) - cross((LSJ(i,:)-
pelviscm(i,:)),Flsj(i,:)) - ([-2*Mhip(i,1) 0 0]) -
cross(CMdist(i,:),Fseat(i,:))*-1);
end

%%

%%%%%%%%%%%%%%%%%%%%%%%%%%%%%%%%%%%%%%%%%%%%%%%%%%%%%%%%%%%%%%%%%%%%%%%%
%%%%%%%%%%%%%%%%%%%%%%%%%%%%%%%%%%%%%%%%%%%%%%%%%%%%%%%%%%%%%%%%%%%%%%%% TRANSFORMATION SECTION%%%%%%%%%%%%%%%%%%%%%%%%%%%%%%%%%%%%%%%%%%%%%%%%%%%%%%%%%%%%%%%%%%%%%%%%
%%%%%%%%%%%%%%%%%%%%%%%%%%%%%%%%%%%%%%%%%%%%%%%%%%%%%%%%%%%%%%%%%%%%%%%%

%%%%%%%%%%%%%%%%%%%%%%%%%%%%%%%%%%%%%%%%%%%%%%%%%%%%%%%%%%%%%%%%%%%%%%%%
%%%%%%%%%%%%%%%%%%%%%%%%%%%%%%%%%%%%%%%%%%%%%%%%%%%%%%%%%%%%%%%%%%%%%%%% PELVIS FRAME %%%%%%%%%%%%%%%%%%%%%%%%%%%%%%%%%%%%%%%%%%%%%%%%%%%%%%%%%%%%%%%%%%%%%%%%%
%%%%%%%%%%%%%%%%%%%%%%%%%%%%%%%%%%%%%%%%%%%%%%%%%%%%%%%%%%%%%%%%%%%%%%%%

right_P SIS_ASIS = midpoint(RP SIS, R ASIS);
left_P SIS_ASIS = midpoint(LP SIS, L ASIS);
ASISmid = midpoint(R ASIS, L ASIS);
P SISmid = midpoint(RP SIS, LP SIS);

for i = 1:length(fobdata)

%I (med-lat vector)
vectorI_pel = right_P SIS_ASIS(i,:) - left_P SIS_ASIS(i,:);
I_pel(i,:) = -directioncosine(vectorI_pel);

%J (ant-pos vector)
vectorJ_pel = ASISmid(i,:) - P SISmid(i,:);
J_pel(i,:) = directioncosine(vectorJ_pel);

%K (vertical vector)
vectorK_pel = cross(I_pel, J_pel);
K_pel = directioncosine(vectorK_pel);

```

```

%%%%%%%%%%%%%%%%%%%%%%%%%%%%%%%%%%%%%%%%%%%%%%%%%%%%%%%%%%%%%%%%%%%%%%%%
%%%%%%%%%%%%%%%%%%%%%%%%%%%%%%%%%%%%%%%%%%%%%%%%%%%%%%%%%%%%%%%%%%%%%%%% FEMORAL FRAME %%%%%%%%%%%%%%%%%%%%%%%%%%%%%%%%%%%%%%%%%%%%%%%%%%%%%%%%%%%%%%%%%%%%%%%%%
%%%%%%%%%%%%%%%%%%%%%%%%%%%%%%%%%%%%%%%%%%%%%%%%%%%%%%%%%%%%%%%%%%%%%%%%

%K (vertical vector)
vectorK_femur = HJC(i,:) - KJC(i,:);
K_femur(i,:) = -directioncosine(vectorK_femur);

%I (med-lat vector)
vectorI_femur = Lepi(i,:) - Mepi(i,:);
I_femur(i,:) = -directioncosine(vectorI_femur);

%J (ant-pos vector)
vectorJ_femur = cross(K_femur, I_femur);
J_femur = directioncosine(vectorJ_femur);

%%%%%%%%%%%%%%%%%%%%%%%%%%%%%%%%%%%%%%%%%%%%%%%%%%%%%%%%%%%%%%%%%%%%%%%%
%%%%%%%%%%%%%%%%%%%%%%%%%%%%%%%%%%%%%%%%%%%%%%%%%%%%%%%%%%%%%%%%%%%%%%%% SHANK FRAME %%%%%%%%%%%%%%%%%%%%%%%%%%%%%%%%%%%%%%%%%%%%%%%%%%%%%%%%%%%%%%%%%%%%%%%%%
%%%%%%%%%%%%%%%%%%%%%%%%%%%%%%%%%%%%%%%%%%%%%%%%%%%%%%%%%%%%%%%%%%%%%%%%

%K (vertical vector)
vectorK_shank = KJC(i,:) - AJC(i,:);
K_shank(i,:) = -directioncosine(vectorK_shank);

%I (med-lat vector)
vectorI_shank = Lmal(i,:) - Mmal(i,:);
I_shank(i,:) = -directioncosine(vectorI_shank);

%J (ant-pos vector)
vectorJ_shank = cross(K_shank, I_shank);
J_shank = directioncosine(vectorJ_shank);

%%%%%%%%%%%%%%%%%%%%%%%%%%%%%%%%%%%%%%%%%%%%%%%%%%%%%%%%%%%%%%%%%%%%%%%%
%%%%%%%%%%%%%%%%%%%%%%%%%%%%%%%%%%%%%%%%%%%%%%%%%%%%%%%%%%%%%%%%%%%%%%%% FOOT FRAME %%%%%%%%%%%%%%%%%%%%%%%%%%%%%%%%%%%%%%%%%%%%%%%%%%%%%%%%%%%%%%%%%%%%%%%%%
%%%%%%%%%%%%%%%%%%%%%%%%%%%%%%%%%%%%%%%%%%%%%%%%%%%%%%%%%%%%%%%%%%%%%%%%

%K (vertical vector)
vectorK_foot = AJC(i,:) - FJC(i,:);
K_foot(i,:) = -directioncosine(vectorK_foot);

%I (med-lat vector)
vectorI_foot = MET5(i,:) - FJC(i,:);
I_foot(i,:) = -directioncosine(vectorI_foot);

%J (ant-pos vector)
vectorJ_foot = cross(K_foot, I_foot);
J_foot = directioncosine(vectorJ_foot);

%add these to the original co-ordinates for the origin to
%give the technical axis unit vectors in terms of the global frame.
Ifoot(i,:) = I_foot(i, :)+AJC(i, :);
Jfoot(i,:) = J_foot(i, :)+AJC(i, :);
Kfoot(i,:) = K_foot(i, :)+AJC(i, :);
% Foot global to local transformation matrix
Tfoot = soder([1 0 0 0 1 0 0 0 1;Ifoot(i,:) Jfoot(i,:) Kfoot(i,:)]);

%add these to the original co-ordinates for the origin to
%give the technical axis unit vectors in terms of the global frame.
Ishank(i,:) = I_shank(i, :)+KJC(i, :);

```

```

Jshank(i,:) = J_shank(i,:)+KJC(i,:);
Kshank(i,:) = K_shank(i,:)+KJC(i,:);
% Shank global to local transformation matrix
Tshank = soder([1 0 0 0 1 0 0 0 1;Ishank(i,:) Jshank(i,:)
Kshank(i,:)]);

%add these to the original co-ordinates for the origin to
%give the technical axis unit vectors in terms of the global frame.
Ifemur(i,:) = I_femur(i,:)+HJC(i,:);
Jfemur(i,:) = J_femur(i,:)+HJC(i,:);
Kfemur(i,:) = K_femur(i,:)+HJC(i,:);
% femur global to local transformation matrix
Tfemur = soder([1 0 0 0 1 0 0 0 1;Ifemur(i,:) Jfemur(i,:)
Kfemur(i,:)]);

%add these to the original co-ordinates for the origin to
%give the technical axis unit vectors in terms of the global frame.
Ipel(i,:) = I_pel(i,:)+LSJ(i,:);
Jpel(i,:) = J_pel(i,:)+LSJ(i,:);
Kpel(i,:) = K_pel(i,:)+LSJ(i,:);
% pelvis global to local transformation matrix
Tpel = soder([1 0 0 0 1 0 0 0 1;Ipel(i,:) Jpel(i,:) Kpel(i,:)]);

% Transformation of Global net moments to Local net joint moments

lcs_Flsj(i,:) = Tpel\[Flsj(i,:) 1]';
lcs_Fhip(i,:) = Tfemur\[Fhip(i,:) 1]';
lcs_Fknee(i,:) = Tshank\[Fknee(i,:) 1]';
lcs_Fankle(i,:) = Tfoot\[Fankle(i,:) 1]';

lcs_Mlsj(i,:) = Tpel\[Mlsj(i,:) 1]';
lcs_Mhip(i,:) = Tfemur\[Mhip(i,:) 1]';
lcs_Mknee(i,:) = Tshank\[Mknee(i,:) 1]';
lcs_Mankle(i,:) = Tfoot\[Mankle(i,:) 1]';

end

allforces = [lcs_Fankle(:,1:3) lcs_Fknee(:,1:3) lcs_Fhip(:,1:3)
lcs_Flsj(:,1:3)];
allmoments = [lcs_Mankle(:,1:3) lcs_Mknee(:,1:3) lcs_Mhip(:,1:3)
lcs_Mlsj(:,1:3)];

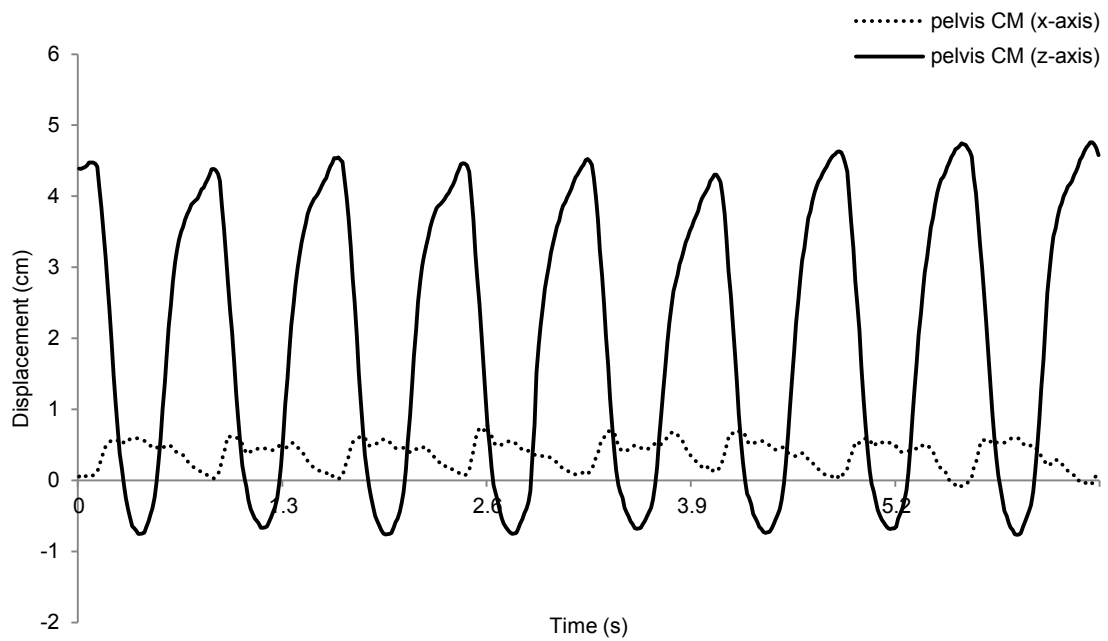
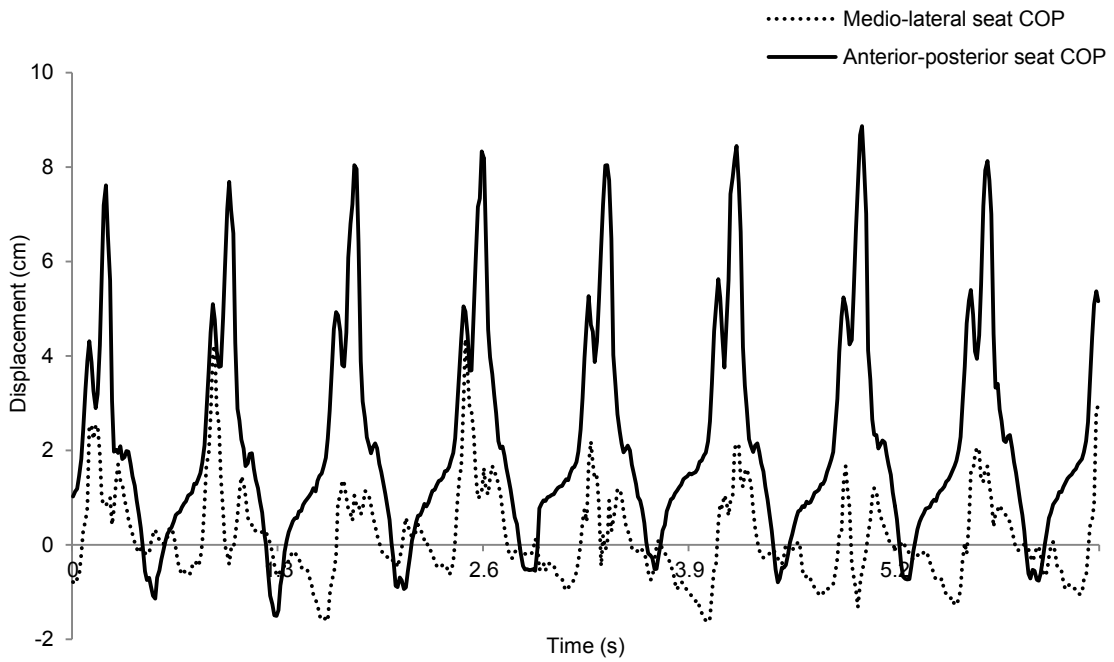
end

```

**Appendix K:**  
**Comparison of seat COP and pelvis CM**  
**trajectories**

---





The above graphs show the anterior-posterior (z-axis) and medio-lateral (x-axis) trajectories of the seat's COP and pelvis' CM trajectories during a portion of a rowing trial. The two are being compared because it was not possible to infer in the inverse dynamics model that force from the rowing seat acted through its COP. This is because seat position was not tracked, therefore global COP positions could not be derived. As such, it had to be assumed that seat force consistently acted through the pelvis' CM.

This was thought to be a realistic assumption as COP at the seat is mostly influenced by movement of the upper body and pelvis.

The graphs above show that pelvis motion in the sagittal plane is swiftly followed by anterior motion of seat COP – although it must be noted that COP motion is greater on the seat in both planes. However, Seat COP motion is well represented by pelvis CM motion, as demonstrated by the shape and comparative sizes of the AP and ML waveforms.